Interactions of Water with Mineral Dust Aerosol: Water Adsorption, Hygroscopicity, Cloud Condensation, and Ice Nucleation

Interactions of Water with Mineral Dust Aerosol: Water Adsorption, Hygroscopicity, and Cloud Condensation and Ice Nucleation Activities

M. J. Tang[1], D. J. Cziczo[2], V. H. Grassian[1,*]

1 Department of Chemistry, University of Iowa, Iowa City, IA 52242, USA

2 Department of Earth, Atmospheric and Planetary Sciences and Civil and Environmental Engineering, Massachusetts Institute of Technology, Cambridge, MA 02139, USA

Abstract: Mineral dust aerosol is one of the major types of aerosol present in the troposphere. The molecular level interactions of water vapor with mineral dust are of global significance. Hygroscopicity, light scattering and absorption, heterogneous reactivity and the ability to form clouds are all related to water-dust interactions. In this review article, experimental techniques to probe water interactions with dust and theoretical frameworks to understand these interactions are discussed. A comprehensive overview of laboratory studies of water adsorption, hygroscopicity, and cloud condensation nucleation and ice nucleation activity of fresh and atmspherically aged mineral dust particles is provided. Finally, we relate laboratory studies and theoretical simulations that provide fundemental insights into these processes on the molecular level with field measurements that illustrate the atmospheric significance of these processes. Overall, the details of water interactions with mineral dust are covered from multiple perspectives in this review article.

19 **CONTENTS**

1 Introduction

1.1 Significance of mineral dust aerosol in the atmosphere

Atmospheric aerosols are ubiquitous in the atmosphere and consist of solid and liquid particles that range in size from a few nanometers to tens of micrometers. In addition to their impacts on air quality, human health, and visibility,[1,2] these particles can alter the energy balance of the earth by scattering and absorbing solar and terrestrial radiation and by influencing the formation and properties of clouds.[3,4] The lack of a complete understanding of the role of aerosols (and thus clouds) on the climate system becomes a bottleneck for reliable and accurate projections of climate change.[5] Mineral dust aerosol is one of the main types of aerosol in the troposphere. Mineral dust particles are mainly emitted from arid and semi-arid regions (e.g., Saharan and Gobi Deserts),[6,7] with an annual flux of ~2000 Tg yr^{-1}.[8,9] It is estimated that natural dust sources account for 75% of the emission and anthropogenic sources account for the other 25%.[10] One outstanding issue is the abundance of relatively bare mineral dust emitted from arid regions versus internally mixed "fertile soil dust" containing both mineral and organic components. Forster et al.[11] suggested the latter contributed 0-20% of the global mineral dust budget, while a more recent satellite-based study [10] coupled to land usage maps suggested ~25%. After being lifted into the troposphere, mineral dust particles have lifetimes of up to several days [9] and can be transported over thousands of kilometres.[12-18]

Table 1. Average emission fluxes and atmospheric loadings of different types of aerosol particles in the troposphere, as estimated by models participating in the aerosol model intercomparison initiative (AeroCom).[8]

aerosol type	emission (Tg yr^{-1})	atmospheric loading (Tg)
mineral dust	1840	19.2
sea spray	16600	7.52

sulfate	179	1.99
primary organic matter	96.6	1.7
black carbon	11.9	0.24

The average emission fluxes and atmospheric abundances of different types of tropospheric aerosol particles, as estimated by models participating in the aerosol model intercomparison initiative (AeroCom),[8] are provided in Table 1. While the emission of mineral dust is the second largest in the troposphere, with sea spray being the largest, it is the most abundant type of aerosol particle by mass with an estimated average atmospheric loading of 19.2 Tg,[8] as much of sea spray particles have diameters larger than 10 μm and thus are quickly removed from the atmosphere through deposition.[19] A substantial fraction of mineral dust particles also have large diameters and thus are quickly removed by dry deposition after they are entrained into the atmosphere.[9] Dust emissions are closely linked to hydrological cycles, and climate variability can change dust emissions, leading to further feedbacks on the climate system.[10,20-28]

Because of the overall loading and lifetime in the atmosphere, mineral dust can impact the Earth's atmosphere and climate in a number of ways. Mineral dust particles can both scatter and absorb solar and terrestrial radiations, thus having direct radiative effects.[29-43] [44]Optical scattering and absorption by mineral dust particles can further change the photolysis rates and thus influence photochemical cycles in the troposphere.[45] Mineral dust particles can also have indirect impact on radiative forcing by acting as cloud condensation nuclei (CCN) to form liquid cloud droplets [46-55] and ice nuclei (IN) to form ice clouds.[56-73] In fact, mineral dust particles may be the dominant IN in the troposphere [74,75] and therefore have a significant impact on the Earth's radiative budget,[76-79] precipitation, and the hydrological cycle.[58,80-83] Additionally, deposited mineral dust particles can be a major contributor of several important elements, including Fe,[84-87] P,[88-91] and Cu,[92,93]

especially into open ocean waters [88,94-97] and the Amazon,[98,99] and therefore have strong effects on biogeochemical cycles and the Earth's climate system.[100-103]

Mineral dust aerosol also influences air quality,[104-106] visibility,[107] and public health in dust-impacted regions.[12,20,104,108-119] For example, clear enhanced effects of particulate matter on respiratory and cerebrovascular diseases were observed during Saharan dust outbreaks in Roma, Italy.[120] A recent modeling study [108] estimated that the fraction of cardiopulmonary deaths caused by mineral dust aerosol is about 1.8% globally, and in countries most affected by dust storms it is up to 15-50%.

The mineralogy of dust particles is very complex, showing large variation with their sources and atmospheric transport processes.[121-130] Different minerals can have very different physical and chemical properties, such as heterogeneous reactivity, refractive index, CCN and IN activity, and therefore have different impacts on atmospheric chemistry, cloud formation, and climate. For example, it has been shown that the kinetics of N_2O_5 uptake onto mineral dust particles vary over almost two orders of magnitude for different minerals,[131-139] and the ice nucleation activity of different minerals can differ by several orders of magnitude.[140,141] It is also suggested that the iron solubility in dust particles is strongly dependent on the mineloragy.[142-144] Mineral dust particles in the troposphere consist of a variety of minerals that can be externally and internally mixed.[145-149] The emission fluxes and atmospheric abundance of the most abundant minerals, estimated by a recent modeling study,[150] are shown in Table 2.

Table 2. Emission fluxes and atmospheric loadings of different mineral phases, estimated by a recent study [150] using the Community Atmosphere Model.

mineral	flux (Tg yr^{-1})	atmospheric loadings (Tg)

quartz	568.9	4.1
illite	370.1	4.2
montmorillonite	246.2	2.8
feldspar	205	1.4
kaolinite	192.3	2.2
calcite	145.1	1.3
hematite	24	0.2
gypsum	15.3	0.1

159

160 Less abundant minerals have not been included in most modeling studies; however, the impact of
161 a mineral in the troposphere is not necessarily proportional to its abundance. For example, the
162 mass fractions of TiO_2 in mineral dust particles are typically a few percents or less,[32,151-153] but its
163 semiconductor properties make it very important in heterogeneous photochemical reactions which
164 may play an important role in the formation or removal of reactive trace gases in the
165 troposphere.[154-156] Saharan dust particles only contain 0.09% phosphorus on average, though the
166 deposition of mineral dust particles from the Sahara desert is a major source of phosphorus for
167 oceans.[97] It has also been suggested that transition metals of trace amounts contained by mineral
168 dust particles (and probably also anthropogenic particles) may significantly enhance the
169 multiphase oxidation of SO_2.[157] Furthermore, the complexity of mineral dust particles can be
170 significantly increased due to their transformations resulting from chemical processing during
171 transport.[158-162]

172

173 In addition, a few minerals with high refractive indexes (such as TiO_2 and Al_2O_3),[138,139,163-165] have
174 recently been proposed as alternative particles to be injected into the stratosphere to scatter more
175 solar radiation back into space, as a geoengineering method [166] to counteract global warming due
176 to increasing levels of greenhouse gases. For example, it is estimated that in order to achieve the

same scattering effect, the use of TiO_2 for stratospheric particle injection requires a factor of ~3 less in mass than that of H_2SO_4 aerosols which are present as a natural aerosol in the stratosphere.[163]

1.2 Overview of the interaction of water with mineral dust aerosol: adsorption, hygroscopic growth, and cloud condensation and ice nucleation

Water is ubiquitous in the troposphere and can exist in the gas, liquid, and solid states. The amount of water vapor contained by air is usually described by relative humidity (RH), typically in %, which is defined as the ratio of its partial pressure to the saturated vapor pressure at the same temperature (T) multiplied by 100, as shown in Eq. (1):

$$RH = 100 \times \frac{P(water)}{P_S(water)} \qquad (1),$$

where P(water) is the partial pressure of water vapor and P_s(water) is the saturated vapor pressure of water. Under sub-saturation conditions, i.e. RH is lower than 100%, some water vapor will partition onto/into mineral dust particles. The amount of water associated with particles, in equilibrium with water vapor in the gas phase, depends on RH, T, and the type of dust particles. The partitioning of water between the gas and particle phase, is called water adsorption in surface science and hygroscopicity in aerosol science. Hygroscopicity is in fact a general term which describes the ability to absorb or release water as a function of water activity and how a substance can attract and hold water molecules from the surrounding environment. In aerosol science, it usually refers to the change in diameter, volume, or mass of particles when exposed to water vapor. Different theories are used to describe water adsorption versus hygroscopicity which differ in fundamental underlying assumptions to describe water partitioning between gas and particle phases under sub-saturation conditions, as discussed in more detail in Section 3.

When RH is larger than 100%, i.e. under super-saturation conditions, dust aerosol particles can be activated to cloud droplets (a process called cloud condensation nucleation).[167] At a given super-saturation, the ability of a particle to be activated to a cloud droplet depends on the particles diameter [168,169] and also its CCN activity, which is determined by its chemical composition and mixing state.[170] When *T* is less than 273 K, mineral dust particles might be activated to form ice particles (ice nucleation) if the relative humidity to ice (RH*i*, defined as the ratio of the partial pressure of water vapor to the saturated pressure of ice at the same temperature) is larger than 100%.[167] In this article RH and RH*i* are referred to relative humidity with respect to liquid water and ice, respectively.

What makes water uptake properties of mineral dust more complicated is that, as well known, during transport mineral dust particles react with a wide range of trace gases in the troposphere.[156,161,171-187] These heterogeneous reactions involve gas-solid interactions. If mineral dust particles are activated to cloud droplets, multiphase reactions can occur in these aqueous cloud droplets.[157,162,188-191] Heterogeneous and multiphase reactions can directly and indirectly change the concentrations of several important trace gases,[161,172,192-198] such as NOx, O_3 and OH radicals, thus imposing significant impacts on tropospheric chemistry. Furthermore, these reactions also lead to a change in surface and sometimes even the bulk chemical composition of mineral dust particles,[126,158,199-210] thereby modifying their interactions with water, including surface adsorption,[211,212] hygroscopicity,[213-215] and cloud condensation nucleation [216-218] and ice nucleation activity.[219-221]

The change in the interaction with water can in turn further influence the reactivity of mineral dust particles towards reactive trace gases. The change in composition and hygroscopicity of dust particles may influence both their refractive index [222] and optical diameters, and the change in

CCN and IN activity can results in the change in the probability of wet deposition,[223,224] thereby impacting their atmospheric lifetime.[224] In addition, heterogeneous chemistry can modify the solubility and/or bio-availability of elements within individual mineral dust particles.[84,88,96,225] The complex interactions of mineral dust particles with reactive trace gases and water, and their impacts on cloud formation, are depicted in Figure 1.

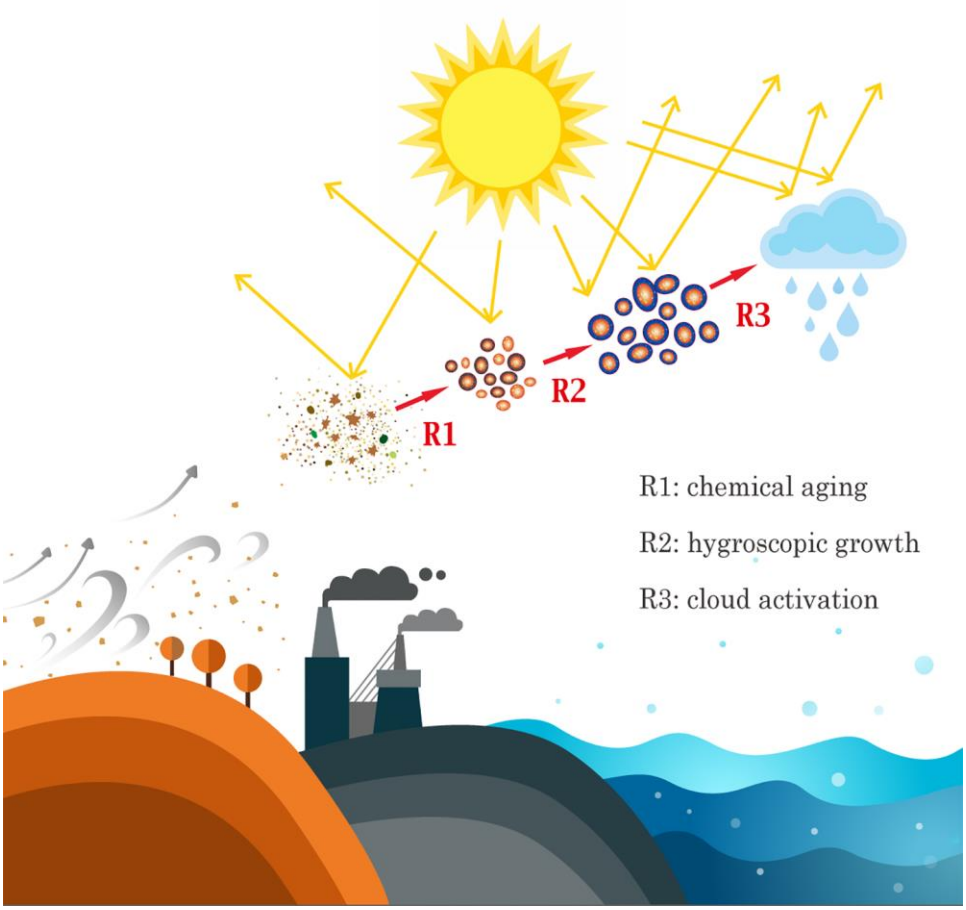

Figure 1. A schematic diagram of the interactions of mineral dust aerosol particles with reactive trace gases and water and their impacts on cloud formation and radiative balance. R1) chemical transformation/aging of mineral dust aerosol particles due to reactions with reactive trace gases; R2) enhanced hygroscopic growth of aged mineral dust aerosol particles; and R3) activation of mineral dust particles to cloud droplets and ice particles.

238 It is important to note that heterogeneous chemistry and photochemistry of mineral dust particles
239 in the atmosphere have been summarized in several comprehensive review papers.[161,171,172] It has
240 been widely recognized that water adsorbed by mineral dust plays a central role in determining the
241 heterogeneous reactivity and photoreactivity towards reactive trace gases in the
242 atmosphere.[137,199,226-228] In particular, a recent review paper [229] described in detail how surface
243 adsorbed water can play a myriad of roles in the surface chemistry and can either enhance or
244 suppress the reactivity of mineral dust particles towards reactive trace gases. For example, Figure
245 2 shows the dependence of the uptake coefficient of N_2O_5, $\gamma(N_2O_5)$, on RH (and thus surface
246 adsorbed water) for different mineral dust particles. Even for the same trace gas, the influence of
247 RH on the uptake kinetics can be very different for different minerals, highlighting the importance
248 of accurate determination of water adsorption as a function of RH for a variety of different minerals
249 that make up dust in the atmosphere. Adsorbed water can also change the reaction products and
250 the partitioning of reaction products among different phases.[229]

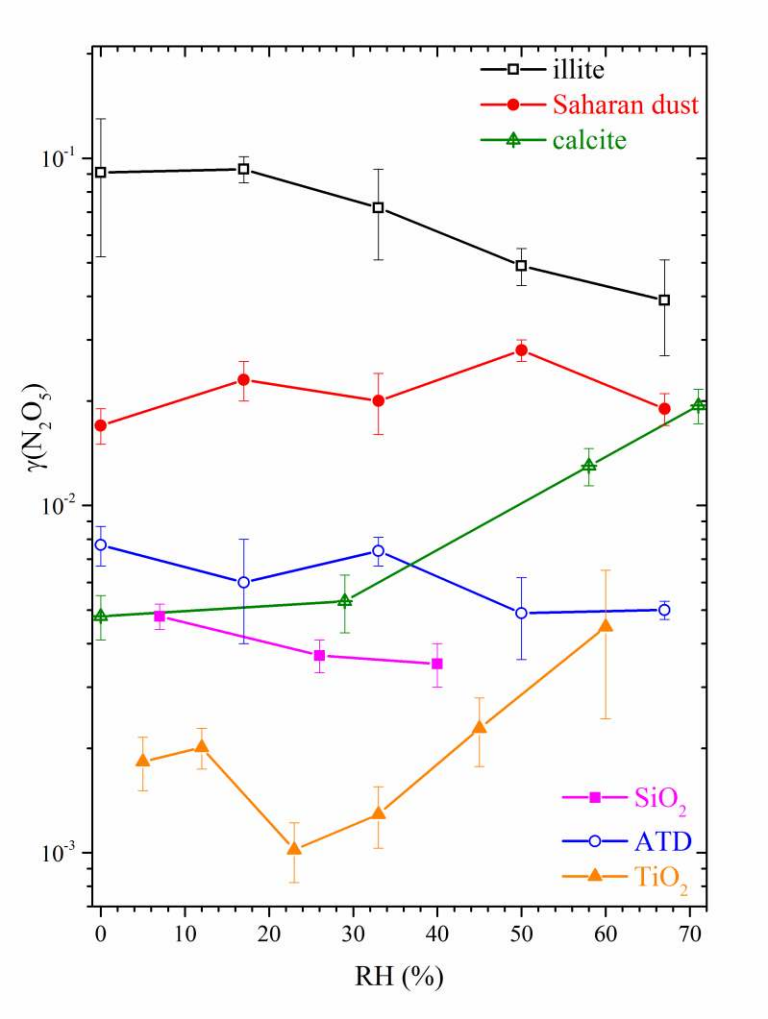

Figure 2. Dependence of $\gamma(N_2O_5)$ on RH for different mineral dust particles. Sources of data: illite,[137] Saharan dust,[136] calcite,[135] SiO_2,[139] Arizona Test Dust (ATD),[137] and TiO_2.[138]

However, the interactions of mineral dust particles with water vapor at temperatures higher than that for ice nucleation has hitherto not been reviewed in the context of atmospheric chemistry and climate, despite that in the last two decades a large number of studies have been published by both the surface science and aerosol science communities. We note that a recent review paper has discussed the multi-faceted roles of surface adsorbed water in heterogeneous reactions of mineral dust particles.[229] Therefore, in this article, we undertake a comprehensive review of the interactions of water with mineral dust particles. Following the Introduction section, we summarize and discuss experimental techniques used to study water adsorption properties, hygroscopicity, and CCN

activity of mineral dust particles (Section 2). In Section 3, we introduce and discuss theories used in this review to describe water adsorption in surface science and hygroscopicity and CCN activity in aerosol science, and we also describe guidelines used to compare experimental data reported in these previous studies. Following this, laboratory studies of water adsorption properties, hygroscopicity, and CCN activity of different mineral dust particles are reviewed in Section 4, in which the effects of chemical aging processes on water interaction are also discussed. We focus on mineral particles and surfaces which are of direct relevance for atmospheric chemistry and microphysics of aerosols and clouds. Therefore, water adsorption on single crystal surfaces,[230-236] although relevant, is not discussed in too much detail in this review. In this section, we also discuss some theoretical studies to illustrate how these studies can provide insight into the fundamental mechanisms of water adsorption on mineral surface on the molecular and sub-molecular levels. In addition, at the end of this section we also summarize results from field measurements which provide evidence that the hygroscopicity of mineral dust particles can be significantly modified due to heterogeneous reactions and cloud processing. Although ice nucleation activity of mineral dust particles has been reviewed in a few excellent recent papers,[140,237-239] these papers are mainly focused on fresh mineral dust particles and only one review article [238] has briefly summarized ice nucleation activity of aged mineral dust particles. Increasing number of laboratory studies suggest that chemical aging processes can significantly change the ice nucleation activity of mineral dust particles. Thus in Section 5, recent work on the effects of chemical aging on the ice nucleation activity of dust particles is reviewed. Finally, in Section 6 we outline several key questions from a physical chemistry view which preclude us from a better understanding of the interactions of mineral dust aerosol particles with water vapor (including water adsorption, hygroscopicity, and CCN and IN activities), and discuss how these challenges can be addressed through future research.

2 An overview of sample preparation methods and experimental techniques

Experimental techniques which have been used to investigate water adsorption properties, hygroscopicity, and CCN activity of mineral dust particles are briefly summarized here. Instead of providing a comprehensive discussion of each techniques, we introduce the basic principles and key features, and refer interested readers to the relevant literature for further details. These techniques can be classified into three groups which are discussed in Sections 2.2-2.4, according to the way particles under investigation exist: 1) particle ensembles or single particles deposited on a substrate; 2) levitated single particles; and 3) an ensemble of particles as an aerosol. A quick overview of these techniques is provided in Table 3 along with their key measurement features. A variety of sample preparation methods have been used in previous studies, and it has been suggested that experimental results may vary with sample preparation methods. Therefore, we first briefly discuss the effects of different particle preparation/generation methods in Section 2.1. In this review paper, we focus on techniques which have been used to quantitatively determine the amount of water adsorbed by mineral dust particles of direct atmospheric relevance. In addition, there have been a large number of studies on water adsorption on single crystals of minerals, for example, $CaCO_3$,[211] α-Al_2O_3,[230,240] TiO_2,[231,232,241], and α-Fe_2O_3.[242] Although surfaces of these single crystals may not completely resemble the complexity of mineral dust particles in the troposphere, studies using well-defined single crystal surfaces can provide a wealth of fundamental information and insights into water adsorption mechanisms and intermolecular interactions between water molecules and water molecules with surface atoms. Techniques used to study the ice nucleation activity have been discussed recently [140,238,239] and thus are not covered here.

Note that one shortcoming of many laboratory studies is that overly simplistic dust samples, when compared to the complex internal mixtures found in the atmosphere,[243,244] [158] are often utilized. For example, atmospheric mineral dust is often associate with surface coatings due to

311 heterogeneous reactions with reactive trace gases,[158,161,202,245] but laboratory studies most often
312 consider unprocessed particles which may be only representative of mineral dust particles freshly
313 emitted into the troposphere.
314
315 **Table 3.** Summary of representative literature on different experimental techniques which have been used
316 to measure water adsorption, hygroscopicity, and CCN activity of mineral dust particles.

techniques	references	main features
QCM	Navea et al., 2010 [246]	Change in particle mass at different RH is quantified by the frequency change of the quartz crystal.
TGA	Gustafsson et al., 2005 [247]	Change in particle mass at different RH is directly measured.
PSA	Ma et al., 2010 [248]	Change in partial pressure of water vapor due to surface adsorption is measured.
ATR-FTIR	Schuttlefield et al., 2007 [249]	IR absorption of surface adsorbed water is measured and can be converted to the amount of adsorbed water.
transmission FTIR	Goodman et al., 2001 [250]	
DRIFTS	Gustafsson et al., 2005 [247]	
AP-XPS	Ketteler et al., 2007 [241]	Chemically specific and quantitative measurements of water and other species adsorbed on the surface can be achieved.
EDB	Pope et al., 2010 [251]	Relative change in mass of a single particle at different RH is determined from the change of the DC voltage used to balance the gravitational force.
optical levitation	Tong et al., 2011 [252]	Particle size change of a single particle at different RH is determined by light scattering.
H-TDMA	Herich et al., 2009 [49]	Mobility diameter change at different RH is measured.
aerosol optical extinction	Attwood and Greenslade, 2011 [253]	Change in aerosol optical extinction properties at different RH is measured, e.g., using an AE-CRD.
aerosol optical scattering	Li-Jones et al., 1998 [254]	Change in aerosol optical scattering properties at different RH is measured, e.g., using a nephelometer.

aerosol optical adsorption	Utry et al., 2015 [255]	Change in aerosol optical scattering properties at different RH is measured, e.g., using a photoacoustic absorption spectrometer.
CCNc	Sullivan et al., 2010 [256]	Concentrations of aerosol particles activated to cloud droplets at a certain super-saturation are measured.

QCM: quartz crystal microbalance. TGA: thermogravimetric analyser. PSA: physisorption analyser. ATR-FTIR: attenuated total reflection Fourier transform infrared spectroscopy. DRIFTS: diffuse reflectance Fourier transform spectroscopy. AP-XPS: atmospheric pressure X-Ray photoelectron spectroscopy. EDB: electrodynamic balance. H-TDMA: hygroscopicity tandem differential mobility analyser. CCNc: cloud condensation nuclei counter.

2.1 Methods used for sample preparation

There are two common methods used to generate mineral dust aerosols: i) wet generation: aerosol particles were generated by atomizing the suspension of mineral dust powders in water;[139,256,257] ii) dry generation: mineral dust particles are directly dispersed and entrained into the air, typically by using a high-speed air jet.[136,258-260] Commercial instruments, such as rotating brusher generators [134,136] and fluidized beds,[220,261] are also available for dry generation of dust aerosol particles. Recent studies have shown that mineral dust particles generated by these two methods can have distinctive hygroscopicity and CCN activities,[49,217,262,263] with wet-generated aerosol particles having higher hygroscopicity and CCN activities. The change of hygroscopicity and CCN activities of dust particles after wet-generation can be due to a couple of reasons: 1) soluble impurities contained by the dust particles are enriched in generated aerosol particles by wet-generation, and 2) some components contained by dust particles may undergo chemical reaction in the water suspension. For example, Sullivan et al.[256] suggest that the formation of $Ca(HCO_3)_2$, due to the reaction of $CaCO_3$ with H_2O and CO_2, causes wet-generated $CaCO_3$ particles to have higher CCN activity than dry-generated $CaCO_3$. This conclusion is further supported by Zhao et al.,[264] who have demonstrated that $Ca(HCO_3)_2$ particles are more hygroscopic than $CaCO_3$

particles. We expect that similar phenomena may occur for clay mineral but less likely for relatively inert minerals such as SiO_2.

Compared to wet generation, dry generation produces dust aerosol particles which may better resemble the composition and thus the hygroscopicity of original powders used to generate those aerosol particles. On the other hand, dust aerosol particles can be activated to cloud droplets and undergo cloud processing several times during their residence in the troposphere,[48,162,223,265-267] and dust aerosol particles produced by wet generation might better resemble the properties of dust particles which were activated cloud droplets. Thus, to summarize, dry and wet generation methods have been shown to produce aerosol particles with different hygroscopicity and CCN activity. Nevertheless, currently it is not clear which method may generate aerosol particles which better resemble dust particles in the troposphere. This is because nascent dust or cloud activated dust may be very different and therefore may best described by dry generation and wet generation techniques, respectively.

To investigate water adsorption on mineral dust particles deposited on a substrate, typically a slurry of dust particles in water is deposited on the supporting substrate, leading to the formation of a relatively uniform dry film after the evaporation of water.[268] Alternatively, other solvents, such as methanol or ethanol, can be used instead of water.[196] In some studies [269,270] dry powders of dust were also directly placed on a substrate, without using any solvents. Whether a solvent is used during deposition of dust particles on a substrate may influence the measured water adsorption and hygroscopicity of dust particles; however, to date this has not been systematically examined.

2.2 Mineral dust particles supported on substrates

2.2.1 Mass measurements of adsorbed water as a function of water vapor pressure

The mass of a particle ensemble can be measured at different RH (in %) to investigate the amount of adsorbed water by using several techniques. For examples, in a quartz crystal microbalance (QCM) experiment, the measured frequency of the quartz crystal reflects the mass of particles loaded on it.[249,271] The frequency change, Δf (Hz), is directly related to the change in mass, Δm, according to the Sauerbrey equation:[246,249,272]

$$\Delta f = -C_f \Delta m \qquad (2),$$

where C_f is the constant sensitivity factor for the specific QCM and can be experimentally calibrated. Usually a slurry of dust particles in water (or other solvents, e.g., methanol) was sprayed onto the quartz crystal and then dried to form a thin film on the quartz crystal.[246,273]

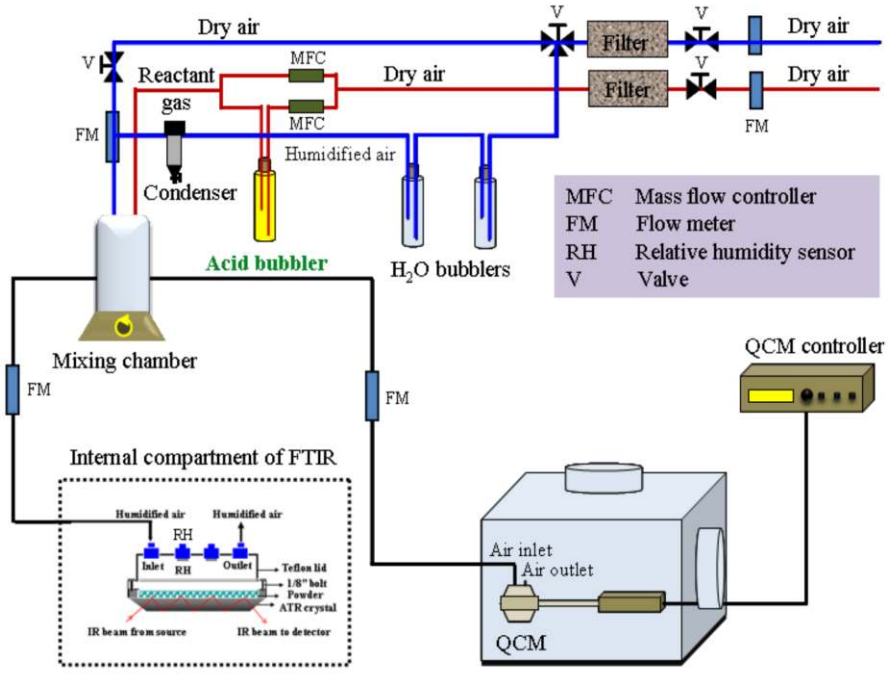

Figure 3. A schematic diagram of ATR-FTIR spectroscopy and quartz crystal microbalance (QCM). Although these measurements are integrated in time and the gas phases above the samples are at the same relative humidity, it should be noted that the ATR-FTIR cell and the QCM cell both have separate thin film samples. Reprinted with permission from ref 274. Copyright 2012 American Chemical Society.

A schematic diagram of a typical QCM set-up,[274] is shown in Figure 3. The change in frequency of the quartz crystal (and thus the change in particle mass) measured at different RH, can be used to determine the amount of adsorbed water. Figure 4 shows the frequency change of a QCM (upper panel) and water adsorption isotherm (lower panel) for SiO_2 particles.[273]

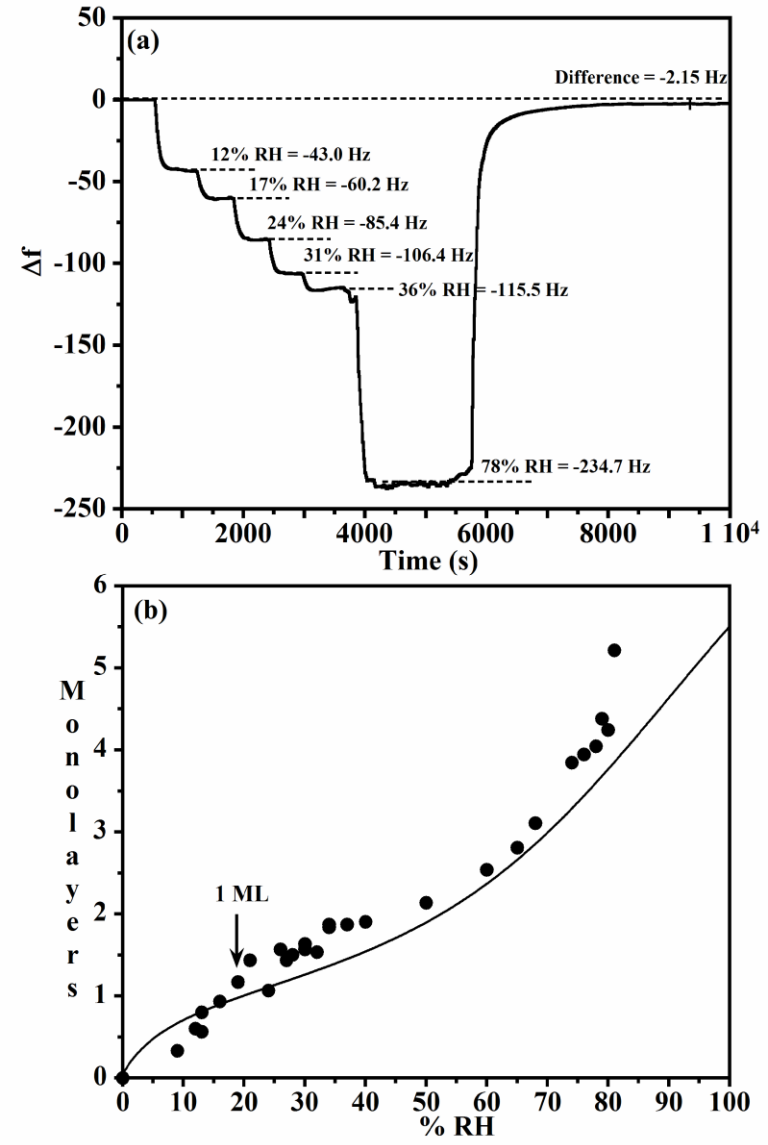

Figure 4. Water adsorption on SiO_2 at different RH as measured by QCM. (a) Change in frequency of the quartz crystal at different RH; b) the number of adsorbed water layers on the surface at different RH, and the curve is the modified three-parameter BET fit reported by Goodman et al.[250] Reprinted with permission from ref 273. Copyright 2007 Society for Applied Spectroscopy.

Thermogravimetric analysers can also be used to investigate water adsorption on mineral dust particles. For example, a Mettlet-Toledo TGA/SDTA851e thermogravimetric analyzer (Mettler-Toledo, USA) with a mass measurement accuracy of ±1 μg, was used to measure the amount of water adsorbed on $CaCO_3$ and Arizona Test Dust particles.[247]

In addition, the amount of surface adsorbed water can also be quantified by measuring the change of water vapor pressure in the gas phase due to adsorption onto the surface, using a physisorption analyser (PSA).[212,248] The change in partial pressure of water vapor due to adsorption on mineral dust particles can be measured to determine the water adsorption isotherm, in a similar way to the BET surface area measurement using N_2. For example, a commercial physisorption analyser, AUTOSORB (Quantachrome, USA), was modified and used to investigate the hygroscopicity of fresh and aged Al_2O_3 and $CaCO_3$ particles.[212,248]

These experimental techniques provide direct quantification of water adsorbed by mineral dust particles. Water may also adsorb on the apparatus wall and cause artifacts, and this effect can be subtracted by blank experiments in which no particles are used.

2.2.2 FTIR measurements of water uptake

Water adsorbed on mineral dust surface at different RH can be monitored by Fourier transform infrared spectroscopy (FTIR), including transmission FTIR,[250] diffuse reflectance Fourier transform spectroscopy (DRIFTS),[247] and attenuated total reflection Fourier transform infrared spectroscopy (ATR-FTIR).[273] As shown in Figure 5, surface adsorbed water has two distinctive IR absorption peaks in the region extending from 1500 to 4000 cm^{-1}, one near 3400 cm^{-1} due to the O-H stretching mode and the other near 1645 cm^{-1} due to H_2O bending mode.[250,273,275]

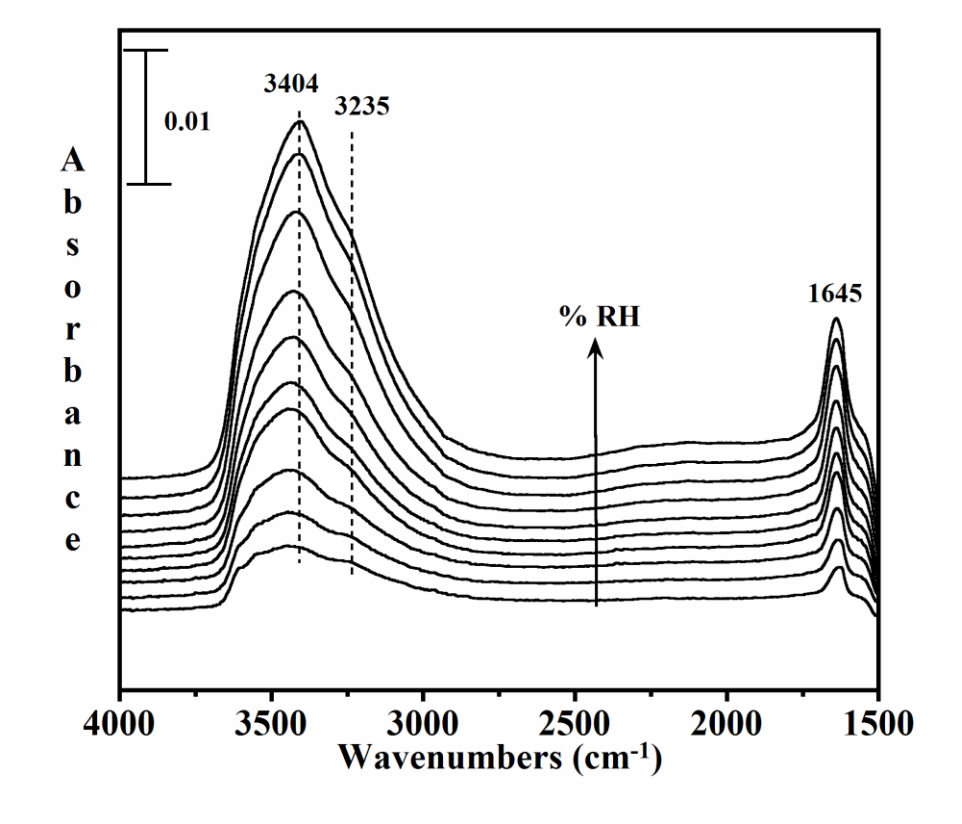

410

411 **Figure 5.** ATR-FTIR spectra following the water uptake on 19.2 mg of SiO_2 at different RHs (5, 8, 13, 20,
412 27, 37, 47, 66, 74, and 78%). Reprinted with permission from ref 273. Copyright 2007 Society for Applied
413 Spectroscopy.

414

415 Since surface hydroxyl groups can also contribute to the O-H stretching mode, it is better to use
416 the H_2O bending mode to analyze molecularly adsorbed water on the surface. The integrated IR
417 absorption can be used to quantify the amount of surface-adsorbed water, using a modified
418 Lambert-Beer law and assuming that the IR absorption cross section of surface-adsorbed water is
419 equal to that of liquid water.[211,240]

420 **2.2.3 Surface analysis techniques used for water uptake measurements**

421 Surface techniques can be very valuable in studying water adsorption and hygroscopicity of
422 mineral dust particle. Some surface techniques are able to provide information on both chemical
423 composition and morphology of the surface under investigation, though absolute quantification of

424 the amount of water associated with the surface may be non-trivial. Here we provide several
425 examples to demonstrate how different surface techniques can be used to understand water
426 adsorption and hygroscopicity of fresh and aged mineral dust particles. In addition to the
427 techniques mentioned in this section, there are many other surface techniques which have been
428 used to study water adsorption on single crystals including scanning probe techniques such as
429 scanning tunneling microscopy (STM).[232,276-278]
430
431 The transformation of solid $CaCO_3$ particles to aqueous droplets, due to the reaction with HNO_3,
432 has been observed in the laboratory for the first time by Krueger et al.,[279] using Scanning Electron
433 Microscopy (SEM) and Energy Dispersive X-ray analysis (EDX). Two years later the atmospheric
434 significance of this finding was supported by a field study,[245] which showed that dust particles
435 collected in Israel have been substantially processed in the atmosphere and could exist in aqueous
436 state even at very low RH (9-11%). Transmission Electron Microscopy can also be used to monitor
437 the morphology change of mineral dust particles. For example, using TEM, Matsuki et al.[159] found
438 that some of the Asian dust particles collected in Beijing are spherical, due to internal mixing with
439 nitrate and sulfate. Liu et al.[215] used a micro-Raman spectrometry to investigate the hygroscopicity
440 of $CaCO_3$ particles after exposure to NO_2. They [215] found that after the reaction, irregular $CaCO_3$
441 particles are converted to spherical droplets at 37% RH and the internally mixed $CaCO_3/Ca(NO_3)_2$
442 particles have the same phase transition properties as pure $Ca(NO_3)_2$ particles.
443
444 Traditionally, X-Ray photoelectron spectroscopy (XPS) is a technique applied to surfaces in ultra-
445 high vacuum, limiting its application under atmospheric relevant conditions (i.e. with pressures
446 close to 1 bar). Over the past decade, advances in atmospheric pressure XPS (AP-XPS) makes it a
447 very promising method to investigate the interaction of gases, including water vapor, with mineral
448 dust particles, because of its chemically specific and quantitative nature.[280-284] Using this technique,

449 Ketteler et al.[241] measured the amounts of adsorbed water and surface OH groups on TiO_2(110)
450 surface over a very large RH range, from $<1\times10^{-4}$ to almost 100%. In addition, they [241] found that
451 AP-XPS can also differentiate the oxygen species (lattice O, OH, and H_2O) on the surface by their
452 difference in O1s binding energies, providing very useful information on mechanisms of water
453 adsorption on the mineral surface. In another study,[242] the coverages of surface-adsorbed water
454 and OH groups on single crystal α-Fe_2O_3(0001) surface were measured as a function of RH, as
455 shown in Figure 6. Though AP-XPS has shown large potential to quantify the amount of adsorbed
456 water and to explore the adsorption mechanisms on a molecular and/or atomic level, to our
457 knowledge AP-XPS has not been used to investigate the interaction of water vapor with clay
458 mineral or authentic dust particles.

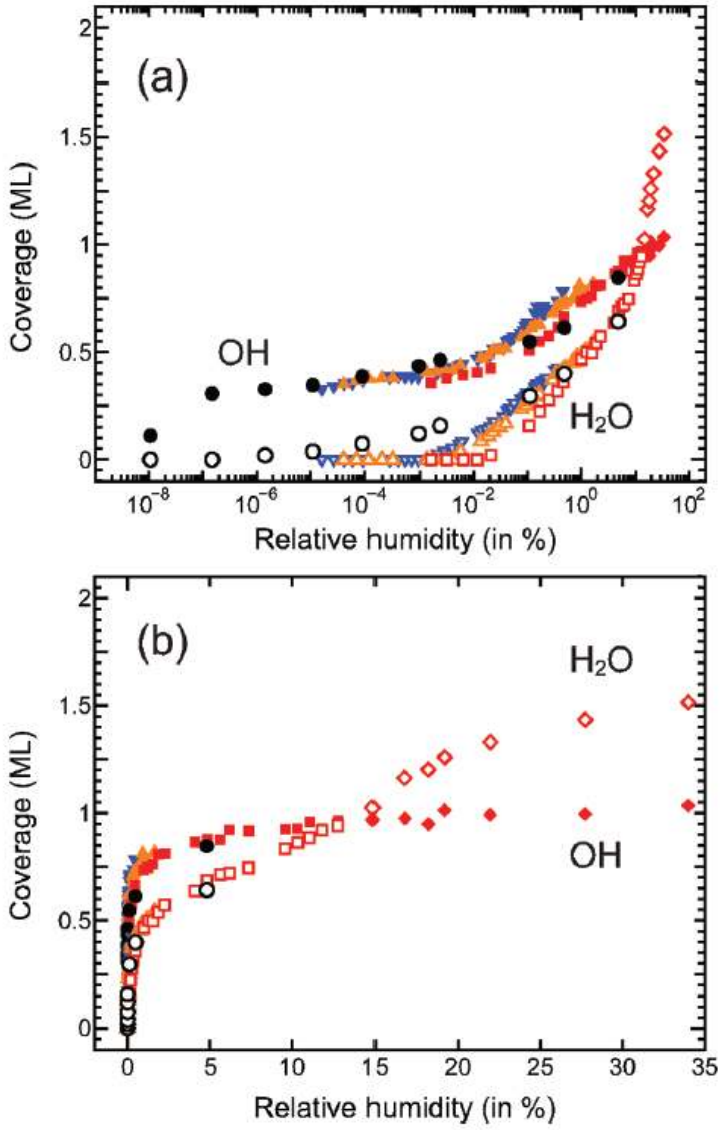

Figure 6. Coverages of surface OH groups (filled symbols) and molecularly adsorbed H_2O (open symbols) on α-Fe_2O_3(0001) surface as a function of RH. RH is plotted on a logarithmic scale in (a) and a linear scale in (b). Measurements were carried out at different experimental conditions: black circles, varying *P*(water) with a constant temperature of 295 K; blue triangles, varying temperature with a constant *P*(water) of 0.02 Torr; orange triangles, varying temperature with a constant *P*(water) of 0.1 Torr; red squares, varying temperature with a constant *P*(water) of 1 Torr; red diamonds, *P*(water) in the range of 1.0-2.0 Torr and temperature in the range of 277-280 K. Reprinted with permission from ref 242. Copyright 2010 American Chemical Society.

Surface vibrational spectroscopy, such as sum frequency generation (SFG), is a nonlinear and interface-specific technique to investigate the structure and dynamics of the interface.[285-287] SFG has been widely used to study the liquid water-air interface under environmental conditions, and have contributed to the elucidation of environmental interfacial processes at the molecular level.[234,288] Several studies also utilized SFG to investigate water adsorption on minerals, including Al_2O_3 and SiO_2. For example, Ma et al.[289] suggested that at 35% RH, α-Al_2O_3(0001) surface can be described as a H-bonding network formed by molecularly adsorbed water and surface hydroxyl groups H-bonded to the adsorbed water. A further study by Liu et al.[290] found that for SiO_2 at 54% RH, isolated silanol OH groups were in fact the major surface species and molecularly adsorbed water only covered a limited fraction of the surface. SFG can provide invaluable insights into the mechanisms of water adsorption on mineral dust particles, though absolute quantification of the adsorbed water is non-trivial.

Many surface spectroscopic methods, such as FTIR, Raman, and SFG, as discussed above, typically provide the average information of the surface under investigation. Atomic force microscopy is a technique which can provide spatial resolution down to sub-nanometres under atmospheric relevant conditions.[291-294] If complemented with spectroscopic measurements, it could help elucidate the mechanisms of water adsorption on mineral dust surface.[229]

Knudsen cell reactors are widely utilized to study the heterogeneous reactions of mineral dust particles with atmospheric reactive trace gases.[151,184,295-297] They have also been used to investigate the interaction of water vapor with mineral dust.[298,299] Because a Knudsen cell reactor is typically operated in the molecular flow regime (with a total pressure of less than 1 mTorr), the partial pressure of water vapor (and thus the RH) used in these experiments is very low. Therefore, these studies are less relevant for atmospheric chemistry and climate, though they can provide valuable

494 insights into the mechanisms of water adsorption on mineral dust. Molecular beam scattering
495 techniques have been used to explore how gas molecules interact with surfaces of atmospheric
496 chemistry interest,[236,300-305] and if applied to study mineral dust surface, can potentially help us
497 understand the fundamental dynamics and kinetics of water adsorption.

498 **2.3 Levitated single particle measurements**

499 Levitation of single particles avoids potential effects due to interaction of different particles and
500 those due to contact with the substrate used to support particles. A few particle levitation
501 techniques, such as the electrodynamic balance (EDB) and optical levitation, have been widely
502 used to study the hygroscopicity of aerosol particles.[306] Acoustic levitation is limited to particles
503 with sizes of larger than 20 μm, which are less relevant for atmospheric aerosols; therefore, this
504 technique is not further described here.[306] In an EDB a combination of AC and DC electric fields
505 is used to trap and levitate a charged particle,[307] with typical sizes of 5 to 50 μm.[306] The mass of
506 the particle is proportional to the balancing DC voltage, and the relative change of the particle
507 mass at different RH, usually compared to that at 0% RH, is determined from the change of the
508 DC voltage used to balance the gravitational force.[251,307] Though this technique seems to be a
509 suitable technique to study the hygroscopic growth of mineral dust particles, to our knowledge it
510 has not been applied to mineral dust particles yet.

511

512 Optical levitation methods, e.g., optical tweezers, can routinely trap and levitate aqueous (and thus
513 spherical) particles of 1-10 μm,[252,306,308-310] limiting their applications to mineral dust particles.
514 However, recent advances show that spherical and quasi-spherical solid particles can also be
515 trapped for many hours.[139,252,311] The size of a particle which is optically levitated can be estimated
516 from the measured intensity of scattered light as a function of scattering angle, i.e. the phase
517 function. Very accurate size measurements have been achieved by using optical tweezers. For
518 example, a precision of better than 1 nm for measuring the diameter of micrometer sized droplets

519 has been reported, with simultaneous measurements of complex refractive indexes.[312,313] However,
520 most of the sizing techniques based on light scattering are strictly applicable to spherical particles
521 and thus may not be suitable for mineral dust particles which are typically non-spherical.
522
523 An advantage of these levitation techniques is that, in addition to online measurements of particle
524 mass/size, several non-intrusive techniques, such as Raman spectroscopy [139,314] and fluorescence
525 spectroscopy,[315] can be used to measure the particle composition change simultaneously.
526 Therefore, these techniques have a large potential to investigate the change of both chemical
527 composition and hygroscopicity of single mineral dust particles due to heterogeneous reactions as
528 a function of time.

529 ## 2.4 Aerosol measurements

530 ### 2.4.1 Hygroscopic tandem differential mobility analyzer measurements

531 Hygroscopicity-tandem differential mobility analyzers (H-TMDA) have been widely used to
532 investigate the hygroscopicity of aerosol particles. Comprehensive discussions of this technique
533 have been provided elsewhere,[316-319] and only a brief description is given here. In a typical H-
534 TDMA set-up, a dry aerosol flow is passed through a bipolar charger and then into the first
535 differential mobility analyzer (DMA) which is used to produce a quasi-momodisperse aerosol flow
536 based on mobility diameters. These size-selected particles are then humidified to a certain RH and
537 then enter the second DMA coupled to a condensation nuclei counter (CPC) to measure the size
538 distribution of the humidified aerosol particles. The change in aerosol particle diameters before
539 and after humidification can be used to derive the hygroscopic growth factors.
540
541 H-TDMA has been widely used to measure the hygroscopicity of mineral dust aerosol
542 particles.[49,247,260,320] However, there are a few issues related to its application to mineral dust
543 particles: 1) dust particles are non-spherical in general, and thus it is non-trivial to interpret the

H-TDMA measurements; 2) the hygroscopicity of dust particles is relatively low, and the mobility diameter change before and after humidification may not be significant; and 3) restructuring of clay minerals may occur during humidification/dehumidification. Very recently Ardon-Dryer et al.[321] used several different techniques to measure the size distribution of size-selected mineral dust aerosol particles using a DMA, and concluded that mobility size selection using a DMA usually does not yield mineral dust particles with desired physical sizes. Similar findings were also reported by Veghte and Freedman.[322]

2.4.2 Optical properties

Water adsorption by mineral dust aerosol particles may lead to change in their size (and probably also refractive indices), thus modifying the optical properties. The change in optical properties of aerosol particles, in principle, can then be used to derive their hygroscopicity.[323] A variety of in-situ instruments are readily available to measure aerosol optical extinction,[324,325] scattering,[254,326-328] and absorption.[255,329] For example, light extinction properties at 532 nm were measured at different RH using a Cavity Ring-Down spectroscopy, to investigate the hygroscopicity of several clay and clay/salt aerosol particles.[253] However, it is non-trivial to convert change in optical diameter at different RH to hygroscopicity for mineral dust aerosol particles, again due to the non-sphericity of dust particles.

2.4.3 Cloud condensation nuclei activity

Under super-saturation (i.e. RH larger than 100%) aerosol particles can be activated to cloud droplets, and the number concentration of activated particles at a given super-saturation can be measured by using cloud condensation nuclei counters (CCNc). If such an instrument is coupled to a CPC in parallel, the activation fraction, defined as the ratio of the concentration of activated particles to the total particle number concentration, can then be determined. The most widely used cloud condensation nuclei counters are commercialized by Droplet Measurement Technologies (Boulder, CO, USA), based on the original design by Roberts and Nenes.[330]

Details on the principle, operation, and calibration of this instrument are provided elsewhere.[330-333] A typical schematic diagram of the experimental set-up used by Kumar et al.[262] to measure the CCN activity of aerosol particles is shown in Figure 7. A dry aerosol flow is delivered through an aerosol neutralizer and then into a DMA to produce a quasi-monodisperse aerosol particles. After that, the aerosol flow is split: one flow is delivered into a CPC to measure the total particle number concentration, and the other flow is delivered into a CCNc to measure the concentration of particles activated to cloud droplets under a given super-saturation ratio (SS).

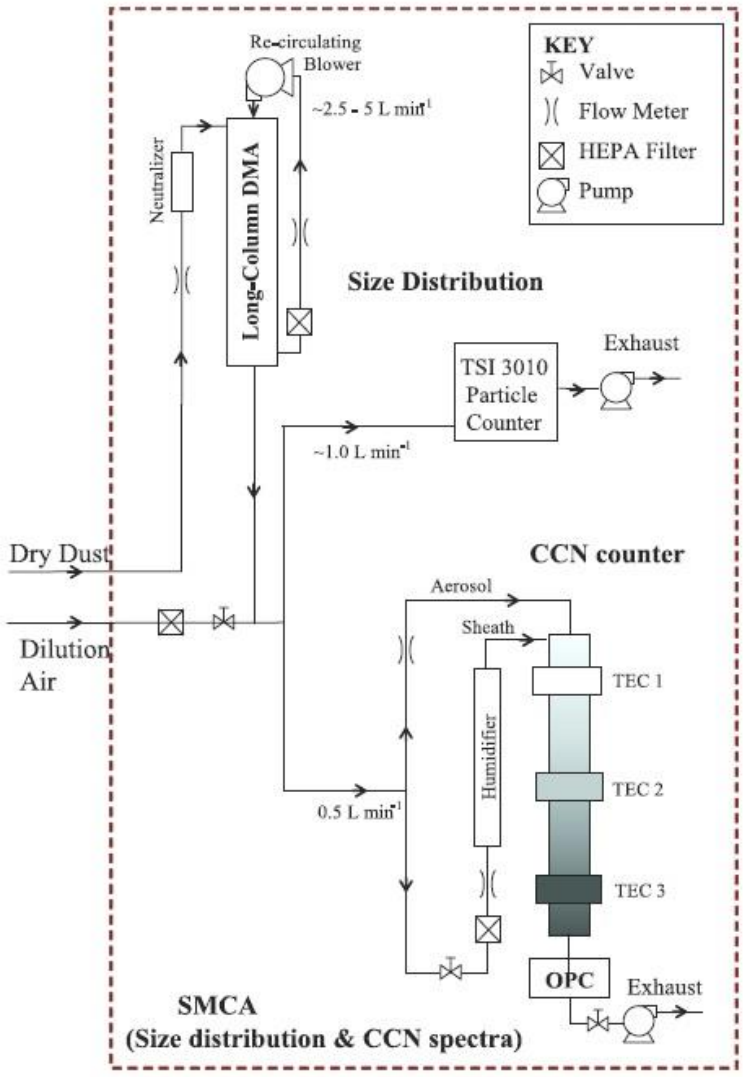

579 **Figure 7.** A schematic diagram of an experimental set-up used to determine the CCN activity of (mineral
580 dust) aerosol particles. Reprinted with permission from ref 262. Copyright 2011 Copernicus Publications.
581
582 There are usually two modes to operate a CCN counter: i) measuring the activation fraction as a
583 function of super-saturation ratio for a given dry particle diameter to determine the critical super-
584 saturation under which 50% of the aerosol particles are activated; ii) measuring the activation
585 fraction as a function of the dry particle diameter under a given super-saturation to determine the
586 critical dry diameter at which 50% of the aerosol particle are activated. This information can then
587 be used to derive the cloud condensation nucleation activity of aerosol particles. This technique
588 has been widely used to measure the cloud condensation nucleation activities of fresh and aged
589 mineral dust particles,[46,49,256,257,259,262] significantly improving our understanding of the role of dust
590 particles in the formation of clouds in the troposphere. Different theories used to describe the CCN
591 activity, and the relation between hygroscopic growth under sub-saturation conditions and CCN
592 activity under super-saturation conditions, are further discussed in more detail in Section 3.

593 **2.5 Discussion**

594 As summarized in this section, a wide range of techniques, based on different measurement
595 principles, have been developed to study water adsorption, hygroscopicity, and CCN activity of
596 mineral dust particles. Experimental techniques used to investigate the hygroscopic growth of
597 mineral dust aerosol particles are based on measurements of changes in diameter at different RH.
598 For examples, H-TDMA measures the change in mobility diameter and AE-CRD measures the
599 change in optical extinction properties which can then be related to particle size using Mie theory
600 which assumes particles are spherical. Since mineral dust particles are typically non-spherical, it
601 is non-trivial to quantify the absolute amount of water associated with aerosol particles at a given
602 RH, though they can provide other important information, such as the dependence of particle
603 mobility and optical properties on RH. Aerosol particle mass analyzers (usually referred to as APM

or PMA) have been widely used to classify aerosol particles based on their mass.[334-338] In principle, two APM and one CPC can be combined to measure changes in the aerosol particle mass as a function as RH, in a similar way as a H-TDMA system is constructed. In brief, dry dust aerosol particles with the same mass is selected by the first APM; after that, the aerosol flow will be humidified to a given RH, and the mass distribution of the humidified dust aerosol particles will be measured by the second APM coupled to a CPC. This instrument has promising potential to quantitatively determine the mass change of mineral dust particles as a function of RH.

Diameter changes of single particles trapped by optical levitation techniques at different RH are usually determined by light scattering. The non-sphericity of mineral dust particles can render the data interpretation difficult. Relative mass changes of single particles levitated in an EDB can be directly measured, regardless of the particle shape. EDB has been used to determine the amount of water adsorbed by pollen particles which are also non-spherical,[339] and therefore can also be used to study water adsorption by mineral dust particles. Nevertheless, it is still unclear if the EDB is sensitive enough to detect small mass changes of dust particle due to water adsorption.

FTIR based techniques have been widely used to monitor adsorbed water by mineral dust particles supported on substrates.[250,268,269] Although in principle adsorbed water can be quantified by its IR absorption bands, this types of analysis typically requires several assumptions which may introduce uncertainties in quantification.[249] In this aspect, techniques which can directly quantify changes in dust particle mass [247,249,271] or water vapor pressure,[212,248] due to the interaction of water vapor with mineral dust, show their advantages. For techniques which use particles supported on substrates, particles are usually not size-selected and therefore it is difficult to investigate the size dependence of the amount of water associated with particles (for the same mass of dry materials, surface adsorption theories indicate that the amount of adsorbed water increases with decreasing

particle diameter while the hygroscopic growth theory implies that it is size-independent, as discussed in detail in Section 3). Many surface science techniques, though they may not quantitatively measure adosrbed water, can nevertheless provide valuable information about chemical composition, morphology, and adsorption mechanisms on the fundamental level, with some examples given in Section 2.2.3.

For CCN activity measurements, it is critical to accurately determine the dry particle diameters. Typically a DMA is used to classify aerosol particles based on their mobility. The mobility diameter is not necessarily equivalent to the geometrical diameter for dust particles, due to their non-sphericity. This has also been supported by experimental work,[321,322] showing that mobility size selection using a DMA usually does not generate mineral dust particles with desired physical sizes. Additionally, after passing through the aerosol neutralizer, dry-generated dust aerosol particles may consist of a substantial fraction of multiply charged particls which in fact have larger diameters and can be activated to cloud droplets at lower supersaturation, compared to single charged particles. Both factors can lead to biases in the reported CCN activity,[259] and therefore charge and shape corrections should be applied in determining the CCN activity of mineral dust particles.

3 Introduction of different theories

Several different theories have been developed to describe the partitioning of water between the gas phase and mineral dust particles under both sub- and super-saturation conditions with respect to liquid water. Most widely used theories are introduced in this section. These theories can be generally classified to two groups, with one originating from surface science and surface chemistry and the other one developed for atmospheric aerosol science.

3.1 Theories and models used to describe sub-saturation conditions

Several different models are available to describe the amount of the absorbate adsorbed at different partial pressures.[340-342] In this review, water is the adsorbate and it partial pressure is expressed as RH instead, and mineral dust particles (or their surfaces) are the adsorbents. Among adsorption models, the Langmuir adsorption isotherm model [341-343] is the first and probably the most widely used adsorption theory, but its application is limited to adsorption below one monolayer. Therefore, it is not suitable to describe water adsorption on mineral dust particles at high RH and thus no further discussion on the Langmuir adsorption isotherm is provided here.

3.1.1 Brunauer-Emmet-Teller adsorption isotherm model

The Brunauer-Emmett-Teller (BET) adsorption isotherm [341,342,344] can be used to describe water adsorption for mineral dust particles:[250]

$$\theta = \frac{c \cdot RH}{(1-RH)(1-RH+c \cdot RH)} \qquad (3),$$

where θ is the surface coverage of adsorbed water, and c is a constant related to the enthalpy of desorption, $\Delta_{des}H^o$ (kJ K^{-1}):

$$c = \exp[(\Delta_{des}H^o - \Delta_{vap}H^o)/RT] \qquad (4),$$

where R is the gas constant (8.314 J mol^{-1} K^{-1}), T is the temperature (K), and $\Delta_{vap}H^o$ is the standard enthalpy of water evaporation (kJ K^{-1}). For the adsorption of water on mineral dust, c is usually found to be >1, suggesting that $\Delta_{des}H^o$ is larger than $\Delta_{vap}H^o$.[250]

It has been found that in many cases that the BET equation, Eq. (3), may overestimate the surface coverage of adsorbed water (θ) at high RH. Therefore, by introducing the third parameter, n, a modified three-parameter BET equation has been proposed to describe the water adsorption on mineral particles:[345]

$$\theta = \frac{c \cdot RH}{(1-RH)} \cdot \frac{1-(n+1) \cdot RH^n + n \cdot RH^{n+1}}{1+(c-1) \cdot RH - c \cdot RH^{n+1}} \qquad (5).$$

Goodman et al.[250] found that the three-parameter BET equation could fit fairly well the water adsorption on several different mineral dust particles for RH ranging from ~0% to >90%. They [250] also described in details how to derive c and n from experimentally measured θ as a function of RH, using Eq. (5). Ma et al.[269] also suggsted that the three-parameter BET equations can fit well water adsorption on five different oxides which they investigated, as shown in Figure 8.

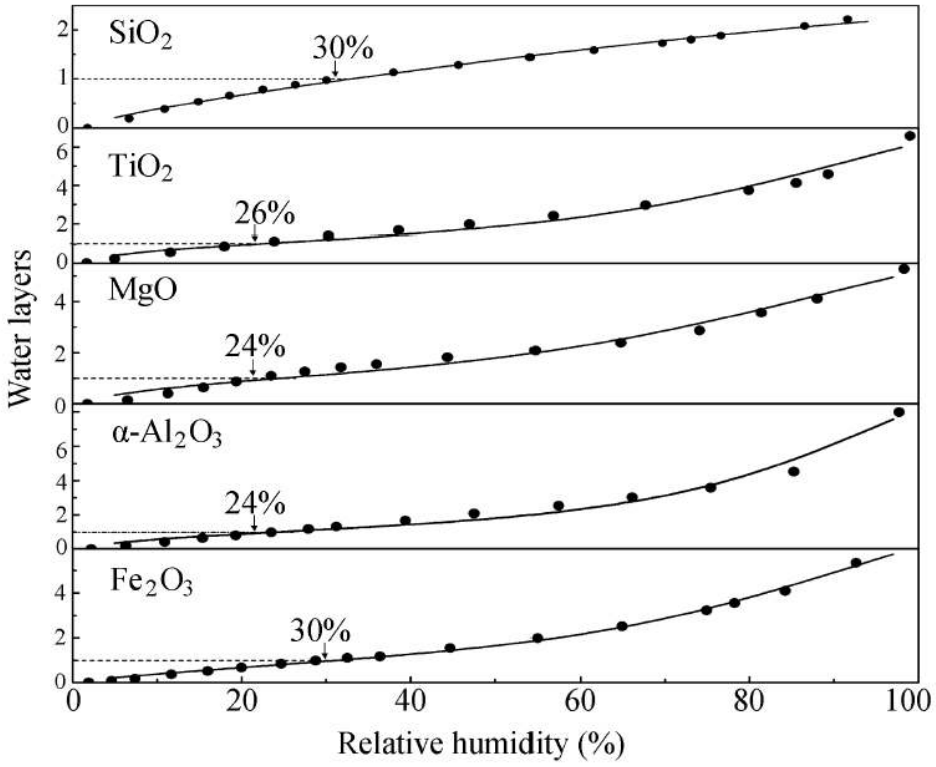

Figure 8. Water adsorption on SiO_2, TiO_2, MgO, α-Al_2O_3, and Fe_2O_3 as a function of RH at 30 °C. Cirlces represent experimental data and curves represent corresponding fitted three-parameter BET isotherms. Relative humidities under which a monolayer of adsorbed water is formed are given in the figure for each minerals. Reprinted with permission from ref 269. Copyright 2011 Elsevier.

3.1.2 Freundlich adsorption isotherm model

The Freundlich adsorption isotherm expresses the mass ratio of the adsorbed water to the dry mineral dust particles as a function of partial pressure or RH:[346,347]

$$\frac{m(water)}{m(mineral)} = A_F \cdot \sqrt[B_F]{RH} \qquad (6),$$

where m(water) and m(mineral) are the mass of adsorbed water and dry mineral dust particles, and A_F and B_F are the empirical Freundlich constants which represent the adsorption capacity and strength, respectively.[268] Eq. (6) can be rearranged to

$$\ln\frac{m(water)}{m(mineral)} = lnA_F + \frac{\ln(RH)}{B_F} \qquad (7),$$

Therefore, simple linear regression of the natural logarithm of the mass ratio (of adsorbed water to dry dust particles) versus the natural logarithm of RH can be used to derive A_F and B_F.

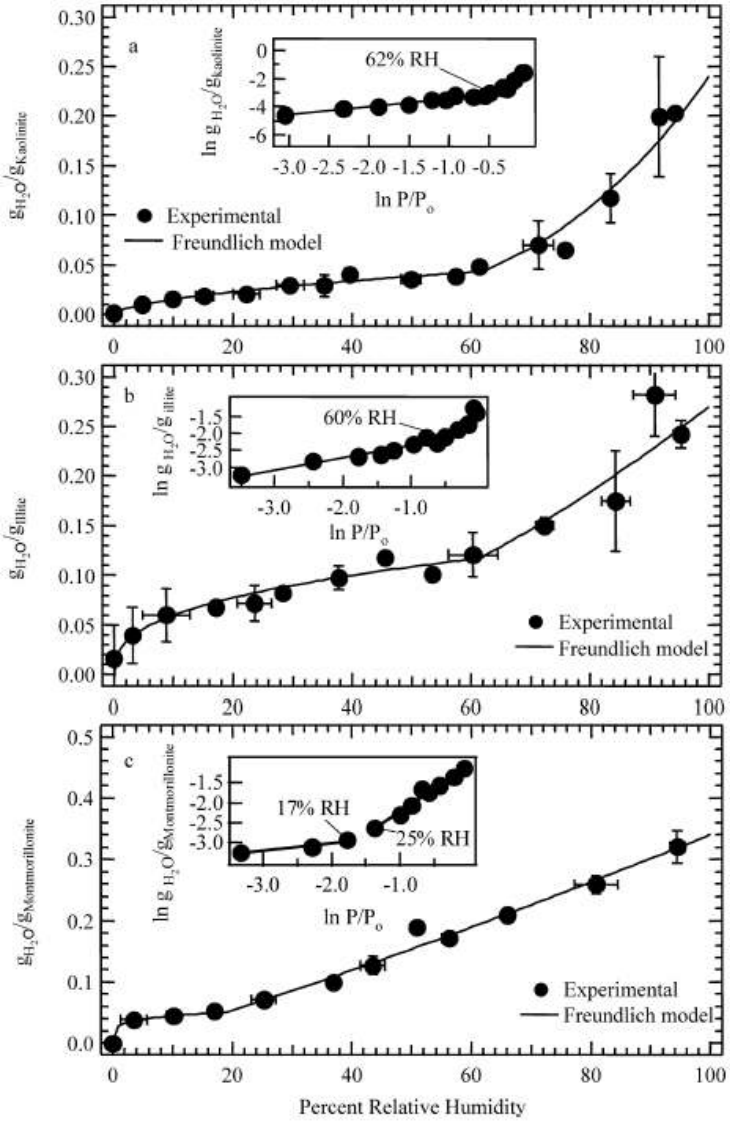

Figure 9. Measured and modeled water adsorption (represented by the mass ratio of adsorbed water to dry mineral) at 298 K as a function of RH on (a) kaolinite, (b) illite, and (c) montmorillonite. The insets

represent the data fitted to the linear form of the Freundlich adsorption isotherm, i.e. Eq. (7). Reprinted with permission from ref 268. Copyright 2011 American Chemical Society.

Hatch et al.[268] measured water adsorption on illite, kaolinite, and montmorillorite particles, and fitted these experimenrtal results using the Freundlich adsorption isotherm, as shown in Figure 9. It was suggested that compared to the two-parameter BET adsorption isotherm, the Freundlich adsorption isotherm can better describe water adsorption by these three clay minerals they investigated.[268]

3.1.3 Frenkel-Halsey-Hill adsorption isotherm model

The Frenkel-Halsey-Hill (FHH) isotherm uses a two-parameter equation to describe RH as a function of surface coverage of adsorbed water, θ:

$$RH = \exp(-A_{FHH} \cdot \theta^{-B_{FHH}}) \quad (8),$$

where A_{FHH} and B_{FHH} are empirical parameters.[341,348] A_{FHH} describes interactions between the surface and first adsorbed water layer and interactions between adjacent adsorbed water molecules. Therefore, it governs the overall extent of water coverage, and higher A_{FHH} values suggest that more water may be adsorbed. B_{FHH} describes interactions between the surface and subsequent adsorbed water layers. Smaller B_{FHH} values mean that attractive forces function over a longer distance from the particle surface. As a result, B_{FHH} significantly influences the shape of the adsorption isotherm, especially at high RH. Consequently, CCN activation described by the FHH activation theory is predominantly determined by the magnitude of B_{FHH},[47,52] and this will be further discussed in Section 3.2.2.

Eq. (8) can be rearranged to

$$\ln[-\ln(RH)] = lnA_{FHH} - B_{FHH} \cdot \ln(\theta) \quad (9).$$

As shown in Eq. (9), A_{FHH} and B_{FHH} can be derived from linear regression of ln[-ln(RH)] versus ln(θ). We can also describe the surface coverage of adsorbed water as a function of RH by rearranging Eq. (9):

$$\theta = \sqrt[B_{FHH}]{\frac{A_{FHH}}{-\ln(RH)}} \qquad (10).$$

3.1.4 Hygroscopic growth theory

The change of the diameter of a particle at elevated RH due to adsorption of water, called hygroscopic growth in aerosol science, can be described by the single hygroscopicity parameter, κ:[169]

$$RH = \frac{GF^3-1}{GF^3-(1-\kappa)} \exp\left(\frac{A_{Kelvin}}{D_{d\cdot GF}}\right) \qquad (11),$$

$$A_{Kelvin} = \frac{4\sigma M_w}{RT\rho_w} \qquad (12),$$

where GF is the growth factor, defined as the ratio of the diameter of a particle at a given RH to that of the dry particle (D_d).[169] The second term in the right part of Eq. (11), $\exp(A_{Kelvin}/D_d{\cdot}GF)$, is due to the Kelvin effect, referring to the increase of vapor pressure on a curved surface of the particle, relative to that for a flat surface. A_{Kelvin} is a constant which describes the Kelvin effect, depending on the surface tension (σ), density (ρ_w) and molar mass (M_w) of water, and temperature. A_{Kelvin} is equal to 2.1×10^{-9} m for a surface tension of 0.072 J m^{-2} (pure water) and temperature of 298.15 K.[217]

The Kelvin effect becomes negligible for large particles, and in this case Eq. (11) can be simplified to

$$RH = \frac{GF^3-1}{GF^3-(1-\kappa)} \qquad (13).$$

Eq. (13) can then be rearranged to express GF as a function of RH:

$$GF = \sqrt[3]{1+\kappa\cdot\frac{RH}{1-RH}} \qquad (14).$$

Calculations show that the difference between calculated GF at 90% using Eq. (11) (i.e. taking into account the Kelvin effect) and that using Eq. (14) (i.e. neglecting the Kelvin effect) is negligible for particles with dry diameters larger than 100 nm. As a result, in this review for simplicity, Eq. (14) is used to calculate hygroscopic growth factors and thus also amounts of adsorbed water at different RH for mineral dust particles.

The surface coverage, θ, can be expressed as the change of particle diameters:[47,349]

$$\theta = \frac{D-D_d}{2D_w} = \frac{GF-1}{2} \cdot \frac{D_d}{D_w} \qquad (15).$$

where D_d and D are the diameters of the dry particle and the wet particle. D_w is the average diameter of a water molecule adsorbed on the particle surface. D_w is sometimes assumed to be 0.275 nm,[47,349] meaning that a water molecule adsorbed on mineral dust surface occupies an area of 5.9×10^{-16} cm^2. Al-Abadleh et al.[211] assumes that the hydroxylated $CaCO_3$ surface can accommodate 1×10^{15} water molecules per cm^2, i.e. a water molecule adsorbed on the surface occupies an area of 1×10^{-15} cm^2 (or 0.1 nm^2), corresponding to D_w of 0.36 nm. In this paper, the diameter of one water molecule adsorbed on a mineral dust particle is always assumed to be 0.36 nm.

3.1.5 Discussion

There is a fundamental difference between adsorption theories originating from surface science and hygroscopicity theories used to describe the interaction of water vapor with mineral particles under sub-saturation conditions. All adsorption theories assume that at given RH and T, the amount of water adsorbed by mineral particles is proportional to the total surface area; therefore, for the same amount (mass or volume) of dry material, the amount of water adsorbed by mineral particles increase with decreasing average particle diameter. On the other hand, hygroscopicity theories assume that the amount of water is proportional to the volume of solute, and thus for the same amount of dry material, the amount of water associated with mineral dust is independent of particle

diameter, if the Kelvin effect is negligible. This difference can make direct comparison of some experimental measurements difficult, and this issue will be discussed further in Section 3.3.

3.2 Theories and models used to describe super-saturation conditions

3.2.1 κ-Köhler activation theory

The saturation ratio of water vapor, S, in equilibrium with an aqueous droplet, can be describe by the Köhler theory,[350] which takes into account the effects of both water activity and surface curvature:

$$S = a_w \cdot \exp(\frac{A_\kappa}{D}) \qquad (16),$$

where a_w is the water activity, and D is the droplet diameter, and A_{Kelvin} is defined in Eq. (12). In fact the definition of S is the same as RH, as shown in Eq. (1). However, to keep consistent with conventional terminology, S is used for super-saturation conditions and RH is used for sub-saturation conditions. The single hygroscopicity parameter, κ, links water activity (a_w), the volume of the dry particle (V_s), and the volume of water (V_w):[169,351]

$$\frac{1}{a_w} = 1 + \kappa \frac{V_s}{V_w} \qquad (17),$$

As shown by Petters and Kreidenweis (2007),[169] inserting Eq. (17) into Eq. (16) and converting volumes to corresponding diameters can yield the "κ-Köhler theory" equation:

$$S(D) = \frac{D^3 - D_d^3}{D^3 - (1-\kappa)\cdot D_d^3} \cdot \exp(\frac{A_\kappa}{D}) \qquad (18).$$

The critical saturation for a dry particle, S_c, is defined as the saturation above which the particle is activated to a cloud droplet. The critical super-saturation, s_c, which is equal to S_c-1, is more widely used in describing cloud condensation nucleation. For a particle with given dry diameter and hygroscopicity, S_c (and thus s_c) can be calculated from the maximum of the κ-Köhler curve, i.e. Eq. (18). Three κ-Köhler curves, for particles with a dry diameter of 50 nm and different hygroscopicity, are plotted in Figure 10 as examples. The maxima of s, i.e., s_c, are 0.47%, 1.03%,

and 2.46% for 50 nm particles with κ values of 0.5, 0.1, and 0.01, respectively. If the supersaturation ratio in the ambient air is larger than the s_c for a given particle, this particle will be activated to a cloud droplet.

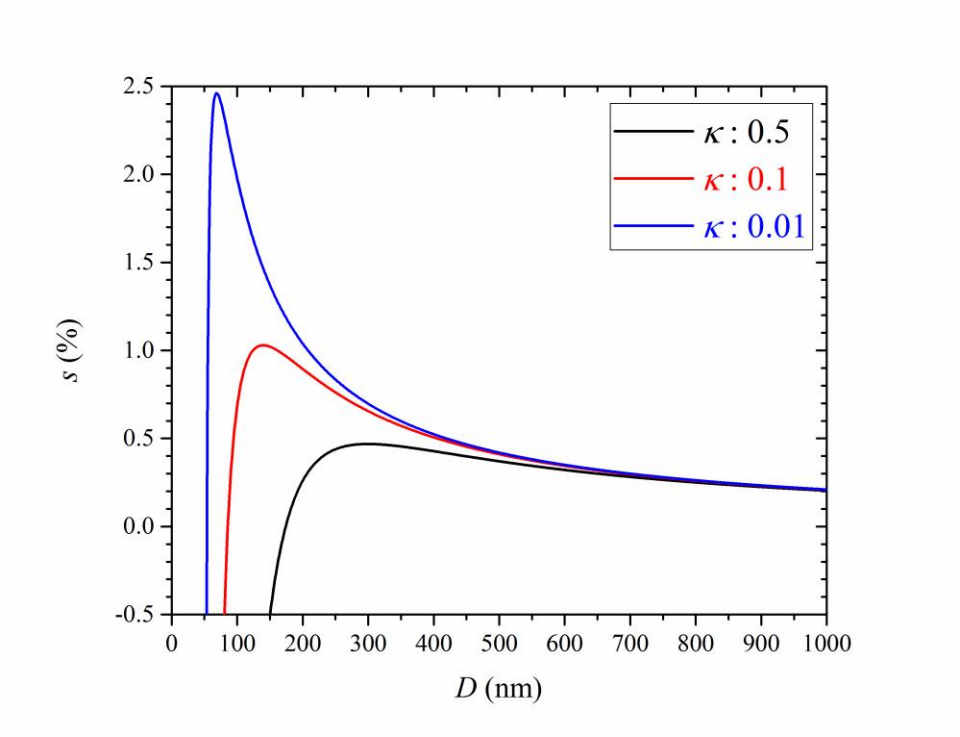

Figure 10. Calculated super-saturations as a function of the diameter of aqueous particles with a dry diameter of 50 nm and different hygroscopicity (κ is equal to 0.5, 0.1, and 0.01, respectively), using Eq. (18). Note that super-saturation (s) instead of saturation (S), is plotted.

The same procedure can be applied to a wide range of D_d and κ to calculate corresponding s_c, and a look-up table for s_c as a function of D_d and κ can then be produced. The critical super-saturation, s_c, for momodisperse aerosol particles with a dry diameter of D_d, or alternatively the critical diameter of polydisperse aerosol particles for a gievn super-saturation, can be measured using the procedure described in Section 2.3.3. Corresponding κ values can then be derived from s_c and D_d, using the look-up table.

3.2.2 Frenkel-Halsey-Hill adsorption activation theory

The FHH adsorption activation theory [349] describes the activity of adsorbed water on the surface of insoluble particles:

$$a_w = \exp[-A_{FHH} \cdot \theta^{-B_{FHH}}] \quad (19),$$

where θ is the surface coverage of water, and A_{FHH} and B_{FHH} are empirical parameters which are described in Eq. (8). Inserting Eq. (19) into Eq. (16) gives

$$S = \exp[-A_{FHH} \cdot \theta^{-B_{FHH}}] \cdot \exp(\frac{A_\kappa}{D_d}) \quad (20).$$

A_{FHH} and B_{FHH} can be derived from to the fit to the s_c-D_d data, as detailed by Kumar et al.[52]

A_{FFH} and B_{FHH} vary with different compounds. Typically, A_{FHH} ranges from 0.1 to 3.0, and B_{FHH} ranges from 0.5 to 3.0.[349] If the dry diameter, A_{FHH} and B_{FHH} are known for a particle, the critical super-saturation can be calculated from the maximum of its FHH adsorption activation curve. Three FHH curves for B_{FHH} values of 0.7, 0.8, and 0.9 (all with an A_{FHH} value of 0.3) are shown in Figure 11, and have s_c values of ~0.26%, ~0.62%, and ~0.89%, respectively. If the supersaturation ratio in the ambient air is larger than the s_c for a given particle, this particle will be activated to a cloud droplet.

If B_{FHH} is small enough, the activation curve may never reach a maximum but instead asymptotes to a negative value, $-s_\infty$. Two FHH curves with B_{FHH} values of 0.5 and 0.6 (and A_{FHH} is 0.3 for both cases), are shown in Figure 11 for illustration. The asymptotic value of s at very large D_p determines if this particle will be activated:[47] if it is smaller than 0, the particle can be spontaneously activated at RH less than 100%; otherwise, the particle will never be activated (i.e. always in stable equilibrium with the environment). However, such observations have not been reported yet, shedding doubt on its atmospheric relevance.

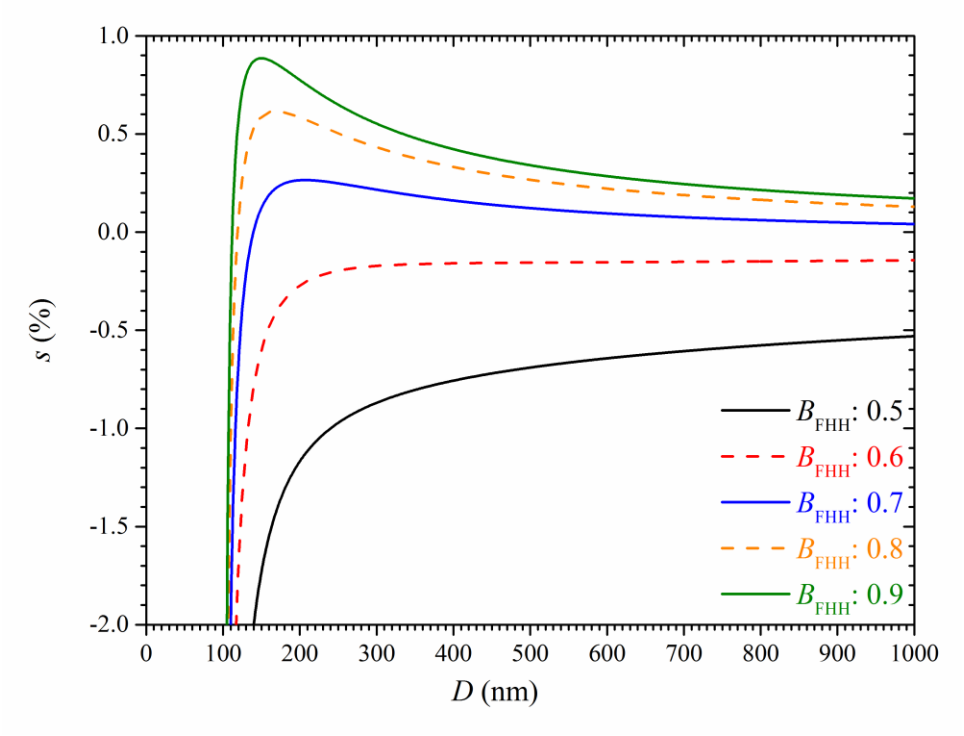

832

833 **Figure 11.** Calculated super-saturations as a function of the diameter of a wet particle, here for a dry
834 diameter of 100 nm, using Eq. (20). A_{FHH} is assumed to be 0.3, and B_{FHH} are assumed to be 0.5, 0.6, 0.7,
835 0.8, and 0.9, respectively. Note that super-saturation (s) instead of saturation (S), is plotted.

836

837 The two empirical FHH parameters, A_{FHH} and B_{FHH}, can be determined by measuring the surface
838 coverage (θ) of adsorbed water as a function of RH under sub-saturation conditions, as discussed
839 in Section 3.1.3. Alternatively, they can also be determined by measuring critical super-saturation
840 as a function of particle diameter under super-saturation conditions.[262,263]

841

842 Activity of adsorbed water can also be described by other water adsorption isotherms (e.g., the
843 BET adsorption isotherm), and corresponding adsorption activation theories, analogous to Eq. (20),
844 can be subsequently derived. For example, the BET adsorption activation theory has been
845 developed and applied to describe cloud activation of black carbon particles.[352] To our knowledge,
846 this theory has not been used to describe cloud activation of mineral dust particles, and therefore
847 it is not discussed further in this review.

848 **3.2.3 Discussion**

849 It has been shown that both κ-Köhler and FHH theories are superior to the original Köhler theory,
850 at the expense of increased complexity, since they can account for the hygroscopic content of
851 mineral dust.[47,52,217] Differences do exist between these two methods. As noted by Kumar et al,[47,52]
852 using FHH theory changes the maximum super-saturations and cloud droplet number with respect
853 to aerosol variations, compared to the κ-Köhler theory. This is because when compared to the κ-
854 Köhler theory, the FHH activation theory requires less water uptake to reach a critical diameter.
855 This is further illustrated by Figure 12, displaying the κ-Köhler and FHH activation curves for a
856 particles with a dry diameter of 100 nm. Both theories suggest that the particle will be activated at
857 a super-saturation of ~0.88%. However, the predicted wet particle diameters when super-saturation
858 is equal to sc are different, with 150 nm predicted by the FHH activation theory and 174 nm
859 predicted by the κ-Köhler theory. As a result, compared to the κ-Köhler theory, the FHH activation
860 theory requires less water uptake for the particle to be activated.
861
862 In addition, the two theories suggest different dependence of s_c on D_d, as shown in Figure 12. Both
863 theories suggest that a particle with a dry diameter of 100 nm has the same s_c. Compared to the κ-
864 Köhler theory, the FHH activation theory predicts that particles with D_d <100 nm will be activated
865 at smaller s_c while they have larger s_c for D_d >100 nm.

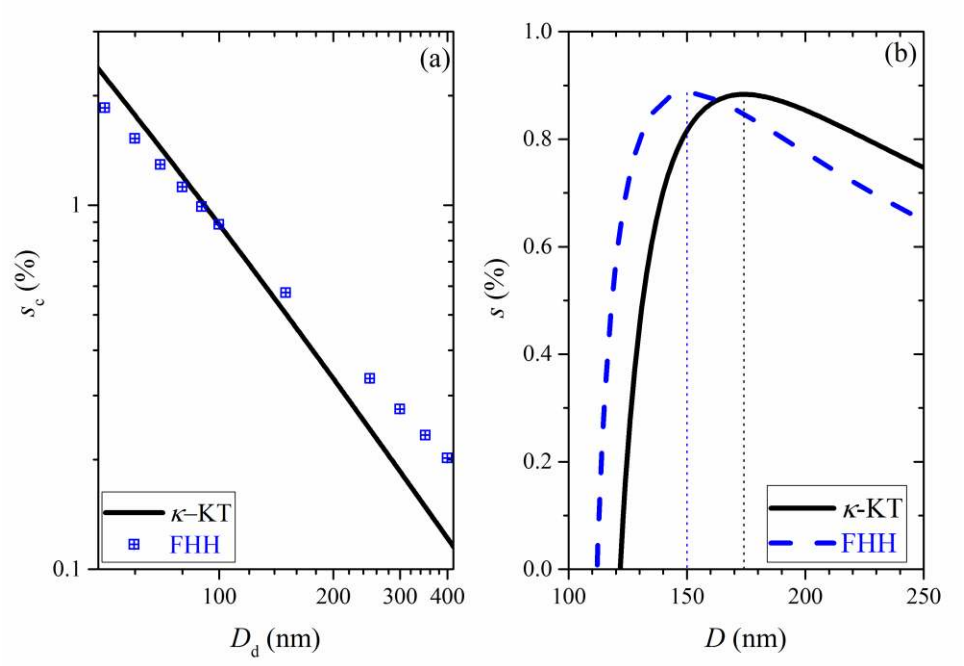

Figure 12. Comparison of κ-Köhler (κ = 0.014) and FHH (A_{FHH} = 0.3, B_{FHH} = 0.9) activation theories. Values of κ, A_{FHH}, and B_{FHH} are chosen in such a way that both theories predict that a particle with a dry diameter (D_d) of 100 nm will have a s_c of ~0.88%. (a) Predicted sc as a function of D_d by κ-Köhler (solid black curve) and FHH (blue squares) activation theories. (b) Calculated activation curves for a particle with a dry diameter of 100 nm by κ-Köhler (solid black curve) and FHH (dashed blue curve) activation theories.

A recent study suggests that the κ-Köhler activation theory provides a better fit to laboratory data with slightly less complexity of calculation.[259] Nevertheless, it still remains under debate which theory can better describe the activation of cloud droplets by mineral dust particles.

3.3 Suggested guidelines used for data comparison

The amounts of water adsorbed or condensed on mineral dust particles are reported in different ways. The following guidelines are used to compare available data for each type of mineral particles:

881 i) Under super-saturation conditions the single hygroscopic parameter, κ, is usually reported. Using
882 Eq. (14), reported κ values can be converted to the hygroscopic growth factors, which are directly
883 measured by H-TDMA under sub-saturation conditions.
884
885 ii) The change in particle diameters due to hygroscopic growth, calculated from measured κ values
886 or directly measured by H-TDMA, can be converted to the surface coverage (θ) of adsorbed water,
887 using Eq. (15). Usage of Eq. (15) requires the knowledge of dry particle diameter. In this review,
888 three different dry particle diameters, i.e. 500, 1000, and 2000 nm, are used when we convert
889 hygroscopic growth factors to surface coverages, θ, using Eq. (15). The dry particle diameter (D_d)
890 and the hygroscopic growth factor at a given RH can be used to calculate the wet particle diameter
891 (D) at this RH, and the number of monolayers (i.e. surface coverage) of adsorbed water is
892 approximately equal to $(D_d\text{-}D)/D_w$, where D_w is the average diameter of the adsorbed water
893 molecules. We choose these three diameters because they may reasonably represent the size range
894 of tropospheric dust particles after long range transport. According to Eq. (15), the calculated θ is
895 proportional to the dry particle diameter used in the calculation. Therefore, large uncertianties may
896 occur when converting hygroscopic growth factors to θ, making data comparison difficult. For
897 example, for the same hygroscopic growth factor, the calculated θ using a dry particle diameter of
898 1000 nm will be twice as large as that using a dry particle diameter of 500 nm. In some CCN
899 activity measurements the two FHH parameters (instead of κ values) are reported;[262,263] in this case,
900 the surface coverage of adsorbed water at different RH can be directly calculated using Eq. (10).
901
902 iii) If the mass ratio of adsorbed water to dry mineral particle is reported, the surface coverage (θ)
903 of adsorbed water can then be calculated by
904 $$\theta = \frac{m(water)}{m(mineral)} \cdot \frac{N_A \cdot A(water)}{M(water) \cdot A_{BET}} \qquad (21),$$

where m(water) and m(mineral) are the masses (g) of adsorbed water and dry mineral, M_m(water) is the molar mass of water (g mol^{-1}), N_A is the Avogadro constant (6.02×10^{23} mol^{-1}), A(water) is the average surface area of one adsorbed water molecule (1×10^{-15} cm^2), and A_{BET} is the BET area (cm^2 g^{-1}) of the mineral.

It should be emphasized that large uncertainties may occur when we convert reported data in other units to θ. The largest uncertainties may come from i) converting hygroscopic growth factors, either directly measured by using H-TDMA or calculated from κ values determined by CCN activity measurements, to surface coverages of adsorbed water, and ii) the nonsphericity (and probably also porosity) of mineral particles. In this review it is always assumed that the mass-, volume-, and surface area-equivalent diameters are equal to mobility diameters. However, this is a clear oversimplification and will inherently yield some uncertainty for mineral dust particles which are typically non-spherical.[353]

4 Water adsorption properties, hygroscopicity, and CCN activity of fresh and aged mineral dust particles

In this section, the interaction of water vapor with different components of mineral dust particles under both sub-saturation and super-saturation conditions are reviewed. Mineral dust particles covered in this section include calcium carbonate ($CaCO_3$, usually in the form of calcite), Arizona Test Dust, illite, kaolinite, montmorillonite, quartz, several metal oxides (TiO_2, Al_2O_3, and Fe_2O_3), and authentic desert dust samples. Laboratory studies on the effects of atmospheric aging through heterogeneous processes are also reviewed. We also discuss some theoretical studies on water adsorption on mineral dust surfaces. After that, we summarize some field measurements that have provided evidence that chemical transformation in the atmosphere could change the interaction of mineral dust particles with water vapor. A brief summary is then provided to conclude this section.

4.1 Calcium carbonate

With respect to the interaction with water vapor, calcium carbonate ($CaCO_3$), usually in the form of calcite, is the most widely investigated component of mineral dust particles. We first review the interactions of water vapor with fresh $CaCO_3$, and then discuss the effects of chemical aging on these interactions.

4.1.1 Fresh $CaCO_3$ particles

As shown in Table 4, the interaction of fresh $CaCO_3$ particles with water vapor has been investigated under both sub-saturation and super-saturation conditions by a number of studies.

Table 4. Water adsorption, hygroscopicity, and CCN activity of fresh $CaCO_3$ particles: summary of previous studies.

references	techniques	aerosol generation method
Al-Hosney et al., 2005 [354]	ATR-FTIR	not applicable
Gustafsson et al., 2005 [247]	DRIFTS, TGA, and H-TDMA	wet generation
Gibson et al., 2006 [355]	H-TDMA and CCNc	wet generation
Gibson et al., 2007 [257]	CCNc	wet generation
Schuttlefield, 2008 [356]	QCM	not applicable
Hatch et al., 2008 [216]	QCM and CCNc	wet generation
Sullivan et al., 2010 [256]	CCNc	wet and dry generation
Zhao et al., 2010 [264]	H-TDMA and CCNc	see text for details
Kumar et al., 2011 [262]	CCNc	dry generation
Kumar et al., 2011 [263]	CCNc	wet generation
Gierlus et al., 2012 [218]	CCNc	wet generation
Ma et al., 2012 [212]	PSA	not applicable
Tang et al., 2015 [357]	CCNc	dry generation

941 Al-Hosney et al.[354] investigated water adsorption on $CaCO_3$ particles at different RH, using ATR-
942 FTIR, and observed that the bending (ca. 1646 cm^{-1}) and stretching (3000-3700 cm^{-1}) modes of
943 adsorbed water both increase with RH. However, absolute amounts of adsorbed water was not
944 reported.[354] DRIFTS was used by Gustafsson et al.[247] to study the water adsorption on $CaCO_3$
945 particles (BET surface area: 17.8 m^2 g^{-1}), and they found that 1 and 4.5 monolayers of adsorbed
946 water is formed at ~55% and 80% RH, respectively. The same study [247] also measured the
947 hygroscopic growth of wet-generated $CaCO_3$ particles at different RH using a H-TDMA, and
948 suggested that the relative change of mobility diameters can be described by the following equation:
949 $\frac{D}{D_0} = (1 - RH)^{-0.073}$ (22).
950 It should be noted that $CaCO_3$ aerosol particles used by Gustafsson et al.[247] are polydisperse, with
951 a first mode at 40 nm and a second mode at 250 nm. Gibson et al.[355] also used a H-TDMA to
952 measure the hygroscopic growth of 100 nm wet-generated $CaCO_3$ particles, and found that the
953 hygroscopic growth factor can be described by an average value of 1.00±0.02 over the entire RH
954 range (0-85%), i.e. the hygroscopic growth of $CaCO_3$ particles is not significant within the
955 experimental uncertainties.
956
957 Ma et al.[212] measured the amount of water adsorbed on $CaCO_3$ (BET area: 0.6 m^2 g^{-1}) at 278 K
958 using a physisorption analyser. They [212] reported that there is one monolayer of adsorbed water
959 formed on the surface at 52% RH, increasing to ~2 layers at 90% RH and ~7 layers at 95% RH.
960 Hatch et al.[216] showed that the mass of adsorbed water on $CaCO_3$ particles (BET surface area: 10.1
961 m^2 g^{-1}) is equal to ~8% of the mass of dry $CaCO_3$ particles at 78% RH, corresponding to
962 approximately 3 monolayers of water. The amount of water adsorbed on $CaCO_3$ particles at
963 different RH was also measured by Schuttlefield et al.,[356] using a QCM.
964

965 Wet-generated $CaCO_3$ particles were reported to have κ values of ~0.043 by Gibson et al.,[355]
966 0.0110±0.0015 by Gibson et al.,[257] ~0.005 by Hatch et al.,[216] and 0.0070±0.0017 by Gierlus et
967 al.[218] from CCN activity measurements. The CCN activity of dry generated $CaCO_3$ particles was
968 studied by Sullivan et al.[217] and Tang et al.,[357] with reported κ values of 0.0008-0.0018 [217] and
969 0.001-0.003.[357] Zhao et al.[264] developed a novel method to produce dry $CaCO_3$ particles, by
970 transforming $Ca(HCO_3)_2$ aerosol particles to $CaCO_3$ particles via thermal decomposition in a tube
971 furnace. They reported a mobility diameter growth factor of 1.01 at 95% RH (corresponding to κ
972 values of 0.0016±0.004) using a H-TDMA and κ values of 0.0019±0.0007 using a CCNc.[264]
973 Kumar et al.[262] also investigated the CCN activity of dry-generated $CaCO_3$ aerosol particles, and
974 they suggested the activation of $CaCO_3$ particles can be better described by the FHH activation
975 theory, with A_{FHH} of 3.00±0.04 and B_{FHH} of 1.30±0.03.
976
977 As summarized above, the CCN activities of $CaCO_3$ aerosol particles were measured by several
978 previous studies. For dry generated $CaCO_3$ particles, different studies reported very similar CCN
979 activities, with measured κ values of ~0.002.[256,264,357] The CCN activity of wet generated $CaCO_3$
980 aerosol particles is significantly higher.[216,218,257,355] The difference in the measured CCN activities
981 of dry and wet generated $CaCO_3$ particles has been investigated,[256,262,263] and it has been concluded
982 that wet generation of $CaCO_3$ aerosol particles will lead to higher CCN activities.
983
984 Using the data comparison guideline discussed in Section 3.3, a κ value of 0.002 means that the
985 hygroscopic growth factors are 1.003, 1.006, and 1.013 at RH of 80%, 90%, and 95%. This shows
986 excellent agreement with H-TDMA measured hygroscopic growth factors reported by the two
987 previous studies (1.00±0.01 for RH <85% [355] and 1.01 at 95% RH [264]).

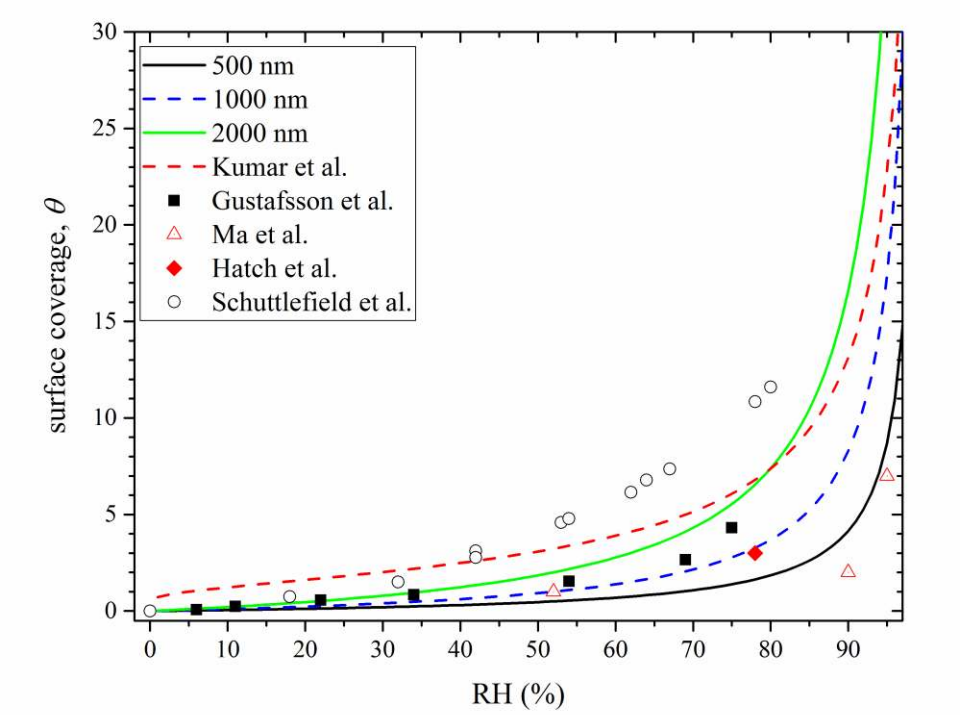

Figure 13. Comparison of measured surface coverages (θ) of adsorbed water on $CaCO_3$ particles reported by previous studies. Squares: Gustafsson et al.;[247] diamonds: Hatch et al.;[216] circles: Schuttlefield et al.;[356] triangles: Ma et al.;[212] dashed red curve: calculated using the two FHH parameters reported by Kumar et al.[262] In addition, an avearge κ values of 0.002 is used to calculated θ using Eq. (14-15) with assumed dry particle diameters of 500 (solid black curve), 1000 (dashed green curve), and 2000 nm (solid green curve).

Surface coverages of adsorbed water, measured by the four previous studies using particles deposited on some substrates,[212,216,247,356] are plotted in Figure 13 for comparison. Reasonably good agreement is found between these four different studies, as shown in Figure 13. However, discrepancies do also occur. For example, Gustafsson et al.[247] and Schuttlefield et al.[356] suggested that 4.5 and ~12 monolayers, respectively, of adsorbed water are formed at 80% RH, while Ma et al.[212] found that only ~2 monolayers of adsorbed water are formed at ~90% RH. Surface coverages of adsorbed water can be calculated using the two FHH parameters reported by Kumar et al.[262] As shown by the dashed red curve in Figure 13, the calculated θ fall into the range of those measured using particles deposited on substrates. We further calculate θ using an average κ value of 0.002

for $CaCO_3$, with assumed dry particle diameters of 500, 1000, and 2000 nm, respectively. The calculated θ are within the same order of magnitude as those directly measured. Considering measurement uncertainties and more importantly, uncertainties related to assumptions used in converting reported κ values into surface coverage (as discussed in Section 3.3), these studies show reasonably good agreement.

There are also a few studies which may not be directly relevant for atmospheric interest but can provide fundamental insight into the mechanisms of water adsorption on $CaCO_3$. For example, Neagle and Rochester [358] measured the mass of calcite samples at different temperatures and found that a cumulative loss of particle mass by 5.2% when increasing temperature from 273 K to 873 K. Synchrotron X-ray reflectivity was used to measure the thickness of water adsorbed on single crystal $CaCO_3$ surface (1014) at different RH by Bohr et al.,[359] and they found that the adsorbed water was constant in thickness (1.55±0.1 nm) while RH was varied from <4% to 90%. The result reported by Bohr et al.[359] appears to disagree with several other studies which suggest that the amount of adsorbed water on $CaCO_3$ significantly increases with RH. The discrepancy may be due to the fact that much less defect sites were present on the single crystals used by Bohr et al.[359]

Most of the aforementioned studies on water adsorption by $CaCO_3$ used techniques which provide information on the average ensemble for the surfaces under investigation, AFM can achieve spatial resolution down to sub-nanometer. AFM has been widely used to study calcite surfaces in dry and humid environments,[292,360-362] revealing that calcite surface is very dynamic and complex in the presence of water vapor. More recently, alternating current AFM height images combined with force measurements and phase imaging were used by Baltrusaitis and Grassian [291] to examine surface structure and chemistry of calcite (1014) surface at 70% for a total period of ~ 3h and at 278 and 296 K. They [291] found that calcite surfaces under ambient conditions are complex and

1029 inhomogeneous in terms of surface composition and phases, containing regions with very different
1030 water contents. Therefore, the heterogeneous reactivity of the surface will also be spatially
1031 controlled and inhomogeneous,[291] though this complication has not been considered or understood.

1032 **4.1.2 Effect of chemical aging**

1033 As summarized in Table 5, a number of previous laboratory studies have examined the change in
1034 water adsorption, hygroscopicity, and CCN activity of $CaCO_3$ particles, using different
1035 experimental techniques and methods to produce aged dust particles.

1036 **Table 5.** Laboratory studies on the effects of chemical aging processes on water adsorption, hygroscopicity, CCN activity of $CaCO_3$ particles:

1037 summary of previous studies

references	techniques	particle aging methods	major findings
Krueger et al., 2003 [214]	SEM-EDX	Particles deposited on supporting substrates were exposed to HNO_3(g) at different RH.	Exposure to 26 ppbv HNO_3 at (41±1)% RH only for 1 hour will change irregular $CaCO_3$ particles to spherical aqueous droplets.
Al-Abadleh et al., 2003 [363]	FTIR	$CaCO_3$ single crystals were exposed to HNO_3(g) at different RH.	$CaCO_3$(104) and $CaCO_3$(110) surfaces exposed to 100 mTorr HNO_3 at 23% RH have similar deliquescence relative humidities as amorphous $Ca(NO_3)_2$ particles.
Gibson et al., 2007 [257]	CCNc	Internally mixed $CaCO_3$/$Ca(NO_3)_2$ aerosol particles were generated by atomizing $CaCO_3$/$Ca(NO_3)_2$/H_2O mixture.	Internally mixed $CaCO_3$/$Ca(NO_3)_2$ particles show much higher CCN activities than $CaCO_3$ particles, and the enhancement increases with the ratio of $Ca(NO_3)_2$ to $CaCO_3$ in the particles.
Hatch et al., 2008 [216]	QCM and CCNc	Aged $CaCO_3$ particles were generated by atomizing $CaCO_3$/H_2O mixtures containing humic acid sodium salt or fulvic acid.	$CaCO_3$ particles internally mixed with humic acid sodium salt and Suwannee River fulvic acid adsorb significantly larger amounts of water, compared to fresh $CaCO_3$ particles.
Liu et al., 2008 [215]	micro Raman spectrometry	$CaCO_3$ particles on supporting surface were exposed to NO_2 at different RH.	After exposure to 100 ppmv NO_2 for 50 min at 37% RH, $CaCO_3$ particles have much higher hygroscopicity compared to fresh particles, and they exhibit the same phase transition behavior as pure $Ca(NO_3)_2$ particles.
Sullivan et al., 2009 [258]	CCNc	Monodisperse $CaCO_3$ aerosol particles were exposed to gaseous HNO_3 in an aerosol flow tube at different RH.	Exposure to HNO_3 can increase the CCN activity of $CaCO_3$ particles from κ = ~0.002 to κ = ~0.1 very quickly. A comparison of different calcium-containing minerals shows a range of CCN activities.

Gierlus et al., 2012 [218]	CCNc	Internally mixed $CaCO_3$ particles were generated by atomizing $CaCO_3/H_2C_2O_4/H_2O$ mixture.	Internally mixed $CaCO_3/CaC_2O_4$ particles only have slightly higher CCN activity, compared to fresh $CaCO_3$ particles.
Ma et al., 2012 [212]	PSA	$CaCO_3$ particles on supporting surface were exposed to gaseous CH_3COOH at different RH.	Reaction with CH_3COOH can significantly enhance the amount of water adsorbed by $CaCO_3$ particles.
Tang et al., 2015 [357]	CCNc	Monodisperse $CaCO_3$ aerosol particles were exposed to N_2O_5 in an aerosol flow tube at 0% RH.	Exposure of $CaCO_3$ aerosol particles to N_2O_5 (~550 to 15000 ppbv·s) at 0% RH increases their κ values from 0.001-0.003 to 0.02-0.04.

1038

1039

Phase transformation of solid dust particles to liquid droplets, i.e. significant change in hygroscopicity, due to heterogeneous chemistry, was first reported by Krueger et al.,[214] using Scanning Electron Microscopy. It is found that exposure to 26 ppbv HNO_3 at (41±1)% RH only for 1 hour will change irregular $CaCO_3$ particles to spherical aqueous droplets.[214] Similar phase change of $CaCO_3$ particles was also observed at (17±1)% RH after exposed to HNO_3 of the same concentration, though it only occurred after much longer exposure time.[214] Energy Dispersive X-Ray (EDX) analysis reveals that the observed phase change of aged $CaCO_3$ particles is caused by the formation of $Ca(NO_3)_2$ (R1),[199] which has a much higher hygroscopicity than $CaCO_3$.

$$CaCO_3(s) + 2HNO_3(g) \rightarrow Ca(NO_3)_2(l) + H_2O(l) + CO_2(g) \qquad (R1)$$

This innovative discovery has been supported by many following studies, which have provided further insights and more quantitative results. For example, Al-Abadleh et al.[211] found that after exposure to 100 mTorr HNO_3 at 23% RH and 295 K, the amount of adsorbed water by $CaCO_3$ single crystals (104 and 110 surface planes) is significantly increased, due to the formation of $Ca(NO_3)_2$ on the surface. Aged $CaCO_3$(104) and $CaCO_3$(110) surfaces have deliquescence relative humidities (DRH) of (9±2)% and (13±5)% at 295 K,[211] similar to that for amorphous $Ca(NO_3)_2$ particles.[364]

In addition to HNO_3, uptake of NO_2 [201,365] and N_2O_5 [131,136,139] also lead to the formation of nitrate on dust particles. Using micro-Raman spectrometry, Liu et al.[215] found that after exposure to 100 ppmv NO_2 for 50 min at 37% RH, fresh $CaCO_3$ particles were converted to internally mixed $CaCO_3$/$Ca(NO_3)_2$ particles with much higher hygroscopicity. This study further showed those internally mixed $CaCO_3$/$Ca(NO_3)_2$ particles, though still containing $CaCO_3$ inclusion, exhibit the same phase transition behavior as pure $Ca(NO_3)_2$ particles.[215]

Heterogeneous reactions of $CaCO_3$ particles with other acidic trace gases, in addition to nitrogen oxides, can also lead to the increase in hygroscopicity. For example, Hatch et al.[216] used a QCM to measure the amount of water adsorbed on fresh $CaCO_3$ and $CaCO_3$ particles mixed with humic acid sodium salt (NaHA) and Suwannee River fulvic acid (SRFA) at different RH. As shown in Figure 14, compared to fresh $CaCO_3$, the amount of water is significantly increased for $CaCO_3$ particles internally mixed with NaHa or SRFA.[216]

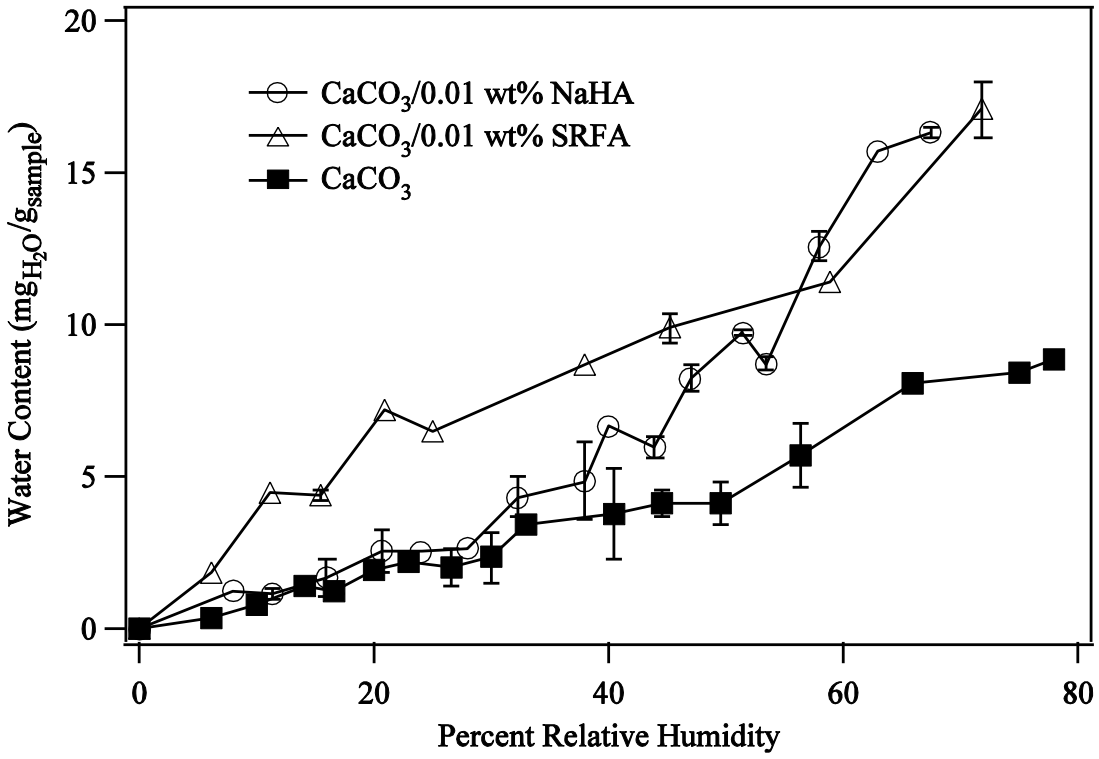

Figure 14. Amounts of water adsorbed on fresh $CaCO_3$ particles and $CaCO_3$ mixed with humic acid sodium salt (NaHA) and Suwannee River fulvic acid (SRFA) at different RH. Reprinted with permission from ref 216. Copyright 2008 Elsevier.

Ma et al.[212] observed that at 90% RH, while fresh $CaCO_3$ particles only contain 0.1% water, internally mixed $CaCO_3/Ca(CH_3COO)_2$ particles formed in the reaction of $CaCO_3$ with acetic acid at 50% RH contains ~70% water. They found that these internally mixed $CaCO_3/Ca(CH_3COO)_2$ particles have almost the same DRH as pure $Ca(CH_3COO)_2$ particles.[212] Exposure to acetic acid at

0% RH also enhances the ability of $CaCO_3$ to adsorb water, though the increase is smaller compared to that at 50% RH.[212]

As discussed previously, several studies suggest that the CCN activity of fresh $CaCO_3$ particles is very low, with κ values of <0.005.[217,264,357] Thermodynamic theories predict that the formation of more hygroscopic materials through atmospheric aging processes on $CaCO_3$ particles will increase their CCN activities.[366,367] Indeed the CCN activities of several pure Ca-containing compounds that could be formed in the atmospheric transformation of $CaCO_3$ particles, are found to have higher κ values. For example, the κ values are ~0.5 for $Ca(NO_3)_2$ and $CaCl_2$,[217,357] similar to that for $(NH_4)_2SO_4$, and 0.05 for CaC_2O_4.[217]

The CCN activities of fresh $CaCO_3$ and internally mixed particles, generated by atomization, have been measured to mimic the effect of chemical aging on the CCN activities of $CaCO_3$ particles.[218,257] For example, internally mixed $CaCO_3/Ca(NO_3)_2$ particles show much higher CCN activities than $CaCO_3$ particles, and the enhancement of CCN activities increases with the mass ratio of $Ca(NO_3)_2$ to $CaCO_3$ in the aqueous mixtures which were atomized to produce aerosol particles.[257] On the other hand, another study [218] found that internally mixed $CaCO_3/CaC_2O_4$ aerosol particles have κ values of 0.0090±0.0019, only slightly higher than 0.0070±0.0017 for fresh $CaCO_3$ aerosol particles generated using a similar method. For a particle with a dry diameter of 200 nm, κ values of 0.0070 and 0.0090 correspond to s_c of 0.442% and 0.402%, respectively. The smaller enhancement in CCN activity of $CaCO_3/CaC_2O_4$ particles, compared to fresh $CaCO_3$ particles, may be explained by relative low CCN activity of CaC_2O_4 particles, with κ values of ~0.05.[217] In addition, mixing humic acid sodium salt (NaHA) and fulvic acid can substantially increase the CCN activities of $CaCO_3$ particles and therefore reduce the critical super-saturation required to activate these particles to cloud droplets.[216] It has been reported that for 235 nm

particles, the critical super-saturation is 0.39% for fresh $CaCO_3$, 0.35% for $CaCO_3$ mixed with 0.01 wt.% NaHA, and 0.32% for $CaCO_3$ mixed with 0.05 wt.% NaHA.[216] Similar but smaller effects have also been observed for $CaCO_3$ particles mixed with fulvic acid.[216]

CCN activity of $CaCO_3$ aerosol particles before and after exposure to reactive trace gases has been measured by a few studies to better mimic the effects of atmospheric aging processes. For examples, Sullivan et al.[258] exposed $CaCO_3$ particles to HNO_3 in the aerosol flow tube and then measured the CCN activities of reacted particles. In this study [258] HNO_3 concentration, RH and exposure time were varied. As shown in Figure 15, they found [258] that the CCN activity of reacted $CaCO_3$ particles was significantly enhanced.

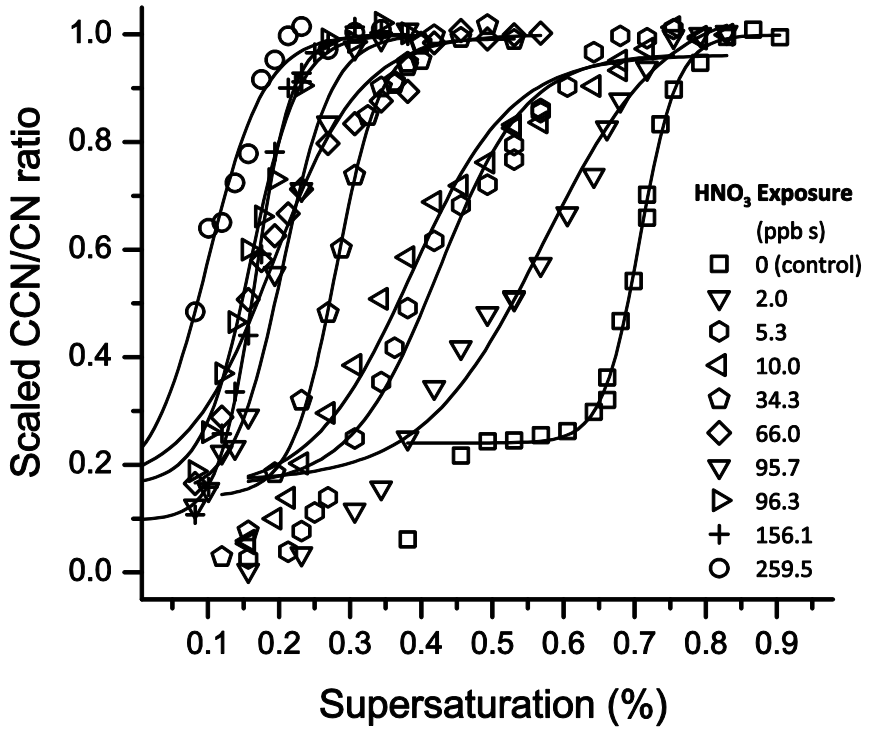

Figure 15. CCN activation curves of fresh and aged (exposure to HNO_3 at 50% RH) $CaCO_3$ aerosol particles with initial mobility diameters of 200 nm. Reprinted with permission from ref 258. Copyright 2009 the PCCP Owner Societies.

It is clear that heterogeneous reactions can significantly change the CCN activity of $CaCO_3$ particles. However, its relevance for cloud formation depends on how fast these changes occur in the troposphere. This important question has just started to be explored. For example, Sullivan et al.[258] investigated the CCN activity of aged particles as a function of HNO_3 exposure, and suggested that the κ values of $CaCO_3$ particles increase with HNO_3 exposure at three different RHs, as shown in Figure 16. Interestingly no RH dependence is found, though the uptake of HNO_3 by $CaCO_3$ particles is enhanced at higher RH.[199,227] It is further concluded by Sullivan et al.[258] that fresh $CaCO_3$ particles will be rapidly converted to aged particles with κ values of >0.1 within 4 h for 10 pptv HNO_3 and within 3 min for 1 ppbv HNO_3. HNO_3 in the troposphere can reach up to several ppbv,[368-370] suggesting that $CaCO_3$ particles can be converted to hygroscopic particles soon after they are emitted into the troposphere.

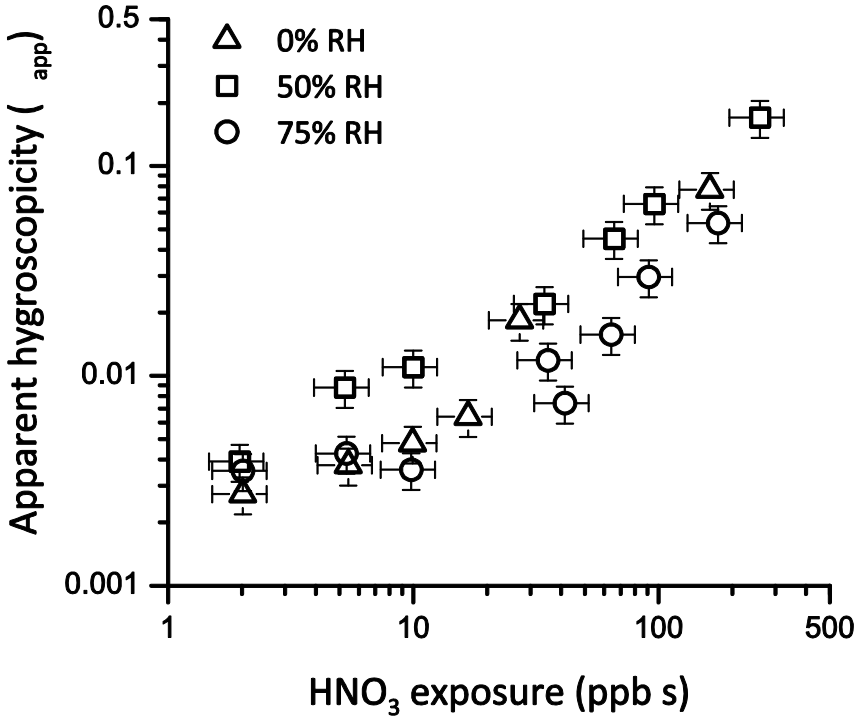

Figure 16. Measured CCN activities (represented by κ values) of aged $CaCO_3$ particles (due to the reaction with HNO_3) as a function of nitric acid exposure at 0%, 50%, and 70% RH. Reprinted with permission from ref 258. Copyright 2009 the PCCP Owner Societies.

N_2O_5 concentrations up to several ppbv have been reported,[371-374] and its reaction with $CaCO_3$ (R2) could lead to the formation of nitrate in particles. In a very recent study, Tang et al.[357] found that CCN activity of $CaCO_3$ particles which had been exposed to N_2O_5 at 0% RH in an aerosol flow tube was enhanced, with κ increased from 0.001-0.003 to 0.02-0.04. It was also found that variation of N_2O_5 exposure from ~550 to 15000 ppbv·s did not lead to change in the CCN activity of aged $CaCO_3$ particles,[357] probably because at 0% RH $CaCO_3$ may be quickly saturated with respect to reaction with N_2O_5.

$$CaCO_3(s) + N_2O_5(g) \rightarrow Ca(NO_3)_2(l) + H_2O(l) + CO_2(g) \qquad (R2)$$

4.2 Arizona Test Dust

Arizona Test Dust (ATD) is in fact one type of authentic dust samples. It is often used as a test dust and a number of previous studies have investigated water adsorption, hygroscopicity and CCN activity of both fresh and aged ATD, as listed in Table 6. Therefore, it is separately discussed here in Section 4.2, instead of being included Section 4.8 together with other authentic dust samples.

4.2.1 Fresh ATD particles

Based on their DRIFTS measurement, Gustafsson et al.[247] suggested that ~2.5 and ~4 monolayers of adsorbed water are formed on ATD particles at ~70% and ~80% RH, respectively, though the BET surface area of their ATD samples was not clearly stated. Gustafsson et al.[247] also measured the hygroscopic growth of wet-generated ATD aerosol particles which have the first mode at 56 nm and the second mode at 250 nm, and suggested that the hygroscopic growth factors of ATD particles at different RH can be described by the following equation:

$$\frac{D}{D_0} = (1 - RH)^{-0.036} \qquad (23)$$

Table 6. Water adsorption, hygroscopicity, and CCN activity of fresh Arizona Test Dust (ATD) particles: summary of previous studies.

references	techniques	aerosol generation method
Gustafsson et al., 2005 [247]	DRIFTS, TGA, and H-TDMA	wet generation
Vlasenko et al., 2005 [260]	H-TDMA	dry generation
Koehler et al., 2009 [46]	H-TDMA and CCNc	dry and wet generation
Herich et al., 2009 [49]	H-TDMA and CCNc	dry and wet generation
Navea et al., 2010 [246]	ATR-FTIR and QCM	not applicable
Sullivan et al., 2010 [261]	CCNc	dry generation
Sullivan et al., 2010 [375]	CCNc	dry generation
Kumar et al., 2011 [262]	CCNc	dry generation
Kumar et al., 2011 [263]	CCNc	wet generation
Yamashita et al., 2011[376]	CCNc	dry generation
Garimella et al., 2014 [259]	CCNc	dry generation

Navea et al.[246] investigated water adsorption on ATD particles using ATR-FTIR and QCM, and reported the mass ratio of adsorbed water to dry particles from 0-70% RH. Vlasenko et al.[260] used a H-TDMA to study the hygroscopic growth of ATD aerosol particles, and found that the hygroscopic growth factors of monodisperse particles with mobility diameters of 55, 100, 250, and 400 nm are all <1.01 for RH up to 90%. Koehler et al.[46] measured the hygroscopic growth and CCN activity of dry- and wet-generated ATD aerosol particles. The H-TDMA measurements show both dry and wet generated ATD particles have a growth factor of 1.09 at 90% RH, corresponding to a κ value of 0.03.[46] The CCN activity measurements suggest that while the dry generated ATD particles have κ values of ~0.025, the CCN activity of wet generated ATD particles is much higher, with κ values of 0.35.[46] This may indicate that compared to dry generation, wet generation can lead to significant increase of CCN activities of mineral dust particles, as suggested by several

1171 other studies.[49,256,263] Therefore, the CCN activity of wet generated ATD particles reported by
1172 Koehler et al.[46] is not included for further discussion.
1173
1174 The interaction of water vapor with dry and wet generated ATD particles was also studied by
1175 Herich et al.[49] under both sub- and super-saturation conditions, using H-TDMA and CCNc,
1176 respectively. They also found that wet-generated ATD particles show significantly higher CCN
1177 activities, due to effects introduced by redistribution of soluble materials among the particles.[49]
1178 The κ value derived from the CCN activity measurement is 0.003.[49] The κ value derived from H-
1179 TDMA measurement appears to be slightly lower than that from CCN activity measurement;
1180 however, the difference may not be significant due to the large uncertainty associated with the
1181 measured growth factors.[49] The CCN activity of dry generated ATD particles was also investigated
1182 by several other studies, with reported κ values being 0.0041,[259] 0.002,[261] 0.0042,[375] and 0.017,[376]
1183 respectively. Kumar et al.[262] investigated the CCN activity of dry generated ATD aerosol particles
1184 and interpreted their results using the FHH activation theory, with A_{FFH} of 2.96±0.03 and B_{FHH} of
1185 1.28±0.03. In another study, Kumar et al.[263] also investigated the CCN activity of wet-generated
1186 ATD aerosol particles, and concluded that compared to dry generation, wet-generation will
1187 significantly increase the CCN activity of ATD particles.

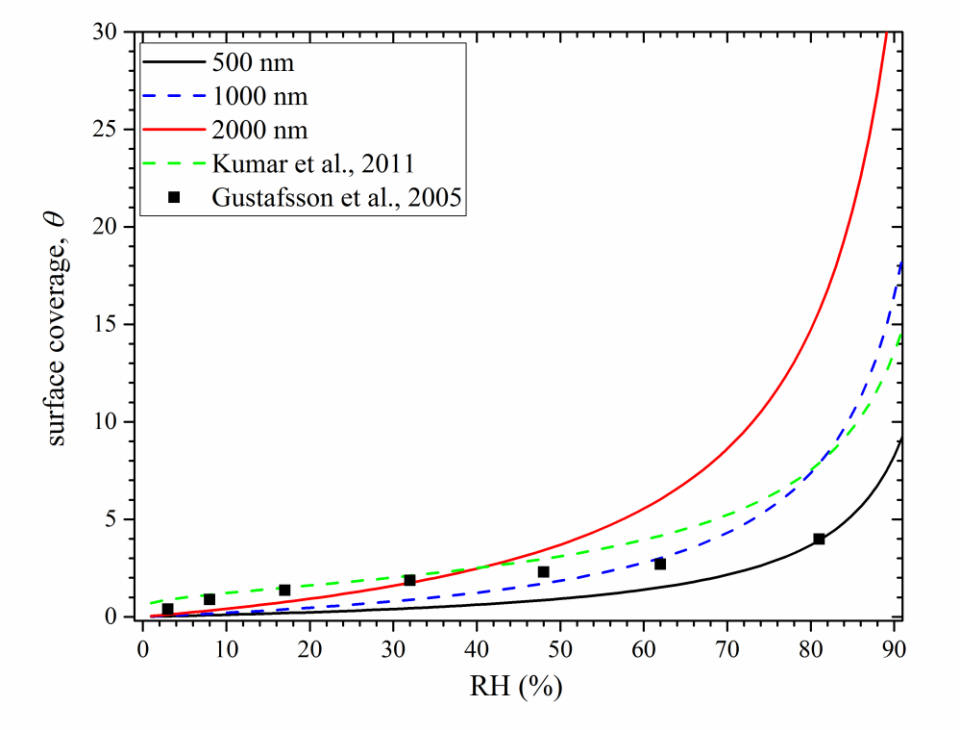

Figure 17. Comparison of measured and calculated surface coverages (θ) of adsorbed water on ATD particles. Black squares: measured by Gustafsson et al;[247] solid black curve: calculated using an average κ value of 0.004 [259,375] and an assumed diameter of 500 nm; dashed blue curve: calculated using a κ value of 0.004 [259,375] and an assumed diameter of 1000 nm; solid red curve: calculated using a κ value of 0.004 [259,375] and an assumed diameter of 2000 nm; dashed green curve: calculated using the two FHH parameters reported by Kumar et al.[262]

Surface coverages of adsorbed water on ATD particles reported by Gustafsson et al.[247] are plotted in Figure 17 together with those calculated using the two FHH parameters derived by Kumar et al.[262] from their CCN activity measurement. In addition, the surface coverages of adsorbed water are also calculated using an average κ value of 0.004 [259,375] for particles with diameters of 500, 1000, and 2000 nm, respectively. As shown in Figure 17, considering the experimental uncertainties and errors in extrapolating measurements done under super-saturation conditions to sub-saturation conditions, these studies show fairly good agreement, though some discrepancies also occur.

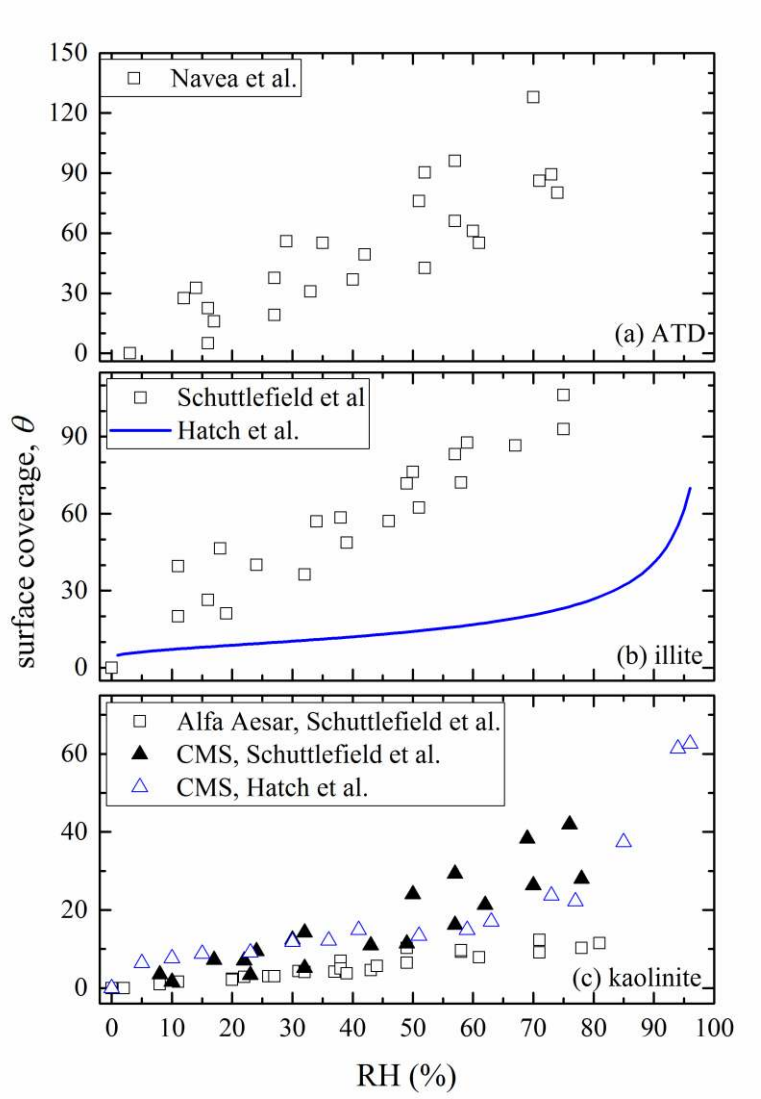

Figure 18. Surface coverage of adsorbed water on ATD (a), illite (b), and kaolinite (c), reported by Navea et al.,[246] Schuttlefield et al,[249] and Hatch et al.[268,348] Alfa Aesar indicates that particles are provided by Alfa Aesar, and CMS indicates that particles are provided by Clay Mineral Society (CMS).

The results reported by Navea et al.,[246] directly measured by using particles deposited a substrate, are shown in Figure 18a. Compared to those plotted in Figure 17, the surface coverages of adsorbed water measured by Navea et al.[246] are significantly higher. Navea et al.[246] deposited a water slurry of ATD particles on the quartz crystal surface in their QCM to form a dry dust film after the evaporation of water. When being mixed with water, clay minerals contained by ATD particles may undergo interaction with liquid water and therefore change their physicochemical properties,

a phenomena known as swelling for some clay minerals.[377] This may begin to explain the relative large difference between Navea et al.[246] and those shown in Figure 17. This may also be due to possible chemical reactions of ATD particles (or some of their components) in the aqueous mixture, leading to compositional changes. However, further studies are needed to explain and resolve this discrepancy.

4.2.2 Effect of chemical aging

The change of hygroscopicity of ATD particles due to heterogeneous reactions has been explored by a few studies. For example, Vlasenko et al.[213] measured the hygroscopic growth of ATD particles after being exposed to HNO_3 (3×10^{13} molecule cm^{-3}, i.e. ~1.2 ppmv) for 3 min at different RH in an aerosol flow tube. As shown in Figure 19, the change in hygroscopicity was negligible for exposure at 30% RH; however, the hygroscopic growth factor at ~85% RH increased from <1.02 to ~1.08 after exposure to the same amount of HNO_3 at 85% RH.[213]

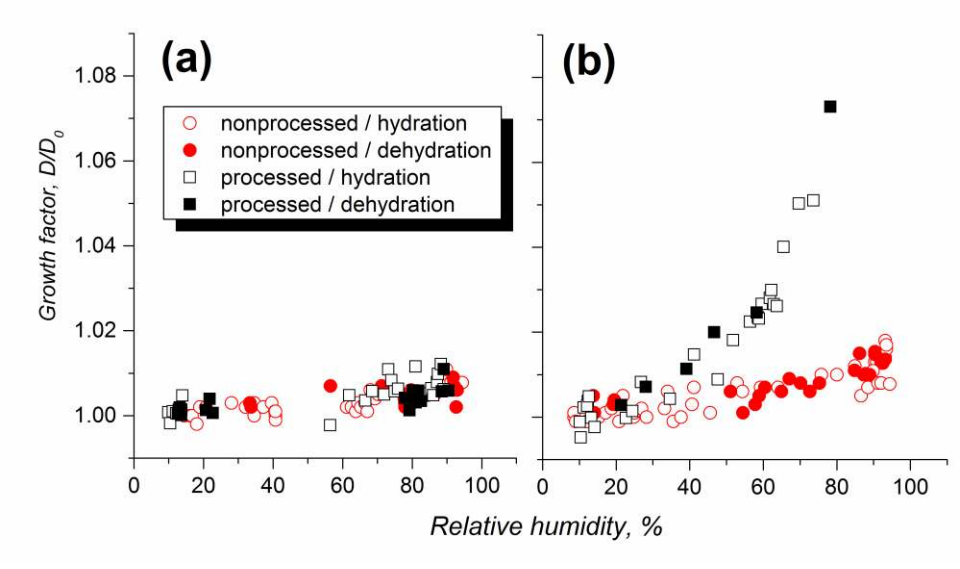

Figure 19. Hygroscopic growth of ATD particles with initial mobility diameters of 100 nm before (red circles) and after (black squares) reaction with HNO_3 of 3×10^{13} molecule cm^{-3} at RH of (a) 30% and (b) 85%. Reprinted with permission from ref 213. Copyright 2006 Copernicus Publications.

It is also found that exposure to HNO_3 [375] and H_2SO_4 [261] vapor could significantly increase the CCN activity of ATD aerosol particles. In another study, Keskinen et al.[378] suggested that secondary organic coatings which are formed from α-pinene ozonolysis can also significantly enhance the CCN activity of ATD particles.

4.3 Illite

Illite is the most abundant clay in mineral dust particles,[150] and its interaction with water vapour has been investigated by several studies. Table 7 summarizes previous studies which have investigated water adsorption, hygroscopicity, and CCN activity of illite particles. The interaction of water vapor with illite particles was investigated by Schuttlefield et al.[249] using ATR-FTIR and QCM, and the amount of water adsorbed by illite was quantified at different RH. Hatch et al.[268] studied water adsorption on illite particles using ATF-FTIR. They found that the two-parameter BET adsorption isotherm failed to describe the experimental data at higher RH while the Feundlich adsorption model could fit the data over the entire RH range.[268] In a following study, Hatch et al.[348] also used the FHH adsorption isotherm to fit their data, with A_{FFH} and B_{FHH} equal to 75±17 and 1.77±0.11.

Table 7. Water adsorption, hygroscopicity, and CCN activity of fresh illite: summary of previous studies.

references	techniques (and aerosol generation method, if applicable)
Schuttlefield et al., 2007 [249]	ATR-FTIR and QCM
Herich et al., 2009 [49]	H-TDMA and CCNc (dry and wet generation)
Attwood and Greenslade, 2011[253]	AE-CRD (wet generation)
Hatch et al., 2011 [268]	ATR-FTIR
Kumar et al., 2011 [262]	CCNc (dry generation)
Kumar et al., 2011 [263]	CCNc (wet generation)
Garimella et al., 2014 [253]	CCNc (dry generation)
Hatch et al., 2014 [348]	ATR-FTIR

Attwood and Greenslade [253] measured the optical extinction of wet-generated illite aerosol particles at 532 nm and at different RH to study their hygroscopicity. The hygroscopic growth factors were found to be 0.90, 0.93, and 1.06 at RH of 50%, 68%, and 90%, respectively.[253] It should be pointed out that the hygroscopic growth reported by Attwood and Greenslade [253] is based on the measured optical extinction coefficients. Hygroscopic growth factors smaller than 1, which have also been reported for ATD particles using H-TDMA,[46,260] can be due to change in particle morphology and even restructure of particles during humidification.[46,253,260] Since it is difficult to convert change in optical extinction cross sections at different RH to the amount of adsorbed water, the result reported by Attwood and Greenslade [253] is not included in further discussion.

Herich et al.[49] produced illite aerosol particles using both dry and wet generation methods, and measured the hygroscopicity and CCN activity of generated illite aerosol particles using H-TDMA and CCNc, respectively. They [49] found that wet-generated illite particles are more CCN active than those generated by dry dispersion, and that the dry-generated illite particles has κ values of 0.002-0.003. Kumar et al.[262,263] also investigated the CCN activity of dry- and wet-generated illite aerosol particles, and suggested that the FHH activation theory could better describe CCN activation of illite particles. A_{FHH} and B_{FHH} were reported to be 1.02±0.38 and 1.12±0.04 for dry-generated illite particles,[262] and 3.00 and 1.27 for wet-generated illite particles.[263] Recently Garimella et al.[259] also studied the CCN activity of dry-generated illite particles, and they suggested that the κ-Köhler activation theory could adequately describe the CCN activation of illite particles, with an average κ value of 0.0072.

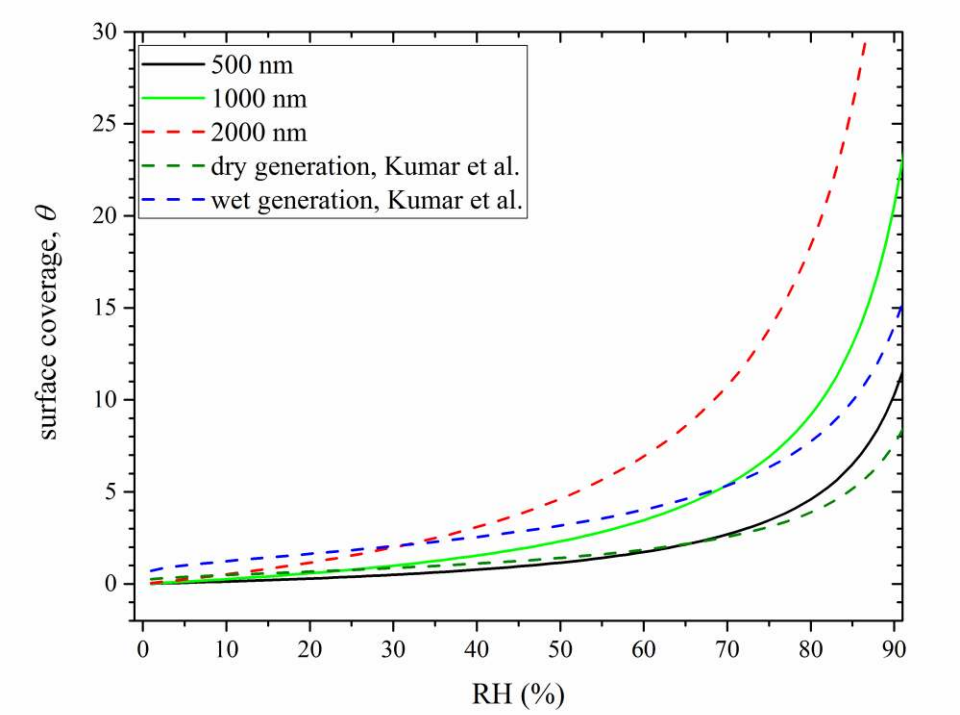

Figure 20. Comparison of calculated surface coverages (θ) of adsorbed water on illite particles. Surface coverages of adsorbed water are calculated using an average κ value of 0.005 and different dry particle diameters of 500 (solid black curve), 1000 (solid green curve), and 2000 nm (dashed red curve), and using A_{FHH} and B_{FHH} for dry- (dashed olive curve) and wet-generated (dashed blue curve) illite aerosol particles reported by Kumar et al.[262,263]

A_{FFH} and B_{FHH} parameters for dry- and wet-generated illite particles, derived by Kumar et al.[262,263] from their CCN activity measurements, are used to calculate surface coverages of adsorbed water under sub-saturation conditions. κ values for dry-generated illite aerosol particles were reported to be 0.002-0.003 by Herich et al.[49] and 0.0072 by Garimella et al.[259] An average κ value of 0.005 is then used here to calculate surface coverage of adsorbed water under sub-saturation conditions for particles with uniform diameters of 500, 1000, and 2000 nm. All the calculated results are shown in Figure 20, exhibiting relatively good agreement in general.

Schuttlefield et al.[249] and Hatch et al.[268,348] experimentally measured water adsorption under sub-saturation conditions on illite particles which were deposited on supporting substrates, and their results are displayed in Figure 18b. Comparison of results shown in Figure 20 to those in Figure 18b suggests that surface coverages of adsorbed water reported by Schuttlefield et al.[249] and Hatch et al.[268,348] are both significantly higher than those using aerosol particles, including those reported by Kumar et al.[263] who generated aerosol particles by atomizing illite/water mixture. Therefore, the difference between studies using particles deposited on substrates and those using aerosol particles cannot be fully explained by the potential change in particle properties due to the interaction of clay with liquid water during the sample preparation stage. Clay minerals are inherently complex with variability between samples. Variability in clay minerals are due to differences in metal cations present and potentially contamination with other clay components (e.g. montmorillonite) can potentially cause the observed difference. Considering the abundance of illite in tropospheric mineral dust particles, more studies are required to better understand its interaction of water vapor.

4.4 Kaolinite

Previous studies which reported water adsorption, hygroscopicity, and CCN activities of fresh kaolinite are summarized in Table 8. ATR-FTIR and QCM were used by Schuttlefield et al.[249] to investigate water adsorption on kaolinite particles at different RH. Two different kaolinite samples were used,[249] with one purchased from Alfa Aesar and the other one provided by the Source Clay Repository (Clay Mineral Society). Hatch et al.[268] also investigated water adsorption on Clay Mineral Society kaolinite using ATR-FTIR, and suggested that the Freundlich adsorption isotherm can better describe their experimental data, compared to the two-parameter BET adsorption isotherm. Recently Hung et al.[270] used a physisorption analyser to study water adsorption on kaolinite provided by Fluka.

Table 8. Water adsorption, hygroscopicity, and CCN activity of fresh kaolinite: summary of previous studies.

references	techniques (and aerosol generation method, if applicable)
Schuttlefield et al., 2007 [249]	ATR-FTIR and QCM
Gibson et al., 2007 [257]	CCNc (wet generation)
Herich et al., 2009 [49]	H-TDMA and CCNc (dry and wet generation)
Hatch et al., 2011 [268]	ATR-FTIR
Attwood and Greenslade, 2011[253]	AE-CRD (wet generation)
Kumar et al., 2011 [263]	CCNc (wet generation)
Hung et al., 2015 [270]	PSA

Optical extinction coefficients were measured at 532 nm using Cavity Ring-Down spectroscopy to determine the hygroscopic growth of Clay Mineral Society kaolinite particles at different RH.[253] The hygroscopic growth factors, relative to the diameter at <10% RH, were measured to be 0.90±0.08, 0.79±0.11 and 0.80±0.17 at RH of 50%, 68%, and 90%, respectively.[253] Hygroscopic growth factors significantly smaller than 1 suggest that restructure of mineral dust particles may occur during humidification, and also make it difficult to derive the amount of adsorbed water from optical extinction measurements. It should be noted that potential restructure of dust particles can also affect H-TDMA measurements. For example, hygroscopic growth factors of ATD particles, as measured by H-TDMA, were reported to be slightly smaller than 1 at some RH.[46,260]

CCN activity of wet-generated Clay Mineral Society kaolinite aerosol particles were studied by Gibson et al.,[257] and the critical super-saturation was measured to be 0.44±0.02 for 200 nm dry particles, corresponding to a κ value of 0.0071. Herich et al.[49] used H-TDMA and CCNc to study the hygroscopicity and CCN activity of kaolinite particles, provided by Fluka and Clay Mineral Society. In the study by Herich et al.,[49] aerosol particles were produced by both dry and wet

generation, and wet generation was found to increase the CCN activity of kaolinite particles. The CCN activity of dry-generated kaolinite particles is quite low, with average κ values of ~0.001.[49] By comparison, another study by Kumar et al.[263] found that wet-generated kaolinite aerosol particles exhibited a κ values of 0.45 which is only slightly lower than that for ammonia sulfate, highlighting that dry and wet generation methods can lead to considerable difference in the CCN activities of resulting dust aerosol particles.

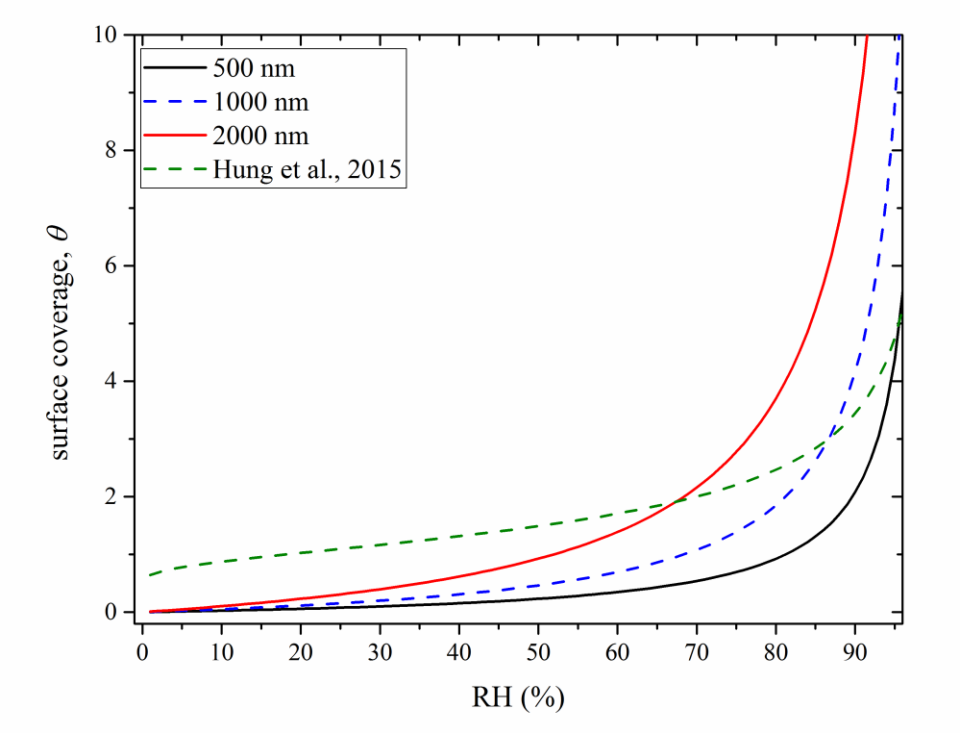

Figure 21. Comparison of surface coverage (θ) of adsorbed water on kaolinite particles experimentally measured by Hung et al.[270] (dashed olive curve) and those calculated using a κ value of 0.001 reported by Herich et al.[49] and assumed particle diameters of 500 (solid black curve), 1000 (dashed blue curve), and 2000 nm (solid red curve).

Surface coverages of adsorbed water on kaolinite particles experimentally by Hung et al.[270] are plotted in Figure 21 together with those calculated using a κ value of 0.001 reported by Herich et al.[49] and assumed particle diameters of 500, 1000, and 2000 nm. As shown in Figure 21, reasonably good agreement is found,

1344 considering the uncertainties (as discussed in Section 3.3) when using the κ value to calculate surface
1345 coverages of adsorbed water.
1346
1347 Experimentally determined surface coverages of adsorbed water on kaolinite particles by Schuttlefield et
1348 al.[249] and Hatch et al.[268] are shown in Figure 18c. Several conclusions can be drawn when comparing these
1349 two studies.[249,268] First of all, Schuttlefield et al.[249] and Hatch et al.[268] used very similar techniques to
1350 measure the amounts of water adsorbed by kaolinite particles from the same source (provided by Clay
1351 Mineral Society), and their results agree quite well with each other, as shown in Figure 18c. Second,
1352 Schuttlefield et al.[249] measured water adsorption on two different kaolinite samples, and significant
1353 difference between these two samples was found. This may suggest the same type of dust particles from
1354 different sources, because of variability within sources, could have very different ability to uptake water
1355 vapor.
1356
1357 Surface coverages of adorbed water on kaolinite particles measured by Schuttlefield et al.[249] and Hatch et
1358 al.,[268] as shown in Figure 18c, are significantly higher than those (as shown Figure 21) directly measured
1359 by Hung et al.[270] and those calculated using the κ value reported by Herich et al.[49] We note that Schuttlefield
1360 et al.,[249] Hatch et al.[268], and Hung et al.[270] all deposited kaolinite particles on supporting substrates. The
1361 observed large discrepancy between the first two studies[249,268] and that by Hung et al.[270] is somehow
1362 unexpected. A potential explanation is that the two studies by Schuttlefield et al.[249] and Hatch et al.[268] placed
1363 particles onto the supporting substrates via depositing water slurry onto them, probably leading to swelling
1364 and changes in the properties of kaolinite particles, while dry kaolinite powders were directly placed onto
1365 the supporting substrate by Hung et al.[270]
1366
1367 Internally mixed kaolinite/ammonia sulfate particles, generated by atomizing kaolinite-ammonia
1368 sulfate-water mixture, were found to have higher CCN activity compared to fresh kaolinite
1369 particles.[257] The internally mixed kaolinite-ammonia sulfate particles have κ values of ~0.017 and
1370 ~0.038, increasing with the mass ratio of ammonia sulfate to kaolinite in the aqueous mixtures

1371 which were atomized to produce aerosol particles.[257] Although this study [257] may not mimic actual
1372 atmospheric aging processes very well, it does suggest that the CCN activity of kaolinite particles
1373 can be substantially enhanced if being mixed more soluble compounds due to heterogeneous
1374 reactions and/or cloud processing.

1375 **4.5 Montmorillonite**

1376 As summarized in Table 9, water adsorption, hygroscopicity, and CCN activity of montmorillonite
1377 particles have been investigated by several studies in the last 2-3 decades. For example, Hall and
1378 Astill [379] used a vacuum microbalance to measure the mass of montmorillorite particles at different
1379 RH (up to 70%) and at different temperature (25-75 ºC). Four homoionic (Ca^{2+}, Li^{+}, Na^{+}, and K^{+})
1380 exchanged forms of Clay Mineral Society montmorillorite (SWy-1) were studied.[379] Water
1381 adsorption by Na-exchanged montmorillorite was also investigated at different RH and 25 ºC by
1382 Cases et al.,[380] using a microbalance. An environmental infrared microbalance was deployed by
1383 Xu et al.[381] to investigate water adsorption on Na-, Li-, Ca-, and Mg-exchanged forms of two
1384 montmorillonite samples (SWy-1 and SAz-1) provided by Clay mineral Society. Gas
1385 chromatography was used by Zent et al.[382] to study water uptake on Na-montmorillorite (Swy-1)
1386 at different RH and at 211 and 273 K.

1387

1388 **Table 9.** Water adsorption, hygroscopicity, and CCN activity of fresh montmorillonite: summary of
1389 previous studies.

references	techniques (and aerosol generation method, if applicable)
Hall and Astill, 1989 [379]	vacuum microbalance
Cases et al., 1992 [380]	microbalance
Xu et al., 2000 [381]	environmental infrared microbalance
Zent et al., 2001 [382]	gas chromatography
Frinak et al., 2005 [383]	Transmission FTIR

Schuttlefield et al., 2007 [249]	ATR-FTIR and QCM
Herich et al., 2009 [49]	H-TDMA and CCNc (dry and wet generation)
Attwood and Greenslade, 2011[253]	AE-CRD (wet generation)
Hatch et al., 2011 [268]	ATR-FTIR
Kumar et al., 2011 [262]	CCNc (dry generation)
Kumar et al., 2011	CCNc (wet generation)
Hatch et al., 2014 [348]	ATR-FTIR
Garimella et al., 2014 [259]	CCNc (dry and wet generation)
Hung et al., 2015 [270]	PSA

More recently, Frinak et al.[383] used transmission FTIR to determine the amount of water adsorbed on montmorillonite (SWy-2) provided by Clay Mineral Society as a function of temperature (212-231 K) and RH. They found that water uptake by montmorillonite is almost as large as ammonia sulfate.[383] It was further suggested by Frinak et al.[383] that though water adsorption on montmorillonite depended strongly on RH, no strong dependence on temperature (212-231 K) was observed.

Frinak et al.[383] also compared their measurement to those reported in previous studies.[379-382] As shown in Figure 22, except that reported by Zent et al.,[382] all the other studies in general show good agreement. A close look reveals that the amount of adsorbed water measured by Cases et al.[380] at RH<30% may be lower than those reported by Hall and Astill,[379] Xu et al.,[381] and Frinak et al.[383]

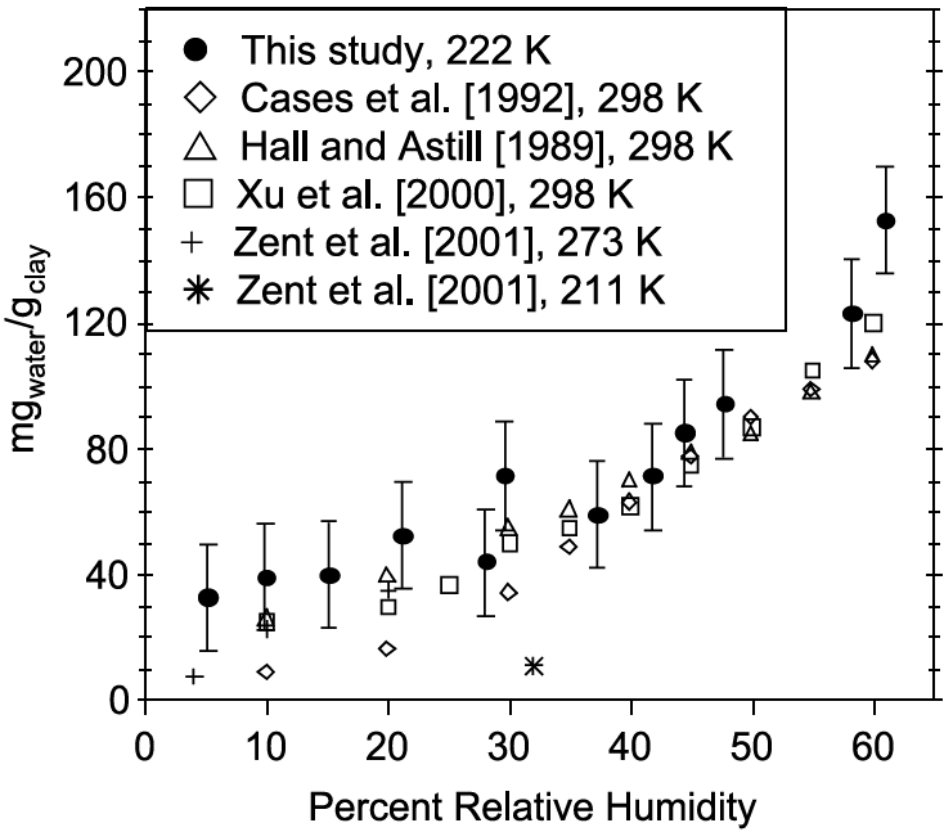

1403

1404 **Figure 22.** Comparison of amounts of water adsorbed on SWy-2 (montmorillorite from Clay Mineral
1405 Society) measured by studies before 2006. Reprinted with permission from ref 383. Copyright 2005 John
1406 Wiley & Sons, Inc.

1407

1408 Water adsorption on three different montmorillonite samples (one from Alfa Aesar, the other two
1409 from Clay Mineral Society: SWy-2 and SAz-1) was investigated by Schuttlefield et al.[249] using
1410 ATR-FTIR and QCM. The amount of water adsorbed by montmorillorite was quantified at room
1411 temperature and at different RH, using QCM.[249] As shown in Figure 23a, montmorillorite particles
1412 from various sources exhibit different ability to adsorb water. At the same RH, the amount of water
1413 adsorbed by SAz-1 is much larger than those by the other two montmorillorite samples, and Alfa
1414 Aesar montmorillorite adsorbs the least amount of water.

1415

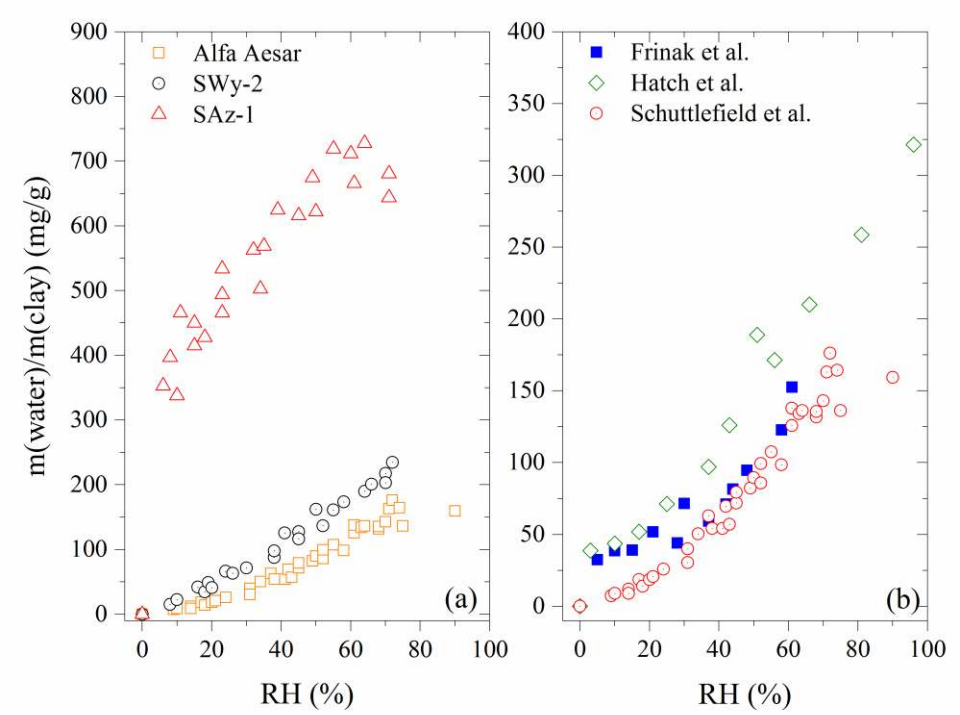

Figure 23. (a) Water adsorption on three different montmorillorite samples as a function of RH, measured by Schuttlefield et al.[249] at room temperature. Squares: Alfa Aesar montmorillorite; circles: SWy-2 provided by Clay Mineral Society; triangles: SAz-1 provide by Clay Mineral Society. (b) Water adsorption on SWy-2 montmorillorite as a function of RH measured three different studies. Squares: measured by Frinak et al.[383] at 222 K; diamonds: measured by Hatch et al.[268] at room temperature; circles: measured by Schuttlefield et al.[249] at room temperature.

ATR-FTIR was used by Hatch et al.[268] to determine the amount of water adsorbed on Clay Mineral Society montmorillorite (SWy-2) particles at room temperature and at different RH, and the experimental result was fitted by the FHH adsorption isotherm with A_{FHH} and B_{FHH} equal to 98±22 and 1.79±0.11.[348] The mass ratios of adsorbed water to dry SWy-2, as a function of RH, measured by Frinak et al.[383] at 222 K and by Schuttlefield et al.,[249] and Hatch et al.[268] at room temperature, are plotted in Figure 23b for comparison. Results reported by studies [379-382] prior to Frinak et al.[383] are already shown in Figure 22, and therefore they are not included in Figure 23b. Considering the experimental uncertainties, all the three studies show very good agreement, even though Frinak et

al.[383] carried out the measurement at 222 K and the other two studies [249,268] were conducted at room temperature. Considering earlier measurements which are plotted in Figure 22, one could conclude that most of the available studies [249,268,379-381,383] in which samples were supported on substrates reported similar water adsorption for SWy-2 montmorillorite, although different experimental techniques were used to quantify the amount of adsorbed water.

Optical extinction of wet-generated Clay Mineral Society montmorillorite particles at 532 nm was measured at room temperature and at different RH by Attwood and Greenslade [253] to study their hygroscopic growth, using Cavity Ring-Down spectroscopy. Their reported hygroscopic growth factors are 1.03 at 50% RH, 1.18% at 68% RH, and 1.4 at 90%, respectively.[253] As discussed in Sections 4.3 and 4.4, their reported hygroscopic growth factors are <1 for illite and kaolinite,[253] likely due to restructure of clay particles at elevated RH. Restructure of montmorillorite particles may also occur during humidification. In addition, since montmorillorite particles are non-spherical, it is non-trivial to convert change in optical properties at different RH to the amount of adsorbed water by the particles. Therefore, the result reported by Attwood and Greenslade [253] for montmorillorite is not included in comparison. Using the same experimental method, in a following study Attwood and Greenslade [384] found that internal mixing with montmorillorite would decrease the deliquescence RH of both ammonia sulfate and sodium chloride.

Using H-TDMA and CCNc, Herich et al.[49] studied the hygroscopicity and CCN activity of montmorillorite particles provided Aldrich and Clay Mineral Society. Aerosol particles were produced by both dry- and wet-generation.[49] Wet generation was found to increase the CCN activity of montmorillonite particles, compared to dry generation.[49] The single hygroscopicity parameter, κ, was determined to be ~0.003 for dry-generated montmorillorite particles and close to 0.02 for wet-generated particles.[49] The CCN activation of dry-generated Na-montmorillorite

provided by Clay Mineral Society was investigated by Garimella et al.,[259] with κ reported to be 0.0088.

Kumar et al.[262,263] investigated the CCN activity of dry and wet-generated Na- and Ca-montmorillonite aerosol particles, and suggested that the FHH adsorption activation theory could better describe the CCN activation of montmorillonite aerosol particles. Reported A_{FHH} and B_{FHH} are 1.23±0.31 and 1.08±0.03 for dry-generated Na-montmorillonite,[262] 2.06±0.72 and 1.23±0.04 for dry-generated Ca-montmorillonite,[262], 0.87 and 1.00 for wet-generated Na-montmorillonite,[263] and 1.09 and 1.04 for wet-generated Ca-montmorillonite,[263] respectively.

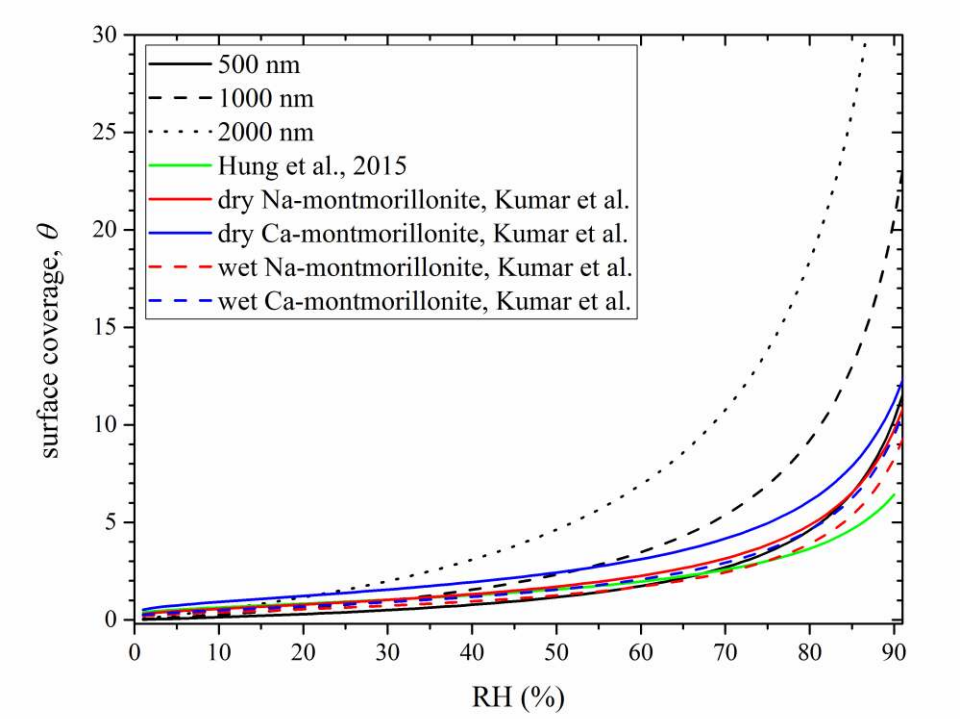

Figure 24. Comparison of surface coverages of adsorbed water on montmorillorite measured by Hung et al.[270] (solid green curve) with those extrapolated from CCN activity measurements. Surface coverages of adsorbed water are also calculated using an average κ of 0.005 [49,259] and assumed dry particle diameters of 500 (solid black curve), 1000 (dashed black curve), and 2000 nm (dotted black curve), respectively. In addition, θ are calculated using A_{FHH} and B_{FHH} values reported by Kumar et al.[262,263] Red curves: calculated using A_{FHH} and B_{FHH} parameters for dry- (solid) and wet-generated (dashed) Na-montmorillorite; blue

curves: calculated using A_{FHH} and B_{FHH} parameters for dry- (solid) and wet-generated (dashed) Ca-montmorillorite.

Recently Hung et al.[270] measured water adsorption on kaolinite K10 powders (provided by Sigma Aldrich) at 28 ^{o}C and at different RH, using a PSA. For comparison, the measurements[49,259,262,263] in which the CCN activity of aerosol particles were investigated are extrapolated to sub-saturation conditions and plotted in Figure 24 together with the surface coverage of adsorbed water directly measured Hung et al.[270] As shown in Figure 24, reasonably good agreement is found, though large errors can occur in these extrapolations, as discussed in Section 3.2.

However, differences can be found when comparing studies plotted in Figures 22-23, to those shown in Figure 24. For example, Schuttlefield et al.[249] suggested that at around 70% RH, approximately 50-60 and 200 monolayers of adsorbed water were formed on SWy-2 and SAz-1 kaolinite particles, compared to approximately 10 or less monolayers at the same RH for studies shown in Figure 24. It should be noted that the surface coverage is calculated by dividing the total amount of adsorbed water by the BET surface area of particles under investigation. The reasons for such relatively large discrepancies are complicated and unclear at this stage. For example, the difference between using particles supported on substrates and aerosol particles cannot explain the discrepancies alone, because Hung et al.[270] also studied particles deposited on a substrate but reported similar results to those using aerosol particles.[49,259,262,263] This can not be explained by clay swelling effects alone which may play a role in several studies, for example, by Frinak et al.,[383] Schuttlefield et al.,[249] and Hatch et al.[268] This is because the calculated surface coverages of adsorbed water from the CCN activity measurement of wet-generated particles by Kumar et al.[263] are not very different from those for dry-generated particles,[262] as shown in Figure 24. In addition, such discrepancies cannot be only due to the usage of different types of montmorillorite particles,

because studies [49,259,262,263,270] included in Figure 24 used montmorillorite from various sources but still showed reasonably good agreement. Careful and systematical measurements in future can help resolve these discrepancies and better understand the interaction of montmorillorite with water vapor.

4.6 Quartz

Table 10 provides a summary of previous studies in which water adsorption, hygroscopicity, and CCN activity of SiO_2, TiO_2, Al_2O_3, and Fe_2O_3 were determined. Section 4.6 discusses previous studies on SiO_2, while those for TiO_2, Al_2O_3, and Fe_2O_3 are reviewed in Section 4.7.

Table 10. Water adsorption, hygroscopicity, and CCN activity of fresh SiO_2, TiO_2, Al_2O_3, and Fe_2O_3: summary of previous studies.

mineral	References	techniques
SiO_2	Goodman et al., 2001 [250]	Transmission FTIR
	Schuttlefield et al., 2007 [273]	ATR-FTIR and QCM
	Ma et al., 2010 [269]	DRIFTS
	Keskinen et al., 2011 [320]	H-TDMA (wet generation)
	Kumar et al., 2011 [262]	CCNc (dry generation)
	Dalirian et al., 2015 [385]	CCNc (wet generation)
TiO_2	Goodman et al., 2001 [250]	Transmission FTIR
	Ketteler et al., 2007 [241]	AP-XPS
	Ma et al., 2010 [269]	DRIFTS
Al_2O_3	Goodman et al., 2001 [250]	Transmission FTIR
	Al-Abadleh and Grassian, 2003 [240]	Transmission FTIR
	Schuttlefield et al., 2007 [249]	ATR-FTIR and QCM
	Ma et al., 2010 [269]	DRIFTS
	Ma et al., 2012 [212]	PSA
Fe_2O_3	Goodman et al., 2001 [250]	Transmission FTIR

Ma et al., 2010 [269]	DRIFTS	

Water adsorbed on SiO_2 particles was measured using transmission FTIR, and its surface coverage at different RH was fitted by a modified three-parameter BET equation with n equal to 10 and c equal to 13.1.[250] Schuttlefield et al.[273] investigated water adsorption on SiO_2 particles by coupling ATR-FTIR with QCM in tandem. In another study, DRIFTS was used by Ma et al.[269] to investigate the interaction of water vapor with SiO_2 surface at different RH, and the result was also fitted with a modified three-parameter BET equation with n equal to 3.8 and c equal to 4.8.

H-TDMA was used to study the hygroscopic growth of spherical SiO_2 aerosol particles of 8-10 nm,[320] and it is suggested that the water adsorption on SiO_2 particles can be described by the FHH adsorption isotherm, with A_{FHH} and B_{FHH} equal to 4.82 and 2.16. It is also suggested that compact agglomerate particles which contain a few primary spherical particles could adsorb ~1.5 times more water at the same RH, compared to small spherical particles.[320] This may probably result from the capillary effects of these small cavities between primary small particles in the agglomerate.[320]

Kumar et al.[262] investigated the CCN activity of SiO_2 aerosol particles under super-saturation conditions. Their measurements were interpretted using the FHH adsorption activation theory, with A_{FHH} and B_{FHH} equal to 2.96 and 1.36, respectively.[262] The CCN activity of SiO_2 aerosol particles were also investigated by Dalirian et al.,[385] and they suggested that the activation of SiO_2 particles can be described by the FHH activation theory with A_{FHH} and B_{FHH} equal to 2.50 and 1.62, respectively.

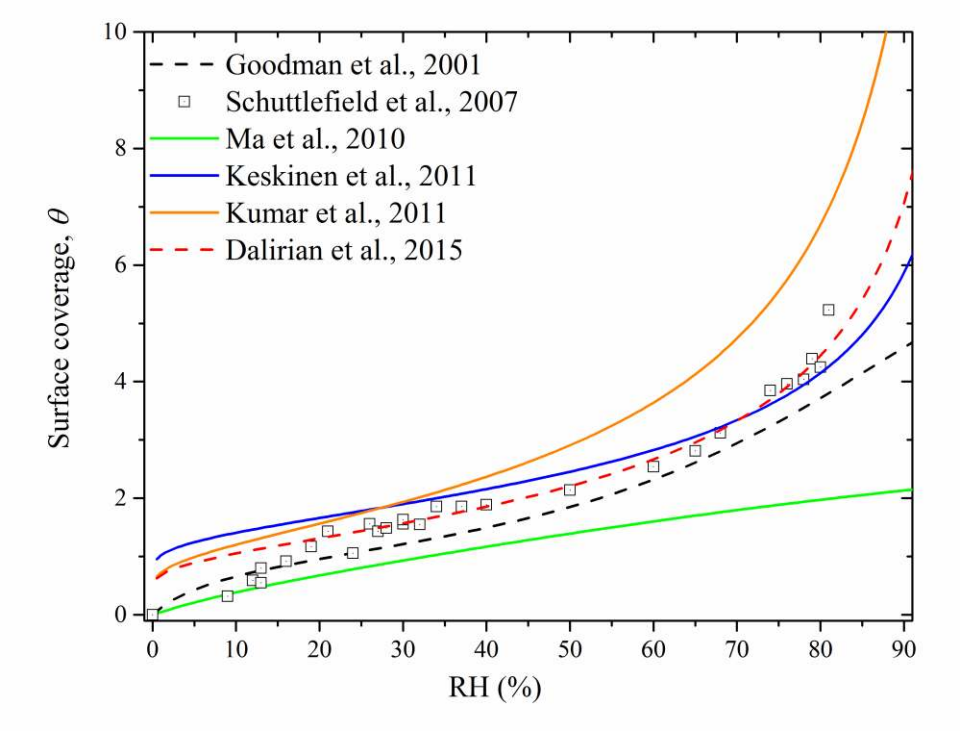

Figure 25. Comparison of surface coverage of adsorbed water on SiO_2 particles reported by Goodman et al.[250] (black dashed curve), Schuttlefield et al.[273] (squares), Ma et al.[269] (green solid curve), Keskinen et al.[320] (blue solid curve), Kumar et al.[262] (orange solid curve) and Dalirian et al.[385] (red dashed curve).

Water adsorption on SiO_2 particles, as measured by previous studies under sub-saturation conditions [250,269,273,320] or calculated using the two FHH parameters derived from CCN activation measurements under super-saturation conditions,[262,385] is plotted in Figure 25 for comparison. In general good agreement is found, though different experimental techniques and different SiO_2 samples were used. Significant discrepancies also exist. For example, the surface coverages of adsorbed water reported by Ma et al.[269] are always lower than those reported by other studies, and the discrepancy becomes more evident for RH >50%. In addition, for RH >50%, the difference between the calculated surface coverages of adsorbed water using the two FHH parameters reported by Kumar et al.[262] and those reported by Goodman et al.,[250] Schuttlefield et al.,[273] Keskinen et al.[320] and Dalirian et al.[385] appears to increase with RH.

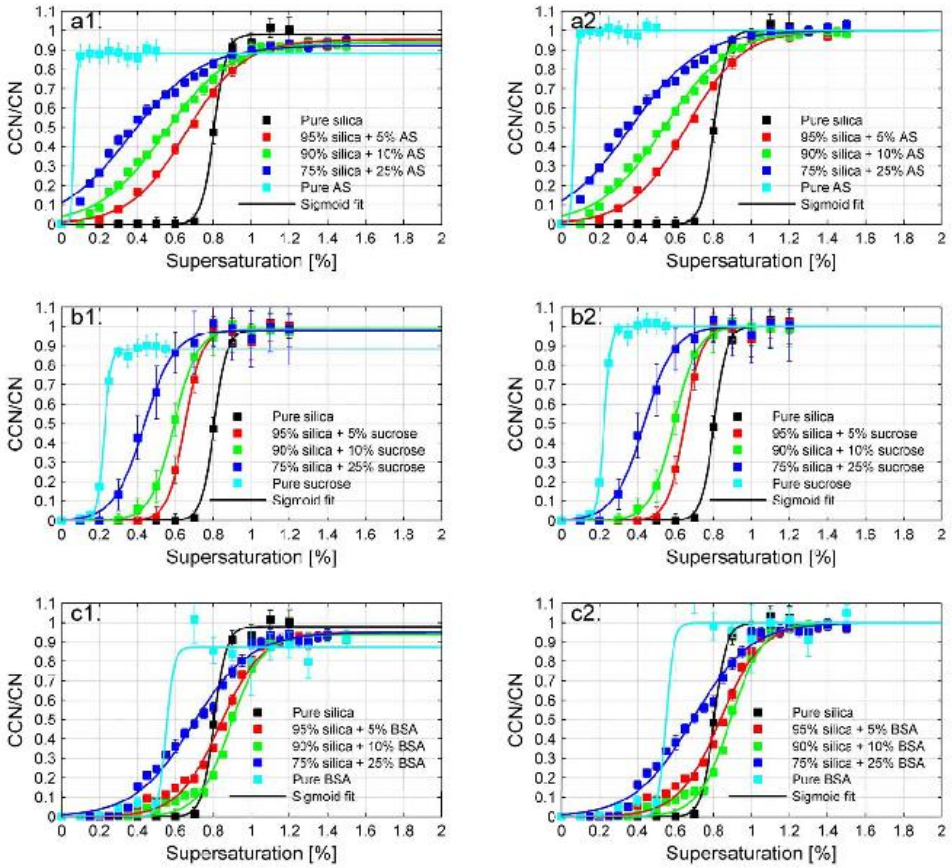

1547

1548 **Figure 26**. CCN activation curves for 150 nm pure SiO_2 particles and SiO_2 particles mixed with (a1-a2)
1549 ammonia sulfate (AS), (b1-b2) sucrose, and (c1-c2) bovine serum albumin. The left three panels show the
1550 un-normalized data and the right three panels show the normalized data. Reprinted with permission from
1551 ref 385. Copyright 2015 Copernicus Publications.

1552

1553 Coating of SiO_2 particles with more hygroscopic materials can increase their CCN activities.
1554 Dalirian et al.[385] generated SiO_2 particles mixed with different amounts of ammonia sulfate (AS),
1555 sucrose, and bovine serum albumin (BSA). As shown in Figure 26, mixing SiO_2 with compounds
1556 with higher CCN activities (compared to SiO_2) can decrease the critical super-saturation ratios and
1557 increase their CCN activity, when compared to pure SiO_2 particles.[385] The extent of decrease in
1558 critical super-saturation ratios depends on the mass fraction of SiO_2, i.e. the less SiO_2 the mixed
1559 particles contain, the more CCN active these particles are. In addition, different materials have
1560 different effects even when their mass fractions are the same. For the three compounds investigated

1561 by Dalirian et al.,[385] ammonia sulfate has the most significant effect because it is most CCN activity
1562 with a κ value of 0.61, while BSA has a smaller effect because its κ value is ~0.13 (and the κ value
1563 is 0.084 for sucrose).[385]

1564 ## 4.7 Metal oxides (TiO_2, Al_2O_3, and Fe_2O_3)

1565 Previous studies which have investigated water adsorption on fresh and/or reacted TiO_2, Al_2O_3,
1566 and Fe_2O_3 particles are summarized in Table 10.

1567 ### 4.7.1 TiO_2

1568 Goodman et al.[250] investigated water adsorption on P25 TiO_2 particles (BET surface area: 50 m^2 g^{-1})
1569 [1]) at different RH using transmission FTIR. It was found that [250] the surface coverage of adsorbed
1570 water can be fitted by the modified three-parameter BET equation, i.e. Eq. (5), with n equal to 8
1571 and c equal to 74.8. Ma et al.[269] used DRIFTS to study the water adsorption on P25 TiO_2 particles,
1572 and suggested that surface coverage of adsorbed water can be fitted with the modified three-
1573 parameter BET equation with n equal to 6.2 and c equal to 5.5. The results reported by these two
1574 studies are plotted in Figure 27, suggesting that the surface coverage of adsorbed water measured
1575 by Goodman et al.[250] is slightly higher than that determined by Ma et al.[269]

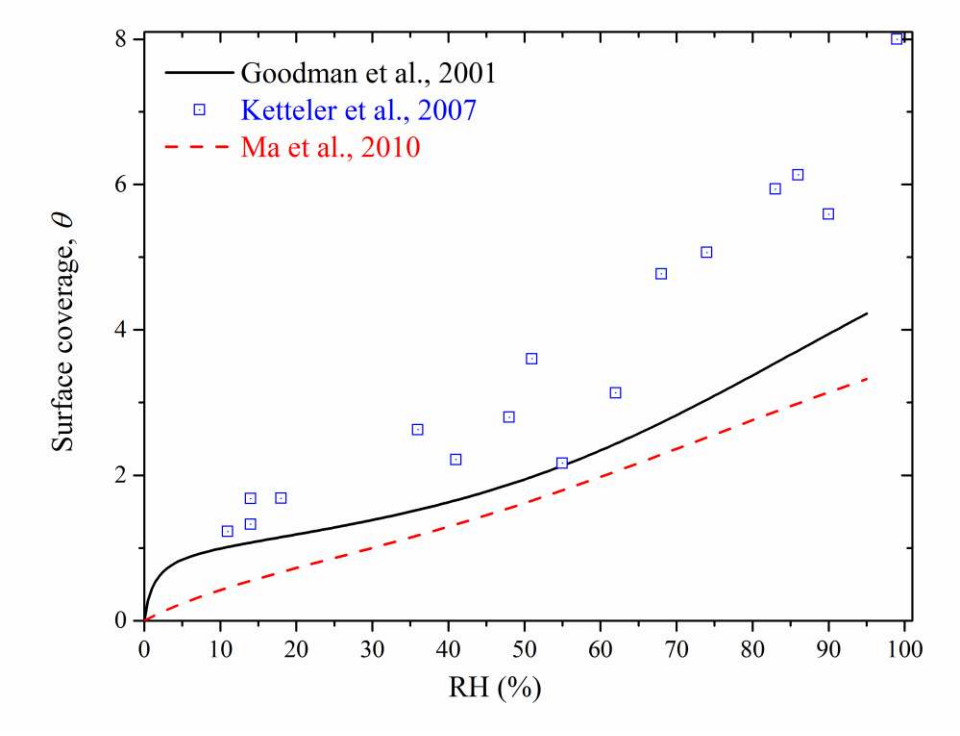

Figure 27. Surface coverage of adsorbed water on TiO_2 particles reported by previous studies. Solid curve: Goodman et al.;[250] squares: Ketteler et al.;[241] dashed curve: Ma et al.[269]

In addition, AP-XPS was also used to study water adsorption on the rutile single crystal surface(110).[241] The AP-XPS measurement suggested that 2 and 3 monolayers of adsorbed water are found at 12% and 25%,[241] and the surface coverage is higher than those reported Goodman et al.[250] and Ma et al.[269] However, it may not be directly comparable because Ketteler et al.[241] used single crystals while P25 TiO_2 particles were used by the other two studies.[250,269] Many previous studies have investigated water adsorption on rutile and anatase singles crystals, as summarized by Chen et al.[155] Since those studies are not of direct atmospheric relevance, they are not further discussed.

4.7.2 Al_2O_3

Transmission FTIR was used to study water adsorption on α-Al_2O_3 particles,[250] and it was suggested that the surface coverage of adsorbed water can be fitted with the modified three-

parameter BET equation with *n* equal to 8 and *c* equal to 25.2. Transmission FTIR was also used to investigate water adsorption on α-Al_2O_3 single crystals;[240] this work is of less atmospheric relevance and thus not further discussed. Water adsorption on α-Al_2O_3 particles was further investigated by Schuttlefield et al.[249] using ATR-FTIR and QCM, and the amount of adsorbed water at different RH was reported. Ma et al.[269] used DRIFTS to measure the amount of water adsorbed on α-Al_2O_3 particles, and suggested that its surface coverage can be described by a modified three-parameter BET equation, with *n* equal to 15.4 and *c* equal to 9.66. In addition, PSA was used by Ma et al.[212] to measure water adsorbed on α-Al_2O_3, and it was shown that one monolayer adsorbed water is formed at ~20% RH.

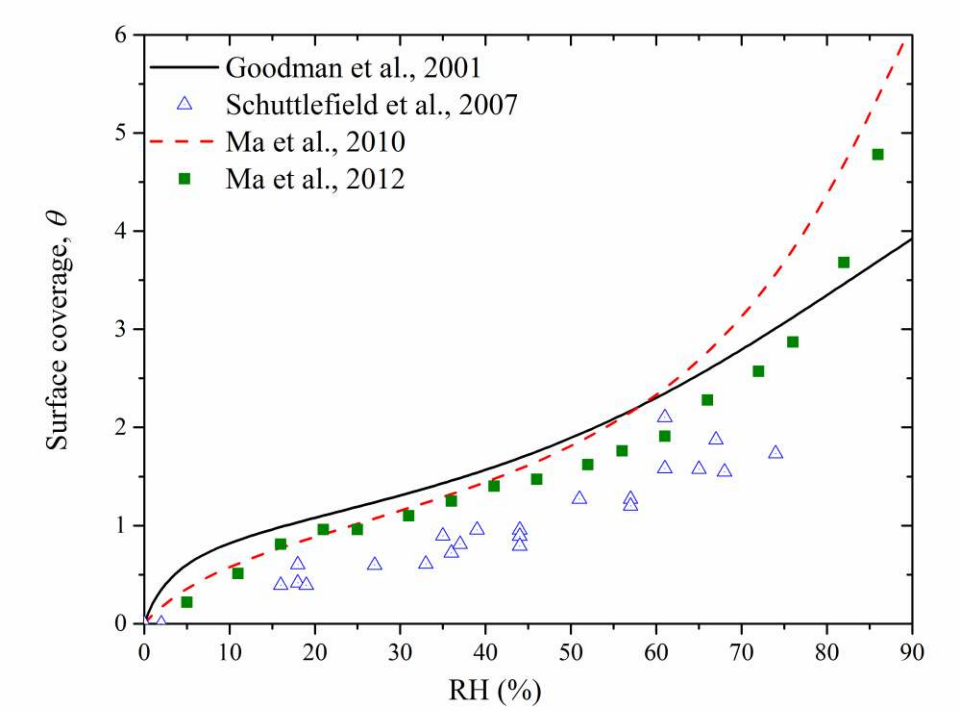

Figure 28. Comparison of surface coverage of adsorbed water on α-Al_2O_3 at different RH, as reported in previous studies. Solid curve: Goodman et al.;[250] dashed curve: Ma et al.;[269] squares: Ma et al.;[212] triangles: chuttlefield et al.[249]

Surface coverages of adsorbed water on α-Al_2O_3, as measured by these four different studies, are displayed together in Figure 28 as a function of RH. As evident in Figure 28, in general different

studies show good agreement, though different methods have been used to quantify the amount of water adsorbed on the particle surface. A close inspection also reveals that for RH > 80%, the discrepancy between Goodman et al.[250] and Ma et al.[212,269] may increase. This may suggest that experimental uncertainties increase with RH.

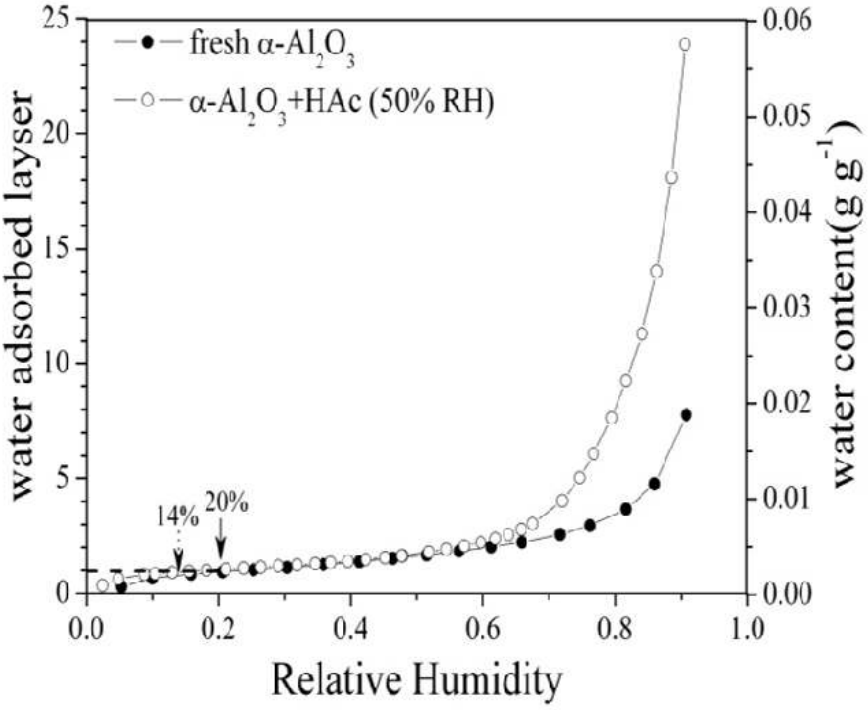

Figure 29. Amounts of water adsorbed on α-Al_2O_3 particles before and after heterogeneous reaction with gaseous acetic acid. Reprinted with permission from ref 212. Copyright 2012 the PCCP Owner Societies.

Heterogeneous reactions can change the hygroscopicity of α-Al_2O_3. For example, Ma et al.[212] measured the amount of water adsorbed on α-Al_2O_3 before and after reaction with acetic acid. As shown in Figure 29, it was found that the RH required to form one monolayer of adsorbed water decreased from ~20% to 14% after the reaction with acetic acid.[212] In addition, at 90% RH the amount of water adsorbed on the surface increased from 1.7% (by mass) for fresh particles to 5.2% (by mass) for reacted particles.[212] The study by Ma et al.[212] suggests that heterogeneous reaction

with acetic acid increases the hygroscopicity of α-Al_2O_3 particles. In contract, another study by Rubasinghege et al.[386] found that exposure to formic acid could largely reduce the amount of water adsorbed by γ-Al_2O_3.

4.7.3 Fe_2O_3

Water adsorption on Fe_2O_3 was investigated by transmission FTIR [250] and DRIFTS [269] respectively. Both studies suggest that the surface coverage of adsorbed water can be described by a modified three-parameter BET equation, with *n* and *c* equal to 4 and 51.1 reported by Goodman et al.[250] and 11.3 and 4.68 derived by Ma et al.[269] As shown in Figure 30, the surface coverage of adsorbed water measured by Goodman et al.[250] is higher for RH < ~55% and lower for RH > ~55% than that measured by Ma et al.[269] In addition, the discrepancy between the two studies seems to increase with RH for RH > ~55%.

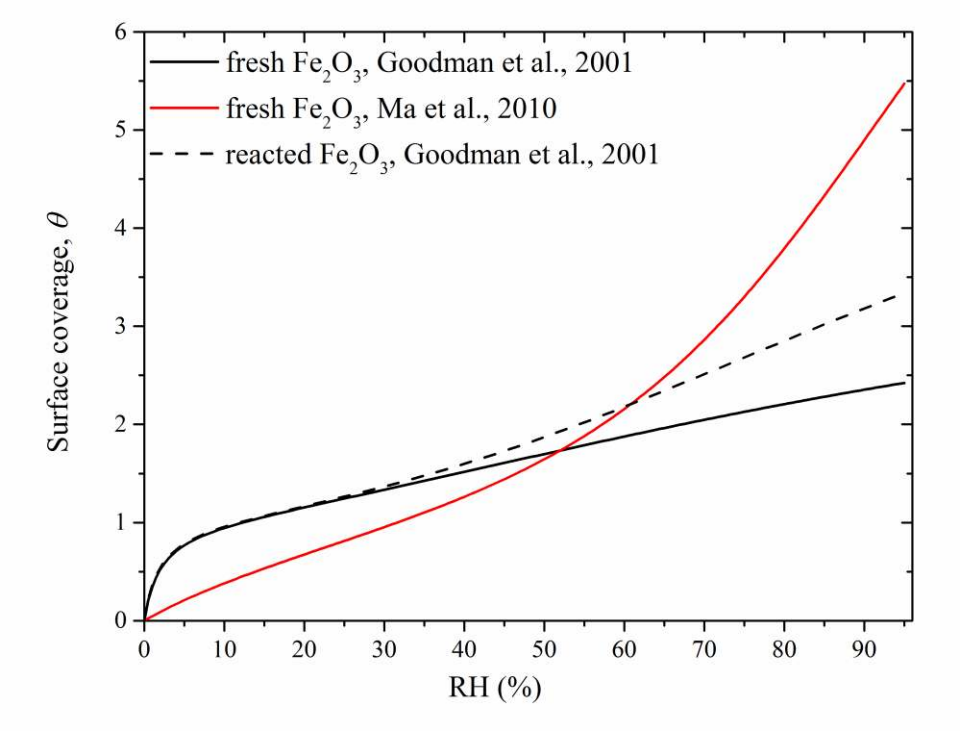

Figure 30. Surface coverages of adsorbed water on Fe_2O_3. Solid black curve: fresh particles measured by Goodman et al.;[250] dashed black curve: reacted particles measured by Goodman et al.;[250] solid red curve: fresh particles measured by Ma et al.[269]

In addition, Goodman et al.[250] found that the exposure to HNO_3 significantly increased the amount of water adsorbed by Fe_2O_3 particles, with n and c equal 6 and 55.3 for aged Fe_2O_3, compared to 4 and 51.1, respectively, for fresh Fe_2O_3.

4.8 Authentic complex dust mixture

Water adsorption properties, hygroscopicity, and CCN activity of a variety of authentic dust samples have been investigated in the last two decades, and Table 11 provides a quick overview of these studies. Arizona Test Dust is also an authentic dust sample; however, it has been separately discussed in Section 4.2 because it has been extensively studied and is often used as a dust standard. A direct comparison between different studies is difficult, because dust particles, even if they have

the same name (for examples, Saharan dust), may be collected from different locations and thus their compositions may show large variations.

Table 11. Water adsorption, hygroscopicity, and CCN activity of authentic dust particles: summary of previous studies.

reference	techniques	dust
Seisel et al., 2004 [298]	Knudsen cell	Saharan dust
Seisel et al., 2005 [299]	Knudsen cell	Saharan dust
Koehler et al., 2007 [387]	H-TDMA and CCNc	Owens (dry) Lake dust
Koehler et al., 2009 [46]	H-TDMA and CCNc	Canary Islands dust, Cairo dust
Herich et al., 2009 [49]	H-TDMA and CCNc	Saharan dust, Chinese dust
Navea et al., 2010 [246]	ATR-FTIR and QCM	Saharan dust, China loess
Yamashita et al., 2011 [376]	CCNc	Asian mineral dust
Kumar et al., 2011 [262]	CCNc	Niger dust, and five different East Asian dust
Kumar et al., 2011 [263]	CCNc	Niger dust, and five different East Asian dust
Ma et al., 2012 [182]	DRIFTS	Asian dust

Using a Knudsen cell reactor coupled to a mass spectrometer, Seisel et al.[298,299] measured the uptake of water vapor by Saharan dust particles over 203-298 K, and the initial uptake coefficient was determined to be $(6.3\pm0.7)\times10^{-2}$, independent of temperature. Yamashita et al.[376] studied the CCN activity of dry-generated Asian mineral dust particles, and reported an average κ of 0.014. Ma et al.[182] collected Asian dust particles in Beijing during a dust storm event, and measured the water adsorption by these dust particles at different RH before and after heterogeneous reaction with SO_2. They [182] found that ~8 monolayers of adsorbed water were found at 90% RH, and that the reaction with SO_2 did not significantly change the hygroscopicity of Asian dust particles they collected.

Koehler et al.[387] measured the hygroscopicity and CCN activity of dust particles collected from Owens Lake region (California, USA), using H-TDMA and CCNc. They [387] found that 35% of the dry-generated particles are very hygroscopic with an average κ of 0.69 and the other 65% are much less hygroscopic with an average κ of ~0.05. Koehler et al.[46] also investigated the hygroscopicity and CCN activity of two North African dust samples: one from the Canary Islands and the other one from outside Cairo. It is suggested that the CCN activity of these dust particles can be represented using the single hygroscopicity parameter of $0.01 < \kappa < 0.08$.[46] In addition, wet-generated Canary Islands dust and Cairo dust were found to be much more hygroscopic, with κ equal to 0.26 and 0.7,[46] suggesting that wet-generation may artificially enhance the hygroscopicity and CCN activity of dust particles.

Using H-TDMA and CCNc, Herich et al.[49] investigated the hygroscopicity and CCN activity of Saharan dust and Chinese dust. Dust aerosol particles were produced by both dry- and wet-generation, and it was found that wet generation could significantly increase the CCN activity of dust particles.[49] The single hygroscopicity parameter, κ, was found to be 0.023 for dry-generated Saharan dust and 0.007 for dry-generated Chinese dust.[49] In addition, Herich et al.[49] found that κ derived from H-TDMA measurement may be smaller than those derived from CCNc measurement; nevertheless, the difference may be within the experimental uncertainties.

QCM was used to study water adsorption on Saharan dust and China Loess at room temperature and at different RH.[246] The results are displayed in Figure 31, suggesting that both Saharan dust and China loess can adsorb substantial amount of water.[246] In addition, it appears that the two samples show somewhat similar water uptake capacities on a per mass basis, although their chemical compositions based on the XPS, SEM-EDX, and ATR-FTIR analyses show large differences.[246]

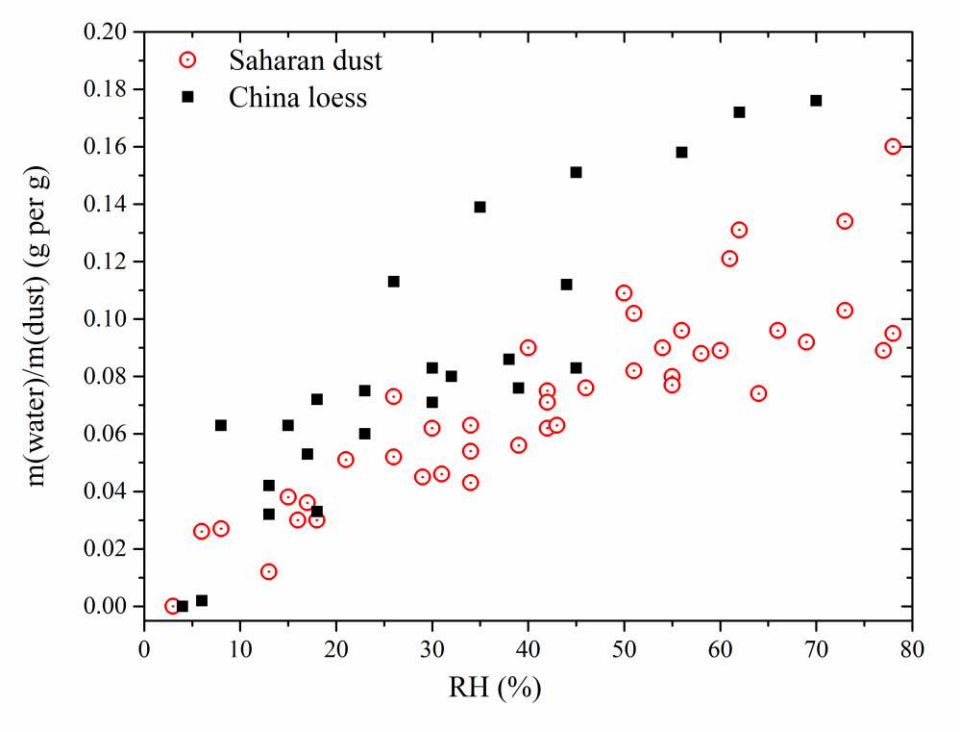

Figure 31. The amounts of water adsorbed by Saharan dust (red circles) and China loess (black squares) at room temperature and at different RH, as measured by Navea et al.[246]

Kumar et al.[262] investigated the CCN activity of six different types of dust particles, one collected from Niger (Sahel) and the other five collected from different locations in East Asian deserts. It was suggested that the FHH adsorption activation theory could better describe the CCN activation of these dry-generated dust aerosol particles,[262] compared to the κ-Köhler activation theory. The measured CCN activity of all the dust particles can be represented by one set of FHH parameters with A_{FHH} equal to ~2.25±0.75 and B_{FHH} equal to ~1.20±0.10.[262] Kumar et al.[263] also measured the CCN activity of wet-generated aerosol particles for these six types of dust, and found that κ for these wet-generated dust aerosol particles varies in the range of 0.14-0.44.[263] It was also suggested that wet-generation can lead to enhancement of the measured CCN activity of dust particles, compared to dry generation.[262,263]

4.9 Theoretical studies on water adsorption on mineral dust surface

There have been several theoretical studies focused on adsorption of gas phase water on mineral surfaces. These studies include but are not limited to calcite,[388-390] kaolinite,[391-395] montmorillonite,[377,396,397] quartz,[398,399] titanium dioxide,[400-402] and FeOOH.[275,403,404] In this review we do not provide a comprehensive review of these studies, but instead we highlight a few these. In particular, we highlight several theoretical studies which have significantly improved our understanding of water adsorption on mineral dust particles of atmospheric relevance at a fundamental level. This discussion is limited to four representative components contained by mineral dust aerosol particles in the troposphere. These components are representative of carbonate minerals (calcite), clay minerals (kaolinite and montmorillonite), and oxide minerals (quartz). A recent review paper [155] summarized some theoretical work for water adsorption on TiO_2(110) surface. In general, it appears that it is non-trivial for theoretical studies to quantitatively predict the amount of water adsorbed by mineral surfaces as a function of RH. However, insights into fundamental processes involved in water-mineral interactions can be gained from these theoretical studies. Recently Gerber et al.[405] provided several excellent examples to illustrate how theoretical studies could help us understand atmospherically relevant chemical reactions at various interfaces/surfaces.

4.9.1 Calcium carbonate

Using molecular dynamics simulations, de Leeuw and Parker [388] investigated the effect of water adsorption on the surface structures and energetics for several different planar calcite surfaces. They found that physisorption of water is energetically favourable for all the planar surfaces, among which the (1014) surface is most stable.[388] Kerist and Parker [406] calculated the free energy of water adsorption on the (1014) calcite surface using molecular dynamics simulations. Their simulations [406] suggested that the free energy of water adsorption is smaller than the enthalpy, indicating that there is a large change in entropy associated with water adsorption on the surface.

Additionally, ab-initio calculations by Kerisit et al.[389] were used to predict the surface phase diagram for the (1014) calcite surface, and they [389] suggested that nonstoichiometric surfaces can be important in determining the chemistry of calcite at high RH.

Rahaman et al.[390] developed a molecular dynamics scheme to study the dynamics of water adsorption on the (1014) calcite surface at different RH. They [390] found that the timescale for the surface to become in equilibrium with the environment is of several nanoseconds, and predicted that water adsorption on the surface would follow a BET-like isotherm. They [390] also suggested that mobility of adsorbed water is enhanced at higher RH, and that at lower RH adsorbed water is more tightly bound to the surface.

4.9.2 Kaolinite

Previous theoretical studies on water adsorption on kaolinite, for example, by Hu and Michaelides,[407-409] mostly focused on the Al-terminated(001) and Si-terminated(001) surfaces. Croteau et al.[392-395] used grand canonical Monte Carlo simulations to investigate adsorption and structure of water on kaolinite surfaces. They [392] found that at 235 K, the Si-surface is hydrophobic and does not display potential to adsorb water when RH is less than 100%, and adsorption on the Al-surface exhibits first-order characteristics. More importantly, they [392] suggested that adsorption on edges, dominated by strong water-surface interactions, is much more continuous and contributes significantly to water uptake by kaolinite.

In a following study, Croteau et al.[393] further investigated water adsorbed on four different surfaces (the Al-terminated surface, the Si-terminated surface, and two edge-like surfaces) of kaolinite at different RH and at two different temperatures (235 and 298 K), using Monte Carlo simulations. Several conclusions have been drawn from their simulations:[393] i) the Si-terminated surface does not uptake significant amount of water, and the Al-terminated surface and the two edge-like

surfaces can adsorb monolayers of water for RH below 100%; ii) the edge-like surfaces have the largest affinity for water; iii) water adsorption on the edge-like surfaces grows continuously until one monolayer is reached, while on the Al-surface the formation of one monolayer adsorbed water appears as a sharp transition (this also indicates that collective behavior occurs among water molecules on the Al-surface but not on the edges) and practically there is no submonolayer adsorption. This suggests that mechanisms of water adsorption on the Al-surface and the edge-like surfaces are distinctively different.[393]

The two previous studies carried out by Croteau et al.[392,393] used atomistically smooth kaolinite surfaces in these simulations, and their predicted surface coverages of adsorbed water are much lower than those experimentally measured by Schuttlefield et al.[249] In an effort to explain the experimental results, Croteau et al.[395] further performed water adsorption simulations at 296 K on kaolinite surfaces which contain trenchlike structures. The structures of different trenches considered by Croteau et al.[395] are shown in Figure 32.

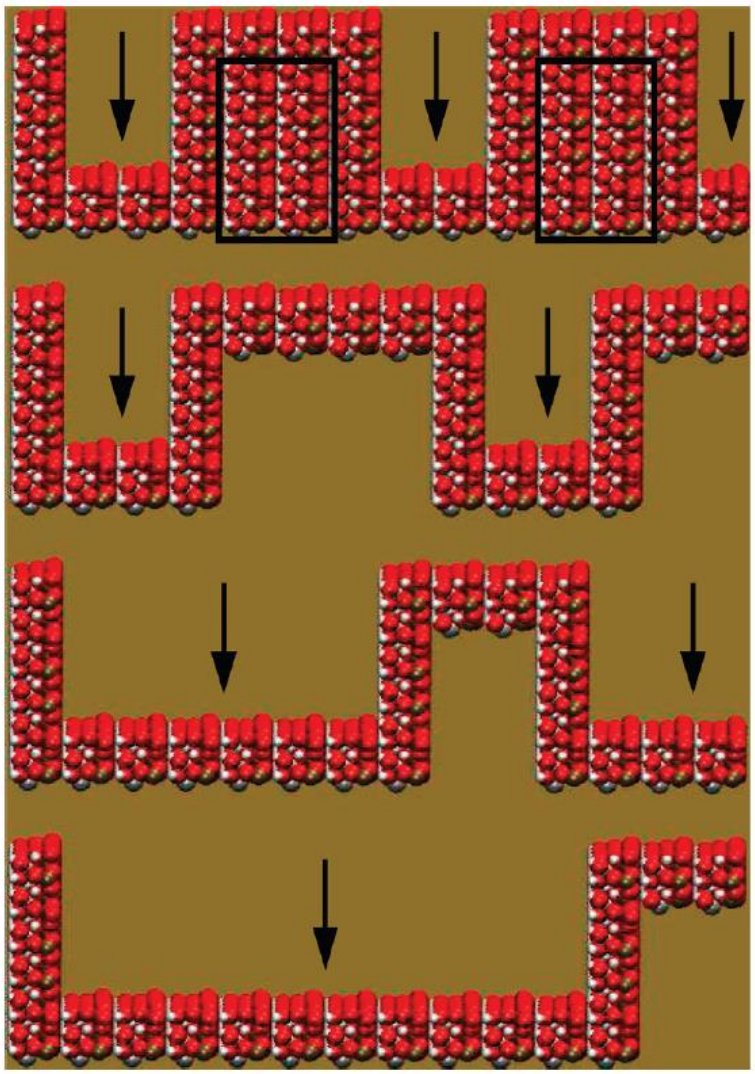

Figure 32. The structures of different trenches on kaolinite surfaces considered by Croteau et al.[395] in their simulations. O, H, Al, and Si atoms are in red, white, gray, and brown. From top to bottom, the trenches are refered as 1, 2, 3, and 4, with trend widths of 14.78, 14.78, 44.34, and 73.91 Å, respectively. Simulations were carried out for trench 1 without (1A) and with (1B) intertrench spacing filled (atoms inside the black rectangle). Black arrows indicate where the trenches are. Reprinted from permission from ref 395. Copyright 2010 American Chemical Society.

Simulated water adsorption on kaolinite surfaces with different trenches at 298 K are shown in Figure 33 as a function of RH. Compared to that for an atomistically smooth edge-like surface, it was found that the amount of adsorbed water is largely increased for surfaces with all the different

trenches.[395] The study by Croteau et al.[395] suggests that surface trenches (and very likely other surface defects) may have strong affinity for water and thus can adsorb multilayers of water. The amounts of adsorbed water on kaolinite predicted by Croteau et al.[395] as a function of RH are on the same order of magnitude as those measured by Hung et al.,[270] but appear to be significantly smaller than those measured by Schuttlefield et al.[249] and Hatch et al.[348]

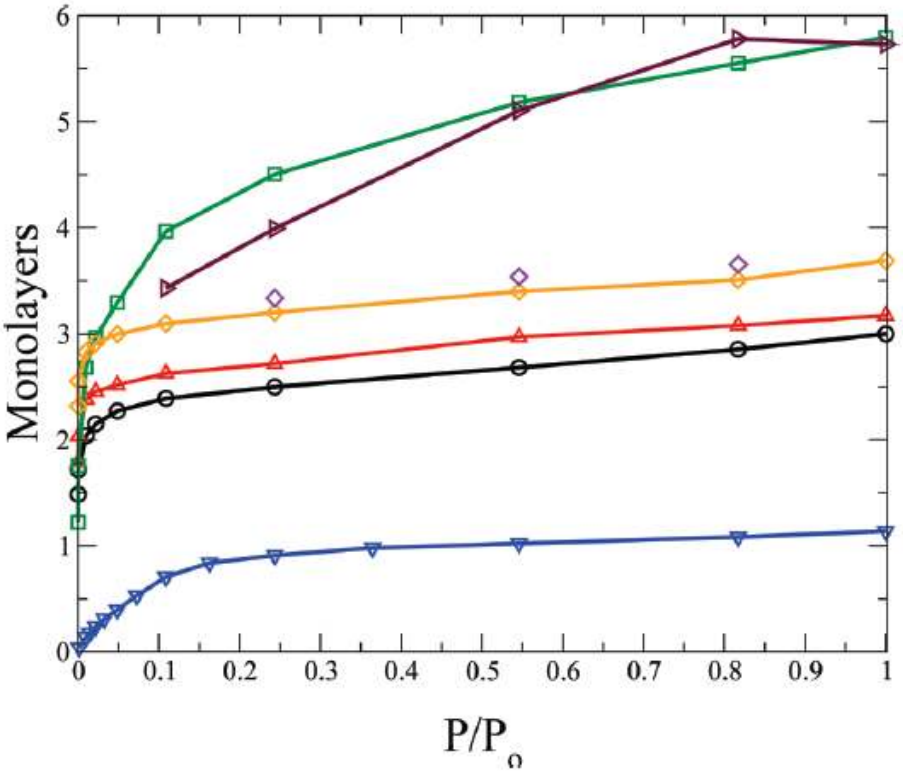

Figure 33. Simulated surface coverages of adsorbed water on an atomistically smooth edge kaolinite surface (blue triangles) and kaolinite surfaces containing different types of trenches as a function of RH (P/P_0, defined as the ratio of partial pressure of water vapor to the saturated vapor pressure of water) at 298 K. Blue triangles: atomistically smooth edge-like surface; red triangles: trenches 1A; orange diamonds: trenches 1B; black circles: trenches 2; green squares: trenches 3; maroon triangles: trenches 4. Trench structures are given in Figure 32. Reprinted from permission from ref 395. Copyright 2010 American Chemical Society.

4.9.3 Montmorillonite

Hensen et al.[396] combined molecular dynamics and Monte Carlo simulations to investigate water adsorption by Li-, Na-, and K-montmorillonite. It is found that water adsorption by these montmorillonite occurs via two mechanism:[396] 1) at low RH, water adsorption is driven by hydration of interlayer counterions, and the extent of water adsorption increases with cation-H_2O hydration energy ($Li^+ > Na^+ > K^+$); 2) at high RH, water molecules are adsorbed near mineral surface, coordinating to the structural OH groups. This enables the formation of an extensive hydrogen bonding network and therefore leads to a sharp increase of adsorbed water with RH.[396]

In a following theoretical study, Hensen and Smit [377] was able to quantitatively predict the amount of water adsorbed by Na-montmorillonite as a function of RH. In addition, their simulations [377] suggested that montmorillonite swelling occurs by migration of counterions (which are initially strongly bound to clay surface) to positions in the clay interlayers where these ions can be fully hydrated.

4.9.4 Quartz

Several review articles [410,411] and books [412,413] have summarized theoretical studies on the interaction of water with silica surfaces, especially for liquid water-quartz interactions. Interested readers are referred to these publications for more information. Density functional theory based molecular dynamics simulations were used by Sulpiz et al.[414] to understand the molecular behavior of quartz-water interface. They [414] suggested that two types of silanol groups exist at the quartz surface: i) out-of-plane silanols with a pKa of 5.6, forming strong and short H-bonds with interfacial water molecules, giving rise to highly correlated hydrogen-bonding network and thus exhibiting a band at ~3200 cm^{-1} in the sum frequency generation (SFG) spectroscopy.[415-417] For simplicity, these water molecules are also referred to as the "ice-like" water because of their similarity in structure to water molecules in bulk ice;[418] ii) in-plane silanols with a pKa of 8.5,

1814 forming weak hydrogen bonds with interfacial water molecules and showing a broad band at ~3400
1815 cm^{-1} in the SFG spectrum.[415-417] Intensity in this region corresponds with OH stretch intensities of
1816 bulk liquid water, and therefore for simplicity these water molecules are sometimes referred to as
1817 "liquid-like" water.[418]
1818
1819 Recently Murdachaew et al.[399] used initio molecular dynamics to study the adsorption of HCl on
1820 the hydroxylated α-quartz (0001) surface, and observed that adsorbed HCl is rapidly dissociated
1821 and ionized on wetted surface at temperatures between 250 and 300 K. Ionization of adsorbed HCl
1822 seems to be enhanced by lattice mismatch between the silica and water layer.[399] The dissociation
1823 and ionization of HCl on SiO_2 surface has several important implications for atmospheric
1824 chemistry. For example, it lowers the pH for silica surface and leads to the charging and
1825 disordering of adsorbed water.[399] These changes could significantly impact chemical processes on
1826 silica surfaces.[399]

1827 **4.10 Chemical aging modifies the interaction of water vapor with mineral dust**
1828 **particles: results from field measurements**

1829 As summarized in previous sections, numerous laboratory studies have suggested that atmospheric
1830 heterogeneous reactions could substantially increase the water adsorption ability, hygroscopicity,
1831 and CCN activity of mineral dust particles. Very frequently tropospheric dust aerosol particles
1832 have been observed to be internally mixed with nitrate, sulfate, chloride, and organic
1833 compounds.[158,159,162,202,206,419-425] [158,159,162,202,206,419-425] More importantly, the effect of atmospheric
1834 aging processes has also been supported by increasing evidence from field measurements. Instead
1835 of providing an exhaustive literature survey, here we highlight some important findings from field
1836 measurements to provide evidence if atmospheric chemical transformation could influence the
1837 interaction of mineral dust particles with water vapor. Tables 12 summarizes the major findings of
1838 field studies which are discussed in the section. A recent review paper by Li et al.[426] summarized

single particle studies on the changes in chemical compositions, morphology, and hygroscopicity of aerosol particles (including mineral dust) collected in East Asia.

1841 **Table 12.** Field measurements of water adsorption, hygrsoscopicity, and CCN activity of mineral dust aerosol particles: summary of major findings

1842 from previous studied included in this review.

reference	Location	major findings
Perry et al., 2004 [427]	Trinidad Head, California, USA	Elemental (Al, Si, and Fe) mass distributions all shifted toward smaller sizes as RH was reduced, indicating that mineral dust particles transported from Asia to the west coast of the United States is somewhat more hygroscopic upon its arrival.
Laskin et al., 2005 [245]	Shoresh, Israel	In agreement with laboratory studies, it was shown that solid nonspherical calcium carbonate particles were converted to spherical liquid droplets which contain $Ca(NO_3)_2$, due to heterogeneous reactions with HNO_3.
Matsuki et al., 2005 [159]	Beijing, China	Some Ca-rich dust particle are spherical under humid conditions, due to the formation of nitrate and sulfate on these particles.
Massling et al. 2007 [428]	off the coasts of Japan, Korea, and China	For all continentally influenced air masses, 1 μm particles can be classified as two groups according to their hygroscopic growth factors at 90% RH: one with growth factors of around 1.0 (representative of dust particles) and the other one with a growth factors of ~2(representative of sea spray particles).
Shi et al., 2008 [429]	southwestern Japan	Nitrate free dust particle, even though they may contain sulfate, did not change their morphology when RH was increased from 15% to 90%; however, dust particles containing nitrate became aqueous droplets even at 15% RH.
Crumeyrolle et al., 2008 [430]	Banizoumbou, Niger	Cloud processing during a mesoscale convective system may enhance the formation of soluble materials associated with dust particles and therefore enhance their CCN activity.
Tobo et al., 2009,[431] Tobo et al., 2010 [432]	Kanazawa, Japan	Some Ca-rich particles contain substantial amount of chloride, and they existed in an amorphous state and were nearly spherical even under high vacuum.

Kim and Park, 2012 [433]	Gwangju, Korea	Dust aerosol particles transported to Korea exhibited enhanced hygroscopicity, compared to fresh aluminum silicate and calcium carbonate.
Begue et al., 2015 [267]	Cabauw, Netherlands	CCN activities of Saharan dust aerosol particles transported to Netherlands were significantly increased due to heterogeneous reactions with anthropogenic pollutants.
Denjean et al., 2015 [434]	Fajardo, Puerto Rico	Supermicron African dust particles, after being transported across the Atlantic in summertime, were largely unprocessed and did not show significant change in hygroscopic properties.

1843

1844

Laskin et al.[245] collected mineral dust particles at Shoresh, Israel, and analyzed the morphology and composition of individual dust particles using scanning electron microscopy with energy dispersive analysis of X-ray (SEM-EDX). For the first time, they [245] provided field evidence that due to heterogeneous reactions with HNO_3, solid nonspherical calcium carbonate particles were converted to spherical liquid droplets which contain $Ca(NO_3)_2$. This important finding has been supported by a number of following studies. For example, Matsuki et al.[159] collected Asian dust particles (>1 μm) in Beijing and analysed them using electron microscopy. As shown in Figure 34, Matsuki et al.[159] found that some Ca-rich dust particle are spherical under humid conditions, due to the formation of nitrate and sulfate on these particles.

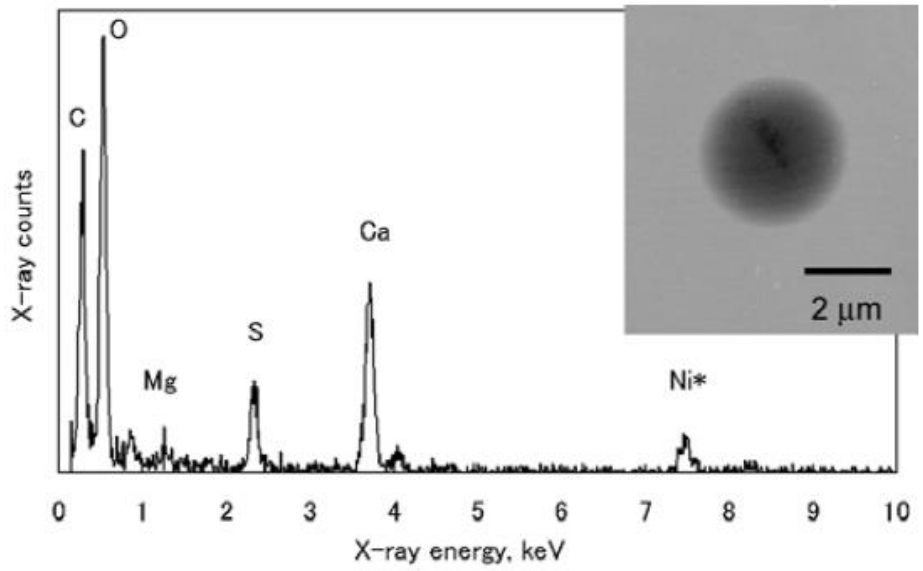

Figure 34. Electron micrograph and X-ray spectrum of a typical Ca-rich spherical particle collected in the boundary layer in Beijing. The signal of Ni in the X-ray spectrum was caused by the Ni-containing grids used to support the films on which particles were collected. Reprinted with permission from ref 159. Copyright 2005 John Wiley & Sons, Inc.

Asian dust particles (>1 μm) were also collected in Southwestern Japan after long-range transport and analyzed with environmental scanning electron microscopy.[429] It was found that nitrate free

dust particle, even though they may contain sulfate, did not change their morphology when RH was increased from 15% to 90%;[429] in contract, dust particles containing nitrate became aqueous droplets even at 15% RH.[429] This suggested that the formation of nitrate coating could substantially increase the hygroscopicity of dust particles, whereas the formation of sulfate did not.[429] This observation can be explained by the fact that $Ca(NO_3)_2$ is more hygroscopic than $CaSO_4$.[217,357]

Tobo et al.[431,432] collected Asian dust particles around Japan Islands and analyzed them by SEM-EDX. They [432] found that substantial amount of chloride was found on Ca-rich particles, and these particles existed in an amorphous state and were nearly spherical even under high vacuum. Consequently, Tobo et al.[432] proposed that in remote marine troposphere where the concentrations of reactive nitrogen species are typically very low, heterogeneous reactions with HCl can also significantly change the composition and thus hygroscopicity of dust particles.

In another study, Asian dust particles were collected in Trinidad Head (California, USA) after long-range transport during three significant dust episodes.[427] Two impactors were used in parallel, one maintained at ambient RH and the other one maintained at a lower RH of 55%.[427] Elemental analysis of collected samples using synchrotron X-ray fluorescence suggested that the elemental (Al, Si, and Fe) mass distributions all shifted toward smaller sizes as the RH was reduced.[427] This may indicate that mineral dust particles transported from Asia to the west coast of the United States is somewhat more hygroscopic upon its arrival, and it was tentatively attributed to the formation of sulfate coatings on dust particles.[427]

Most of studies which investigated the hygroscopicity of ambient dust particles require collection of dust particles followed by offline analysis. In an airborne field campaign in West African, aerosol properties in a layer between 1300 and 3000 m were measured during the passage of a

1887 mesoscale convective system (MCS).[430] After passage of the MCS, a significant increase in CCN
1888 fraction was observed together with higher contribution of sulfate, nitrate, and chloride to the total
1889 aerosol mass.[430] A mesoscale model was used to interpret the results, and it was concluded that
1890 cloud processing during the MCS could enhance the formation of soluble materials associated with
1891 dust particles and therefore enhance their CCN activity.[430] In another study, Kim and Park [433]
1892 measured the hygroscopicity of Asian dust aerosol particles using a system similar to H-TDMA.
1893 They [433] found that dust aerosol particles transported to Korea exhibited enhanced hygroscopicity
1894 compared to fresh aluminum silicate and calcium carbonate, due to heterogeneous reactions and
1895 cloud processing. More recently, it is suggested that the CCN activity of Saharan dust aerosol
1896 particles transported to Netherlands were significantly increased due to heterogeneous reactions
1897 with anthropogenic pollutants.[267]
1898
1899 However, not all the field measurements conclude that after long-range transport in the troposphere,
1900 the hygroscopicity of mineral dust aerosol particles will be significantly enhanced. Massling et
1901 al.[428] measured the hygroscopic growth of 1 μm (dry diameter) particles off the coats of Japan,
1902 Korea, and China in spring 2001 during the ACE-Asia study. It is found that for all continentally
1903 influenced air masses, 1 μm particles can be classified as two groups according to their hygroscopic
1904 growth factors at 90% RH: one with growth factors of around 1.0 and the other one with a growth
1905 factors of ~2.[19,428 435,436]The first one was suggested to be representative of dust particles, and the
1906 second one appears to be similar to sea spray particles.[437] This study may indicate that the change
1907 in hygroscopicity of Asian dust particles after long-range transport can be very small, though lack
1908 of particle composition measurements makes it difficult to draw more convincing conclusions. A
1909 recent field campaign in Fajardo, Puerto Rico found that supermicron African dust particles, after
1910 being transported across the Atlantic in summertime, did not show significant change in
1911 hygroscopic properties.[434] Measurements of chemical composition suggest that most of mineral

dust was chemically unprocessed and externally mixed, and only a minor portion of mineral dust was internally mixed with sulfate and/and chloride.[434] In addition, Kaaden et al.[438] measured the hygroscopic growth of aerosol particles at Tinfou, Morocco, and found that particles larger than 720 nm were completely hydrophobic. The hygroscopic growth of aerosol particles at Cape Verde was investigated by Schladitz et al.,[439] who found that the κ value was almost 0 for particles with volume equivalent diameters of >250 nm. Both studies [438,439] seem to suggest that Saharan dust particles they detected are largely hydrophobic; nevertheless, both measurements are very close to source regions and therefore it is highly likely that those dust particles have not aged much in the atmosphere and my not have been exposed very much to acidic gases.

Discrepancies reported by the aforementioned field measurements of hygroscopicity of mineral dust particles may due to their different exposure histories (and thus the effective aging extents) and their variations in mineralogy. Several single particle studies [159,245,429,432,440] seem to indicate that the major components of hygroscopic aged dust particles could be carbonates (e.g., calcite and dolomite), which can undergo rapid reactions with acidic trace gases, leading to the formation of very hygroscopic salts, such as $Ca(NO_3)_2$ and $CaCl_2$. The only solid conclusion which can be drawn up to now is that some dust particles can be converted to aqueous droplets after long-range transport, but it is still unclear to which extent the hygroscopicity distribution of mineral dust aerosol particles will change during their residence time in the troposphere. In addition, there will be a very strong dependence on the mineralogy as noted above.

4.11 Summary

4.11.1 Fresh dust particles

Table 13 summarizes CCN activity, as represented by κ, of $CaCO_3$, ATD, illite, kaolinite, montmorillonite, and African and Asian dust particles reported in previous studies. Only studies using dry-generated aerosol particles are included, because wet-generation may enhance the CCN

activity of dust particles.[49,256,259,262,263] In order for simple and direct comparison, CCN activity measurements interpreted using the FHH adsorption activation theory are not included, but they have been discussed in previous subsections. Garimella et al.[259] provided an intercomparison of measured critical super-saturations as a function of particles diameter for several types of dry-generated mineral dust particles. H-TDMA measurements have also been used to derive κ; however, these measurements can be significantly influenced by the non-sphericity of dust particles. Therefore, Table 13 does not include H-TDMA measurements.

Table 13. Summary of single hygroscopicity parameter (κ) of $CaCO_3$, ATD, illite, kaolinite, montmorillonite, and African and Asian dust particles reported in previous studies. Only studies in which the CCN activity of dry-generated mineral aerosol particles were measured are included.

mineral	reported κ	reference
$CaCO_3$	0.0008-0.0018	Sullivan et al., 2010 [256]
	0.0019±0.0007	Zhao et al., 2010 [264]
	0.0013-0.0033	Tang et al., 2015 [357]
ATD	~0.025	Koehler et al., 2009 [46]
	~0.003	Herich et al., 2009 [49]
	0.002	Sullivan et al., 2010 [261]
	0.0042	Sullivan et al., 2010 [375]
	0.017	Yamashita et al., 2011 [376]
	0.0041	Garimella et al., 2014 [259]
illite	0.002-0.003	Herich et al., 2009 [49]
	0.0072	Garimella et al., 2014 [259]
kaolinite	~0.001	Herich et al., 2009 [49]
montmorillonite	~0.003	Herich et al., 2009 [49]
	0.0088	Garimella et al., 2014 [259]
North African dust	0.01-0.08	Koehler et al., 2009 [46]

Saharan dust	0.023	Herich et al., 2009 [49]
Chinese dust	0.007	Herich et al., 2009 [49]
Asian dust	0.014	Yamashita et al., 2011 [376]

1948

1949 κ values given in Table 13 reveal that there is fairly good agreement between previous studies. It
1950 appears that the CCN activity of $CaCO_3$, ATD, illite, kaolinite, and montmorillonite particles is
1951 very low and can be described with a κ value of less than 0.01. Authentic dust samples collected
1952 in Africa and Asia show somehow slightly higher κ value, probably because those samples contain
1953 more soluble components which increase their CCN activity.

1954

1955 In this section, we have compared measurements carried out under sub-saturation conditions using
1956 particles supported on substrates and those using aerosol particles performed under sub- and super-
1957 saturations conditions. Despite experimental and theoretical issues which can make such
1958 comparisons difficult (as discussed in Sections 2-3), reasonably good agreement has been found
1959 for $CaCO_3$, SiO_2, TiO_2 , Al_2O_3, and Fe_2O_3. On the other hand, as discussed in Sections 4.2-4.5,
1960 large discrepancies exist between studies using aerosol particles and those using particles
1961 supported on substrates for ATD, illite, kaolinite, and montmorillonite, and surface coverages of
1962 adsorbed water interpreted from measurements using aerosol particles are much lower. Even
1963 among studies which used very similar sample preparation methods and experimental techniques,
1964 significant disagreement are also observed for some clay minerals, with illite as an example shown
1965 in Figure 18b.

1966

1967 In experiments in which particles were supported on substrates, normally a slurry of dust particles
1968 in a solvent (e.g., water, methanol, or ethanol) was deposited on the supporting substrates to form
1969 a film. We speculate that though this type of sample preparation methods may not lead to

substantial change in physicochemical properties for relative simple minerals such as Al_2O_3 and SiO_2, it has the potential to cause some artifacts for clays and authentic dust samples. The effects of different sample preparation menthods needs to be carefully and systematically examined in future studies.

The interactions of mineral dust particles with water vapor at temperatures above the onset of ice nucleation can influence their heterogeneous reactivity, hygroscopic growth, and CCN activity; therefore, a better understanding of these interactions is very important. Efforts are required to reduce the existing large discrepancies among different studies. In a well-coordinated collaboration, same mineral dust samples can be distributed to different groups which may use a variety of experimental techniques to study their interactions with water vapor, and reported results can be directly compared in order to find out the advantages and limitations of different experiment techniques. Very recently a similar campaign has been successfully carried out to investigate the ice nucleation activity of illite particles,[441] and similar actions will also definitely be beneficial for investigation of water adsorption, hygroscopicity, and CCN activity of mineral dust particles.

Compared to the κ-Köhler theory, the FHH theory is less used to interpret the hygroscopic growth and CCN activity of mineral dust particles. The two FHH parameters (A_{FHH} and B_{FHH}) reported for mineral dust particles, are compiled in Table 14. Direct comparison of hygroscopicity or CCN activity from the two FHH parameters is difficult, and interested readers can calculate the surface coverage of adsorbed water as a function of RH, using Eqs. (10) or (20).

1991 **Table 14.** Summary of A_{FHH} and B_{FHH} parameteres of mineral dust particles reported in the literature.

mineral	sample preparation method	A_{FHH}	B_{FHH}	reference
$CaCO_3$	dry-generated aerosol particles	3.00±0.04	1.30±0.03	Kumar et al., 2011 [262]
	wet-generated aerosol particles	1.74	1.22	Kumar et al., 2011 [263]
ATD	dry-generated aerosol particles	2.96±0.03	1.28±0.03	Kumar et al., 2011 [262]
illite	dry-generated aerosol particles	1.02±0.38	1.12±0.04	Kumar et al., 2011 [262]
	wet-generated aerosol particles	3.00	1.27	Kumar et al., 2011 [263]
	particles supported on substrates	75±17	1.77±0.11	Hatch et al., 2014 [348]
kaolinite	particles supported on substrates	1.70	2.25	Hung et al., 2015 [270]
montmorillonite	dry-generated aerosol particles [a]	2.06±0.72	1.23±0.04	Kumar et al., 2011 [262]
	dry-generated aerosol particles [b]	1.23±0.31	1.08±0.03	Kumar et al., 2011 [262]
	wet-generated aerosol particles [a]	1.09	1.04	Kumar et al., 2011 [263]
	wet-generated aerosol particles [b]	0.87	1.00	Kumar et al., 2011 [263]
	particles supported on substrates	98±22	1.79±0.11	Hatch et al., 2014 [348]
	particles supported on substrates	1.25	1.33	Hung et al., 2015 [270]
SiO_2	dry-generated aerosol particles	2.95±0.05	1.36±0.03	Kumar et al., 2011 [262]

1992

1993 [a]: Ca-montmorillonite; [b]: Na-montmorillonite

It is noteworthy that most of the previous measurements have only been performed at around room temperature, near 295 K. However, the relevant temperatures in the troposphere range approximately from 200 to 300 K, and mineral dust particles mainly exist in the free troposphere where the temperature is much lower than room temperature. Therefore, the effects of temperature on the water adsorption, hygroscopicity, and CCN activity of mineral dust particles, which have been seldom examined, deserve further investigation.

4.11.2 Aged dust particles

Due to numerous studies over the last 1-2 decades, it is widely recognized that heterogeneous reactions, mostly through the formation of more soluble materials (although sometimes insoluble compounds can also be formed), can lead to significant enhancement of water adsorption, hygroscopicity, and CCN activity of mineral dust particles. Nevertheless, most of previous studies are either rather qualitative or their direct atmospheric relevance is lacking. Further research, which are carried out at atmospherically relevant conditions to quantitatively understand the effects of atmospheric chemical transformation, will be very helpful.

Most of previous studies on the atmospheric aging effects focuses on $CaCO_3$, probably the most reactive mineral contained by tropospheric dust aerosol particles. It is recommended that future studies should also examine the effect of aging processes for more abundant clay minerals and authentic dust samples which have more direct relevance for tropospheric dust aerosol particles.

5 Effects of chemical aging on ice nucleation activity of mineral dust particles

The formation of ice crystals in clouds is of particular scientific interest, because more than 50% of the global precipitation is initiated via the ice phase.[442] Ice formation may occur in clouds through both homogeneous and heterogeneous ice nucleation. Different ice nucleation mechanisms are depicted in Figure 35.[443] Homogeneous ice nucleation requires the temperature to be lower than -36 ^{o}C,[167,444] while heterogeneous ice nucleation can occur at higher

temperature.[167,445,446] Heterogeneous ice nucleation can be classified into four modes:[167] 1) deposition nucleation, which occurs on particles in the absence of the formation of liquid water (below water saturation); 2 and 3) condensation freezing and immersion freezing: ice formation occurs either during the simultaneous action of IN as CCN (condensation freezing) or during the subsequent lifting and cooling of cloud droplets containing insoluble particles (immersion freezing), 4) contact freezing, which occurs via collisions of particles with supercooled cloud droplets.

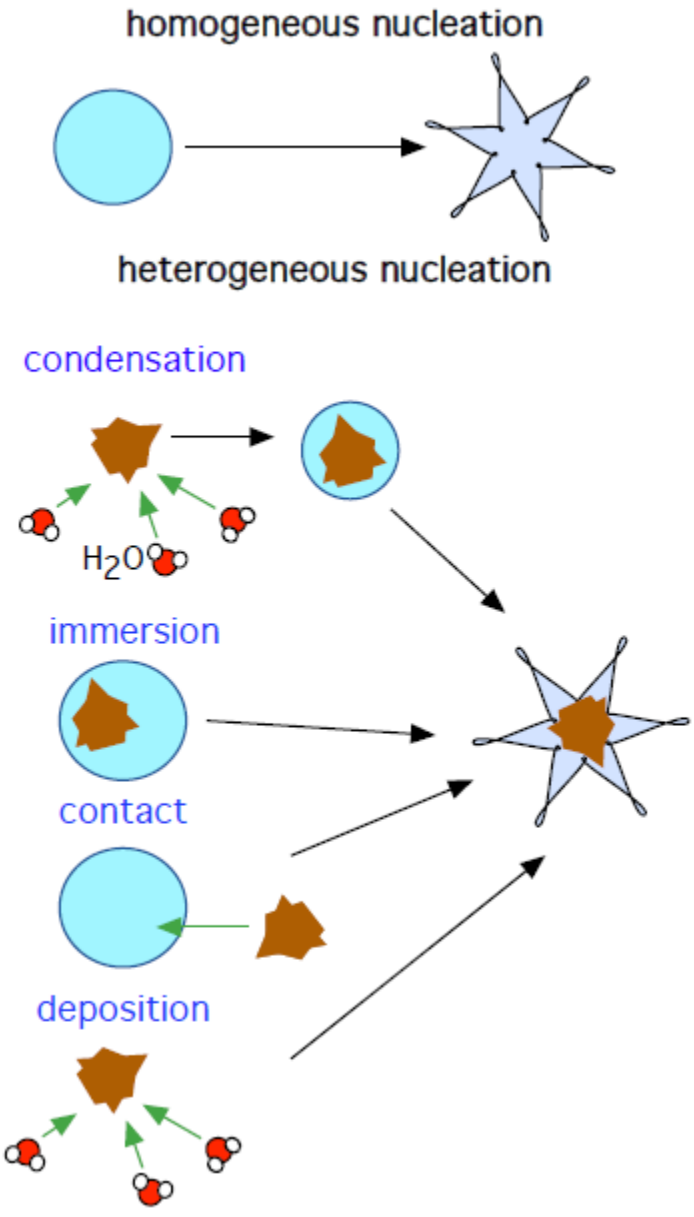

Figure 35. Illustration of homogeneous nucleation and heterogeneous nucleation mechanisms. Heterogeneous nucleation can occur via deposition nucleation, concensation freezing, immeriosn freezing, and contact freezing.Reprinted with permission from ref 443 by Freedman. Copyright 2011 American Chemical Society.

Mineral dust particles may be the most abundant IN in the troposphere,[58,74,75] and the ice nucleation activity of fresh mineral dust particles (and also other types of aerosol particles) has been recently discussed in several excellent review papers.[140,167,237,238,447,448] In the last several years, numerous laboratory studies have suggested that atmospheric aging processes can substantially change the ice nucleation activity of mineral dust particles, as will be discussed here. Hoose and Möhler [238] briefly summarized the effect of atmospheric chemical reactions on the IN activity of mineral dust particles and below we expand on this discussion.

The impacts of change in IN activity due to atmospheric aging processes have been supported by several modeling studies. For example, using parameterizations based on their laboratory measurements, Kulkarni et al.[449] simulated the influence of particle coatings on the ice crystal number concentration and the ice water content in clouds over the Southern Great Plain (SGP) site near Lamont, Oklahoma, USA. As shown in Figure 36a, under water sub-saturation conditions where only deposition nucleation is possible, the modeled monthly mean ice crystal number for the coated case (aged dust particles) was about one order of magnitude lower than the uncoated case (fresh dust particles).[449] Under water super-saturation conditions (Figure 36b), both the simulated ice crystal number and ice water content are higher in the uncoated case than in the coated case;[449] the difference between them in regions with pressure <600 hPa is significantly smaller,[449] and this is partly due to that the difference between the IN activity of uncoated and coated dust particles (illite in this case) is smaller at lower temperatures.[449] Girard et al.[450] used the

Global Multiscale Environmental Model to assess the potential influence of acid coatings on cloud and radiation processes in the Arctic during January and February 2007. Their modeling results [450] suggest that acid coating on dust particles may have significant impacts on cloud microphysics and radiation over the Central Arctic. More specifically, modification in the cloud microstructures, due to acid coating, could change the radiation at the top of the atmosphere by 0 and -6 W m^{-2} over the region which is covered by the Arctic air masses.[450]

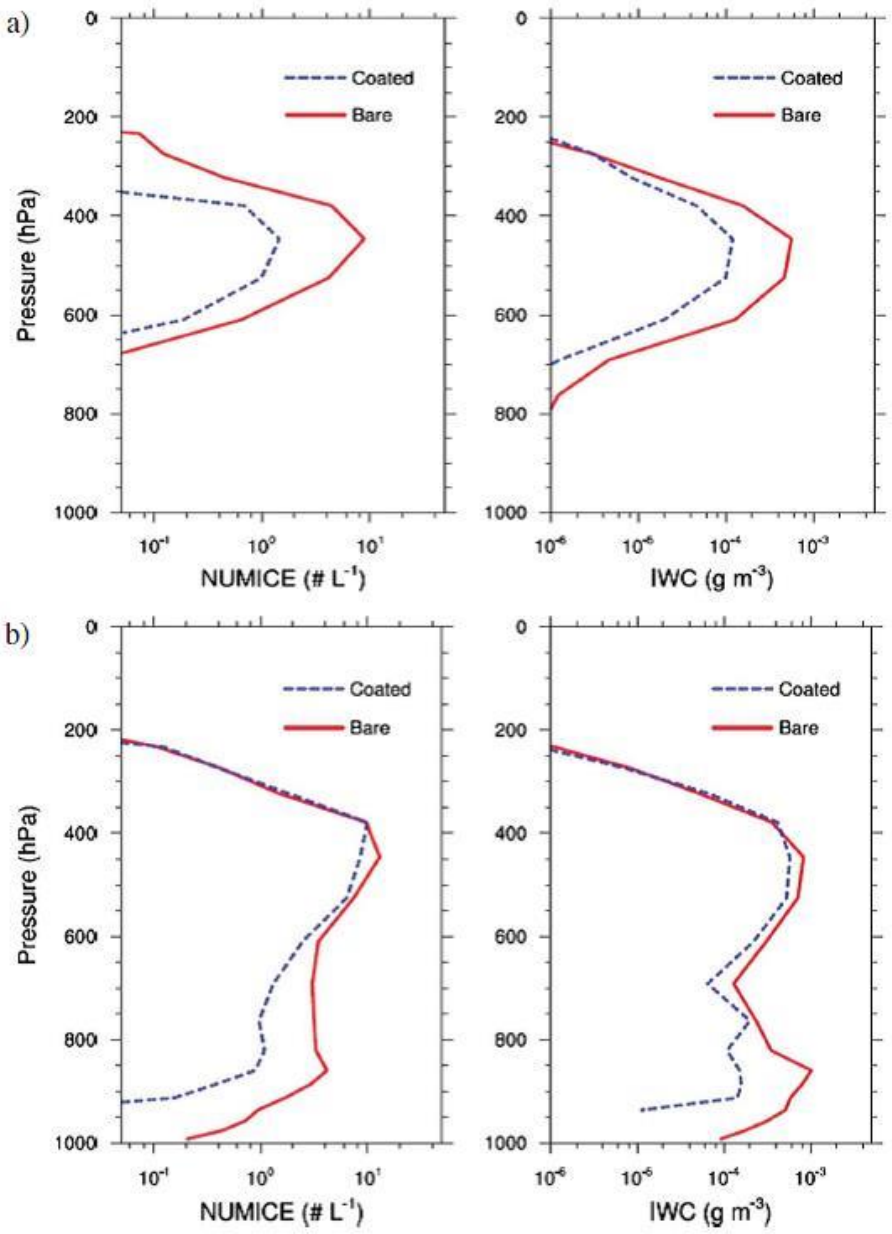

Figure 36. Modeled monthly mean profiles of the ice crystal number concentration (NUMICE) and ice water content (IWC) over the SGP site in (a) deposition ice nucleation mode and (b) condensation/immersion freezing mode. Reprinted with permission from ref 449. Copyright 2014 John Wiley & Sons, Inc.

In this section, we have taken a comprehensive approach to review laboratory studies on the potential effects of atmospheric aging processes on the IN activity of mineral dust particles. This section is divided into several subsections, according to the types of coatings formed on dust particles and/or the trace gases used to react with dust particles to form these coatings.

5.1 Sulfate coating and exposure to SO_2

Table 15 summarizes previous laboratory studies which investigated the efffects of sulfate coating and reaction with SO_2 on the IN activity of mineral dust particles. Previous studies were mainly focused the influence of H_2SO_4 and $(NH_4)_2SO_4$ coating on the IN activity of mineral dust particles, and only one study [451] explored the impact due to the heterogeneous reaction with SO_2.

2075 **Table 15.** Summary of laboratory studies on the effects of chemical aging processes on the IN activity of mineral dust particles: sulfate coatings and

2076 reaction with SO_2

coating or trace gases used to form coating	mineral dust	ice nucleation mode	references	major finding
H_2SO_4	aluminum oxide, alumina-silicate, iron oxide	deposition	Archuleta et al.[452]	H_2SO_4 coating largely reduced the IN activity of alumina-silicate particles, had no significant impact for aluminium oxide particles, and may increase the IN activity of iron oxides.
	ATD	deposition	Knopf and Koop[453]	No significant difference in IN activity was observed between fresh and H_2SO_4-coated ATD particles in the deposition nucleation mode.
	ATD, illite	deposition, immersion, condensation	Cziczo et al.[219]	H_2SO_4 coating reduced the IN activity of ATD and illite particles, and the extent of reduction depended on the coating thickness.
	kaolinite	deposition	Eastwood et al.[454]	H_2SO_4 coating reduced the IN activity of kaolinite particles in the deposition nucleation mode.
	illite, kaolinite, montmorillonite, quartz	deposition	Chernoff and Bertram[455]	H_2SO_4 coating substantially reduced the IN activity of illite, kaolinite, montmorillonite, and quartz particles.

ATD	immersion	Niedermeier et al.[456]	H_2SO_4 coatings could substantially reduce the IN activity of ATD particles in the immersion freezing mode.
ATD	deposition, immersion, condensation	Sullivan et al.[261]	H_2SO_4 coatings always reduced the IN activity of ATD particles, and the extent of decrease was much larger in the deposition nucleation mode than in the immersion/condensation freezing modes.
ATD	immersion	Niedermeier et al.[221]	Expsoure of H_2SO_4-coated ATD particles to water vapor resulted in further decrease in the IN activity.
kaolinite	deposition, immersion, condensation	Tobo et al.[440]	H_2SO_4 coating reduced the IN activity of kaolinite particles in both deposition nucleation and immersion/condensation freezing modes.
kaolinite	deposition, immersion	Wex et al.[457]	For immersion freezing, H_2SO_4 coating (with a thickness of a few nm or less) largely reduced the IN activity of Fluka kaolinite but did not lead to a significant change for CMS kaolinite. In the deposition nucleation mode, for both types of kaolinite particles, H_2SO_4 coating led to a decrease in IN activity at RH <95% but an increase in IN activity for RH >95%.

	ATD, illite, montmorillonite, K-feldspar, quartz	deposition, immersion, condensation	Kulkarni et al.[449]	H_2SO_4 coating reduced the IN actitivity of all the dust particles in the deposition nucleation modes, but its effects were not observable in the immersion/condensation freezing modes.
	kaolinite, montmorillonite	deposition	Sihvonen et al.[458]	Treatments of kaolinite and montmorillonite with H_2SO_4 led to compositional and structural changes of the surfaces, causing reduction in IN activity in the deposition nucleation modes.
	feldspar, ATD, illite, kaolinite	immersion	Augustin-Bauditz et al.[459]	H_2SO_4 coating could reduce the IN activity (in the immersion freezing mode) of all the dust particles under investigation, and the largest effect was obserevd for feldspar.
$(NH_4)_2SO_4$	ATD, illite	deposition, immersion, condensation	Cziczo et al.[219]	$(NH_4)_2SO_4$ coatings could reduce the IN activity of ATD and illite particles, and the extent of reduction depended on the coating thickness.
	kaolinite	deposition	Eastwood et al.[454]	$(NH_4)_2SO_4$ coating reduced the IN activity of kaolinite particles in the deposition nucleation mode, though the effects appeared to be less significant compared to H_2SO_4.
	ATD	immersion	Niedermeier et al.[456]	$(NH_4)_2SO_4$ coatings could substantially reduce the IN activity of ATD particles in the immersion freezing mode. Compared to H_2SO_4, the effects of $(NH_4)_2SO_4$ were more significant.

	ATD	deposition, immersion, condensation	Sullivan et al.[261]	In the immersion/condensation freezing modes, exposure of H_2SO_4-coated ATD particles to NH_3 would further suppress the IN activity.
	ATD	immersion	Niedermeier et al.[221]	Expsoure of ATD particles to H_2SO_4 followed by NH_3 led to a signficant reduction in IN activity, compared to fresh particles.
NH_4HSO_4	illite, kaolinite, montmorillonite, quartz	deposition	Chernoff and Bertram [455]	NH_4HSO_4 coatings substantially reduced the IN activity of illite, kaolinite, montmorillonite, and quartz particles, and the effects varied with temperature.
SO_2	montmorillonite	deposition	Salam et al.[451]	After exposure to pure SO_2 for 2.5 h or 45 ppmv SO2 for 70 h at ~0% RH, no significant change in IN activity in the deposition nucleation mode was observed for montmorillonite.

2077

5.1.1 Sulfate coating

Archuleta et al.[452] measured the ice nucleation activity of fresh and H_2SO_4-coated submicron aluminium oxides, alumina-silicate, and iron oxide particles under deposition nucleation mode conditions between -60 and -45 ^oC, and found that H_2SO_4 coating influenced the IN activity of different minerals in different ways. For example, although the coating had no significant impact for aluminium oxide particles, it largely reduced the IN activity of alumina-silicate particles.[452] For iron oxides, H_2SO_4 coatings statistically reduced the required RHi (relative humidity with respect to ice) to freeze for iron oxides;[452] in other words, the H_2SO_4 coating may increase the IN activity of iron oxides.

IN activity of fresh and coated ATD and illite aerosol particles were investigated in deposition nucleation, immersion freezing, and condensation freezing modes by Cziczo et al.,[219] using the Aerosol Interactions and Dynamics in the Atmosphere (AIDA) chamber in Karlsruhe, Germany. It was found [219] that coating with H_2SO_4 or $(NH_4)_2SO_4$ would largely reduce the IN activity of ATD particles, and that the super-saturations required by freezing coated ATD particles often approached those for homogeneous freezing of aqueous H_2SO_4 and $(NH_4)_2SO_4$ solution alone. Inhibition of ice nucleation by H_2SO_4 and $(NH_4)_2SO_4$ coatings was also observed for illite particles, though the effect was smaller compared to ATD particles.[219] In addition, they [219] observed that dust particles coated with less material were activated earlier than those coated with more material, suggesting that the amount of coating determines to which extent the IN activity of dust particles is reduced. Another study by Niedermeier et al.[456] suggested that H_2SO_4 and $(NH_4)_2SO_4$ both could significantly reduce the IN activity of ATD particles in the immersion freezing mode (233.15-239.15 K), and the effect of $(NH_4)_2SO_4$ coating is more significant than H_2SO_4. In contrast, an earlier study by Knopf and Koop [453] did not observe significant difference in the ice nucleation ability between fresh and H_2SO_4-coated ATD particles in the deposition nucleation mode.

Eastwood et al.[454] investigated the deposition nucleation properties (represented by ice nucleation onset conditions, defined as the RHi and temperature at which the first ice nucleation event was observed) of fresh and coated kaolinite particles over 233-246 K. As shown in Figure 37, it was found that H_2SO_4 coatings drastically reduced the ice nucleating ability of kaolinite particles, increasing the RH*i* required for ice nucleation by approximately 30% across the entire temperature range they investigated.[454] On the other hand, the decease of ice nucleation activity due to $(NH_4)_2SO_4$ coating was much smaller at 245 K compared to that at 236 K.[454] Tobo et al.[440] also suggested that H_2SO_4 coating reduced the IN activity of kaolinite aerosol particles for both deposition nucleation and immersion/condensation freezing modes for temperature between -34 to -26 ºC.

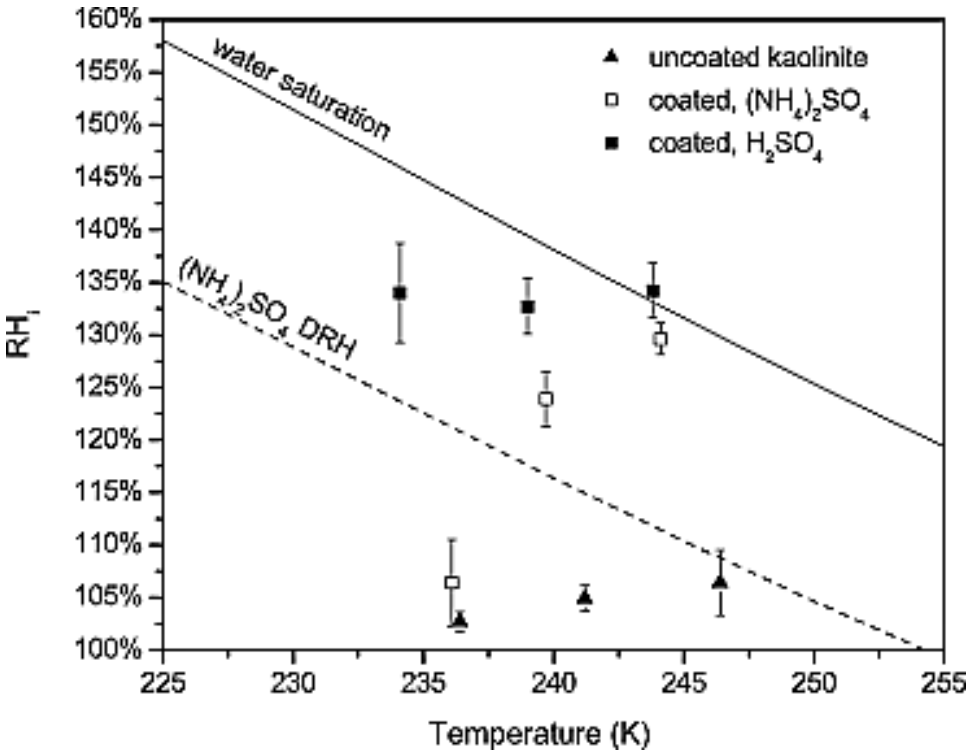

Figure 37. Summary of ice nucleation onset conditions for uncoated, H_2SO_4-, and $(NH_4)_2SO_4$-coated kaolinite particles. The error bars represent 95% confidence intervals based on at least six measurements per data point. Reprinted with permission from ref 454. Copyright 2009 John Wiley & Sons, Inc.

The effects of H_2SO_4 and NH_4HSO_4 coatings on the IN activity of several mineral dust particles in the deposition nucleation mode from 234-247 K were examined by Chernoff and Bertram.[455] They [455] found that H_2SO_4 coatings increased the onset RH*i* (and thus reduced the IN activity) by ~30% for kaolinite and illite and ~20% for montmorillonite and quartz. Additionally, it was found by Chernoff and Bertram [455] that NH_4HSO_4 coatings also impair the IN activity of kaolinite particles, increasing the onset RH*i* by 18-26%, depending on the temperature under which the ice nucleation occurred.

Sullivan et al.[261] investigated the change in ice nucleation properties of 300 nm ATD particles (in both deposition nucleation and immersion/condensation freezing modes) after being exposure to H_2SO_4 alone or H_2SO_4 followed by NH_3, and some representative results are shown in Figure 38. Several conclusions have been drawn by this study:[261] i) heating of ATD particles in a thermal denuder up to 200 ºC did not lead to significant change in their IN activity; ii) H_2SO_4 coating always reduced the IN activity of ATD, compared to fresh particles, and the extent of decrease is much larger in the deposition nucleation mode than the immersion/condensation freezing modes; iii) heating the H_2SO_4-coated ATD particles further decreased IN activity in the immersion/condensation freezing mode, probably because heating may accelerate the reaction of coated H_2SO_4 with ATD particle surface; and iv) in the immersion/condensation freezing modes, subsequent exposure of H_2SO_4-coated ATD particles to NH_3 would further suppress the IN activity.

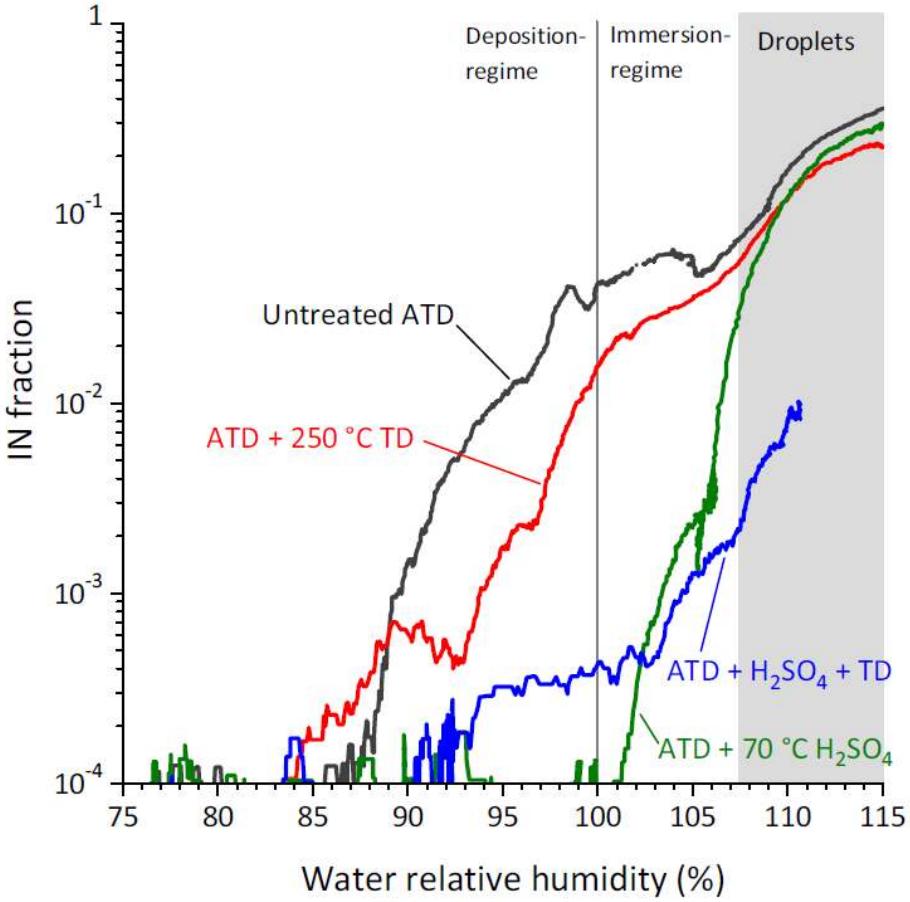

2138

2139 **Figure 38.** Measured fractions of 300 nm fresh and aged ATD particles which were activated to ice crystals
2140 at -30 ºC as a function of RH. Black curve: untreated ATD; red curve: ATD heated in the thermodenuder
2141 (TD) at 250 ºC; green curve: ATD coated with sulphuric acid; blue curve: ATD coated with sulfuric acid
2142 and then heated in the TD at 250 ºC. In the region (RH >107%) covered by the grey box, measurements
2143 were not reliable because droplets could survive in the evaporation region (of the ice nuclei counter) and
2144 therefore could not be distinguished from ice crystals. Reprinted with permission from ref 261. Copyright
2145 2010 Copernicus Publications.

2146

2147 Using an Aerosol Mass Spectrometer and an Aerosol Time of Flight Mass Spectrometer, Reitz et
2148 al.[220] simultaneously measured the composition of H_2SO_4-coated ATD particles (the IN activity of
2149 which were studied by Sullivan et al.[261]), and found that condensation of H_2SO_4 vapor onto ATD
2150 particles not only resulted in the formation of a H_2SO_4 coating on the particle surface but also led

2151 to reactions which produced metal (including Na, K, Mg, Al, and etc.) sulfate, ammonium metal
2152 sulfate, and ammonia sulfate on the surface. These surface modifications may be responsible for
2153 that observed decrease in IN activity of ATD particles.[220] In the same campaign as Sullivan et al.[261]
2154 and Reitz et al.,[220] Niedermeier et al.[221] found that additional exposure of H_2SO_4-coated ATD
2155 particles to water vapor could further strongly reduce their IN activity, and this may be caused by
2156 that the presence of water could accelerate the chemical reaction of H_2SO_4 coating with particle
2157 surface, leading to further depletion of ice nucleation active sites on the surface.
2158
2159 Using the Leipzig Aerosol Cloud Interaction Simulator, Augustin-Bauditz et al.[459] measured the
2160 IN activity of fresh (with mobility diameters of 300 nm) and H_2SO_4-coated dust particles in the
2161 immersion freezing mode. As shown in Figure 39, H_2SO_4 coating could reduce the IN activity of
2162 all the dust particles (including feldspar, ATD, illite, and kaolinite) from around -38 ^oC to -32 ^oC,
2163 and the largest suppression in IN activity was observed for feldspar particles.[459]
2164

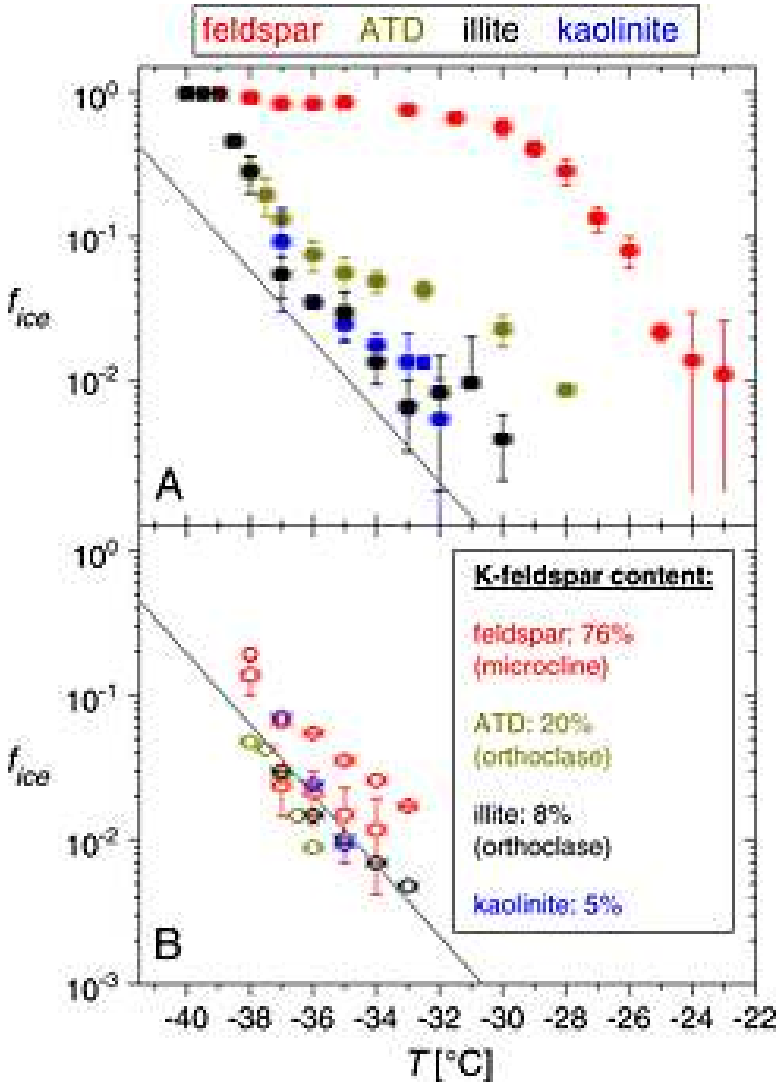

2165

2166 **Figure 39.** Measured ice nucleation fractions of (a) uncoated particles and (b) particles coated with sulfuric
2167 acid (circles: coating at 70 ºC; squares: coating at 80 ºC). Reprinted with permission from ref 459. Copyright
2168 2014 John Wiley & Sons, Inc.

2169

2170 Sihvonen et al.[458] found that the treatment with H_2SO_4 could cause reduction in IN activity for
2171 kaolinite and illite particles in the deposition nucleation mode. They [458] also used X-ray diffraction,
2172 TEM, and inductively coupled plasma-atomic emission spectroscopy to measure the physical and
2173 chemical changes of dust particle treated with H_2SO_4. Formation of new products and structural
2174 change of the surface were observed, both probably explaining the suppression of IN activities

2175 after treatment with H_2SO_4.[458] This study [458] shows the importance of post-analysis of modified
2176 dust particles to better understand the impact of chemical processing on IN activity.
2177
2178 Kulkarni et al.[449] studied the IN activity of 200 nm fresh and H_2SO_4-coated ATD, illite,
2179 montmorillonite, K-feldspar, and quartz particles as a function of temperature (-35 to -25 ^oC) and
2180 RH (75-110%). It was found [449] that H_2SO_4 coating led to reduction in IN activity of all five
2181 different types of dust particles in the deposition nucleation mode; nevertheless, its effect under
2182 water-super-saturation conditions (i.e. in immersion/condensation freezing modes) was not
2183 observable for any type of dust particles.[449] X-ray diffraction measurements showed that coating
2184 dust particles with H_2SO_4 changed the surface crystalline nature and resulted in surface structural
2185 disorders.[449] Therefore, it was further concluded that the suppression of IN activity of dust particles
2186 in the deposition freezing mode due to H_2SO_4 coating was caused by the lack of structured order
2187 of the surface after treatment with H_2SO_4.[449]
2188
2189 The effect of H_2SO_4 (with a thickness of a few nm or less) on the IN activity of two different types
2190 of kaolinite particles was investigated by Wex et al.[457] in the deposition nucleation and immersion
2191 freezing mode. For immersion freezing, while H_2SO_4 substantially reduced the IN activity of Fluka
2192 kaolinite particles, it did not lead to significant change to Clay Mineral Society kaolinite.[457] The
2193 following explanation was provided:[457] Fluka kaolinite contained K-feldspar which is very IN
2194 active [141] but the other type of kaolinite did not, and H_2SO_4 coating could efficiently react with K-
2195 feldspar and thus largely reduce its IN activity. Under water sub-saturation conditions, H_2SO_4
2196 coating suppressed the ice nucleation of kaolinite particles for RH <95% while a significant
2197 increase in ice nucleation activity was observed for RH >95%.[457] For RH in the range of 95-100 %,
2198 H_2SO_4 coating kaolinite particles may become aqueous droplets with solid inclusion, and therefore
2199 immersion freezing actually dominated over deposition freezing.[457]

Though many studies have shown that sulfate coating could significantly modify the IN activity of mineral dust particles, fundamental understanding of deactivation mechanisms on the molecular level is lacking. Yang et al.[460] explored why sulfuric acid coatings influence the IN activity of mineral dust particles. They [460] probed the structure of water at the interface between mica (used as a surrogate as dust particles) and aqueous D_2SO_4 solutions of different concentrations using sum frequency generation vibrational spectroscopy. In this study [460] deuterated water and sulfuric acid were used to avoid the overlap with the IR absorption peak of mica at 3620 cm^{-1}.[461] The spectra of interfacial D_2O molecules show two peaks at around 2375 and 2550 cm^{-1}. These two peaks are sometimes called the "ice-like" and the "liquid-like" peaks, because their peak positions are similar to those of bulk ice and liquid water, respectively.[286,462] It is usually believed that the interfacial water molecules observed by SFG are more ordered than those in the bulk because SFG is largely depressed in a disordered medium.[463] As shown in Figure 40, Yang et al.[460] found that when the concentration of D_2SO_4 in the aqueous solution increased from 0 to 5 M, the two peaks at 2375 and 2550 cm^{-1} both gradually disappeared.

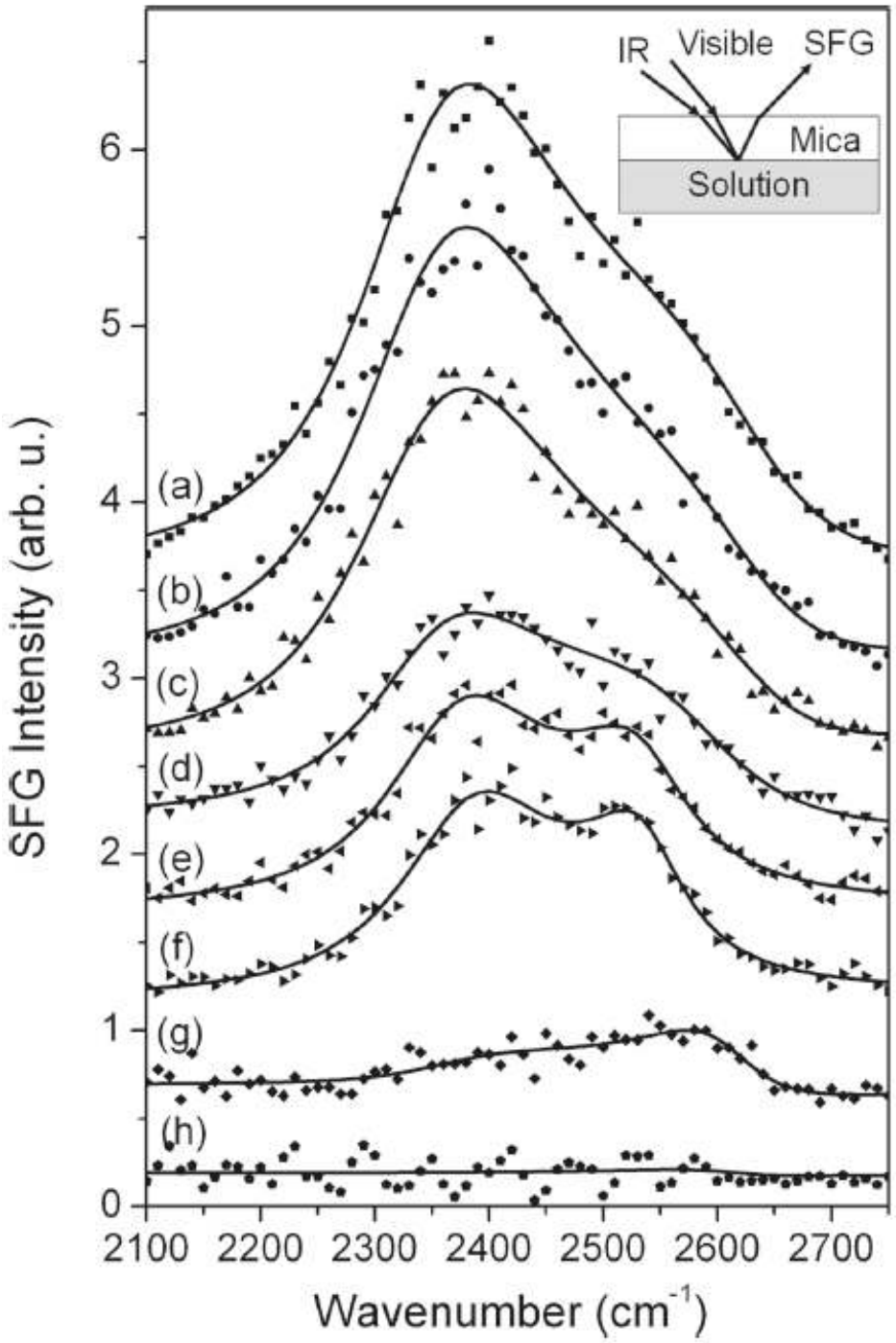

2215

2216 **Figure 40.** SFG spectra of D_2O/mica interfaces with D_2SO_4 concentrations of (a) 0, (b) 5×10^{-6}, (c) 5×10^{-5}, (d) 5×10^{-4}, (e) 0.005, (f) 0.05, (g) 0.5, and (h) 5 M. The inset shows the schematic layout of the spectroscopic setup. Reprinted with permission from ref 460. Copyright 2011 American Chemical Society.

2219

The observation shown in Figure 40 is interpreted as the reduction of ordered water structures at the interface with increasing D_2SO_4 concentrations.[460] It was further suggested by Yang et al.[460] that IN activity is correlated with the presence of structured water at the interface. The reduction in ordered water structure was due to the combination of several factors,[460] including i) reduced mica surface potential at low pH, ii) adsorption of sulfate on mica surface, iii) decrease of free water molecules at higher H_2SO_4 in the aqueous solution. Though it has provided fundamental insights into the structure of the mineral-aqueous solution interface, the study by Yang et al.[460] was carried at room temperature instead of those at which ice nucleation may occur.

Very recently second harmonic generation spectroscopy has been used to monitor the mineral-water interface during the occurrence of immersion freezing in an in-situ and online manner.[464] Local ordering of water on the mica (which provides a good ice nucleating surface) was observed by SFG during cooling down to the freezing point;[464] in contract, no significant change in water structure at sapphire (which is a poor ice nucleator) surface was observed during cooling.[464] This is supported by a recent molecular dynamics simulation study,[465] suggesting that layering and ordering of interfacial liquid water are critical to heterogeneous nucleation of ice. This novel application developed by Abdelmonem et al.[464] has a great potential to help understand how heterogeneous ice nucleation occurs in general and more specifically how chemical aging alters the IN activity at the molecular level.

5.1.2 Exposure to SO_2

To our knowledge only one previous study [451] explored the effect of SO_2 exposure on the IN activity of mineral dust particles. No significant change in deposition ice nucleation efficiency was observed for montmorillonite particles after being exposed to pure SO_2 for 2.5 h or 45 ppmv SO_2 for 70 h at room temperature and ~0% RH.[451]

5.2 Organic coatings

Several previous studies have investigated how organic coatings can alter the IN activities of mineral dust particles, and an overview of these studies is provided in Table 16.

Table 16. Summary of laboratory studies on the effects of chemical aging processes on the IN activity of mineral dust particles: organic coatings, and reactions with HNO_3, NH_3, and O_3.

coating or trace gases used to form coating	mineral dust	ice nucleation mode	references	major finding
organic coating	ATD, kaolinite	deposition, immersion, condensation	Möhler et al.[466]	Organic coating formed by ozonolysis of α-pinene could substantially reduced the IN activity of ATD and illite particles, and the extent of decrease depended on the coating thickness.
	ATD	immersion	Niedermeier et al.[456]	ATD particles coated with succinic acid had lower IN activity in the immersion freezing mode, compared to fresh ATD particles
	kaolinite	deposition, immersion, condensation	Tobo et al.,[440]	Levoglusocan coating significantly reduced the IN activity of kaolinite particles in the deposition nucleation mode, while its impact was not observable in the immersion/condensation freezing modes.
	kaolinite	deposition, immersion	Wex et al.,[457]	In the immersion freezing mode, neither succinic acid or levoglusocan changed the IN activity of kaolinite particles. In the deposition nucleation mode, both organic coatings suppressed the IN activity of kaolinite particles for RH below 95%, while a significant increase in IN activity was observed for RH >95%.

HNO_3	ATD	deposition, immersion, condensation	Sullivan et al.[375]	In the immersion/condensation freezing modes, exposure to HNO_3(g) has no significant impact on IN activity. For RH <97%, heterogeneous reaction with HNO_3(g) significantly reduced the IN activity of ATD particles; while around the RH of 97-100 % no significant difference in IN activity was observed between fresh and aged particles
	kaolinite and montmorillonite	deposition	Sihvonen et al.[458]	In the deposition nucleation mode, treatment with HNO_3 reduced the IN activity of kaolinite but did not significantly affect the ice nucleation properties of montmorillonite.
	ATD, illite, K-feldspar, and quartz	deposition, immersion, condensation	Kulkarni et al.[467]	In deposition nucleation mode, aged dust particles, except quartz, showed reduced IN activity compared to fresh particles. In the immersion/condensation freezing modes, fresh and aged dust particles exhibited equivalent IN activity.
NH_3	montmorillonite	deposition	Salam et al.[468]	Exposure to pure and 25 ppmv NH_3 could enhance the IN activity of montmorillonite particles in the deposition nucleation mode.
	montmorillonite	deposition	Salam et al.[451]	Exposure to ~100 pptv NH_3 for 70 h increased the ice nucleation efficiency of montmorillonite by a factor of ~2.

O_3	montmorillonite	deposition	Salam et al.[451]	Exposure of montmorillonite to 200 ppbv O_3 for 70 h at room temperature and at 0% RH did not significantly change the IN activity in the deposition nucleation mode.
	ATD and kaolinite	deposition, immersion	Kanji et al.,[469]	The change in IN activity after exposure to O_3 was found to be complex, depending on O_3 concentrations, ice nucleation modes, and minerals.

2251

The ice nucleation activity (in deposition and immersion/condensation freezing modes) of ATD and kaolinite aerosol particles with and without secondary organic matter (SOM) coating formed by the ozonolysis of α-pinene was investigated using the AIDA chamber at 205-210 K.[466] It was found that the SOM coating could substantially suppress the IN activity of both ATD and illite particles, and the suppression extent depended on the thickness of the coating.[466] Almost all the fresh ATD and illite particles with diameters of 0.1-1.0 μm were efficient deposition mode IN at RH*i* between 105 and 120%.[466] However, if coated with 17 wt% SOM, only ~20% of ATD particles were activated to ice crystals at RH*i* between 115 and 130%;[466] and only 10% of illite particles were ice-active at RH*i* between 160 and 170%, if coated with 41 wt% SOM.[466] In another study by Niedermeier et al.,[456] ATD particles coated with succinic acid were found to have lower IN activity in the immersion freezing mode (233.15-239.15 K), compared to fresh ATD particles.

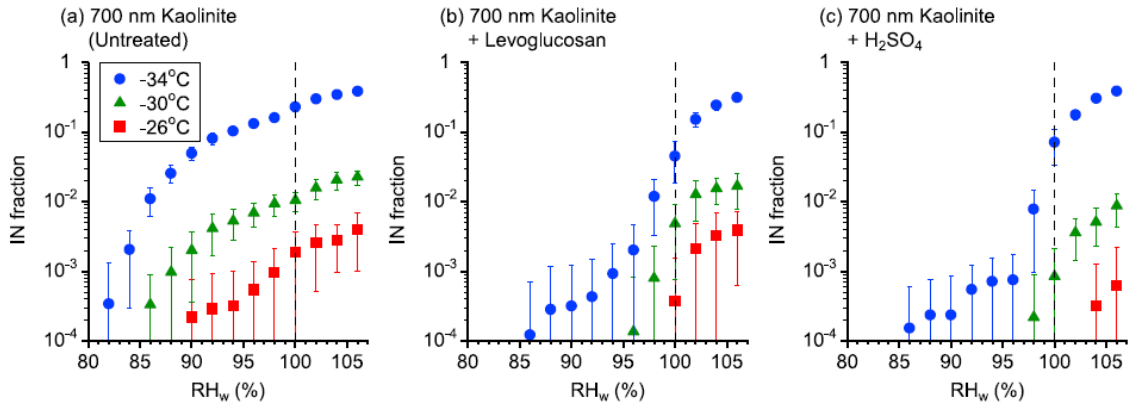

Figure 41. Fractions of 700 nm kaolinite particles which were activated to ice particles at -34 (circles), -30 (triangles), and -26 ºC (squares) as a function of RH. (a) fresh kaolinite particles, (b) kaolinite particles treated with levoglucosan at 93 ºC, and (c) kaolinite particles treated with H_2SO_4 at 70 ºC. Dashed lines indicate liquid water saturated conditions. Error bars indicate the standard deviation from multiple measurements. Reprinted with permission from ref 440. Copyright 2014 John Wiley & Sons, Inc.

Tobo et al.[440] investigated the effects of levoglusocan coating on the IN activity of kaolinite particles. As shown in Figure 41, they [440] found that for temperature ranging from -34 to -26 ºC,

levoglusocan coating significantly reduced the IN activity of kaolinite particles for the deposition nucleation mode while its impact was not observable for immersion/condensation freezing modes. Wex et al.[457] systematically examined how succinic acid and levoglusocan coatings with a thickness of a few nm or less could change the IN activity of kaolinite particles in deposition nucleation and immersion freezing modes. In the immersion freezing mode, neither organic compounds changed the IN activity of kaolinite particles.[457] Under water sub-saturation conditions, the effect of organic coatings were more complicated:[457] i) for RH below 95%, both organic coatings were found to suppress the ice nucleation of kaolinite particles; ii) on the other hand, a significant increase in ice nucleation activity was observed for RH >95%, probably because in this RH range mainly immersion freezing instead of deposition nucleation took place (i.e. coated kaolinite particles at RH >95% may become aqueous particles with solid inclusion).

5.3 Exposure to HNO_3

Nitrate has been frequently observed to internally mixed with mineral dust particles in the troposphere by field measurements [158-160,202,429] due to the heterogeneous reactions with HNO_3,[199,227,365,470-473] N_2O_5,[131-134,136,139] NO_2,[474-478] and NO_3 radicals.[177,479] Nevertheless, only a few studies [375,458,467] have investigated whether and how nitrate coatings could alter the IN activity of mineral dust particles, as summarized in Table 16.

The effects of HNO_3 exposure on the IN activity of ATD aerosol particles were investigated by Sullivan et al.,[375] who reacted 200 nm ATD particles with HNO_3(g) in an aerosol flow tube at room temperature and at different RH and then measured their ice nucleation properties at -30 ºC as a function of RH. As shown in Figure 42, for RH <97% under which deposition nucleation occurred, heterogeneous reaction with HNO_3(g) significantly reduced the IN activity of ATD particles;[375] however, for RH>100% where immersion/condensation freezing dominated, the effect of exposure to HNO_3(g) was insignificant.[375] In addition, around the RH of 97-100 % no significant difference

in IN activity was observed between fresh and coated particles.[375] At 97-100 % RH deposition nucleation dominated for fresh particles; however, at this RH range aged particles may become aqueous particles (due to the formation of nitrate coating) and thus immersion/condensation freezing can become the main ice nucleation mechanism. The change in ice nucleation modes could cause fresh and aged particles to be activated under similar conditions, though their compositions differ.

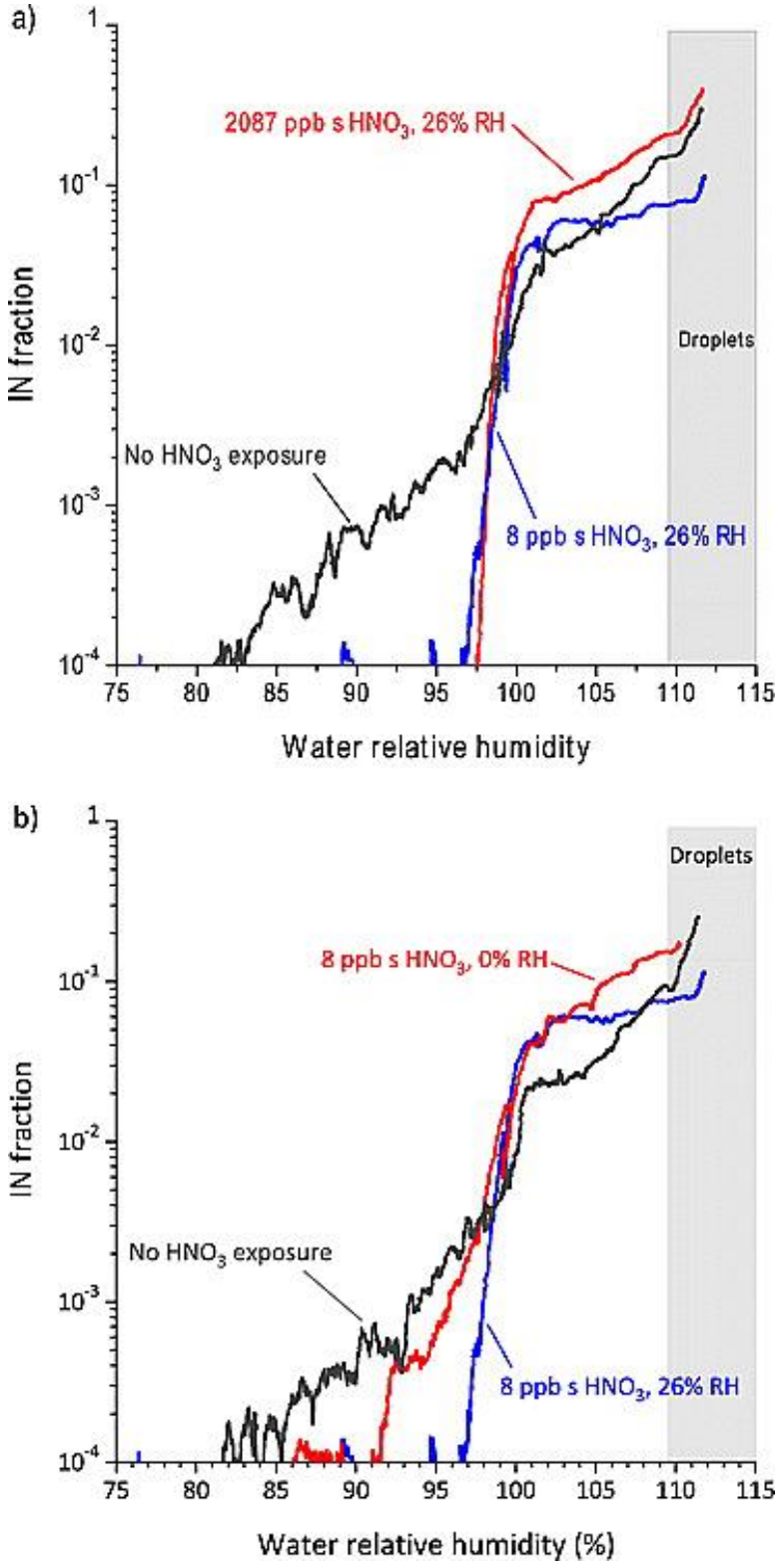

2303

2304 **Figure 42**. Fractions of 200 nm fresh and HNO_3-exposed ATD aerosol particles that were activated to ice

2305 crystals at -30 ºC as a function of RH. (a) black curve: no HNO_3 exposure; blue curve: HNO_3 exposure of

2306 8 ppbv·s at 26% RH; red curve: HNO_3 exposure of 2087 ppbv·s at 26% RH. (b) Black curve: no HNO_3

exposure; blue curve: HNO_3 exposure of 8 ppbv·s at 26% RH; red curve: HNO_3 exposure of 8 ppbv·s at 0% RH. In the region covered by the grey box, droplets may interfere with IN measurements and therefore these measurement may not be reliable. Reprinted with permission from ref 375. Copyright 2010 John Wiley & Sons, Inc.

In addition, exposure to HNO_3 at 26% RH, compared to that at 0%, will more significantly reduce the deposition nucleation activity of ATD particles for RH<97%,[375] as shown in Figure 42. This may be explained by the fact that heterogeneous reaction of HNO_3 with ATD particles is accelerated and thus more particulate nitrate is formed at higher RH.[213]

Sihvonen et al.[458] showed that in the deposition nucleation mode, while treatment with HNO_3 decreased the IN activity of kaolinite, it did not significantly affect the ice nucleation properties of montmorillonite. In another study, Kulkarni et al.[467] investigated the ice nucleation activity of ATD, illite, K-feldspar, and quartz as a function of temperature and RH before and after reaction with HNO_3. They [467] found that at subsaturated conditions (i.e. in deposition nucleation mode), aged dust particles, except quartz, showed reduced IN activity compared to fresh particles. In contract, at super-saturation conditions (i.e. in immersion/condensation freezing modes), fresh and aged dust particles exhibited equivalent IN activity.[467]

5.4 Exposure to NH_3

As summarized in Table 16, the impacts of heterogeneous reaction with NH_3 have been investigated by two previous studies.[451,468] Salam et al.[468] studied the ice nucleation activity of NH_3-exposed montmorillonite particles under the deposition nucleation mode and provided the first experimental evidence that exposure to NH_3 could enhance the IN activity of mineral dust particles. They [468] suggested that ice nucleation activity of montmorillonite particles increased with exposure time to NH_3. It was further observed by Salam et al.[468] that compared to fresh

montmorillonite particles, the activation temperature (defined as the highest temperature at which >1% particles were activated to ice crystals) at RH of 100% and 90% was 15 °C higher for particles exposed to pure NH_3, and was 5 °C higher for particles exposed to 25 ppmv NH_3. In a following study, Salam et al.[451] further measured the deposition ice nucleation activity of montmorillonite particles after exposed to NH_3 of ~100 pptv (a typical atmospheric concentration) for 70 h, and found that this exposure increased the ice nucleation efficiency of montmorillonite by a factor of around two.

5.5 Exposure to O_3

The influence of heterogeneous reaction with O_3 on the IN activity of mineral dust particles have also been explored,[451,469] as shown in Table 16. Salam et al.[451] exposed montmorillonite particles to 200 ppbv O_3 for 70 h at room temperature and ~0% RH. No clear change in deposition nucleation efficiency was observed after exposure, compared to fresh particles.[451] Kanji et al.[469] systematically investigated the IN activity of ATD and kaolinite aerosol particles in deposition and immersion modes (between 233 and 263 K) before and after exposure to 0.4-4.3 ppmv O_3 at room temperature and 0% RH in a stainless steel aerosol chamber. Complex response of IN activity to O_3 exposure was reported:[469] 1) after exposure to 430 ppbv O_3 for ~130 min, kaolinite particles showed enhanced ice nucleation activity in both deposition and immersion modes over the temperature range (233-263 K) they studied, whereas the change of IN activity was insignificant for ATD particles in either deposition or immersion nucleation modes; 2) compared to fresh particles, kaolinite particles exposed to 1.4 ppmv O_3 for ~130 min showed a lower ice nucleation activity over 232-240 K in the deposition mode, and only slight suppression of IN activity was observed for the immersion over 233-263 K; 3) additionally, ATD particles exposed to 4.3 ppmv O_3 for ~130 min, compared to unexposed particles, showed significantly lower IN activity in both deposition and immersion modes over 233-263 K.

5.6 Summary

Increasing numbers of laboratory studies have shown that chemical aging processes can substantially change the IN activity of mineral dust particles. Furthermore, several modeling studies have suggested that these changes can have important impacts on cloud microphysics, radiation, and thus the climate. In the last two decades significant progress has been made in this field, and a comprehensive and systematic picture is emerging. Nevertheless, our understanding in the effects of atmospheric aging processes on the IN activity of mineral dust particles is still not comprehensive or quantitative.

The same coating formed on dust particles may influence on the IN activity for different minerals and different ice nucleation modes in different ways. In addition, it is not unusual that inconsistent results have been reported by different studies for the same coating on the same type of dust in the same ice nucleation mode. For example, most studies suggest that sulfuric acid coating typically reduces the IN activity, while the effect of HNO_3 coating is largely unclear. This may be partly due to the fact that it is still nontrivial or even challenging to measure the IN activity of aerosol particles. What makes it more complicated is that the formation of coating could change the mode in which dust particles are activated to ice crystals (e.g., from deposition nucleation to condensation/immersion freezing, due to the increase in CCN activity of aged dust particles).[375] Several studies have revealed that the extent of IN activity changes depends on the thickness of coatings;[219,375,466] however, a quantitative understanding of effects of chemical aging processes on IN activity of mineral dust particles is still lacking.

Furthermore, it is still not clear at the molecular level why and how chemical processes with acids usually turn to reduce the IN activity of mineral dust particles. It may be largely due to the fact that we still do not understand why some minerals are more ice nucleation active than others and

the nature of ice nucleation active sites on the surface.[443,480] Five factors have been empirically proposed to promote heterogeneous ice nucleation.[167] 1) It is typically assumed that the number of ice nucleation active sites is proportional to the particle surface area.[238,481-484] 2) Heterogeneous ice nucleation is preferentially initiated by surfaces of insoluble materials. 3) The ability of a surface to form hydrogen bonds usually promotes water adsorption and ice nucleation. 4) Surfaces which have similar crystallographic structures to that of ice will promote ice nucleation. 5) Morphological, chemical, and electrical heterogeneities on the surface can also promote ice nucleation. Several hypotheses have been suggested to explain why exposure to acid gases (e.g., H_2SO_4 and HNO_3) may suppress the IN activity of mineral dust particles. Laboratory studies [220,261,458] have shown that reaction products which are more soluble (and thus less IN active) can lead to the loss of or cover the active sites. Chemical aging processes can also lead to structural changes of surfaces, alter their crystalline nature, and cause structural disorders,[443,449,458] therefore reducing their ice nucleation activity. The patterns in which surfaces interact with water can also be changed due to chemical processes, resulting in changes in heterogeneous ice formation.[460] In addition, a few recent studies [457,459] also suggest that the loss/deactivation of feldspar (which is very IN active) heterogeneities may be responsible for the decrease in IN activity of clay minerals.

6 Concluding remarks and recommendations for future studies

Interactions of mineral dust particles with water vapor influence their heterogeneous reactivity towards reactive trace gases, their hygroscopicity and hence their ability to directly scatter and absorb solar and terrestrial radiation, and their activity to serve as CCN and IN and therefore their roles in indirect radiative forcing. Additionally, atmospheric heterogeneous and multiphase reactions will change their chemical compositions after mineral dust particles are lifted into the troposphere, as a result modifying the interactions of mineral dust particles with water vapor. A complete and in-depth understanding of the interactions of fresh and aged dust particles with water

vapor will help us assess the roles of mineral dust aerosols in many aspects of atmosphere chemistry and climate change.

In this article we provide a comprehensive review of water adsorption, hygroscopicity, and CCN activity of fresh and aged mineral dust particles, and the effects of chemical aging on the IN activity of mineral dust particles. As shown in this review, previous studies have largely improved our understanding of the interactions of mineral dust particles with water vapor. Brief summaries are provided in Section 4.11 for water adsorption, hygroscopicity, and CCN activities of fresh and aged mineral dust particles and in Section 5.6 for the IN activity of aged mineral dust particles. However, there still remain many open questions which can only be satisfactorily answered through a close collaboration among laboratory studies, field measurements, modeling work, and theoretical analysis. Several future directions are recommended here in order to address these challenges:

(1) Large discrepancies still exist for water adsorption and hygroscopicity of fresh mineral dust particles reported by different studies, especially for clay minerals. Reasons for these discrepancies are largely unclear. Further measurements are recommended to solve these discrepancies, and well-coordinated collaborations in which same dust samples are distributed to different groups and experimental results are intercompared will be very helpful. Most experimental data are only presented in graphical forms, yet numerical tabulation of the data can enhance their accessibility and usability.

(2) Previous studies which measured water adsorption and hygroscopicity of fresh mineral dust particles were mainly carried out at RH lower than 80%. It is recommended that future measurements should be extended to RH above 90% or even 99%. Nevertheless, it is non-trivial

2430 to do these measurements at RH very close to 100%. In addition, most previous studies have been
2431 performed at or near room temperature, but temperature varies from ~200 to ~300 K in the
2432 troposphere, and profound effects of temperature on the hygroscopicity have been reported for
2433 some materials of atmospheric relevance.[485-487] Therefore, the effects of temperature on the water
2434 adsorption and hygroscopicity of mineral dust particles need to be systematically investigated by
2435 future studies.
2436
2437 (3) Large numbers of previous laboratory studies have suggested that chemical aging could
2438 substantially increase the water adsorption ability, hygroscopicity, and CCN activity of mineral
2439 dust particles. However, most of these studies focused on $CaCO_3$, and the effect of chemical aging
2440 should also been examined for more abundant minerals and real dust samples. It is also
2441 recommended that future laboratory work should be carried out at atmospherically relevant
2442 conditions (e.g., concentrations of reactive trace gases, reaction time, and RH etc.). Studies of this
2443 type can help to answer how rapidly water adsorption, hygroscopicity, and CCN activity of mineral
2444 dust particles will be changed during their residence in the atmosphere.
2445
2446 (4) The interactions of mineral dust particles with water vapor influences, and is influenced by,
2447 interactions with reactive trace gases. Such complex interactions are likely to involve mass transfer
2448 [306,488-492] and chemical reactions in and between all three different phases (gas, liquid, and solid)
2449 in nonlinear manners.[172,173,493-499] Multiphase models have been developed in order to integrate
2450 these processes and have been applied to study chemical reactions and phase transition of organic
2451 particles.[499-502] If developed for and applied to mineral dust chemistry, they can be very helpful for
2452 a better understanding of the complex interactions between mineral dust particles, water, and
2453 reactive trace gases.
2454

(5) Many field measurements have shown that coated dust particles in the troposphere have different phase transition properties when compared to uncoated dust particles. However, most of these studies are of a qualitative nature. It will be useful for future field measurements to quantitatively and simultaneously determine 1) the amount and type of coating formed on ambient mineral dust particles, and 2) the change of water adsorption, hygroscopicity, or CCN activity of these coated mineral dust particles. Measurements of this type, though very challenging, will largely improve our understanding of the effects of chemical aging processes in the atmosphere.

(6) The impacts of heterogeneous reactions on trace gases and compositions of mineral dust particles have been assessed by many regional and global models in the last 2-3 decades. However, their effects on the hygroscopicity and CCN activity of mineral dust particles have seldom been investigated by modeling studies. Modeling analyses will give a better understanding, on a much larger spatial and temporal scale, of the atmospheric relevance of change in hygroscopicity and CCN activity of mineral dust particles due to chemical aging processes.

(7) Compared to the effects of atmospheric aging processes on hygroscopicity and CCN activity, the impact on IN activity has been much less widely investigated. While sulfate coatings have received some attention, much less has been paid to the effects of nitrate and organic species on the IN activity of mineral dust particles. In order for a more comprehensive understanding, further studies are needed on the effect of different coatings, especially nitrate and organic, on the IN activity of mineral dust particles. It is also highly desirable to carry out aging experiments at atmospheric relevant conditions, and to control the amount of coatings and/or exposure conditions in more quantitative and atmospherically relevent ways. One of the current limitations on our ability to understand how chemical aging changes the IN activity of mineral dust particles is to correctly mimic atmospheric processing of aerosol particles in the laboratory. For example, it is

critical that surface coating composition and thickness realistically mimic what is present in the atmosphere. Since coatings, in particular, appear to effectively deactivate effective mineral dust ice nuclei,[74,219] future studies will need to consider how to properly compare laboratory particles to atmospheric measurements.

(8) Mechanisms that change IN activity of dust particles due to atmospheric aging processes are largely unknown on a molecular level, and a collaborative effort from experts in aerosol/cloud chemistry microphysics, surface science and surface chemistry, and theoretical chemistry will be very beneficial.

(9) Field measurements are required to understand if and to which extent the IN activity of mineral dust particles in the troposphere is influenced by a variety of aging processes during transport. Modeling studies are encouraged to include more laboratory-derived and realistic parameterizations for the effects of aging processes on IN activity in their simulations, in order to better evaluate the effects of atmospheric aging processes on IN activity, cloud microphysics, and climate impacts.

Author information

Corresponding author

*Phone: (319)335-1392. Fax: (319)353-1115. E-mail: vicki-grassian@uiowa.edu.

Notes

The authors declare no competing financial interest.

Biographies

Mingjin Tang is currently a postdoctoral fellow in Professor Grassian's group, Department of Chemistry, University of Iowa, USA. Before arriving in the USA in the beginning of 2015, he received his BSc (in 2005) and MSc (in 2008) from Peking University (China) under the supervision of Professor Tong Zhu, and then received his PhD (in 2011) in Max Planck Institute for Chemistry and Johannes Gutenberg-Universität Mainz (Germany), advised by Drs. John N Crowley, Ulrich Pöschl, and Thorsten Hoffmann. After a short postdoc in Max Planck Institute for Chemistry, he joined Dr. Markus Kalberer's group at Department of Chemistry, University of Cambridge (UK) as a postdoctoral fellow. His research interest focuses on the fundamental physical chemistry of atmospheric aerosol particles and how physicochemical changes of aerosol particles influence air quality, clouds, and climate. He would like to thank Professor Tong Zhu for bringing him into atmospheric heterogeneous and multiphase chemistry studies as a young scientist in Peking University.

Daniel J. Cziczo is currently the Victor P. Starr Professor of Atmospheric Chemistry in the Department of Earth, Atmospheric and Planetary Sciences and Civil and Environmental Engineering at the Massachusetts Institute of Technology, USA. His research revolves around the interrelationship of particulate matter and cloud formation. His group utilizes laboratory and field studies to elucidate how small particles interact with water vapor to form droplets and ice crystals which are important players in the Earth's climate system. Experiments include using small cloud chambers in the laboratory to mimic atmospheric conditions that lead to cloud formation and observing clouds in situ from remote mountaintop sites or through the use of research aircraft.

As of January 2016, Vicki H. Grassian is a Distinguished Professor at the University of California San Diego (UCSD) with appointments in Chemistry and Biochemistry, Nanoengineering and

Scripps Institution of Oceanography. She is also Distinguished Chair of Physical Chemistry and currently serves as co-director at the Center for Aerosol Impacts on Climate and the Environment centered at UCSD. Prior to her move to UCSD, she was the F. Wendell Miller Professor in Chemistry at the University of Iowa. Her research area focuses on environmental molecular surface science, heterogeneous and multiphase chemistry of atmospheric aerosol particles, the impact of atmospheric aerosol on air quality and climate, and environmental and health aspects of nanoscience and nanotechnology.

Acknowledgement

The preparation of this review paper was initiated when M. J. T was working in University of Cambridge (UK) as a postdoctoral fellow under the supervision of Dr. M Kalberer. M. J. T. would like to thank Dr. Kalberer for his support and useful discussion, and the Isaac Newton Trust (Trinity College, University of Cambridge, UK) for sponsoring him with a research scholarship. V. H. G acknowledges that this work was supported by the NSF under grant CHE-1305723. Any opinions, findings, and conclusions or recommendations expressed in this material are those of the authors and do not necessarily reflect the views of National Science Foundation. D. J. C. acknowledges funding from NASA (Grant NNX13AO15G) and the Victor P. Starr Career Development Chair for funding that made this work possible.

References

(1) Seinfeld, J. H.; Pandis, S. N. *Atmospheric Chemistry and Physics: From air pollution to climate change*; Wiley Interscience: New York, 2006.

(2) Finlayson-Pitts, B. J.; Pitts, J. N. *Chemistry of the Upper and Lower Atmosphere: Theory, Experiments, and Applications*; Academic Press: San Diego, 2000.

(3) Stevens, B.; Feingold, G. Untangling aerosol effects on clouds and precipitation in a buffered system. *Nature* **2009**, *461*, 607-613.

(4) Carslaw, K. S.; Lee, L. A.; Reddington, C. L.; Pringle, K. J.; Rap, A.; Forster, P. M.; Mann, G. W.; Spracklen, D. V.; Woodhouse, M. T.; Regayre, L. A. *et al.* Large contribution of natural aerosols to uncertainty in indirect forcing. *Nature* **2013**, *503*, 67-71.

(5) IPCC *Climate Change 2013: The Physical Science Basis*; Cambridge University Press: Cambridge, UK, 2013.
(6) Laurent, B.; Marticorena, B.; Bergametti, G.; Léon, J. F.; Mahowald, N. M. Modeling mineral dust emissions from the Sahara desert using new surface properties and soil database. *J. Geophys. Res.-Atmos* **2008**, *113*, D14218, doi: 14210.11029/12007JD009484.
(7) Laurent, B.; Marticorena, B.; Bergametti, G.; Mei, F. Modeling mineral dust emissions from Chinese and Mongolian deserts. *Glob. Planet. Change* **2006**, *52*, 121-141.
(8) Textor, C.; Schulz, M.; Guibert, S.; Kinne, S.; Balkanski, Y.; Bauer, S.; Berntsen, T.; Berglen, T.; Boucher, O.; Chin, M. *et al.* Analysis and quantification of the diversities of aerosol life cycles within AeroCom. *Atmos. Chem. Phys.* **2006**, *6*, 1777-1813.
(9) Huneeus, N.; Schulz, M.; Balkanski, Y.; Griesfeller, J.; Prospero, J.; Kinne, S.; Bauer, S.; Boucher, O.; Chin, M.; Dentener, F. *et al.* Global dust model intercomparison in AeroCom phase I. *Atmos. Chem. Phys.* **2011**, *11*, 7781-7816.
(10) Ginoux, P.; Prospero, J. M.; Gill, T. E.; Hsu, N. C.; Zhao, M. Global-scale attribution of anthropogenic and natural dust sources and their emission rates based on MODIS Deep Blue aerosol products. *Rev. Geophys.* **2012**, *50*, RG3005, doi: 3010.1029/2012RG000388.
(11) Forster, P.; Ramaswamy, V.; Artaxo, P.; Berntsen, T.; Betts, R.; Fahey, D. W.; Haywood, J.; Lean, J.; Lowe, D. C.; Myhre, G. *et al.* In *Climate Change 2007: The Physical Science Basis. Contribution of Working Group I to the Fourth Assessment Report of the Intergovernmental Panel on Climate Change*; Solomon, S., Qin, D., Manning, M., Chen, Z., Marquis, M., Averyt, K. B., Tignor, M., Miller, H. L., Eds.; Cambridge University Press: Cambridge, United Kingdom, 2007.
(12) Prospero, J. M. Long-range transport of mineral dust in the global atmosphere: Impact of African dust on the environment of the southeastern United States. *Proc. Natl. Acad. Sci. U. S. A.* **1999**, *96*, 3396-3403.
(13) Uno, I.; Eguchi, K.; Yumimoto, K.; Takemura, T.; Shimizu, A.; Uematsu, M.; Liu, Z.; Wang, Z.; Hara, Y.; Sugimoto, N. Asian dust transported one full circuit around the globe. *Nature Geosci.* **2009**, *2*, 557-560.
(14) Schepanski, K.; Tegen, I.; Macke, A. Saharan dust transport and deposition towards the tropical northern Atlantic. *Atmos. Chem. Phys.* **2009**, *9*, 1173-1189.
(15) Hande, L. B.; Engler, C.; Hoose, C.; Tegen, I. Seasonal variability of Saharan desert dust and ice nucleating particles over Europe. *Atmos. Chem. Phys.* **2015**, *15*, 4389-4397.
(16) Fairlie, T. D.; Jacob, D. J.; Dibb, J. E.; Alexander, B.; Avery, M. A.; van Donkelaar, A.; Zhang, L. Impact of mineral dust on nitrate, sulfate, and ozone in transpacific Asian pollution plumes. *Atmos. Chem. Phys.* **2010**, *10*, 3999-4012.
(17) Fairlie, T. D.; Jacob, D. J.; Park, R. J. The impact of transpacific transport of mineral dust in the United States. *Atmos. Environ.* **2007**, *41*, 1251-1266.
(18) Prospero, J. M.; Mayol-Bracero, O. L. Understanding the Transport and Impact of African Dust on the Caribbean Basin. *Bull. Amer. Meteorol. Soc.* **2013**, *94*, 1329-1337.
(19) Quinn, P. K.; Collins, D. B.; Grassian, V. H.; Prather, K. A.; Bates, T. S. Chemistry and Related Properties of Freshly Emitted Sea Spray Aerosol. *Chem. Rev.* **2015**, *115*, 4383-4399.
(20) Prospero, J. M.; Lamb, P. J. African droughts and dust transport to the Caribbean: Climate change implications. *Science* **2003**, *302*, 1024-1027.
(21) Mahowald, N. M.; Kloster, S.; Engelstaedter, S.; Moore, J. K.; Mukhopadhyay, S.; McConnell, J. R.; Albani, S.; Doney, S. C.; Bhattacharya, A.; Curran, M. A. J. *et al.*

Observed 20th century desert dust variability: impact on climate and biogeochemistry. *Atmos. Chem. Phys.* **2010**, *10*, 10875-10893.
(22) Tegen, I.; Lacis, A. A.; Fung, I. The influence on climate forcing of mineral aerosols from disturbed soils. *Nature* **1996**, *380*, 419-422.
(23) Tegen, I.; Harrison, S. P.; Kohfeld, K.; Prentice, I. C.; Coe, M.; Heimann, M. Impact of vegetation and preferential source areas on global dust aerosol: Results from a model study. *J. Geophys. Res.-Atmos.* **2002**, *107*, 4576, DOI: 4510.1029/2001JD000963.
(24) Tegen, I.; Werner, M.; Harrison, S. P.; Kohfeld, K. E. Relative importance of climate and land use in determining present and future global soil dust emission. *Geophys. Res. Lett.* **2004**, *31*, L05105, doi: 05110.01029/02003GL019216.
(25) Muhs, D. R. The geologic records of dust in the Quaternary. *Aeolian Res.* **2013**, *9*, 3-48.
(26) Muhs, D.; Prospero, J.; Baddock, M.; Gill, T. In *Mineral Dust*; Knippertz, P., Stuut, J.-B. W., Eds.; Springer: Netherlands, 2014.
(27) Mahowald, N. Aerosol Indirect Effect on Biogeochemical Cycles and Climate. *Science* **2011**, *334*, 794-796.
(28) Choobari, O. A.; Zawar-Reza, P.; Sturman, A. The global distribution of mineral dust and its impacts on the climate system: A review. *Atmos. Res.* **2014**, *138*, 152-165.
(29) Li, X.; Maring, H.; Savoie, D.; Voss, K.; Prospero, J. M. Dominance of mineral dust in aerosol light-scattering in the North Atlantic trade winds. *Nature* **1996**, *380*, 416-419.
(30) Balkanski, Y.; Schulz, M.; Claquin, T.; Guibert, S. Reevaluation of Mineral aerosol radiative forcings suggests a better agreement with satellite and AERONET data. *Atmos. Chem. Phys.* **2007**, *7*, 81-95.
(31) Sokolik, I. N.; Toon, O. B. Direct radiative forcing by anthropogenic airborne mineral aerosols. *Nature* **1996**, *381*, 681-683.
(32) Linke, C.; Möhler, O.; Veres, A.; Mohácsi, Á.; Bozóki, Z.; Szabó, G.; Schnaiter, M. Optical properties and mineralogical composition of different Saharan mineral dust samples: a laboratory study. *Atmos. Chem. Phys.* **2006**, *6*, 3315-3323.
(33) Sokolik, I. N.; Winker, D. M.; Bergametti, G.; Gillette, D. A.; Carmichael, G.; Kaufman, Y. J.; Gomes, L.; Schuetz, L.; Penner, J. E. Introduction to special section: Outstanding problems in quantifying the radiative impacts of mineral dust. *J. Geophys. Res.-Atmos.* **2001**, *106*, 18015-18027.
(34) Huang, X.; Song, Y.; Zhao, C.; Cai, X.; Zhang, H.; Zhu, T. Direct Radiative Effect by Multicomponent Aerosol over China. *J. Climate* **2015**, *28*, 3472-3495.
(35) Wu, Z. J.; Cheng, Y. F.; Hu, M.; Wehner, B.; Sugimoto, N.; Wiedensohler, A. Dust events in Beijing, China (2004–2006): comparison of ground-based measurements with columnar integrated observations. *Atmos. Chem. Phys.* **2009**, *9*, 6915-6932.
(36) Di Biagio, C.; Boucher, H.; Caquineau, S.; Chevaillier, S.; Cuesta, J.; Formenti, P. Variability of the infrared complex refractive index of African mineral dust: experimental estimation and implications for radiative transfer and satellite remote sensing. *Atmos. Chem. Phys.* **2014**, *14*, 11093-11116.
(37) McConnell, C. L.; Formenti, P.; Highwood, E. J.; Harrison, M. A. J. Using aircraft measurements to determine the refractive index of Saharan dust during the DODO Experiments. *Atmos. Chem. Phys.* **2010**, *10*, 3081-3098.
(38) Lemaitre, C.; Flamant, C.; Cuesta, J.; Raut, J. C.; Chazette, P.; Formenti, P.; Pelon, J. Radiative heating rates profiles associated with a springtime case of Bodele and Sudan dust transport over West Africa. *Atmos. Chem. Phys.* **2010**, *10*, 8131-8150.
(39) Tanre, D.; Haywood, J.; Pelon, J.; Leon, J. F.; Chatenet, B.; Formenti, P.; Francis, P.; Goloub, P.; Highwood, E. J.; Myhre, G. Measurement and modeling of the Saharan dust

radiative impact: Overview of the Saharan Dust Experiment (SHADE). *J. Geophys. Res.-Atmos.* **2003**, *108*, 8574, doi: 8510.1029/2002jd003273.
(40) Highwood, E.; Ryder, C. In *Mineral Dust*; Knippertz, P., Stuut, J.-B. W., Eds.; Springer: Netherlands, 2014.
(41) Kim, K. W.; He, Z.; Kim, Y. J. Physicochemical characteristics and radiative properties of Asian dust particles observed at Kwangju, Korea, during the 2001 ACE-Asia intensive observation period. *J. Geophys. Res.-Atmos* **2004**, *109*, D19S02, doi: 10.1029/2003JD003693.
(42) Jung, J.; Kim, Y. J.; Lee, K. Y.; Cayetano, M. G.; Batmunkh, T.; Koo, J. H.; Kim, J. Spectral optical properties of long-range transport Asian dust and pollution aerosols over Northeast Asia in 2007 and 2008. *Atmos. Chem. Phys.* **2010**, *10*, 5391-5408.
(43) Miller, R.; Knippertz, P.; Pérez García-Pando, C.; Perlwitz, J.; Tegen, I. In *Mineral Dust*; Knippertz, P., Stuut, J.-B. W., Eds.; Springer: Netherlands, 2014.
(44) Schladitz, A.; Müller, T.; Nordmann, S.; Tesche, M.; Groß, S.; Freudenthaler, V.; Gasteiger, J.; Wiedensohler, A. In situ aerosol characterization at Cape Verde Part 2: Parametrization of relative humidity- and wavelength-dependent aerosol optical properties. *Tellus B* **2011**, *63*.
(45) Jeong, G. R.; Sokolik, I. N. Effect of mineral dust aerosols on the photolysis rates in the clean and polluted marine environments. *J. Geophys. Res.-Atmos.* **2007**, *112*, D21308, doi: 21310.21029/22007jd008442.
(46) Koehler, K. A.; Kreidenweis, S. M.; DeMott, P. J.; Petters, M. D.; Prenni, A. J.; Carrico, C. M. Hygroscopicity and cloud droplet activation of mineral dust aerosol. *Geophys. Res. Lett.* **2009**, *36*, L08805, doi: 08810.01029/02009gl037348.
(47) Kumar, P.; Sokolik, I. N.; Nenes, A. Parameterization of cloud droplet formation for global and regional models: including adsorption activation from insoluble CCN. *Atmos. Chem. Phys.* **2009**, *9*, 2517-2532.
(48) Twohy, C. H.; Kreidenweis, S. M.; Eidhammer, T.; Browell, E. V.; Heymsfield, A. J.; Bansemer, A. R.; Anderson, B. E.; Chen, G.; Ismail, S.; DeMott, P. J. *et al.* Saharan dust particles nucleate droplets in eastern Atlantic clouds. *Geophys. Res. Lett.* **2009**, *36*, L01807, doi: 01810.01029/02008gl035846.
(49) Herich, H.; Tritscher, T.; Wiacek, A.; Gysel, M.; Weingartner, E.; Lohmann, U.; Baltensperger, U.; Cziczo, D. J. Water uptake of clay and desert dust aerosol particles at sub- and supersaturated water vapor conditions. *Phys. Chem. Chem. Phys.* **2009**, *11*, 7804-7809.
(50) Manktelow, P. T.; Carslaw, K. S.; Mann, G. W.; Spracklen, D. V. The impact of dust on sulfate aerosol, CN and CCN during an East Asian dust storm. *Atmos. Chem. Phys.* **2010**, *10*, 365-382.
(51) Karydis, V. A.; Kumar, P.; Barahona, D.; Sokolik, I. N.; Nenes, A. On the effect of dust particles on global cloud condensation nuclei and cloud droplet number. *J. Geophys. Res.-Atmos.* **2011**, *116*, D23204, doi: 23210.21029/22011jd016283.
(52) Kumar, P.; Nenes, A.; Sokolik, I. N. Importance of adsorption for CCN activity and hygroscopic properties of mineral dust aerosol. *Geophys. Res. Lett.* **2009**, *36*, L24804, doi: 24810.21029/22009gl040827.
(53) Solomos, S.; Kallos, G.; Kushta, J.; Astitha, M.; Tremback, C.; Nenes, A.; Levin, Z. An integrated modelling study on the effects of mineral dust and sea salt particles on clouds and precipitation. *Atmos. Chem. Phys.* **2011**, *11*, 873-892.
(54) Nenes, A.; Murray, B.; Bougiatioti, A. In *Mineral Dust*; Knippertz, P., Stuut, J.-B. W., Eds.; Springer: Netherlands, 2014.

(55) Zhang, H.; McFarquhar, G. M.; Cotton, W. R.; Deng, Y. Direct and indirect impacts of Saharan dust acting as cloud condensation nuclei on tropical cyclone eyewall development. *Geophys. Res. Lett.* **2009**, *36*, L06802, doi: 06810.01029/02009GL037276.
(56) DeMott, P. J.; Sassen, K.; Poellot, M. R.; Baumgardner, D.; Rogers, D. C.; Brooks, S. D.; Prenni, A. J.; Kreidenweis, S. M. African dust aerosols as atmospheric ice nuclei. *Geophys. Res. Lett.* **2003**, *30*, 1732, doi: 1710.1029/2003gl017410.
(57) Klein, H.; Nickovic, S.; Haunold, W.; Bundke, U.; Nillius, B.; Ebert, M.; Weinbruch, S.; Schuetz, L.; Levin, Z.; Barrie, L. A. *et al.* Saharan dust and ice nuclei over Central Europe. *Atmos. Chem. Phys.* **2010**, *10*, 10211-10221.
(58) Creamean, J. M.; Suski, K. J.; Rosenfeld, D.; Cazorla, A.; DeMott, P. J.; Sullivan, R. C.; White, A. B.; Ralph, F. M.; Minnis, P.; Comstock, J. M. *et al.* Dust and Biological Aerosols from the Sahara and Asia Influence Precipitation in the Western U.S. *Science* **2013**, *339*, 1572-1578.
(59) Hoose, C.; Lohmann, U.; Erdin, R.; Tegen, I. The global influence of dust mineralogical composition on heterogeneous ice nucleation in mixed-phase clouds. *Environ. Res. Lett.* **2008**, *3*, 025003.
(60) Field, P. R.; Mohler, O.; Connolly, P.; Kramer, M.; Cotton, R.; Heymsfield, A. J.; Saathoff, H.; Schnaiter, M. Some ice nucleation characteristics of Asian and Saharan desert dust. *Atmos. Chem. Phys.* **2006**, *6*, 2991-3006.
(61) DeMott, P. J.; Cziczo, D. J.; Prenni, A. J.; Murphy, D. M.; Kreidenweis, S. M.; Thomson, D. S.; Borys, R.; Rogers, D. C. Measurements of the concentration and composition of nuclei for cirrus formation. *Proc. Natl. Acad. Sci. U. S. A.* **2003**, *100*, 14655-14660.
(62) DeMott, P. J.; Prenni, A. J.; Liu, X.; Kreidenweis, S. M.; Petters, M. D.; Twohy, C. H.; Richardson, M. S.; Eidhammer, T.; Rogers, D. C. Predicting global atmospheric ice nuclei distributions and their impacts on climate. *Proc. Natl. Acad. Sci. U. S. A.* **2010**, *107*, 11217-11222.
(63) Zimmermann, F.; Weinbruch, S.; Schutz, L.; Hofmann, H.; Ebert, M.; Kandler, K.; Worringen, A. Ice nucleation properties of the most abundant mineral dust phases. *J. Geophys. Res.-Atmos.* **2008**, *113*, D23204, doi: 23210.21029/22008jd010655.
(64) Stith, J. L.; Ramanathan, V.; Cooper, W. A.; Roberts, G. C.; DeMott, P. J.; Carmichael, G.; Hatch, C. D.; Adhikary, B.; Twohy, C. H.; Rogers, D. C. *et al.* An overview of aircraft observations from the Pacific Dust Experiment campaign. *J. Geophys. Res.-Atmos.* **2009**, *114*, D05207, doi: 05210.01029/02008jd010924.
(65) Ryder, C. L.; McQuaid, J. B.; Flamant, C.; Rosenberg, P. D.; Washington, R.; Brindley, H. E.; Highwood, E. J.; Marsham, J. H.; Parker, D. J.; Todd, M. C. *et al.* Advances in understanding mineral dust and boundary layer processes over the Sahara from Fennec aircraft observations. *Atmos. Chem. Phys.* **2015**, *15*, 8479-8520.
(66) Burrows, S. M.; Hoose, C.; Pöschl, U.; Lawrence, M. G. Ice nuclei in marine air: biogenic particles or dust? *Atmos. Chem. Phys.* **2013**, *13*, 245-267.
(67) Pratt, K. A.; DeMott, P. J.; French, J. R.; Wang, Z.; Westphal, D. L.; Heymsfield, A. J.; Twohy, C. H.; Prenni, A. J.; Prather, K. A. In situ detection of biological particles in cloud ice-crystals. *Nature Geoscience* **2009**, *2*, 397-400.
(68) Baustian, K. J.; Cziczo, D. J.; Wise, M. E.; Pratt, K. A.; Kulkarni, G.; Hallar, A. G.; Tolbert, M. A. Importance of aerosol composition, mixing state, and morphology for heterogeneous ice nucleation: A combined field and laboratory approach. *J. Geophys. Res.-Atmos.* **2012**, *117*, D06217, doi: 06210.01029/02011jd016784.
(69) Cziczo, D. J.; Froyd, K. D. Sampling the composition of cirrus ice residuals. *Atmos. Res.* **2014**, *142*, 15-31.

(70) Ebert, M.; Worringen, A.; Benker, N.; Mertes, S.; Weingartner, E.; Weinbruch, S. Chemical composition and mixing-state of ice residuals sampled within mixed phase clouds. *Atmos. Chem. Phys.* **2011**, *11*, 2805-2816.
(71) Kamphus, M.; Ettner-Mahl, M.; Klimach, T.; Drewnick, F.; Keller, L.; Cziczo, D. J.; Mertes, S.; Borrmann, S.; Curtius, J. Chemical composition of ambient aerosol, ice residues and cloud droplet residues in mixed-phase clouds: single particle analysis during the Cloud and Aerosol Characterization Experiment (CLACE 6). *Atmos. Chem. Phys.* **2010**, *10*, 8077-8095.
(72) DeMott, P. J.; Prenni, A. J.; McMeeking, G. R.; Sullivan, R. C.; Petters, M. D.; Tobo, Y.; Niemand, M.; Möhler, O.; Snider, J. R.; Wang, Z. *et al.* Integrating laboratory and field data to quantify the immersion freezing ice nucleation activity of mineral dust particles. *Atmos. Chem. Phys.* **2015**, *15*, 393-409.
(73) Prenni, A. J.; Petters, M. D.; Kreidenweis, S. M.; Heald, C. L.; Martin, S. T.; Artaxo, P.; Garland, R. M.; Wollny, A. G.; Poschl, U. Relative roles of biogenic emissions and Saharan dust as ice nuclei in the Amazon basin. *Nat. Geosci.* **2009**, *2*, 401-404.
(74) Cziczo, D. J.; Froyd, K. D.; Hoose, C.; Jensen, E. J.; Diao, M.; Zondlo, M. A.; Smith, J. B.; Twohy, C. H.; Murphy, D. M. Clarifying the Dominant Sources and Mechanisms of Cirrus Cloud Formation. *Science* **2013**, *340*, 1320-1324.
(75) Hoose, C.; Kristjansson, J. E.; Burrows, S. M. How important is biological ice nucleation in clouds on a global scale? *Environ. Res. Lett.* **2010**, *5*, 024009.
(76) Lohmann, U.; Feichter, J. Global indirect aerosol effects: a review. *Atmos. Chem. Phys.* **2005**, *5*, 715-737.
(77) Baker, M. B. Cloud microphysics and climate. *Science* **1997**, *276*, 1072-1078.
(78) Gettelman, A.; Liu, X.; Barahona, D.; Lohmann, U.; Chen, C. Climate impacts of ice nucleation. *J. Geophys. Res.-Atmos.* **2012**, *117*.
(79) Wiacek, A.; Peter, T. On the availability of uncoated mineral dust ice nuclei in cold cloud regions. *Geophys. Res. Lett.* **2009**, *36*.
(80) Rosenfeld, D.; Lohmann, U.; Raga, G. B.; O'Dowd, C. D.; Kulmala, M.; Fuzzi, S.; Reissell, A.; Andreae, M. O. Flood or drought: How do aerosols affect precipitation? *Science* **2008**, *321*, 1309-1313.
(81) Yin, Y.; Wurzler, S.; Levin, Z.; Reisin, T. G. Interactions of mineral dust particles and clouds: Effects on precipitation and cloud optical properties. *J. Geophys. Res.-Atmos.* **2002**, *107*, 4724, doi: 4710.1029/2001jd001544.
(82) Ramanathan, V.; Crutzen, P. J.; Kiehl, J. T.; Rosenfeld, D. Atmosphere - Aerosols, climate, and the hydrological cycle. *Science* **2001**, *294*, 2119-2124.
(83) Rosenfeld, D.; Rudich, Y.; Lahav, R. Desert dust suppressing precipitation: A possible desertification feedback loop. *Proc. Natl. Acad. Sci. U. S. A.* **2001**, *98*, 5975-5980.
(84) Shi, Z. B.; Krom, M. D.; Jickells, T. D.; Bonneville, S.; Carslaw, K. S.; Mihalopoulos, N.; Baker, A. R.; Benning, L. G. Impacts on iron solubility in the mineral dust by processes in the source region and the atmosphere: A review. *Aeolian Res.* **2012**, *5*, 21-42.
(85) Boyd, P. W.; Ellwood, M. J. The biogeochemical cycle of iron in the ocean. *Nature Geosci* **2010**, *3*, 675-682.
(86) Boyd, P. W.; Jickells, T.; Law, C. S.; Blain, S.; Boyle, E. A.; Buesseler, K. O.; Coale, K. H.; Cullen, J. J.; de Baar, H. J. W.; Follows, M. *et al.* Mesoscale Iron Enrichment Experiments 1993-2005: Synthesis and Future Directions. *Science* **2007**, *315*, 612-617.
(87) Moore, J. K.; Braucher, O. Sedimentary and mineral dust sources of dissolved iron to the world ocean. *Biogeosciences* **2008**, *5*, 631-656.

(88) Nenes, A.; Krom, M. D.; Mihalopoulos, N.; Van Cappellen, P.; Shi, Z.; Bougiatioti, A.; Zarmpas, P.; Herut, B. Atmospheric acidification of mineral aerosols: a source of bioavailable phosphorus for the oceans. *Atmos. Chem. Phys.* **2011**, *11*, 6265-6272.
(89) Okin, G. S.; Baker, A. R.; Tegen, I.; Mahowald, N. M.; Dentener, F. J.; Duce, R. A.; Galloway, J. N.; Hunter, K.; Kanakidou, M.; Kubilay, N. *et al.* Impacts of atmospheric nutrient deposition on marine productivity: Roles of nitrogen, phosphorus, and iron. *Glob. Biogeochem. Cycle* **2011**, *25*, GB2022, doi: 2010.1029/2010GB003858.
(90) Okin, G. S.; Mahowald, N.; Chadwick, O. A.; Artaxo, P. Impact of desert dust on the biogeochemistry of phosphorus in terrestrial ecosystems. *Glob. Biogeochem. Cycle* **2004**, *18*, GB2005, doi: 2010.1029/2003GB002145.
(91) Mahowald, N.; Jickells, T. D.; Baker, A. R.; Artaxo, P.; Benitez-Nelson, C. R.; Bergametti, G.; Bond, T. C.; Chen, Y.; Cohen, D. D.; Herut, B. *et al.* Global distribution of atmospheric phosphorus sources, concentrations and deposition rates, and anthropogenic impacts. *Glob. Biogeochem. Cycle* **2008**, *22*, GB4026, doi: 4010.1029/2008GB003240.
(92) Jordi, A.; Basterretxea, G.; Tovar-Sánchez, A.; Alastuey, A.; Querol, X. Copper aerosols inhibit phytoplankton growth in the Mediterranean Sea. *Proc. Natl. Acad. Sci. U.S.A.* **2012**, *109*, 21246-21249.
(93) Paytan, A.; Mackey, K. R. M.; Chen, Y.; Lima, I. D.; Doney, S. C.; Mahowald, N.; Labiosa, R.; Post, A. F. Toxicity of atmospheric aerosols on marine phytoplankton. *Proc. Natl. Acad. Sci. U.S.A.* **2009**, *106*, 4601-4605.
(94) Mahowald, N. M.; Baker, A. R.; Bergametti, G.; Brooks, N.; Duce, R. A.; Jickells, T. D.; Kubilay, N.; Prospero, J. M.; Tegen, I. Atmospheric global dust cycle and iron inputs to the ocean. *Glob. Biogeochem. Cycle* **2005**, *19*, GB4025, doi:4010.1029/2004GB002402.
(95) Schulz, M.; Prospero, J. M.; Baker, A. R.; Dentener, F.; Ickes, L.; Liss, P. S.; Mahowald, N. M.; Nickovic, S.; García-Pando, C. P.; Rodríguez, S. *et al.* Atmospheric Transport and Deposition of Mineral Dust to the Ocean: Implications for Research Needs. *Environ. Sci. Technol.* **2012**, *46*, 10390-10404.
(96) Meskhidze, N.; Chameides, W. L.; Nenes, A. Dust and pollution: A recipe for enhanced ocean fertilization? *J. Geophys. Res.-Atmos.* **2005**, *110*, D03301, doi: 03310.01029/02004jd005082.
(97) Paytan, A.; McLaughlin, K. The Oceanic Phosphorus Cycle. *Chem. Rev.* **2007**, *107*, 563-576.
(98) Bristow, C. S.; Hudson-Edwards, K. A.; Chappell, A. Fertilizing the Amazon and equatorial Atlantic with West African dust. *Geophys. Res. Lett.* **2010**, *37*, L14807, doi: 14810.11029/12010GL043486.
(99) Yu, H.; Chin, M.; Yuan, T.; Bian, H.; Remer, L. A.; Prospero, J. M.; Omar, A.; Winker, D.; Yang, Y.; Zhang, Y. *et al.* The Fertilizing Role of African Dust in the Amazon Rainforest: A First Multiyear Assessment Based on CALIPSO Lidar Observations. *Geophys. Res. Lett.* **2015**, *42*, GL063040, doi: 063010.061002/062015GL063040.
(100) Mahowald, N.; Ward, D. S.; Kloster, S.; Flanner, M. G.; Heald, C. L.; Heavens, N. G.; Hess, P. G.; Lamarque, J.-F.; Chuang, P. Y. Aerosol Impacts on Climate and Biogeochemistry. *Annu. Rev. Environ. Resour.* **2011**, *36*, 45-74.
(101) Jickells, T. D.; An, Z. S.; Andersen, K. K.; Baker, A. R.; Bergametti, G.; Brooks, N.; Cao, J. J.; Boyd, P. W.; Duce, R. A.; Hunter, K. A. *et al.* Global iron connections between desert dust, ocean biogeochemistry, and climate. *Science* **2005**, *308*, 67-71.
(102) Garrison, V. H.; Shinn, E. A.; Foreman, W. T.; Griffin, D. W.; Holmes, C. W.; Kellogg, C. A.; Majewski, M. S.; Richardson, L. L.; Ritchie, K. B.; Smith, G. W. African and Asian Dust: From Desert Soils to Coral Reefs. *BioScience* **2003**, *53*, 469-480.

(103) Jickells, T.; Boyd, P.; Hunter, K. In *Mineral Dust*; Knippertz, P., Stuut, J.-B. W., Eds.; Springer: Netherlands, 2014.
(104) Zhu, T.; Shang, J.; Zhao, D. F. The roles of heterogeneous chemical processes in the formation of an air pollution complex and gray haze. *Sci. China-Chem.* **2011**, *54*, 145-153.
(105) Lelieveld, J.; Evans, J. S.; Fnais, M.; Giannadaki, D.; Pozzer, A. The contribution of outdoor air pollution sources to premature mortality on a global scale. *Nature* **2015**, *525*, 367-371.
(106) Morman, S.; Plumlee, G. In *Mineral Dust*; Knippertz, P., Stuut, J.-B. W., Eds.; Springer: Netherlands, 2014.
(107) Mahowald, N. M.; Ballantine, J. A.; Feddema, J.; Ramankutty, N. Global trends in visibility: implications for dust sources. *Atmos. Chem. Phys.* **2007**, *7*, 3309-3339.
(108) Giannadaki, D.; Pozzer, A.; Lelieveld, J. Modeled global effects of airborne desert dust on air quality and premature mortality. *Atmos. Chem. Phys.* **2014**, *14*, 957-968.
(109) De Longueville, F.; Hountondji, Y.-C.; Henry, S.; Ozer, P. What do we know about effects of desert dust on air quality and human health in West Africa compared to other regions? *Sci. Total Environ.* **2010**, *409*, 1-8.
(110) de Longueville, F.; Ozer, P.; Doumbia, S.; Henry, S. Desert dust impacts on human health: an alarming worldwide reality and a need for studies in West Africa. *Int. J. Biometeorol.* **2013**, *57*, 1-19.
(111) Perez, L.; Tobias, A.; Querol, X.; Künzli, N.; Pey, J.; Alastuey, A.; Viana, M.; Valero, N.; González-Cabré, M.; Sunyer, J. Coarse Particles From Saharan Dust and Daily Mortality. *Epidemiology* **2008**, *19*, 800-807.
(112) Karanasiou, A.; Moreno, N.; Moreno, T.; Viana, M.; de Leeuw, F.; Querol, X. Health effects from Sahara dust episodes in Europe: Literature review and research gaps. *Environ. Int.* **2012**, *47*, 107-114.
(113) Meng, Z.; Lu, B. Dust events as a risk factor for daily hospitalization for respiratory and cardiovascular diseases in Minqin, China. *Atmos. Environ.* **2007**, *41*, 7048-7058.
(114) Kwon, H.-J.; Cho, S.-H.; Chun, Y.; Lagarde, F.; Pershagen, G. Effects of the Asian Dust Events on Daily Mortality in Seoul, Korea. *Environ. Res.* **2002**, *90*, 1-5.
(115) Fubini, B.; Otero Arean, C. Chemical aspects of the toxicity of inhaled mineral dusts. *Chem. Soc. Rev.* **1999**, *28*, 373-381.
(116) Thalib, L.; Al-Taiar, A. Dust storms and the risk of asthma admissions to hospitals in Kuwait. *Sci. Total Environ.* **2012**, *433*, 347-351.
(117) Yang, C.-Y.; Chen, Y.-S.; Chiu, H.-F.; Goggins, W. B. Effects of Asian dust storm events on daily stroke admissions in Taipei, Taiwan. *Environ. Res.* **2005**, *99*, 79-84.
(118) Tobías, A.; Pérez, L.; Díaz, J.; Linares, C.; Pey, J.; Alastruey, A.; Querol, X. Short-term effects of particulate matter on total mortality during Saharan dust outbreaks: A case-crossover analysis in Madrid (Spain). *Sci. Total Environ.* **2011**, *412–413*, 386-389.
(119) Chen, Y.-S.; Sheen, P.-C.; Chen, E.-R.; Liu, Y.-K.; Wu, T.-N.; Yang, C.-Y. Effects of Asian dust storm events on daily mortality in Taipei, Taiwan. *Environ. Res.* **2004**, *95*, 151-155.
(120) Alessandrini, E. R.; Stafoggia, M.; Faustini, A.; Gobbi, G. P.; Forastiere, F. Saharan dust and the association between particulate matter and daily hospitalisations in Rome, Italy. *Occup. Environ. Med.* **2013**, *70*, 432-434.
(121) Claquin, T.; Schulz, M.; Balkanski, Y. J. Modeling the mineralogy of atmospheric dust sources. *J. Geophys. Res.-Atmos.* **1999**, *104*, 22243-22256.

(122) Nickovic, S.; Vukovic, A.; Vujadinovic, M.; Djurdjevic, V.; Pejanovic, G. Technical Note: High-resolution mineralogical database of dust-productive soils for atmospheric dust modeling. *Atmos. Chem. Phys.* **2012**, *12*, 845-855.
(123) Journet, E.; Balkanski, Y.; Harrison, S. P. A new data set of soil mineralogy for dust-cycle modeling. *Atmos. Chem. Phys.* **2014**, *14*, 3801-3816.
(124) Formenti, P.; Schutz, L.; Balkanski, Y.; Desboeufs, K.; Ebert, M.; Kandler, K.; Petzold, A.; Scheuvens, D.; Weinbruch, S.; Zhang, D. Recent progress in understanding physical and chemical properties of African and Asian mineral dust. *Atmos. Chem. Phys.* **2011**, *11*, 8231-8256.
(125) Klaver, A.; Formenti, P.; Caquineau, S.; Chevaillier, S.; Ausset, P.; Calzolai, G.; Osborne, S.; Johnson, B.; Harrisone, M.; Dubovik, O. Physico-chemical and optical properties of Sahelian and Saharan mineral dust: in situ measurements during the GERBILS campaign. *Q. J. R. Meteorol. Soc.* **2011**, *137*, 1193-1210.
(126) Fitzgerald, E.; Ault, A. P.; Zauscher, M. D.; Mayol-Bracero, O. L.; Prather, K. A. Comparison of the mixing state of long-range transported Asian and African mineral dust. *Atmos. Environ.* **2015**, *115*, 19-25.
(127) Scheuvens, D.; Schütz, L.; Kandler, K.; Ebert, M.; Weinbruch, S. Bulk composition of northern African dust and its source sediments - A compilation. *Earth-Sci. Rev.* **2013**, *116*, 170-194.
(128) Scheuvens, D.; Kandler, K. In *Mineral Dust*; Knippertz, P., Stuut, J.-B. W., Eds.; Springer: Netherlands, 2014.
(129) Perlwitz, J. P.; Pérez García-Pando, C.; Miller, R. L. Predicting the mineral composition of dust aerosols – Part 1: Representing key processes. *Atmos. Chem. Phys.* **2015**, *15*, 11593-11627.
(130) Perlwitz, J. P.; Pérez García-Pando, C.; Miller, R. L. Predicting the mineral composition of dust aerosols – Part 2: Model evaluation and identification of key processes with observations. *Atmos. Chem. Phys.* **2015**, *15*, 11629-11652.
(131) Seisel, S.; Borensen, C.; Vogt, R.; Zellner, R. Kinetics and mechanism of the uptake of N_2O_5 on mineral dust at 298 K. *Atmos. Chem. Phys.* **2005**, *5*, 3423-3432.
(132) Karagulian, F.; Santschi, C.; Rossi, M. J. The heterogeneous chemical kinetics of N_2O_5 on $CaCO_3$ and other atmospheric mineral dust surrogates. *Atmos. Chem. Phys.* **2006**, *6*, 1373-1388.
(133) Mogili, P. K.; Kleiber, P. D.; Young, M. A.; Grassian, V. H. N_2O_5 hydrolysis on the components of mineral dust and sea salt aerosol: Comparison study in an environmental aerosol reaction chamber. *Atmos. Environ.* **2006**, *40*, 7401-7408.
(134) Wagner, C.; Hanisch, F.; Holmes, N.; de Coninck, H.; Schuster, G.; Crowley, J. N. The interaction of N_2O_5 with mineral dust: aerosol flow tube and Knudsen reactor studies. *Atmos. Chem. Phys.* **2008**, *8*, 91-109.
(135) Wagner, C.; Schuster, G.; Crowley, J. N. An aerosol flow tube study of the interaction of N_2O_5 with calcite, Arizona dust and quartz. *Atmos. Environ.* **2009**, *43*, 5001-5008.
(136) Tang, M. J.; Thieser, J.; Schuster, G.; Crowley, J. N. Kinetics and mechanism of the heterogeneous reaction of N2O5 with mineral dust particles. *Phys. Chem. Chem. Phys.* **2012**, *14*, 8551-8561.
(137) Tang, M. J.; Schuster, G.; Crowley, J. N. Heterogeneous reaction of N2O5 with illite and Arizona test dust particles. *Atmos. Chem. Phys.* **2014**, *14*, 245-254.
(138) Tang, M. J.; Telford, P. J.; Pope, F. D.; Rkiouak, L.; Abraham, N. L.; Archibald, A. T.; Braesicke, P.; Pyle, J. A.; McGregor, J.; Watson, I. M. *et al.* Heterogeneous reaction of N2O5 with airborne TiO2 particles and its implication for stratospheric particle injection. *Atmos. Chem. Phys.* **2014**, *14*, 6035-6048.

(139) Tang, M. J.; Camp, J. C. J.; Rkiouak, L.; McGregor, J.; Watson, I. M.; Cox, R. A.; Kalberer, M.; Ward, A. D.; Pope, F. D. Heterogeneous Interaction of SiO2 with N2O5: Aerosol Flow Tube and Single Particle Optical Levitation-Raman Spectroscopy Studies. *J. Phys. Chem. A* **2014**, *118*, 8817-8827.
(140) Murray, B. J.; O'Sullivan, D.; Atkinson, J. D.; Webb, M. E. Ice nucleation by particles immersed in supercooled cloud droplets. *Chem. Soc. Rev.* **2012**, *41*, 6519-6554.
(141) Atkinson, J. D.; Murray, B. J.; Woodhouse, M. T.; Whale, T. F.; Baustian, K. J.; Carslaw, K. S.; Dobbie, S.; O/'Sullivan, D.; Malkin, T. L. The importance of feldspar for ice nucleation by mineral dust in mixed-phase clouds. *Nature* **2013**, *498*, 355-358.
(142) Journet, E.; Desboeufs, K. V.; Caquineau, S.; Colin, J.-L. Mineralogy as a critical factor of dust iron solubility. *Geophys. Res. Lett.* **2008**, *35*, L07805, doi: 07810.01029/02007GL031589.
(143) Cwiertny, D. M.; Baltrusaitis, J.; Hunter, G. J.; Laskin, A.; Scherer, M. M.; Grassian, V. H. Characterization and acid-mobilization study of iron-containing mineral dust source materials. *J. Geophys. Res.-Atmos.* **2008**, *113*, D05202, doi: 05210.01029/02007JD009332.
(144) Fu, H. B.; Cwiertny, D. M.; Carmichael, G. R.; Scherer, M. M.; Grassian, V. H. Photoreductive dissolution of Fe-containing mineral dust particles in acidic media. *J. Geophys. Res.-Atmos.* **2010**, *115*, D11304, doi: 11310.11029/12009JD012702.
(145) Formenti, P.; Caquineau, S.; Desboeufs, K.; Klaver, A.; Chevaillier, S.; Journet, E.; Rajot, J. L. Mapping the physico-chemical properties of mineral dust in western Africa: mineralogical composition. *Atmos. Chem. Phys.* **2014**, *14*, 10663-10686.
(146) Jeong, G. Y. Bulk and single-particle mineralogy of Asian dust and a comparison with its source soils. *J. Geophys. Res.-Atmos.* **2008**, *113*, D02208, doi: 02210.01029/02007jd008606.
(147) Avila, A.; QueraltMitjans, I.; Alarcon, M. Mineralogical composition of African dust delivered by red rains over northeastern Spain. *J. Geophys. Res.-Atmos.* **1997**, *102*, 21977-21996.
(148) Caquineau, S.; Gaudichet, A.; Gomes, L.; Legrand, M. Mineralogy of Saharan dust transported over northwestern tropical Atlantic Ocean in relation to source regions. *J. Geophys. Res.-Atmos.* **2002**, *107*, 4251, doi: 4210.1029/2000jd000247.
(149) Kandler, K.; Schutz, L.; Deutscher, C.; Ebert, M.; Hofmann, H.; Jackel, S.; Jaenicke, R.; Knippertz, P.; Lieke, K.; Massling, A. *et al.* Size distribution, mass concentration, chemical and mineralogical composition and derived optical parameters of the boundary layer aerosol at Tinfou, Morocco, during SAMUM 2006. *Tellus Ser. B-Chem. Phys. Meteorol.* **2009**, *61*, 32-50.
(150) Scanza, R. A.; Mahowald, N.; Ghan, S.; Zender, C. S.; Kok, J. F.; Liu, X.; Zhang, Y.; Albani, S. Modeling dust as component minerals in the Community Atmosphere Model: development of framework and impact on radiative forcing. *Atmos. Chem. Phys.* **2015**, *15*, 537-561.
(151) Hanisch, F.; Crowley, J. N. Ozone decomposition on Saharan dust: an experimental investigation. *Atmos. Chem. Phys.* **2003**, *3*, 119-130.
(152) Adedokun, J. A.; Emofurieta, W. O.; Adedeji, O. A. Physical, mineralogical and chemical properties of harmattan dust at Ile-Ife, Nigeria. *Theor. Appl. Climatol.* **1989**, *40*, 161-169.
(153) Hsu, S.-C.; Liu, S. C.; Huang, Y.-T.; Chou, C. C. K.; Lung, S. C. C.; Liu, T.-H.; Tu, J.-Y.; Tsai, F. Long-range southeastward transport of Asian biosmoke pollution: Signature detected by aerosol potassium in Northern Taiwan. *J. Geophys. Res.-Atmos* **2009**, *114*, D14301, doi: 14310.11029/12009JD011725.

(154) George, C.; D'Anna, B.; Herrmann, H.; Weller, C.; Vaida, V.; Donaldson, D. J.; Bartels-Rausch, T.; Ammann, M. In *Atmospheric and Aerosol Chemistry*; McNeill, V. F., Ariya, P. A., Eds.; Springer Berlin Heidelberg, 2014; Vol. 339.
(155) Chen, H. H.; Nanayakkara, C. E.; Grassian, V. H. Titanium Dioxide Photocatalysis in Atmospheric Chemistry. *Chem. Rev.* **2012**, *112*, 5919-5948.
(156) George, C.; Ammann, M.; D'Anna, B.; Donaldson, D. J.; Nizkorodov, S. A. Heterogeneous Photochemistry in the Atmosphere. *Chem. Rev.* **2015**, *115*, 4218-4258.
(157) Harris, E.; Sinha, B.; van Pinxteren, D.; Tilgner, A.; Fomba, K. W.; Schneider, J.; Roth, A.; Gnauk, T.; Fahlbusch, B.; Mertes, S. *et al.* Enhanced Role of Transition Metal Ion Catalysis During In-Cloud Oxidation of SO2. *Science* **2013**, *340*, 727-730.
(158) Sullivan, R. C.; Guazzotti, S. A.; Sodeman, D. A.; Prather, K. A. Direct observations of the atmospheric processing of Asian mineral dust. *Atmos. Chem. Phys.* **2007**, *7*, 1213-1236.
(159) Matsuki, A.; Iwasaka, Y.; Shi, G. Y.; Zhang, D. Z.; Trochkine, D.; Yamada, M.; Kim, Y. S.; Chen, B.; Nagatani, T.; Miyazawa, T. *et al.* Morphological and chemical modification of mineral dust: Observational insight into the heterogeneous uptake of acidic gases. *Geophys. Res. Lett.* **2005**, *32*, L22806, doi: 22810.21029/22005gl024176.
(160) Mori, I.; Nishikawa, M.; Tanimura, T.; Quan, H. Change in size distribution and chemical composition of kosa (Asian dust) aerosol during long-range transport. *Atmos. Environ.* **2003**, *37*, 4253-4263.
(161) Usher, C. R.; Michel, A. E.; Grassian, V. H. Reactions on mineral dust. *Chem. Rev.* **2003**, *103*, 4883-4939.
(162) Matsuki, A.; Schwarzenboeck, A.; Venzac, H.; Laj, P.; Crumeyrolle, S.; Gomes, L. Cloud processing of mineral dust: direct comparison of cloud residual and clear sky particles during AMMA aircraft campaign in summer 2006. *Atmos. Chem. Phys.* **2010**, *10*, 1057-1069.
(163) Pope, F. D.; Braesicke, P.; Grainger, R. G.; Kalberer, M.; Watson, I. M.; Davidson, P. J.; Cox, R. A. Stratospheric aerosol particles and solar-radiation management. *Nature Clim. Change* **2012**, *2*, 713-719.
(164) Ferraro, A. J.; Highwood, E. J.; Charlton-Perez, A. J. Stratospheric heating by potential geoengineering aerosols. *Geophys. Res. Lett.* **2011**, *38*, L24706, doi: 24710.21029/22011gl049761.
(165) Weisenstein, D. K.; Keith, D. W. Solar geoengineering using solid aerosol in the stratosphere. *Atmos. Chem. Phys. Discuss.* **2015**, *15*, 11799-11851.
(166) Crutzen, P. J. Albedo enhancement by stratospheric sulfur injections: A contribution to resolve a policy dilemma? *Clim. Change* **2006**, *77*, 211-219.
(167) Pruppacher, H. R.; Klett, J. D. *Microphysics of Clouds and Precipitation* Kluwer Academic Publishers: Dordrecht, Netherlands 1994.
(168) Dusek, U.; Frank, G. P.; Hildebrandt, L.; Curtius, J.; Schneider, J.; Walter, S.; Chand, D.; Drewnick, F.; Hings, S.; Jung, D. *et al.* Size Matters More Than Chemistry for Cloud-Nucleating Ability of Aerosol Particles. *Science* **2006**, *312*, 1375-1378.
(169) Petters, M. D.; Kreidenweis, S. M. A single parameter representation of hygroscopic growth and cloud condensation nucleus activity. *Atmos. Chem. Phys.* **2007**, *7*, 1961-1971.
(170) McFiggans, G.; Artaxo, P.; Baltensperger, U.; Coe, H.; Facchini, M. C.; Feingold, G.; Fuzzi, S.; Gysel, M.; Laaksonen, A.; Lohmann, U. *et al.* The effect of physical and chemical aerosol properties on warm cloud droplet activation. *Atmos. Chem. Phys.* **2006**, *6*, 2593-2649.
(171) Cwiertny, D. M.; Young, M. A.; Grassian, V. H. Chemistry and photochemistry of mineral dust aerosol. *Annu. Rev. Phys. Chem.* **2008**, *59*, 27-51.

(172) Crowley, J. N.; Ammann, M.; Cox, R. A.; Hynes, R. G.; Jenkin, M. E.; Mellouki, A.; Rossi, M. J.; Troe, J.; Wallington, T. J. Evaluated kinetic and photochemical data for atmospheric chemistry: Volume V - heterogeneous reactions on solid substrates. *Atmos. Chem. Phys.* **2010**, *10*, 9059-9223.
(173) Kolb, C. E.; Cox, R. A.; Abbatt, J. P. D.; Ammann, M.; Davis, E. J.; Donaldson, D. J.; Garrett, B. C.; George, C.; Griffiths, P. T.; Hanson, D. R. *et al.* An overview of current issues in the uptake of atmospheric trace gases by aerosols and clouds. *Atmos. Chem. Phys.* **2010**, *10*, 10561-10605.
(174) Tong, S. R.; Wu, L. Y.; Ge, M. F.; Wang, W. G.; Pu, Z. F. Heterogeneous chemistry of monocarboxylic acids on α-Al_2O_3 at different relative humidities. *Atmos. Chem. Phys.* **2010**, *10*, 7561-7574.
(175) Wu, L. Y.; Tong, S. R.; Wang, W. G.; Ge, M. F. Effects of temperature on the heterogeneous oxidation of sulfur dioxide by ozone on calcium carbonate. *Atmos. Chem. Phys.* **2011**, *11*, 6593-6605.
(176) Tang, M. J.; Li, M. Q.; Zhu, T. Heterogeneous reactions of gaseous methanesulfonic acid with calcium carbonate and kaolinite particles. *Sci. China-Chem.* **2010**, *53*, 2657-2662.
(177) Tang, M. J.; Thieser, J.; Schuster, G.; Crowley, J. N. Uptake of NO_3 and N_2O_5 to Saharan dust, ambient urban aerosol and soot: a relative rate study. *Atmos. Chem. Phys.* **2010**, *10*, 2965-2974.
(178) Fu, H. B.; Wang, X.; Wu, H. B.; Yin, Y.; Chen, J. M. Heterogeneous uptake and oxidation of SO2 on iron oxides. *J. Phys. Chem. C* **2007**, *111*, 6077-6085.
(179) Kong, L. D.; Zhao, X.; Sun, Z. Y.; Yang, Y. W.; Fu, H. B.; Zhang, S. C.; Cheng, T. T.; Yang, X.; Wang, L.; Chen, J. M. The effects of nitrate on the heterogeneous uptake of sulfur dioxide on hematite. *Atmos. Chem. Phys.* **2014**, *14*, 9451-9467.
(180) Zhao, X.; Kong, L. D.; Sun, Z. Y.; Ding, X. X.; Cheng, T. T.; Yang, X.; Chen, J. M. Interactions between Heterogeneous Uptake and Adsorption of Sulfur Dioxide and Acetaldehyde on Hematite. *J. Phys. Chem. A* **2015**, *119*, 4001-4008.
(181) He, H.; Wang, Y.; Ma, Q.; Ma, J.; Chu, B.; Ji, D.; Tang, G.; Liu, C.; Zhang, H.; Hao, J. Mineral dust and NOx promote the conversion of SO2 to sulfate in heavy pollution days. *Sci. Rep.* **2014**, *4*, 4172, doi: 4110.1038/srep04172.
(182) Ma, Q.; Liu, Y.; Liu, C.; Ma, J.; He, H. A case study of Asian dust storm particles: Chemical composition, reactivity to SO2 and hygroscopic properties. *J. Environ. Sci.* **2012**, *24*, 62-71.
(183) Wu, L.-Y.; Tong, S.-R.; Zhou, L.; Wang, W.-G.; Ge, M.-F. Synergistic Effects between SO2 and HCOOH on α-Fe2O3. *J. Phys. Chem. A* **2013**, *117*, 3972-3979.
(184) Zhou, L.; Wang, W. G.; Gai, Y. B.; Ge, M. F. Knudsen cell and smog chamber study of the heterogeneous uptake of sulfur dioxide on Chinese mineral dust. *J. Environ. Sci.* **2014**, *26*, 2423-2433.
(185) Zhao, Y.; Chen, Z. M.; Shen, X. L.; Huang, D. Heterogeneous reactions of gaseous hydrogen peroxide on pristine and acidic gas-processed calcium carbonate particles: Effects of relative humidity and surface coverage of coating. *Atmos. Environ.* **2013**, *67*, 63-72.
(186) Zhao, Y.; Chen, Z. M.; Shen, X. L.; Zhang, X. A. Kinetics and Mechanisms of Heterogeneous Reaction of Gaseous Hydrogen Peroxide on Mineral Oxide Particles. *Environ. Sci. Technol.* **2011**, *45*, 3317-3324.
(187) Arimoto, R.; Kim, Y. J.; Kim, Y. P.; Quinn, P. K.; Bates, T. S.; Anderson, T. L.; Gong, S.; Uno, I.; Chin, M.; Huebert, B. J. *et al.* Characterization of Asian Dust during ACE-Asia. *Glob. Planet. Change* **2006**, *52*, 23-56.

(188) Deguillaume, L.; Leriche, M.; Desboeufs, K.; Mailhot, G.; George, C.; Chaumerliac, N. Transition metals in atmospheric liquid phases: Sources, reactivity, and sensitive parameters. *Chem. Rev.* **2005**, *105*, 3388-3431.
(189) Jacob, D. J. Heterogeneous chemistry and tropospheric ozone. *Atmos. Environ.* **2000**, *34*, 2131-2159.
(190) Hoose, C.; Lohmann, U.; Bennartz, R.; Croft, B.; Lesins, G. Global simulations of aerosol processing in clouds. *Atmos. Chem. Phys.* **2008**, *8*, 6939-6963.
(191) Desboeufs, K.; Journet, E.; Rajot, J. L.; Chevaillier, S.; Triquet, S.; Formenti, P.; Zakou, A. Chemistry of rain events in West Africa: evidence of dust and biogenic influence in convective systems. *Atmos. Chem. Phys.* **2010**, *10*, 9283-9293.
(192) Dentener, F. J.; Carmichael, G. R.; Zhang, Y.; Lelieveld, J.; Crutzen, P. J. Role of mineral aerosol as a reactive surface in the global troposphere. *J. Geophys. Res.-Atmos.* **1996**, *101*, 22869-22889.
(193) de Reus, M.; Fischer, H.; Sander, R.; Gros, V.; Kormann, R.; Salisbury, G.; Van Dingenen, R.; Williams, J.; Zollner, M.; Lelieveld, J. Observations and model calculations of trace gas scavenging in a dense Saharan dust plume during MINATROC. *Atmos. Chem. Phys.* **2005**, *5*, 1787-1803.
(194) Bauer, S. E.; Balkanski, Y.; Schulz, M.; Hauglustaine, D. A.; Dentener, F. Global modeling of heterogeneous chemistry on mineral aerosol surfaces: Influence on tropospheric ozone chemistry and comparison to observations. *J. Geophys. Res.-Atmos.* **2004**, *109*, D02304, doi: 02310.01029/02003JD003868.
(195) Matthews, P. S. J.; Baeza-Romero, M. T.; Whalley, L. K.; Heard, D. E. Uptake of HO2 radicals onto Arizona test dust particles using an aerosol flow tube. *Atmos. Chem. Phys.* **2014**, *14*, 7397-7408.
(196) Romanias, M. N.; El Zein, A.; Bedjanian, Y. Heterogeneous Interaction of H2O2 with TiO2 Surface under Dark and UV Light Irradiation Conditions. *J. Phys. Chem. A* **2012**, *116*, 8191-8200.
(197) El Zein, A.; Romanias, M. N.; Bedjanian, Y. Heterogeneous Interaction of H2O2 with Arizona Test Dust. *J. Phys. Chem. A* **2014**, *118*, 441-448.
(198) Sullivan, R. C.; Guazzotti, S. A.; Sodeman, D. A.; Tang, Y. H.; Carmichael, G. R.; Prather, K. A. Mineral dust is a sink for chlorine in the marine boundary layer. *Atmos. Environ.* **2007**, *41*, 7166-7179.
(199) Goodman, A. L.; Underwood, G. M.; Grassian, V. H. A laboratory study of the heterogeneous reaction of nitric acid on calcium carbonate particles. *J. Geophys. Res.-Atmos.* **2000**, *105*, 29053-29064.
(200) Prince, A. P.; Kleiber, P. D.; Grassian, V. H.; Young, M. A. Reactive uptake of acetic acid on calcite and nitric acid reacted calcite aerosol in an environmental reaction chamber. *Phys. Chem. Chem. Phys.* **2008**, *10*, 142-152.
(201) Li, H. J.; Zhu, T.; Zhao, D. F.; Zhang, Z. F.; Chen, Z. M. Kinetics and mechanisms of heterogeneous reaction of NO_2 on $CaCO_3$ surfaces under dry and wet conditions. *Atmos. Chem. Phys.* **2010**, *10*, 463-474.
(202) Li, W. J.; Shao, L. Y. Observation of nitrate coatings on atmospheric mineral dust particles. *Atmos. Chem. Phys.* **2009**, *9*, 1863-1871.
(203) Li, W. J.; Shao, L. Y. Transmission electron microscopy study of aerosol particles from the brown hazes in northern China. *J. Geophys. Res.-Atmos.* **2009**, *114*, D09302, doi: 09310.01029/02008jd011285.
(204) Huang, X.; Song, Y.; Zhao, C.; Li, M.; Zhu, T.; Zhang, Q.; Zhang, X. Pathways of sulfate enhancement by natural and anthropogenic mineral aerosols in China. *J. Geophys. Res.-Atmos* **2014**, *119*, 14165-14179.

(205) Tang, Y. H.; Carmichael, G. R.; Seinfeld, J. H.; Dabdub, D.; Weber, R. J.; Huebert, B.; Clarke, A. D.; Guazzotti, S. A.; Sodeman, D. A.; Prather, K. A. *et al.* Three-dimensional simulations of inorganic aerosol distributions in east Asia during spring 2001. *J. Geophys. Res.-Atmos.* **2004**, *109*, D19s23, doi: 10.1029/2003jd004201.
(206) Hand, V. L.; Capes, G.; Vaughan, D. J.; Formenti, P.; Haywood, J. M.; Coe, H. Evidence of internal mixing of African dust and biomass burning particles by individual particle analysis using electron beam techniques. *J. Geophys. Res.-Atmos.* **2010**, *115*, D13301, doi: 13310.11029/12009jd012938.
(207) Formenti, P.; Elbert, W.; Maenhaut, W.; Haywood, J.; Andreae, M. O. Chemical composition of mineral dust aerosol during the Saharan Dust Experiment (SHADE) airborne campaign in the Cape Verde region, September 2000. *J. Geophys. Res.-Atmos.* **2003**, *108*, 8576, doi: 8510.1029/2002jd002648.
(208) Sullivan, R. C.; Prather, K. A. Investigations of the diurnal cycle and mixing state of oxalic acid in individual particles in Asian aerosol outflow. *Environ. Sci. Technol.* **2007**, *41*, 8062-8069.
(209) Trochkine, D.; Iwasaka, Y.; Matsuki, A.; Yamada, M.; Kim, Y. S.; Nagatani, T.; Zhang, D.; Shi, G. Y.; Shen, Z. Mineral aerosol particles collected in Dunhuang, China, and their comparison with chemically modified particles collected over Japan. *J. Geophys. Res.-Atmos* **2003**, *108*.
(210) Matsuki, A.; Iwasaka, Y.; Shi, G. Y.; Chen, H. B.; Osada, K.; Zhang, D.; Kido, M.; Inomata, Y.; Kim, Y. S.; Trochkine, D. *et al.* Heterogeneous Sulfate Formation on Dust Surface and Its Dependence on Mineralogy: Balloon-Borne Observations from Balloon-Borne Measurements in The Surface Atmosphere of Beijing, China. *Water Air Soil Pollut: Focus* **2005**, *5*, 101-132.
(211) Al-Abadleh, H. A.; Krueger, B. J.; Ross, J. L.; Grassian, V. H. Phase transitions in calcium nitrate thin films. *Chem. Commun.* **2003**, 2796-2797.
(212) Ma, Q. X.; Liu, Y. C.; Liu, C.; He, H. Heterogeneous reaction of acetic acid on MgO, α-Al2O3, and CaCO3 and the effect on the hygroscopic behavior of these particles. *Phys. Chem. Chem. Phys.* **2012**, *14*, 8403-8409.
(213) Vlasenko, A.; Sjogren, S.; Weingartner, E.; Stemmler, K.; Gaggeler, H. W.; Ammann, M. Effect of humidity on nitric acid uptake to mineral dust aerosol particles. *Atmos. Chem. Phys.* **2006**, *6*, 2147-2160.
(214) Krueger, B. J.; Grassian, V. H.; Laskin, A.; Cowin, J. P. The transformation of solid atmospheric particles into liquid droplets through heterogeneous chemistry: Laboratory insights into the processing of calcium containing mineral dust aerosol in the troposphere. *Geophys. Res. Lett.* **2003**, *30*, 1148, doi: 1110.1029/2002gl016563.
(215) Liu, Y. J.; Zhu, T.; Zhao, D. F.; Zhang, Z. F. Investigation of the hygroscopic properties of $Ca(NO_3)_2$ and internally mixed $Ca(NO_3)_2/CaCO_3$ particles by micro-Raman spectrometry. *Atmos. Chem. Phys.* **2008**, *8*, 7205-7215.
(216) Hatch, C. D.; Gierlus, K. M.; Schuttlefield, J. D.; Grassian, V. H. Water adsorption and cloud condensation nuclei activity of calcite and calcite coated with model humic and fulvic acids. *Atmos. Environ.* **2008**, *42*, 5672-5684.
(217) Sullivan, R. C.; Moore, M. J. K.; Petters, M. D.; Kreidenweis, S. M.; Roberts, G. C.; Prather, K. A. Effect of chemical mixing state on the hygroscopicity and cloud nucleation properties of calcium mineral dust particles. *Atmos. Chem. Phys.* **2009**, *9*, 3303-3316.
(218) Gierlus, K. M.; Laskina, O.; Abernathy, T. L.; Grassian, V. H. Laboratory study of the effect of oxalic acid on the cloud condensation nuclei activity of mineral dust aerosol. *Atmos. Environ.* **2012**, *46*, 125-130.

(219) Cziczo, D. J.; Froyd, K. D.; Gallavardin, S. J.; Moehler, O.; Benz, S.; Saathoff, H.; Murphy, D. M. Deactivation of ice nuclei due to atmospherically relevant surface coatings. *Environ. Res. Lett.* **2009**, *4*, 044013.
(220) Reitz, P.; Spindler, C.; Mentel, T. F.; Poulain, L.; Wex, H.; Mildenberger, K.; Niedermeier, D.; Hartmann, S.; Clauss, T.; Stratmann, F. *et al.* Surface modification of mineral dust particles by sulphuric acid processing: implications for ice nucleation abilities. *Atmos. Chem. Phys.* **2011**, *11*, 7839-7858.
(221) Niedermeier, D.; Hartmann, S.; Clauss, T.; Wex, H.; Kiselev, A.; Sullivan, R. C.; DeMott, P. J.; Petters, M. D.; Reitz, P.; Schneider, J. *et al.* Experimental study of the role of physicochemical surface processing on the IN ability of mineral dust particles. *Atmos. Chem. Phys.* **2011**, *11*, 11131-11144.
(222) Laskina, O.; Young, M. A.; Kleiber, P. D.; Grassian, V. H. Infrared extinction spectroscopy and micro-Raman spectroscopy of select components of mineral dust mixed with organic compounds. *J. Geophys. Res.-Atmos.* **2013**, *118*, 6593-6606.
(223) Abdelkader, M.; Metzger, S.; Mamouri, R. E.; Astitha, M.; Barrie, L.; Levin, Z.; Lelieveld, J. Dust–air pollution dynamics over the eastern Mediterranean. *Atmos. Chem. Phys.* **2015**, *15*, 9173-9189.
(224) Fan, S. M.; Horowitz, L. W.; Levy, H.; Moxim, W. J. Impact of air pollution on wet deposition of mineral dust aerosols. *Geophys. Res. Lett.* **2004**, *31*, 4.
(225) Meskhidze, N.; Chameides, W. L.; Nenes, A.; Chen, G. Iron mobilization in mineral dust: Can anthropogenic SO_2 emissions affect ocean productivity? *Geophys. Res. Lett.* **2003**, *30*, 2085, doi: 2010.1029/2003GL018035.
(226) Pradhan, M.; Kalberer, M.; Griffiths, P. T.; Braban, C. F.; Pope, F. D.; Cox, R. A.; Lambert, R. M. Uptake of Gaseous Hydrogen Peroxide by Submicrometer Titanium Dioxide Aerosol as a Function of Relative Humidity. *Environ. Sci. Technol.* **2010**, *44*, 1360-1365.
(227) Liu, Y.; Gibson, E. R.; Cain, J. P.; Wang, H.; Grassian, V. H.; Laskin, A. Kinetics of heterogeneous reaction of $CaCO_3$ particles with gaseous HNO_3 over a wide range of humidity. *J. Phys. Chem. A* **2008**, *112*, 1561-1571.
(228) Nicolas, M.; Ndour, M.; Ka, O.; D'anna, B.; George, C. Photochemistry of atmospheric dust: ozone decomposition on illuminatd titanium dioxide. *Environ. Sci. Technol.* **2009**, *43*, 7347-7442.
(229) Rubasinghege, G.; Grassian, V. H. Role(s) of adsorbed water in the surface chemistry of environmental interfaces. *Chem. Commun.* **2013**, *49*, 3071-3094.
(230) Ewing, G. E. Ambient Thin Film Water on Insulator Surfaces. *Chem. Rev.* **2006**, *106*, 1511-1526.
(231) Henderson, M. A. Structural Sensitivity in the Dissociation of Water on TiO2 Single-Crystal Surfaces. *Langmuir* **1996**, *12*, 5093-5098.
(232) Schaub, R.; Thostrup, P.; Lopez, N.; Lægsgaard, E.; Stensgaard, I.; Nørskov, J. K.; Besenbacher, F. Oxygen Vacancies as Active Sites for Water Dissociation on Rutile TiO_2(110). *Phys. Rev. Lett.* **2001**, *87*, 266104.
(233) Beaglehole, D.; Radlinska, E. Z.; Ninham, B. W.; Christenson, H. K. Inadequacy of Lifshitz theory for thin liquid films. *Phys. Rev. Lett.* **1991**, *66*, 2084-2087.
(234) Miranda, P. B.; Xu, L.; Shen, Y. R.; Salmeron, M. Icelike Water Monolayer Adsorbed on Mica at Room Temperature. *Phys. Rev. Lett.* **1998**, *81*, 5876-5879.
(235) Zhang, Z.; Bondarchuk, O.; Kay, B. D.; White, J. M.; Dohnálek, Z. Imaging Water Dissociation on TiO2(110): Evidence for Inequivalent Geminate OH Groups. *J. Phys. Chem. B* **2006**, *110*, 21840-21845.

(236) Smith, R. S.; Li, Z.; Chen, L.; Dohnálek, Z.; Kay, B. D. Adsorption, Desorption, and Displacement Kinetics of H2O and CO2 on TiO2(110). *J. Phys. Chem. B* **2014**, *118*, 8054-8061.
(237) Cantrell, W.; Heymsfield, A. Production of ice in tropospheric clouds - A review. *Bull. Amer. Meteorol. Soc.* **2005**, *86*, 795-807.
(238) Hoose, C.; Moehler, O. Heterogeneous ice nucleation on atmospheric aerosols: a review of results from laboratory experiments. *Atmos. Chem. Phys.* **2012**, *12*, 9817–9854.
(239) Ladino, L. A.; Stetzer, O.; Lohmann, U. Contact freezing: a review of experimental studies. *Atmos. Chem. Phys.* **2013**, *13*, 9745-9769.
(240) Al-Abadleh, H. A.; Grassian, V. H. FT-IR study of water adsorption on aluminum oxide surfaces. *Langmuir* **2003**, *19*, 341-347.
(241) Ketteler, G.; Yamamoto, S.; Bluhm, H.; Andersson, K.; Starr, D. E.; Ogletree, D. F.; Ogasawara, H.; Nilsson, A.; Salmeron, M. The Nature of Water Nucleation Sites on TiO2(110) Surfaces Revealed by Ambient Pressure X-ray Photoelectron Spectroscopy. *J. Phys. Chem. C* **2007**, *111*, 8278-8282.
(242) Yamamoto, S.; Kendelewicz, T.; Newberg, J. T.; Ketteler, G.; Starr, D. E.; Mysak, E. R.; Andersson, K. J.; Ogasawara, H.; Bluhm, H.; Salmeron, M. *et al.* Water Adsorption on α-Fe2O3(0001) at near Ambient Conditions. *J. Phys. Chem. C* **2010**, *114*, 2256-2266.
(243) Murphy, D. M.; Thomson, D. S.; Mahoney, T. M. J. In situ measurements of organics, meteoritic material, mercury, and other elements in aerosols at 5 to 19 kilometers. *Science* **1998**, *282*, 1664-1669.
(244) Cziczo, D. J.; Murphy, D. M.; Hudson, P. K.; Thomson, D. S. Single particle measurements of the chemical composition of cirrus ice residue during CRYSTAL-FACE. *J. Geophys. Res.-Atmos.* **2004**, *109*, D04201, doi: 04210.01029/02003jd004032.
(245) Laskin, A.; Iedema, M. J.; Ichkovich, A.; Graber, E. R.; Taraniuk, I.; Rudich, Y. Direct observation of completely processed calcium carbonate dust particles. *Faraday Discuss.* **2005**, *130*, 453-468.
(246) Navea, J. G.; Chen, H. H.; Huang, M.; Carmichael, G. R.; Grassian, V. H. A comparative evaluation of water uptake on several mineral dust sources. *Environ. Chem.* **2010**, *7*, 162-170.
(247) Gustafsson, R. J.; Orlov, A.; Badger, C. L.; Griffiths, P. T.; Cox, R. A.; Lambert, R. M. A comprehensive evaluation of water uptake on atmospherically relevant mineral surfaces: DRIFT spectroscopy, thermogravimetric analysis and aerosol growth measurements. *Atmos. Chem. Phys.* **2005**, *5*, 3415-3421.
(248) Ma, Q. X.; Liu, Y. C.; He, H. The Utilization of Physisorption Analyzer for Studying the Hygroscopic Properties of Atmospheric Relevant Particles. *J. Phys. Chem. A* **2010**, *114*, 4232-4237.
(249) Schuttlefield, J. D.; Cox, D.; Grassian, V. H. An investigation of water uptake on clays minerals using ATR-FTIR spectroscopy coupled with quartz crystal microbalance measurements. *J. Geophys. Res.-Atmos.* **2007**, *112*, D21303, doi: 21310.21029/22007JD008973.
(250) Goodman, A. L.; Bernard, E. T.; Grassian, V. H. Spectroscopic study of nitric acid and water adsorption on oxide particles: Enhanced nitric acid uptake kinetics in the presence of adsorbed water. *J. Phys. Chem. A* **2001**, *105*, 6443-6457.
(251) Pope, F. D.; Dennis-Smither, B. J.; Griffiths, P. T.; Clegg, S. L.; Cox, R. A. Studies of Single Aerosol Particles Containing Malonic Acid, Glutaric Acid, and Their Mixtures with Sodium Chloride. I. Hygroscopic Growth. *J. Phys. Chem. A* **2010**, *114*, 5335-5341.

(252) Tong, H. J.; Reid, J. P.; Bones, D. L.; Luo, B. P.; Krieger, U. K. Measurements of the timescales for the mass transfer of water in glassy aerosol at low relative humidity and ambient temperature. *Atmos. Chem. Phys.* **2011**, *11*, 4739-4754.
(253) Attwood, A. R.; Greenslade, M. E. Optical Properties and Associated Hygroscopicity of Clay Aerosols. *Aerosol Sci. Technol.* **2011**, *45*, 1350-1359.
(254) Li-Jones, X.; Maring, H. B.; Prospero, J. M. Effect of relative humidity on light scattering by mineral dust aerosol as measured in the marine boundary layer over the tropical Atlantic Ocean. *J. Geophys. Res.-Atmos* **1998**, *103*, 31113-31121.
(255) Utry, N.; Ajtai, T.; Pintér, M.; Tombácz, E.; Illés, E.; Bozóki, Z.; Szabó, G. Mass-specific optical absorption coefficients and imaginary part of the complex refractive indices of mineral dust components measured by a multi-wavelength photoacoustic spectrometer. *Atmos. Meas. Tech.* **2015**, *8*, 401-410.
(256) Sullivan, R. C.; Moore, M. J. K.; Petters, M. D.; Kreidenweis, S. M.; Qafoku, O.; Laskin, A.; Roberts, G. C.; Prather, K. A. Impact of Particle Generation Method on the Apparent Hygroscopicity of Insoluble Mineral Particles. *Aerosol Sci. Technol.* **2010**, *44*, 830-846.
(257) Gibson, E. R.; Gierlus, K. M.; Hudson, P. K.; Grassian, V. H. Generation of internally mixed insoluble and soluble aerosol particles to investigate the impact of atmospheric aging and heterogeneous processing on the CCN activity of mineral dust aerosol. *Aerosol Sci. Technol.* **2007**, *41*, 914-924.
(258) Sullivan, R. C.; Moore, M. J. K.; Petters, M. D.; Kreidenweis, S. M.; Roberts, G. C.; Prather, K. A. Timescale for hygroscopic conversion of calcite mineral particles through heterogeneous reaction with nitric acid. *Phys. Chem. Chem. Phys.* **2009**, *11*, 7826-7837.
(259) Garimella, S.; Huang, Y. W.; Seewald, J. S.; Cziczo, D. J. Cloud condensation nucleus activity comparison of dry- and wet-generated mineral dust aerosol: the significance of soluble material. *Atmos. Chem. Phys.* **2014**, *14*, 6003-6019.
(260) Vlasenko, A.; Sjogren, S.; Weingartner, E.; Gaggeler, H. W.; Ammann, M. Generation of submicron Arizona test dust aerosol: Chemical and hygroscopic properties. *Aerosol Sci. Technol.* **2005**, *39*, 452-460.
(261) Sullivan, R. C.; Petters, M. D.; DeMott, P. J.; Kreidenweis, S. M.; Wex, H.; Niedermeier, D.; Hartmann, S.; Clauss, T.; Stratmann, F.; Reitz, P. *et al.* Irreversible loss of ice nucleation active sites in mineral dust particles caused by sulphuric acid condensation. *Atmos. Chem. Phys.* **2010**, *10*, 11471-11487.
(262) Kumar, P.; Sokolik, I. N.; Nenes, A. Measurements of cloud condensation nuclei activity and droplet activation kinetics of fresh unprocessed regional dust samples and minerals. *Atmos. Chem. Phys.* **2011**, *11*, 3527-3541.
(263) Kumar, P.; Sokolik, I. N.; Nenes, A. Cloud condensation nuclei activity and droplet activation kinetics of wet processed regional dust samples and minerals. *Atmos. Chem. Phys.* **2011**, *11*, 8661-8676.
(264) Zhao, D. F.; Buchholz, A.; Mentel, T. F.; Müller, K. P.; Borchardt, J.; Kiendler-Scharr, A.; Spindler, C.; Tillmann, R.; Trimborn, A.; Zhu, T. *et al.* Novel method of generation of Ca(HCO3)2 and CaCO3 aerosols and first determination of hygroscopic and cloud condensation nuclei activation properties. *Atmos. Chem. Phys.* **2010**, *10*, 8601-8616.
(265) Wurzler, S.; Reisin, T. G.; Levin, Z. Modification of mineral dust particles by cloud processing and subsequent effects on drop size distributions. *J. Geophys. Res.-Atmos* **2000**, *105*, 4501-4512.
(266) Smoydzin, L.; Teller, A.; Tost, H.; Fnais, M.; Lelieveld, J. Impact of mineral dust on cloud formation in a Saharan outflow region. *Atmos. Chem. Phys.* **2012**, *12*, 11383-11393.

(267) Begue, N.; Tulet, P.; Pelon, J.; Aouizerats, B.; Berger, A.; Schwarzenboeck, A. Aerosol processing and CCN formation of an intense Saharan dust plume during the EUCAARI 2008 campaign. *Atmos. Chem. Phys.* **2015**, *15*, 3497-3516.
(268) Hatch, C. D.; Wiese, J. S.; Crane, C. C.; Harris, K. J.; Kloss, H. G.; Baltrusaitis, J. Water Adsorption on Clay Minerals As a Function of Relative Humidity: Application of BET and Freundlich Adsorption Models. *Langmuir* **2011**, *28*, 1790-1803.
(269) Ma, Q. X.; He, H.; Liu, Y. C. In situ DRIFTS study of hygroscopic behavior of mineral aerosol. *J. Environ. Sci.* **2010**, *22*, 555-560.
(270) Hung, H. M.; Wang, K. C.; Chen, J. P. Adsorption of nitrogen and water vapor by insoluble particles and the implication on cloud condensation nuclei activity. *J. Aerosol. Sci.* **2015**, *86*, 24-31.
(271) Arenas, K. J. L.; Schill, S. R.; Malla, A.; Hudson, P. K. Deliquescence Phase Transition Measurements by Quartz Crystal Microbalance Frequency Shifts. *J. Phys. Chem. A* **2012**, *116*, 7658-7667.
(272) Lu, C. S.; Lewis, O. Investigation of film‐thickness determination by oscillating quartz resonators with large mass load. *J. Appl. Phys.* **1972**, *43*, 4385-4390.
(273) Schuttlefield, J.; Al-Hosney, H.; Zachariah, A.; Grassian, V. H. Attenuated total reflection Fourier transform infrared spectroscopy to investigate water uptake and phase transitions in atmospherically relevant particles. *Appl. Spectrosc.* **2007**, *61*, 283-292.
(274) Wijenayaka, L. A.; Rubasinghege, G.; Baltrusaitis, J.; Grassian, V. H. Surface Chemistry of alpha-FeOOH Nanorods and Microrods with Gas-Phase Nitric Acid and Water Vapor: Insights into the Role of Particle Size, Surface Structure, and Surface Hydroxyl Groups in the Adsorption and Reactivity of alpha-FeOOH with Atmospheric Gases. *J. Phys. Chem. C* **2012**, *116*, 12566-12577.
(275) Song, X. W.; Boily, J. F. Water Vapor Adsorption on Goethite. *Environ. Sci. Technol.* **2013**, *47*, 7171-7177.
(276) Wendt, S.; Schaub, R.; Matthiesen, J.; Vestergaard, E. K.; Wahlström, E.; Rasmussen, M. D.; Thostrup, P.; Molina, L. M.; Lægsgaard, E.; Stensgaard, I. *et al.* Oxygen vacancies on TiO2(1 1 0) and their interaction with H2O and O2: A combined high-resolution STM and DFT study. *Surf. Sci.* **2005**, *598*, 226-245.
(277) Wendt, S.; Matthiesen, J.; Schaub, R.; Vestergaard, E. K.; Lægsgaard, E.; Besenbacher, F.; Hammer, B. Formation and Splitting of Paired Hydroxyl Groups on Reduced TiO2(110). *Phys. Rev. Lett.* **2006**, *96*, 066107.
(278) He, Y.; Tilocca, A.; Dulub, O.; Selloni, A.; Diebold, U. Local ordering and electronic signatures of submonolayer water on anatase TiO2(101). *Nat Mater* **2009**, *8*, 585-589.
(279) Krueger, B. J.; Grassian, V. H.; Iedema, M. J.; Cowin, J. P.; Laskin, A. Probing heterogeneous chemistry of individual atmospheric particles using scanning electron microscopy and energy-dispersive X-ray analysis. *Anal. Chem.* **2003**, *75*, 5170-5179.
(280) Salmeron, M.; Schlogl, R. Ambient pressure photoelectron spectroscopy: A new tool for surface science and nanotechnology. *Surf. Sci. Rep.* **2008**, *63*, 169-199.
(281) Lampimäki, M.; Schreiber, S.; Zelenay, V.; Křepelová, A.; Birrer, M.; Axnanda, S.; Mao, B.; Liu, Z.; Bluhm, H.; Ammann, M. Exploring the Environmental Photochemistry on the TiO2(110) Surface in Situ by Near Ambient Pressure X-ray Photoelectron Spectroscopy. *J. Phys. Chem. C* **2015**, *119*, 7076-7085.
(282) Lampimaki, M.; Zelenay, V.; Krepelova, A.; Liu, Z.; Chang, R.; Bluhm, H.; Ammann, M. Ozone-Induced Band Bending on Metal-Oxide Surfaces Studied under Environmental Conditions. *ChemPhysChem* **2013**, *14*, 2419 – 2425.
(283) Rosseler, O.; Sleiman, M.; Montesinos, V. N.; Shavorskiy, A.; Keller, V.; Keller, N.; Litter, M. I.; Bluhm, H.; Salmeron, M.; Destaillats, H. Chemistry of NOx on TiO2

Surfaces Studied by Ambient Pressure XPS: Products, Effect of UV Irradiation, Water, and Coadsorbed K+. *J. Phys. Chem. Lett.* **2013**, *4*, 536-541.
(284) Starr, D. E.; Liu, Z.; Havecker, M.; Knop-Gericke, A.; Bluhm, H. Investigation of solid/vapor interfaces using ambient pressure X-ray photoelectron spectroscopy. *Chem. Soc. Rev.* **2013**, *42*, 5833-5857.
(285) Perry, A.; Neipert, C.; Space, B.; Moore, P. B. Theoretical modeling of interface specific vibrational spectroscopy: Methods and applications to aqueous interfaces. *Chem. Rev.* **2006**, *106*, 1234-1258.
(286) Shen, Y. R.; Ostroverkhov, V. Sum-frequency vibrational spectroscopy on water interfaces: Polar orientation of water molecules at interfaces. *Chem. Rev.* **2006**, *106*, 1140-1154.
(287) Ebben, C. J.; Ault, A. P.; Ruppel, M. J.; Ryder, O. S.; Bertram, T. H.; Grassian, V. H.; Prather, K. A.; Geiger, F. M. Size-Resolved Sea Spray Aerosol Particles Studied by Vibrational Sum Frequency Generation. *J. Phys. Chem. A* **2013**, *117*, 6589-6601.
(288) Jubb, A. M.; Hua, W.; Allen, H. C. Environmental Chemistry at Vapor/Water Interfaces: Insights from Vibrational Sum Frequency Generation Spectroscopy. *Annu. Rev. Phys. Chem.* **2012**, *63*, 107-130.
(289) Ma, G.; Liu, D. F.; Allen, H. C. Piperidine adsorption on hydrated alpha-alumina (0001) surface studied by vibrational sum frequency generation spectroscopy. *Langmuir* **2004**, *20*, 11620-11629.
(290) Liu, D. F.; Ma, G.; Xu, M.; Allen, H. C. Adsorption of ethylene glycol vapor on α-Al2O3(0001) and amorphous SiO2 surfaces: Observation of molecular orientation and surface hydroxyl groups as sorption sites. *Environ. Sci. Technol.* **2005**, *39*, 206-212.
(291) Baltrusaitis, J.; Grassian, V. H. Calcite (1014) surface in humid environments. *Surf. Sci.* **2009**, *603*, L99-L104.
(292) Stipp, S. L. S.; Konnerup-Madsen, J.; Franzreb, K.; Kulik, A.; Mathieu, H. J. Spontaneous movement of ions through calcite at standard temperature and pressure. *Nature* **1998**, *396*, 356-359.
(293) Carpick, R. W.; Salmeron, M. Scratching the Surface: Fundamental Investigations of Tribology with Atomic Force Microscopy. *Chem. Rev.* **1997**, *97*, 1163-1194.
(294) Xu, L.; Lio, A.; Hu, J.; Ogletree, D. F.; Salmeron, M. Wetting and Capillary Phenomena of Water on Mica. *J. Phys. Chem. B* **1998**, *102*, 540-548.
(295) Caloz, F.; Fenter, F. F.; Tabor, K. D.; Rossi, M. J. Paper I: Design and construction of a Knudsen-cell reactor for the study of heterogeneous reactions over the temperature range 130-750 K: Performances and limitations. *Rev. Sci. Instrum.* **1997**, *68*, 3172-3179.
(296) Underwood, G. M.; Miller, T. M.; Grassian, V. H. Transmission FT-IR and Knudsen cell study of the heterogeneous reactivity of gaseous nitrogen dioxide on mineral oxide particles. *J. Phys. Chem. A* **1999**, *103*, 6184-6190.
(297) Liu, Y.; Ma, J.; Liu, C.; He, H. Heterogeneous uptake of carbonyl sulfide onto kaolinite within a temperature range of 220–330 K. *J. Geophys. Res.-Atmos* **2010**, *115*, D24311, doi: 24310.21029/22010JD014778.
(298) Seisel, S.; Lian, Y.; Keil, T.; Trukhin, M. E.; Zellner, R. Kinetics of the interaction of water vapour with mineral dust and soot surfaces at T=298 K. *Phys. Chem. Chem. Phys.* **2004**, *6*, 1926-1932.
(299) Seisel, S.; Pashkova, A.; Lian, Y.; Zellner, R. Water uptake on mineral dust and soot: A fundamental view of the hydrophilicity of atmospheric particles? *Faraday Discuss.* **2005**, *130*, 437-451.
(300) Nathanson, G. M.; Davidovits, P.; Worsnop, D. R.; Kolb, C. E. Dynamics and kinetics at the gas-liquid interface. *J. Phys. Chem.* **1996**, *100*, 13007-13020.

(301) Kong, X.; Thomson, E. S.; Papagiannakopoulos, P.; Johansson, S. M.; Pettersson, J. B. C. Water Accommodation on Ice and Organic Surfaces: Insights from Environmental Molecular Beam Experiments. *J. Phys. Chem. B* **2014**, *118*, 13378-13386.
(302) Nathanson, G. M. Molecular beam studies of gas-liquid interfaces. *Annu. Rev. Phys. Chem.* **2004**, *55*, 231-255.
(303) Burden, D. K.; Johnson, A. M.; Nathanson, G. M. HCl Uptake through Films of Pentanoic Acid and Pentanoic Acid/Hexanol Mixtures at the Surface of Sulfuric Acid. *J. Phys. Chem. A* **2009**, *113*, 14131-14140.
(304) Kong, X.; Papagiannakopoulos, P.; Thomson, E. S.; Marković, N.; Pettersson, J. B. C. Water Accommodation and Desorption Kinetics on Ice. *J. Phys. Chem. A* **2014**, *118*, 3973-3979.
(305) Thomson, E. S.; Kong, X.; Papagiannakopoulos, P.; Pettersson, J. B. C. Deposition-mode ice nucleation reexamined at temperatures below 200 K. *Atmos. Chem. Phys.* **2015**, *15*, 1621-1632.
(306) Krieger, U. K.; Marcolli, C.; Reid, J. P. Exploring the complexity of aerosol particle properties and processes using single particle techniques. *Chem. Soc. Rev.* **2012**, *41*, 6631-6662.
(307) Peng, C.; Chan, C. K. The water cycles of water-soluble organic salts of atmospheric importance. *Atmos. Environ.* **2001**, *35*, 1183-1192.
(308) Reid, J. P.; Sayer, R. M. Heterogeneous atmospheric aerosol chemistry: laboratory studies of chemistry on water droplets. *Chem. Soc. Rev.* **2003**, *32*, 70-79.
(309) King, M. D.; Thompson, K. C.; Ward, A. D. Laser Tweezers Raman Study of Optically Trapped Aerosol Droplets of Seawater and Oleic Acid Reacting with Ozone: Implications for Cloud-Droplet Properties. *J. Am. Chem. Soc.* **2004**, *126*, 16710-16711.
(310) Hunt, O. R.; Ward, A. D.; King, M. D. Heterogeneous oxidation of nitrite anion by gas-phase ozone in an aqueous droplet levitated by laser tweezers (optical trap): is there any evidence for enhanced surface reaction? *Phys. Chem. Chem. Phys.* **2015**, *17*, 2734-2741.
(311) Rkiouak, L.; Tang, M. J.; Camp, J. C. J.; McGregor, J.; Watson, I. M.; Cox, R. A.; Kalberer, M.; Ward, A. D.; Pope, F. D. Optical trapping and Raman Spectroscopy of solid aerosol particles. *Phys. Chem. Chem. Phys.* **2014**, *16*, 11426-11434.
(312) Miles, R. E. H.; Walker, J. S.; Burnham, D. R.; Reid, J. P. Retrieval of the complex refractive index of aerosol droplets from optical tweezers measurements. *Phys. Chem. Chem. Phys.* **2012**, *14*, 3037-3047.
(313) Power, R. M.; Burnham, D. R.; Reid, J. P. Toward optical-tweezers-based force microscopy for airborne microparticles. *Appl. Optics* **2014**, *53*, 8522-8534.
(314) Lee, A. K. Y.; Ling, T. Y.; Chan, C. K. Understanding hygroscopic growth and phase transformation of aerosols using single particle Raman spectroscopy in an electrodynamic balance. *Faraday Discuss.* **2008**, *137*, 245-263.
(315) Choi, M. Y.; Chan, C. K. Investigation of Efflorescence of Inorganic Aerosols Using Fluorescence Spectroscopy. *J. Phys. Chem. A* **2005**, *109*, 1042-1048.
(316) Swietlicki, E.; Hansson, H. C.; Hameri, K.; Svenningsson, B.; Massling, A.; McFiggans, G.; McMurry, P. H.; Petaja, T.; Tunved, P.; Gysel, M. *et al.* Hygroscopic properties of submicrometer atmospheric aerosol particles measured with H-TDMA instruments in various environments - a review. *Tellus Ser. B-Chem. Phys. Meteorol.* **2008**, *60*, 432-469.
(317) Weingartner, E.; Gysel, M.; Baltensperger, U. Hygroscopicity of Aerosol Particles at Low Temperatures. 1. New Low-Temperature H-TDMA Instrument: Setup and First Applications. *Environ. Sci. Technol.* **2002**, *36*, 55-62.

(318) Duplissy, J.; Gysel, M.; Sjogren, S.; Meyer, N.; Good, N.; Kammermann, L.; Michaud, V.; Weigel, R.; Martins dos Santos, S.; Gruening, C. *et al.* Intercomparison study of six HTDMAs: results and recommendations. *Atmos. Meas. Tech.* **2009**, *2*, 363-378.
(319) Wex, H.; Petters, M. D.; Carrico, C. M.; Hallbauer, E.; Massling, A.; McMeeking, G. R.; Poulain, L.; Wu, Z.; Kreidenweis, S. M.; Stratmann, F. Towards closing the gap between hygroscopic growth and activation for secondary organic aerosol: Part 1 – Evidence from measurements. *Atmos. Chem. Phys.* **2009**, *9*, 3987-3997.
(320) Keskinen, H.; Romakkaniemi, S.; Jaatinen, A.; Miettinen, P.; Saukko, E.; Jorma, J.; Mäkelä, J. M.; Virtanen, A.; Smith, J. N.; Laaksonen, A. On-Line Characterization of Morphology and Water Adsorption on Fumed Silica Nanoparticles. *Aerosol Sci. Technol.* **2011**, *45*, 1441-1447.
(321) Ardon-Dryer, K.; Garimella, S.; Huang, Y. W.; Christopoulos, C.; Cziczo, D. J. Evaluation of DMA Size Selection of Dry Dispersed Mineral Dust Particles. *Aerosol Sci. Technol.* **2015**, *49*, 828-841.
(322) Veghte, D. P.; Freedman, M. A. The Necessity of Microscopy to Characterize the Optical Properties of Size-Selected, Nonspherical Aerosol Particles. *Anal. Chem.* **2012**, *84*, 9101-9108.
(323) Garland, R. M.; Ravishankara, A. R.; Lovejoy, E. R.; Tolbert, M. A.; Baynard, T. Parameterization for the relative humidity dependence of light extinction: Organic-ammonium sulfate aerosol. *J. Geophys. Res.-Atmos.* **2007**, *112*, D19303, doi: 19310.11029/12006JD008179.
(324) Langridge, J. M.; Richardson, M. S.; Lack, D.; Law, D.; Murphy, D. M. Aircraft Instrument for Comprehensive Characterization of Aerosol Optical Properties, Part I: Wavelength-Dependent Optical Extinction and Its Relative Humidity Dependence Measured Using Cavity Ringdown Spectroscopy. *Aerosol Sci. Technol.* **2011**, *45*, 1305-1318.
(325) Washenfelder, R. A.; Flores, J. M.; Brock, C. A.; Brown, S. S.; Rudich, Y. Broadband measurements of aerosol extinction in the ultraviolet spectral region. *Atmos. Meas. Tech.* **2013**, *6*, 861-877.
(326) Baynard, T.; Garland, R. M.; Ravishankara, A. R.; Tolbert, M. A.; Lovejoy, E. R. Key factors influencing the relative humidity dependence of aerosol light scattering. *Geophys. Res. Lett.* **2006**, *33*, L06813, doi: 06810.01029/02005GL024898.
(327) Meland, B.; Kleiber, P. D.; Grassian, V. H.; Young, M. A. Visible light scattering study at 470, 550, and 660 nm of components of mineral dust aerosol: Hematite and goethite. *J. Quant. Spectrosc. Radiat. Transf.* **2011**, *112*, 1108-1118.
(328) Malm, W. C.; Day, D. E.; Kreidenweis, S. M. Light Scattering Characteristics of Aerosols as a Function of Relative Humidity: Part I—A Comparison of Measured Scattering and Aerosol Concentrations Using the Theoretical Models. *J. Air Waste Manage. Assoc.* **2000**, *50*, 686-700.
(329) Lack, D. A.; Lovejoy, E. R.; Baynard, T.; Pettersson, A.; Ravishankara, A. R. Aerosol absorption measurement using photoacoustic spectroscopy: Sensitivity, calibration, and uncertainty developments. *Aerosol Sci. Technol.* **2006**, *40*, 697-708.
(330) Roberts, G. C.; Nenes, A. A continuous-flow streamwise thermal-gradient CCN chamber for atmospheric measurements. *Aerosol Sci. Technol.* **2005**, *39*, 206-221.
(331) Lance, S.; Medina, J.; Smith, J. N.; Nenes, A. Mapping the operation of the DMT Continuous Flow CCN counter. *Aerosol Sci. Technol.* **2006**, *40*, 242-254.
(332) Good, N.; Coe, H.; McFiggans, G. Instrumentational operation and analytical methodology for the reconciliation of aerosol water uptake under sub- and supersaturated conditions. *Atmos. Meas. Tech.* **2010**, *3*, 1241-1254.

(333) Lathem, T. L.; Nenes, A. Water Vapor Depletion in the DMT Continuous-Flow CCN Chamber: Effects on Supersaturation and Droplet Growth. *Aerosol Sci. Technol.* **2011**, *45*, 604-615.
(334) Ehara, K.; Hagwood, C.; Coakley, K. J. Novel method to classify aerosol particles according to their mass-to-charge ratio—Aerosol particle mass analyser. *J. Aerosol. Sci.* **1996**, *27*, 217-234.
(335) Park, K.; Cao, F.; Kittelson, D. B.; McMurry, P. H. Relationship between Particle Mass and Mobility for Diesel Exhaust Particles. *Environ. Sci. Technol.* **2003**, *37*, 577-583.
(336) Khalizov, A. F.; Zhang, R. Y.; Zhang, D.; Xue, H. X.; Pagels, J.; McMurry, P. H. Formation of highly hygroscopic soot aerosols upon internal mixing with sulfuric acid vapor. *J. Geophys. Res.-Atmos.* **2009**, *114*, D05208, doi: 05210.01029/02008JD010595.
(337) Abegglen, M.; Durdina, L.; Brem, B. T.; Wang, J.; Rindlisbacher, T.; Corbin, J. C.; Lohmann, U.; Sierau, B. Effective density and mass–mobility exponents of particulate matter in aircraft turbine exhaust: Dependence on engine thrust and particle size. *J. Aerosol. Sci.* **2015**, *88*, 135-147.
(338) Amaral, S. S.; de Carvalho, J. A.; Costa, M. A. M.; Pinheiro, C. An Overview of Particulate Matter Measurement Instruments. *Atmosphere* **2015**, *6*, 1327-1345.
(339) Pope, F. D. Pollen grains are efficient cloud condensation nuclei. *Environ. Res. Lett.* **2010**, *5*, 044015.
(340) Atkins, P. W. *Physical Chemistry (Sixth Edition)*; Oxford University Press: Oxford, UK, 1998.
(341) Lowell, S.; Shields, J. E.; Thomas, M. A.; Thommes, M. *Characterization of Porous Solids and Powders: Surface Area, Pore Size and Density*; Springer: Netherlands, 2010.
(342) Crittenden, B.; Thomas, W. J. *Adsorption Technology & Design*; Butterworth-Heinemann: Oxford, UK, 1998.
(343) Langmuir, I. The consitution and fundmental properties of solids and liquids. Part I. Solids. *J. Am. Chem. Soc.* **1916**, *38*, 2221-2295.
(344) Brunauer, S.; Emmett, P. H.; Teller, E. Adsorption of Gases in Multimolecular Layers. *J. Am. Chem. Soc.* **1938**, *60*, 309-319.
(345) Joyner, L. G.; Weinberger, E. B.; Montgomery, C. W. Surface Area Measurements of Activated Carbons, Silica Gel and other Adsorbents. *J. Am. Chem. Soc.* **1945**, *67*, 2182-2188.
(346) Sips, R. On the Structure of a Catalyst Surface. *J. Chem. Phys.* **1948**, *16*, 490-495.
(347) Skopp, J. Derivation of the Freundlich Adsorption Isotherm from Kinetics. *J. Chem. Educ.* **2009**, *86*, 1341.
(348) Hatch, C. D.; Greenaway, A. L.; Christie, M. J.; Baltrusaitis, J. Water adsorption constrained Frenkel–Halsey–Hill adsorption activation theory: Montmorillonite and illite. *Atmos. Environ.* **2014**, *87*, 26-33.
(349) Sorjamaa, R.; Laaksonen, A. The effect of H_2O adsorption on cloud drop activation of insoluble particles: a theoretical framework. *Atmos. Chem. Phys.* **2007**, *7*, 6175-6180.
(350) Kohler, H. The nucleus in and the growth of hygroscopic droplets. *Trans. Faraday Soc.* **1936**, *32*, 1152-1161.
(351) Farmer, D. K.; Cappa, C. D.; Kreidenweis, S. M. Atmospheric Processes and Their Controlling Influence on Cloud Condensation Nuclei Activity. *Chem. Rev.* **2015**, *115*, 4199-4217.
(352) Henson, B. F. An adsorption model of insoluble particle activation: Application to black carbon. *J. Geophys. Res.-Atmos* **2007**, *112*, D24S16, doi: 10.1029/2007JD008549.

(353) DeCarlo, P. F.; Slowik, J. G.; Worsnop, D. R.; Davidovits, P.; Jimenez, J. L. Particle morphology and density characterization by combined mobility and aerodynamic diameter measurements. Part 1: Theory. *Aerosol Sci. Technol.* **2004**, *38*, 1185-1205.
(354) Al-Hosney, H. A.; Grassian, V. H. Water, sulfur dioxide and nitric acid adsorption on calcium carbonate: A transmission and ATR-FTIR study. *Phys. Chem. Chem. Phys.* **2005**, *7*, 1266-1276.
(355) Gibson, E. R.; Hudson, P. K.; Grassian, V. H. Aerosol chemistry and climate: Laboratory studies of the carbonate component of mineral dust and its reaction products. *Geophys. Res. Lett.* **2006**, *33*, L13811, doi: 13810.11029/12006GL026386.
(356) Schuttlefield, J. D. *Laboratory studies of reactions of atmospheric gases with components of mineral dust aerosol and research in chemical education, PhD Dissertation*; The University of Iowa, Iowa City, USA, 2008.
(357) Tang, M. J.; Whitehead, J.; Davidson, N. M.; Pope, F. D.; Alfarra, M. R.; McFiggans, G.; Kalberer, M. Cloud condensation nucleation activities of calcium carbonate and its atmospheric ageing products. *Phys. Chem. Chem. Phys.* **2015**, *17*, 32194-32203.
(358) Neagle, W.; Rochester, C. H. Infrared study of the adsorption of water and ammonia on calcium carbonate. *J. Chem. Soc., Faraday Trans.* **1990**, *86*, 181-183.
(359) Bohr, J.; Wogelius, R. A.; Morris, P. M.; Stipp, S. L. S. Thickness and structure of the water film deposited from vapour on calcite surfaces. *Geochim. Cosmochim. Acta* **2010**, *74*, 5985-5999.
(360) Stipp, S. L. S.; Eggleston, C. M.; Nielsen, B. S. Calcite Surface-Structure Observed at Microtopographic and Molecular Scales with Atomic-Force Microscopy (Afm). *Geochim. Cosmochim. Acta* **1994**, *58*, 3023-3033.
(361) Stipp, S. L. S. Toward a conceptual model of the calcite surface: Hydration, hydrolysis, and surface potential. *Geochim. Cosmochim. Acta* **1999**, *63*, 3121-3131.
(362) Hausner, D. B.; Reeder, R. J.; Strongin, D. R. Humidity-induced restructuring of the calcite surface and the effect of divalent heavy metals. *J. Colloid Interface Sci.* **2007**, *305*, 101-110.
(363) Al-Abadleh, H. A.; Grassian, V. H. Phase transitions in magnesium nitrate thin films: A transmission FT-IR study of the deliquescence and efflorescence of nitric acid reacted magnesium oxide interfaces. *J. Phys. Chem. B* **2003**, *107*, 10829-10839.
(364) Tang, I. N.; Fung, K. H. Hydration and Raman scattering studies of levitated microparticles: $Ba(NO_3)_2$, $Sr(NO_3)_2$, and $Ca(NO_3)_2$. *J. Chem. Phys.* **1997**, *106*, 1653-1660.
(365) Seisel, S.; Borensen, C.; Vogt, R.; Zellner, R. The heterogeneous reaction of HNO_3 on mineral dust and gamma-alumina surfaces: a combined Knudsen cell and DRIFTS study. *Phys. Chem. Chem. Phys.* **2004**, *6*, 5498-5508.
(366) Kelly, J. T.; Wexler, A. S. Thermodynamics of carbonates and hydrates related to heterogeneous reactions involving mineral aerosol. *J. Geophys. Res.-Atmos* **2005**, *110*, D11201, doi: 11210.11029/12004jd005583.
(367) Kelly, J. T.; Chuang, C. C.; Wexler, A. S. Influence of dust composition on cloud droplet formation. *Atmos. Environ.* **2007**, *41*, 2904-2916.
(368) Huey, L. G.; Dunlea, E. J.; Lovejoy, E. R.; Hanson, D. R.; Norton, R. B.; Fehsenfeld, F. C.; Howard, C. J. Fast time response measurements of HNO_3 in air with a chemical ionization mass spectrometer. *J. Geophys. Res.-Atmos.* **1998**, *103*, 3355-3360.
(369) Hanke, M.; Umann, B.; Uecker, J.; Arnold, F.; Bunz, H. Atmospheric measurements of gas-phase HNO_3 and SO_2 using chemical ionization mass spectrometry during the MINATROC field campaign 2000 on Monte Cimone. *Atmos. Chem. Phys.* **2003**, *3*, 417-436.

(370) Bey, I.; Jacob, D. J.; Logan, J. A.; Yantosca, R. M. Asian chemical outflow to the Pacific in spring: Origins, pathways, and budgets. *J. Geophys. Res.-Atmos* **2001**, *106*, 23097-23113.
(371) Brown, S. S.; Stark, H.; Ryerson, T. B.; Williams, E. J.; Nicks, D. K.; Trainer, M.; Fehsenfeld, F. C.; Ravishankara, A. R. Nitrogen oxides in the nocturnal boundary layer: Simultaneous in situ measurements of NO3, N2O5, NO2, NO, and O3. *J. Geophys. Res.-Atmos* **2003**, *108*, 4299.
(372) Osthoff, H. D.; Roberts, J. M.; Ravishankara, A. R.; Williams, E. J.; Lerner, B. M.; Sommariva, R.; Bates, T. S.; Coffman, D.; Quinn, P. K.; Dibb, J. E. *et al.* High levels of nitryl chloride in the polluted subtropical marine boundary layer. *Nature Geosci.* **2008**, *1*, 324-328.
(373) Thornton, J. A.; Kercher, J. P.; Riedel, T. P.; Wagner, N. L.; Cozic, J.; Holloway, J., S.; Dube, W. P.; Wolfe, G. M.; Quinn, P. K.; Middlebrook, A. M. *et al.* A large atomic chlorine source inferred from mid-continental reactive nitrogen chemistry. *Nature* **2010**, *464*, 271-174.
(374) Crowley, J. N.; Thieser, J.; Tang, M. J.; Schuster, G.; Bozem, H.; Beygi, Z. H.; Fischer, H.; Diesch, J. M.; Drewnick, F.; Borrmann, S. *et al.* Variable lifetimes and loss mechanisms for NO3 and N2O5 during the DOMINO campaign: contrasts between marine, urban and continental air. *Atmos. Chem. Phys.* **2011**, *11*, 10853-10870.
(375) Sullivan, R. C.; Minambres, L.; DeMott, P. J.; Prenni, A. J.; Carrico, C. M.; Levin, E. J. T.; Kreidenweis, S. M. Chemical processing does not always impair heterogeneous ice nucleation of mineral dust particles. *Geophys. Res. Lett.* **2010**, *37*, L24805, doi: 24810.21029/22010GL045540.
(376) Yamashita, K.; Murakami, M.; Hashimoto, A.; Tajiri, T. CCN Ability of Asian Mineral Dust Particles and Their Effects on Cloud Droplet Formation. *J. Meteorol. Soc. Jpn.* **2011**, *89*, 581-587.
(377) Hensen, E. J. M.; Smit, B. Why clays swell. *J. Phys. Chem. B* **2002**, *106*, 12664-12667.
(378) Keskinen, H.; Kortelainen, A. M.; Jaatinen, A.; Yli-Pirila, P.; Joutsensaari, J.; Romakkaniemi, S.; Hao, L. Q.; Torvela, T.; Miettinen, P.; Virtanen, A. *et al.* Increased hygroscopicity of Arizona Test Dust seeds by secondary organic aerosol coating from alpha-pinene ozonolysis. *Boreal Environ. Res.* **2014**, *19*, 182-190.
(379) Hall, P. L.; Astill, D. M. Adsorption of water by homoionic exchange forms of Wyoming montmorillonite (SWY-1). *Clays Clay Miner.* **1989**, *37*, 355-363.
(380) Cases, J. M.; Berend, I.; Besson, G.; Francois, M.; Uriot, J. P.; Thomas, F.; Poirier, J. E. Mechanism of adsorption and desorption of water vapor by homoionic montmorillonite. 1. The sodium-exchanged form. *Langmuir* **1992**, *8*, 2730-2739.
(381) Xu, W. Z.; Johnston, C. T.; Parker, P.; Agnew, S. F. Infrared study of water sorption on Na-, Li-, Ca-, and Mg-exchanged (SWy-1 and SAz-1) montmorillonite. *Clays Clay Miner.* **2000**, *48*, 120-131.
(382) Zent, A. P.; Howard, D. J.; Quinn, R. C. H2O adsorption on smectites: Application to the diurnal variation of H2O in the Martian atmosphere. *J. Geophys. Res.-Planets* **2001**, *106*, 14667-14674.
(383) Frinak, E. K.; Mashburn, C. D.; Tolbert, M. A.; Toon, O. B. Infrared characterization of water uptake by low-temperature Na-montmorillonite: Implications for Earth and Mars. *J. Geophys. Res.-Atmos.* **2005**, *110*, D09308, doi: 09310.01029/02004JD005647.
(384) Attwood, A. R.; Greenslade, M. E. Deliquescence Behavior of Internally Mixed Clay and Salt Aerosols by Optical Extinction Measurements. *J. Phys. Chem. A* **2012**, *116*, 4518-4527.

(385) Dalirian, M.; Keskinen, H.; Ahlm, L.; Ylisirniö, A.; Romakkaniemi, S.; Laaksonen, A.; Virtanen, A.; Riipinen, I. CCN activation of fumed silica aerosols mixed with soluble pollutants. *Atmos. Chem. Phys.* **2015**, *15*, 3815-3829.
(386) Rubasinghege, G.; Ogden, S.; Baltrusaitis, J.; Grassian, V. H. Heterogeneous Uptake and Adsorption of Gas-Phase Formic Acid on Oxide and Clay Particle Surfaces: The Roles of Surface Hydroxyl Groups and Adsorbed Water in Formic Acid Adsorption and the Impact of Formic Acid Adsorption on Water Uptake. *J. Phys. Chem. A* **2013**, *117*, 11316-11327.
(387) Koehler, K. A.; Kreidenweis, S. M.; DeMott, P. J.; Prenni, A. J.; Petters, M. D. Potential impact of Owens (dry) Lake dust on warm and cold cloud formation. *J. Geophys. Res.-Atmos.* **2007**, *112*, D12210, doi: 12210.11029/12007jd008413.
(388) deLeeuw, N. H.; Parker, S. C. Atomistic simulation of the effect of molecular adsorption of water on the surface structure and energies of calcite surfaces. *J. Chem. Soc.-Faraday Trans.* **1997**, *93*, 467-475.
(389) Kerisit, S.; Marmier, A.; Parker, S. C. Ab initio surface phase diagram of the {10(1)over-bar4} calcite surface. *J. Phys. Chem. B* **2005**, *109*, 18211-18213.
(390) Rahaman, A.; Grassian, V. H.; Margulis, C. J. Dynamics of water adsorption onto a calcite surface as a function of relative humidity. *J. Phys. Chem. C* **2008**, *112*, 2109-2115.
(391) Tunega, D.; Gerzabek, M. H.; Lischka, H. Ab initio molecular dynamics study of a monomolecular water layer on octahedral and tetrahedral kaolinite surfaces. *J. Phys. Chem. B* **2004**, *108*, 5930-5936.
(392) Croteau, T.; Bertram, A. K.; Patey, G. N. Adsorption and Structure of Water on Kaolinite Surfaces: Possible Insight into Ice Nucleation from Grand Canonical Monte Carlo Calculations. *J. Phys. Chem. A* **2008**, *112*, 10708-10712.
(393) Croteau, T.; Bertram, A. K.; Patey, G. N. Simulation of Water Adsorption on Kaolinite under Atmospheric Conditions. *J. Phys. Chem. A* **2009**, *113*, 7826-7833.
(394) Croteau, T.; Bertram, A. K.; Patey, G. N. Observations of High-Density Ferroelectric Ordered Water in Kaolinite Trenches using Monte Carlo Simulations. *J. Phys. Chem. A* **2010**, *114*, 8396-8405.
(395) Crotean, T.; Bertram, A. K.; Patey, G. N. Water adsorption on kaolinite surfaces containing trenches. *J. Phys. Chem. A* **2010**, *114*, 2171-2178.
(396) Hensen, E. J. M.; Tambach, T. J.; Bliek, A.; Smit, B. Adsorption isotherms of water in Li-, Na-, and K-montmorillonite by molecular simulation. *J. Chem. Phys.* **2001**, *115*, 3322-3329.
(397) Tambach, T. J.; Hensen, E. J. M.; Smit, B. Molecular simulations of swelling clay minerals. *J. Phys. Chem. B* **2004**, *108*, 7586-7596.
(398) Argyris, D.; Tummala, N. R.; Striolo, A.; Cole, D. R. Molecular structure and dynamics in thin water films at the silica and graphite surfaces. *J. Phys. Chem. C* **2008**, *112*, 13587-13599.
(399) Murdachaew, G.; Gaigeot, M.-P.; Halonen, L.; Gerber, R. B. Dissociation of HCl into Ions on Wet Hydroxylated (0001) α-Quartz. *J. Phys. Chem. Lett.* **2013**, *4*, 3500-3507.
(400) Lindan, P. J. D.; Harrison, N. M.; Gillan, M. J. Mixed dissociative and molecular adsorption of water on the rutile (110) surface. *Phys. Rev. Lett.* **1998**, *80*, 762-765.
(401) Jug, K.; Nair, N. N.; Bredow, T. Molecular dynamics investigation of water adsorption on rutile surfaces. *Surf. Sci.* **2005**, *590*, 9-20.
(402) Harris, L. A.; Quong, A. A. Molecular chemisorption as the theoretically preferred pathway for water adsorption on ideal rutile TiO2(110). *Phys. Rev. Lett.* **2004**, *93*, 086105.

(403) Rustad, J. R.; Boily, J. F. Density functional calculation of the infrared spectrum of surface hydroxyl groups on goethite (α-FeOOH). *Am. Mineral.* **2010**, *95*, 414-417.
(404) Song, X. W.; Boily, J. F. Water vapor interactions with FeOOH particle surfaces. *Chem. Phys. Lett.* **2013**, *560*, 1-9.
(405) Gerber, R. B.; Varner, M. E.; Hammerich, A. D.; Riikonen, S.; Murdachaew, G.; Shemesh, D.; Finlayson-Pitts, B. J. Computational Studies of Atmospherically-Relevant Chemical Reactions in Water Clusters and on Liquid Water and Ice Surfaces. *Accounts Chem. Res.* **2015**, *48*, 399-406.
(406) Kerisit, S.; Parker, S. C. Free energy of adsorption of water and metal ions on the {1014} calcite surface. *J. Am. Chem. Soc.* **2004**, *126*, 10152-10161.
(407) Hu, X. L.; Michaelides, A. Water on the hydroxylated (001) surface of kaolinite: From monomer adsorption to a flat 2D wetting layer. *Surf. Sci.* **2008**, *602*, 960-974.
(408) Hu, X. L.; Michaelides, A. Ice formation on kaolinite: Lattice match or amphoterism? *Surf. Sci.* **2007**, *601*, 5378-5381.
(409) Hu, X. L.; Michaelides, A. The kaolinite (001) polar basal plane. *Surf. Sci.* **2010**, *604*, 111-117.
(410) Yang, J.; Wang, E. G. Reaction of water on silica surfaces. *Curr. Opin. Solid State Mater. Sci.* **2006**, *10*, 33-39.
(411) Rimola, A.; Costa, D.; Sodupe, M.; Lambert, J. F.; Ugliengo, P. Silica Surface Features and Their Role in the Adsorption of Biomolecules: Computational Modeling and Experiments. *Chem. Rev.* **2013**, *113*, 4216-4313.
(412) Legrand, A. P. *The Surface Properties of Silicas*; Wiley: Chichester, U.K., 1998.
(413) Papirer, E. *Adsorption on Silica Surfaces*; CRC Press: Boca Raton, USA, 2000.
(414) Sulpizi, M.; Gaigeot, M. P.; Sprik, M. The Silica-Water Interface: How the Silanols Determine the Surface Acidity and Modulate the Water Properties. *J. Chem. Theory Comput.* **2012**, *8*, 1037-1047.
(415) Du, Q.; Freysz, E.; Shen, Y. R. Vibrational spectra of water molecules at quartz/water interfaces. *Phys. Rev. Lett.* **1994**, *72*, 238-241.
(416) Ostroverkhov, V.; Waychunas, G. A.; Shen, Y. R. Vibrational spectra of water at water/α-quartz (0001) interface. *Chem. Phys. Lett.* **2004**, *386*, 144-148.
(417) Ostroverkhov, V.; Waychunas, G. A.; Shen, Y. R. New information on water interfacial structure revealed by phase-sensitive surface spectroscopy. *Phys. Rev. Lett.* **2005**, *94*, 046102.
(418) Richmond, G. L. Molecular bonding and interactions at aqueous surfaces as probed by vibrational sum frequency spectroscopy. *Chem. Rev.* **2002**, *102*, 2693-2724.
(419) Falkovich, A. H.; Ganor, E.; Levin, Z.; Formenti, P.; Rudich, Y. Chemical and mineralogical analysis of individual mineral dust particles. *J. Geophys. Res.-Atmos* **2001**, *106*, 18029-18036.
(420) Falkovich, A. H.; Schkolnik, G.; Ganor, E.; Rudich, Y. Adsorption of organic compounds pertinent to urban environments onto mineral dust particles. *J. Geophys. Res.-Atmos.* **2004**, *109*, D02208, doi: 02210.01029/02003JD003919.
(421) Maxwell-Meier, K.; Weber, R.; Song, C.; Orsini, D.; Ma, Y.; Carmichael, G. R.; Streets, D. G. Inorganic composition of fine particles in mixed mineral dust-pollution plumes observed from airborne measurements during ACE-Asia. *J. Geophys. Res.-Atmos.* **2004**, *109*, D19s07, doi: 10.1029/2003jd004464.
(422) Ro, C. U.; Hwang, H.; Chun, Y.; Van Grieken, R. Single-particle characterization of four "Asian Dust" samples collected in Korea, using low-Z particle electron probe X-ray microanalysis. *Environ. Sci. Technol.* **2005**, *39*, 1409-1419.

(423) Shi, Z. B.; Shao, L. T.; Jones, T. P.; Lu, S. L. Microscopy and mineralogy of airborne particles collected during severe dust storm episodes in Beijing, China. *J. Geophys. Res.-Atmos.* **2005**, *110*, D01303, doi: 01310.01029/02004jd005073.
(424) Geng, H.; Park, Y.; Hwang, H.; Kang, S.; Ro, C. U. Elevated nitrogen-containing particles observed in Asian dust aerosol samples collected at the marine boundary layer of the Bohai Sea and the Yellow Sea. *Atmos. Chem. Phys.* **2009**, *9*, 6933-6947.
(425) Li, W. J.; Shao, L. Y.; Shi, Z. B.; Chen, J. M.; Yang, L. X.; Yuan, Q.; Yan, C.; Zhang, X. Y.; Wang, Y. Q.; Sun, J. Y. *et al.* Mixing state and hygroscopicity of dust and haze particles before leaving Asian continent. *J. Geophys. Res.-Atmos* **2014**, *119*, 1044-1059.
(426) Li, W.; Shao, L.; Zhang, D.; Ro, C.-U.; Hu, M.; Bi, X.; Geng, H.; Matsuki, A.; Niu, H.; Chen, J. A review of single aerosol particle studies in the atmosphere of East Asia: morphology, mixing state, source, and heterogeneous reactions. *J. Clean. Prod.* **2015**, *112*, 1330-1349.
(427) Perry, K. D.; Cliff, S. S.; Jimenez-Cruz, M. P. Evidence for hygroscopic mineral dust particles from the Intercontinental Transport and Chemical Transformation Experiment. *J. Geophys. Res.-Atmos* **2004**, *109*, D23S28, doi: 10.1029/2004JD004979.
(428) Massling, A.; Leinert, S.; Wiedensohler, A.; Covert, D. Hygroscopic growth of sub-micrometer and one-micrometer aerosol particles measured during ACE-Asia. *Atmos. Chem. Phys.* **2007**, *7*, 3249-3259.
(429) Shi, Z.; Zhang, D.; Hayashi, M.; Ogata, H.; Ji, H.; Fujiie, W. Influences of sulfate and nitrate on the hygroscopic behaviour of coarse dust particles. *Atmos. Environ.* **2008**, *42*, 822-827.
(430) Crumeyrolle, S.; Gomes, L.; Tulet, P.; Matsuki, A.; Schwarzenboeck, A.; Crahan, K. Increase of the aerosol hygroscopicity by cloud processing in a mesoscale convective system: a case study from the AMMA campaign. *Atmos. Chem. Phys.* **2008**, *8*, 6907-6924.
(431) Tobo, Y.; Zhang, D. Z.; Nakata, N.; Yamada, M.; Ogata, H.; Hara, K.; Iwasaka, Y. Hygroscopic mineral dust particles as influenced by chlorine chemistry in the marine atmosphere. *Geophys. Res. Lett.* **2009**, *36*, L05817, doi: 05810.01029/02008gl036883.
(432) Tobo, Y.; Zhang, D.; Matsuki, A.; Iwasaka, Y. Asian dust particles converted into aqueous droplets under remote marine atmospheric conditions. *Proc. Natl. Acad. Sci. U. S. A.* **2010**, *107*, 17905-17910.
(433) Kim, J. S.; Park, K. Atmospheric Aging of Asian Dust Particles During Long Range Transport. *Aerosol Sci. Technol.* **2012**, *46*, 913-924.
(434) Denjean, C.; Caquineau, S.; Desboeufs, K.; Laurent, B.; Maille, M.; Quiñones Rosado, M.; Vallejo, P.; Mayol-Bracero, O. L.; Formenti, P. Long-range transport across the Atlantic in summertime does not enhance the hygroscopicity of African mineral dust. *Geophys. Res. Lett.* **2015**, *42*, 7835-7843.
(435) Bates, T. S.; Quinn, P. K.; Frossard, A. A.; Russell, L. M.; Hakala, J.; Petaja, T.; Kulmala, M.; Covert, D. S.; Cappa, C. D.; Li, S. M. *et al.* Measurements of ocean derived aerosol off the coast of California. *J. Geophys. Res.-Atmos.* **2012**, *117*, D00V15, doi: 10.1029/2012jd017588.
(436) Fuentes, E.; Coe, H.; Green, D.; McFiggans, G. On the impacts of phytoplankton-derived organic matter on the properties of the primary marine aerosol - Part 2: Composition, hygroscopicity and cloud condensation activity. *Atmos. Chem. Phys.* **2011**, *11*, 2585-2602.
(437) Laskina, O.; Morris, H. S.; Grandquist, J. R.; Qin, Z.; Stone, E. A.; Tivanski, A. V.; Grassian, V. H. Size Matters in the Water Uptake and Hygroscopic Growth of

Atmospherically Relevant Multicomponent Aerosol Particles. *J. Phys. Chem. A* **2015**, *119*, 4489-4497.
(438) Kaaden, N.; Massling, A.; Schladitz, A.; Müller, T.; Kandler, K.; SchüTz, L.; Weinzierl, B.; Petzold, A.; Tesche, M.; Leinert, S. *et al.* State of mixing, shape factor, number size distribution, and hygroscopic growth of the Saharan anthropogenic and mineral dust aerosol at Tinfou, Morocco. *Tellus B* **2009**, *61*, 51-63.
(439) Schladitz, A.; Müller, Thomas; Nowak, A.; Kandler, K.; Lieke, K.; Massling, A.; Wiedensohler, A. In situ aerosol characterization at Cape Verde. Part 1: particle number size distributions, hygroscopic growth and state of mixing of the marine and Saharan dust aerosol. *Tellus B* **2011**, *63*, 531-548.
(440) Tobo, Y.; DeMott, P. J.; Raddatz, M.; Niedermeier, D.; Hartmann, S.; Kreidenweis, S. M.; Stratmann, F.; Wex, H. Impacts of chemical reactivity on ice nucleation of kaolinite particles: A case study of levoglucosan and sulfuric acid. *Geophys. Res. Lett.* **2012**, *39*, L19803, doi: 19810.11029/12012gl053007.
(441) Hiranuma, N.; Augustin-Bauditz, S.; Bingemer, H.; Budke, C.; Curtius, J.; Danielczok, A.; Diehl, K.; Dreischmeier, K.; Ebert, M.; Frank, F. *et al.* A comprehensive laboratory study on the immersion freezing behavior of illite NX particles: a comparison of 17 ice nucleation measurement techniques. *Atmos. Chem. Phys.* **2015**, *15*, 2489-2518.
(442) Lau, K. M.; Wu, H. T. Warm rain processes over tropical oceans and climate implications. *Geophys. Res. Lett.* **2003**, *30*, 2290, doi: 2210.1029/2003gl018567.
(443) Freedman, M. A. Potential Sites for Ice Nucleation on Aluminosilicate Clay Minerals and Related Materials. *J. Phys. Chem. Lett.* **2015**, *6*, 3850-3858.
(444) DeMott, P. J.; Möhler, O.; Stetzer, O.; Vali, G.; Levin, Z.; Petters, M. D.; Murakami, M.; Leisner, T.; Bundke, U.; Klein, H. *et al.* Resurgence in Ice Nuclei Measurement Research. *Bull. Amer. Meteorol. Soc.* **2011**, *92*, 1623-1635.
(445) Vali, G. Nucleation terminology. *Bull. Amer. Meteorol. Soc.* **1985**, *66*, 1426-1427.
(446) Vali, G.; DeMott, P. J.; Möhler, O.; Whale, T. F. Technical Note: A proposal for ice nucleation terminology. *Atmos. Chem. Phys.* **2015**, *15*, 10263-10270.
(447) Martin, S. T. Phase transitions of aqueous atmospheric particles. *Chem. Rev.* **2000**, *100*, 3403-3453.
(448) Szyrmer, W.; Zawadzki, I. Biogenic and Anthropogenic Sources of Ice-Forming Nuclei: A Review. *Bull. Amer. Meteorol. Soc.* **1997**, *78*, 209-228.
(449) Kulkarni, G.; Sanders, C.; Zhang, K.; Liu, X.; Zhao, C. Ice nucleation of bare and sulfuric acid-coated mineral dust particles and implication for cloud properties. *J. Geophys. Res.-Atmos* **2014**, *119*, 9993-10011.
(450) Girard, E.; Dueymes, G.; Du, P.; Bertram, A. K. Assessment of the effects of acid-coated ice nuclei on the Arctic cloud microstructure, atmospheric dehydration, radiation and temperature during winter. *Int. J. Climatol.* **2013**, *33*, 599-614.
(451) Salam, A.; Lesins, G.; Lohmann, U. Laboratory study of heterogeneous ice nucleation in deposition mode of montmorillonite mineral dust particles aged with ammonia, sulfur dioxide, and ozone at polluted atmospheric concentrations. *Air Qual. Atmos. Health* **2008**, *1*, 135-142.
(452) Archuleta, C. M.; DeMott, P. J.; Kreidenweis, S. M. Ice nucleation by surrogates for atmospheric mineral dust and mineral dust/sulfate particles at cirrus temperatures. *Atmos. Chem. Phys.* **2005**, *5*, 2617-2634.
(453) Knopf, D. A.; Koop, T. Heterogeneous nucleation of ice on surrogates of mineral dust. *J. Geophys. Res.-Atmos.* **2006**, *111*, D12201, doi: 12210.11029/12005jd006894.
(454) Eastwood, M. L.; Cremel, S.; Wheeler, M.; Murray, B. J.; Girard, E.; Bertram, A. K. Effects of sulfuric acid and ammonium sulfate coatings on the ice nucleation properties

of kaolinite particles. *Geophys. Res. Lett.* **2009**, *36*, L02811, doi: 02810.01029/02008gl035997.
(455) Chernoff, D. I.; Bertram, A. K. Effects of sulfate coatings on the ice nucleation properties of a biological ice nucleus and several typs of minerals. *J. Geophys. Res.-Atmos.* **2010**, *115*, D20205, doi: 20210.21029/22010JD014254.
(456) Niedermeier, D.; Hartmann, S.; Shaw, R. A.; Covert, D.; Mentel, T. F.; Schneider, J.; Poulain, L.; Reitz, P.; Spindler, C.; Clauss, T. *et al.* Heterogeneous freezing of droplets with immersed mineral dust particles – measurements and parameterization. *Atmos. Chem. Phys.* **2010**, *10*, 3601-3614.
(457) Wex, H.; DeMott, P. J.; Tobo, Y.; Hartmann, S.; Rösch, M.; Clauss, T.; Tomsche, L.; Niedermeier, D.; Stratmann, F. Kaolinite particles as ice nuclei: learning from the use of different kaolinite samples and different coatings. *Atmos. Chem. Phys.* **2014**, *14*, 5529-5546.
(458) Sihvonen, S. K.; Schill, G. P.; Lyktey, N. A.; Veghte, D. P.; Tolbert, M. A.; Freedman, M. A. Chemical and Physical Transformations of Aluminosilicate Clay Minerals Due to Acid Treatment and Consequences for Heterogeneous Ice Nucleation. *J. Phys. Chem. A* **2014**, *118*, 8787-8796.
(459) Augustin-Bauditz, S.; Wex, H.; Kanter, S.; Ebert, M.; Niedermeier, D.; Stolz, F.; Prager, A.; Stratmann, F. The immersion mode ice nucleation behavior of mineral dusts: A comparison of different pure and surface modified dusts. *Geophys. Res. Lett.* **2014**, *41*, 7375-7382.
(460) Yang, Z.; Bertram, A. K.; Chou, K. C. Why Do Sulfuric Acid Coatings Influence the Ice Nucleation Properties of Mineral Dust Particles in the Atmosphere? *J. Phys. Chem. Lett.* **2011**, *2*, 1232-1236.
(461) Serratosa, J. M.; Bradley, W. F. Infra-Red Absorption of OH Bonds in Micas. *Nature* **1958**, *181*, 111-111.
(462) Du, Q.; Freysz, E.; Shen, Y. R. Surface Vibrational Spectroscopic Studies of Hydrogen Bonding and Hydrophobicity. *Science* **1994**, *264*, 826-828.
(463) Sovago, M.; Campen, R. K.; Wurpel, G. W. H.; Müller, M.; Bakker, H. J.; Bonn, M. Vibrational Response of Hydrogen-Bonded Interfacial Water is Dominated by Intramolecular Coupling. *Phys. Rev. Lett.* **2008**, *100*, 173901.
(464) Abdelmonem, A.; Lützenkirchen, J.; Leisner, T. Probing ice-nucleation processes on the molecular level using second harmonic generation spectroscopy. *Atmos. Meas. Tech.* **2015**, *8*, 3519-3526.
(465) Lupi, L.; Molinero, V. Does Hydrophilicity of Carbon Particles Improve Their Ice Nucleation Ability? *J. Phys. Chem. A* **2014**, *118*, 7330-7337.
(466) Möhler, O.; Benz, S.; Saathoff, H.; Schnaiter, M.; Wagner, R.; Schneider, J.; Walter, S.; Ebert, V.; Wagner, S. The effect of organic coating on the heterogeneous ice nucleation efficiency of mineral dust aerosols. *Environ. Res. Lett.* **2008**, *3*, 025007.
(467) Kulkarni, G.; Zhang, K.; Zhao, C.; Nandasiri, M.; Shutthanandan, V.; Liu, X.; Fast, J.; Berg, L. Ice formation on nitric acid coated dust particles: Laboratory and modeling studies. *J. Geophys. Res.-Atmos* **2015**, *120*, 7682-7698.
(468) Salam, A.; Lohmann, U.; Lesins, G. Ice nucleation of ammonia gas exposed montmorillonite mineral dust particles. *Atmos. Chem. Phys.* **2007**, *7*, 3923-3931.
(469) Kanji, Z. A.; Welti, A.; Chou, C.; Stetzer, O.; Lohmann, U. Laboratory studies of immersion and deposition mode ice nucleation of ozone aged mineral dust particles. *Atmos. Chem. Phys.* **2013**, *13*, 9097-9118.
(470) Fenter, F. F.; Caloz, F.; Rossi, M. J. Experimental-Evidence for the Efficient Dry Deposition of Nitric-Acid on Calcite. *Atmos. Environ.* **1995**, *29*, 3365-3372.

(471) Hanisch, F.; Crowley, J. N. Heterogeneous reactivity of gaseous nitric acid on Al_2O_3, $CaCO_3$, and atmospheric dust samples: A Knudsen cell study. *J. Phys. Chem. A* **2001**, *105*, 3096-3106.
(472) Mashburn, C. D.; Frinak, E. K.; Tolbert, M. A. Heterogeneous uptake of nitric acid on Na-montmorillonite clay as a function of relative humidity. *J. Geophys. Res.-Atmos.* **2006**, *111*, D15213, doi: 15210.11029/12005JD006525.
(473) Vlasenko, A.; Huthwelker, T.; Gaggeler, H. W.; Ammann, M. Kinetics of the heterogeneous reaction of nitric acid with mineral dust particles: an aerosol flow tube study. *Phys. Chem. Chem. Phys.* **2009**, *11*, 7921-7930.
(474) Underwood, G. M.; Li, P.; Al-Abadleh, H.; Grassian, V. H. A Knudsen cell study of the heterogeneous reactivity of nitric acid on oxide and mineral dust particles. *J. Phys. Chem. A* **2001**, *105*, 6609-6620.
(475) Gustafsson, R. J.; Orlov, A.; Griffiths, P. T.; Cox, R. A.; Lambert, R. M. Reduction of NO_2 to nitrous acid on illuminated titanium dioxide aerosol surfaces: implications for photocatalysis and atmospheric chemistry. *Chem. Commun.* **2006**, 3936-3938.
(476) Angelini, M. M.; Garrard, R. J.; Rosen, S. J.; Hinrichs, R. Z. Heterogeneous reactions of gaseous HNO_3 and NO_2 on the clay minerals kaolinite and pyrophyllite. *J. Phys. Chem. A* **2007**, *111*, 3326-3335.
(477) Ndour, M.; D'Anna, B.; George, C.; Ka, O.; Balkanski, Y.; Kleffmann, J.; Stemmler, K.; Ammann, M. Photoenhanced uptake of NO_2 on mineral dust: Laboratory experiments and model simulations. *Geophys. Res. Lett.* **2008**, *35*, L05812, doi: 05810.01029/02007gl032006.
(478) Ndour, M.; Nicolas, M.; D'Anna, B.; Ka, O.; George, C. Photoreactivity of NO_2 on mineral dusts originating from different locations of the Sahara desert. *Phys. Chem. Chem. Phys.* **2009**, *11*, 1312-1319.
(479) Karagulian, F.; Rossi, M. J. The heterogeneous chemical kinetics of NO_3 on atmospheric mineral dust surrogates. *Phys. Chem. Chem. Phys.* **2005**, *7*, 3150-3162.
(480) Zolles, T.; Burkart, J.; Häusler, T.; Pummer, B.; Hitzenberger, R.; Grothe, H. Identification of Ice Nucleation Active Sites on Feldspar Dust Particles. *J. Phys. Chem. A* **2015**, *119*, 2692-2700.
(481) Steinke, I.; Hoose, C.; Möhler, O.; Connolly, P.; Leisner, T. A new temperature- and humidity-dependent surface site density approach for deposition ice nucleation. *Atmos. Chem. Phys.* **2015**, *15*, 3703-3717.
(482) Connolly, P. J.; Moehler, O.; Field, P. R.; Saathoff, H.; Burgess, R.; Choularton, T.; Gallagher, M. Studies of heterogeneous freezing by three different desert dust samples. *Atmos. Chem. Phys.* **2009**, *9*, 2805-2824.
(483) Niemand, M.; Möhler, O.; Vogel, B.; Vogel, H.; Hoose, C.; Connolly, P.; Klein, H.; Bingemer, H.; DeMott, P.; Skrotzki, J. *et al.* A Particle-Surface-Area-Based Parameterization of Immersion Freezing on Desert Dust Particles. *J. Atmos. Sci.* **2012**, *69*, 3077-3092.
(484) Phillips, V. T. J.; DeMott, P. J.; Andronache, C. An empirical parameterization of heterogeneous ice nucleation for multiple chemical species of aerosol. *J. Atmos. Sci.* **2008**, *65*, 2757-2783.
(485) Gysel, M.; Weingartner, E.; Baltensperger, U. Hygroscopicity of Aerosol Particles at Low Temperatures. 2. Theoretical and Experimental Hygroscopic Properties of Laboratory Generated Aerosols. *Environ. Sci. Technol.* **2002**, *36*, 63-68.
(486) Zeng, G.; Kelley, J.; Kish, J. D.; Liu, Y. Temperature-Dependent Deliquescent and Efflorescent Properties of Methanesulfonate Sodium Studied by ATR-FTIR Spectroscopy. *J. Phys. Chem. A* **2014**, *118*, 583-591.

(487) Christensen, S. I.; Petters, M. D. The Role of Temperature in Cloud Droplet Activation. *J. Phys. Chem. A* **2012**, *116*, 9706-9717.
(488) Tang, M. J.; Cox, R. A.; Kalberer, M. Compilation and evaluation of gas phase diffusion coefficients of reactive trace gases in the atmosphere: volume 1. Inorganic compounds. *Atmos. Chem. Phys.* **2014**, *14*, 9233-9247.
(489) Tang, M. J.; Shiraiwa, M.; Pöschl, U.; Cox, R. A.; Kalberer, M. Compilation and evaluation of gas phase diffusion coefficients of reactive trace gases in the atmosphere: Volume 2. Diffusivities of organic compounds, pressure-normalised mean free paths, and average Knudsen numbers for gas uptake calculations. *Atmos. Chem. Phys.* **2015**, *15*, 5585-5598.
(490) Shiraiwa, M.; Ammann, M.; Koop, T.; Poschl, U. Gas uptake and chemical aging of semisolid organic aerosol particles. *Proc. Natl. Acad. Sci. U. S. A.* **2011**, *108*, 11003-11008.
(491) Zobrist, B.; Soonsin, V.; Luo, B. P.; Krieger, U. K.; Marcolli, C.; Peter, T.; Koop, T. Ultra-slow water diffusion in aqueous sucrose glasses. *Phys. Chem. Chem. Phys.* **2011**, *13*, 3514-3526.
(492) Vaden, T. D.; Imre, D.; Beranek, J.; Shrivastava, M.; Zelenyuk, A. Evaporation kinectis and phase of laboratory and ambient secondary organic aerosol. *Proc. Natl. Acad. Sci. U. S. A.* **2011**, *108*, 2190-2195.
(493) Davidovits, P.; Hu, J. H.; Worsnop, D. R.; Zahniser, M. S.; Kolb, C. E. Entry of gas molecules into liquids. *Faraday Discuss.* **1995**, *100*, 65-81.
(494) Pöschl, U. Atmospheric aerosols: Composition, transformation, climate and health effects. *Angew. Chem.-Int. Edit.* **2005**, *44*, 7520-7540.
(495) Davidovits, P.; Kolb, C. E.; Williams, L. R.; Jayne, J. T.; Worsnop, D. R. Update 1 of: Mass Accommodation and Chemical Reactions at Gas-Liquid Interfaces. *Chem. Rev.* **2011**, *111*, PR76-PR109.
(496) Pöschl, U. Gas–particle interactions of tropospheric aerosols: Kinetic and thermodynamic perspectives of multiphase chemical reactions, amorphous organic substances, and the activation of cloud condensation nuclei. *Atmos. Res.* **2011**, *101*, 562-573.
(497) Ammann, M.; Cox, R. A.; Crowley, J. N.; Jenkin, M. E.; Mellouki, A.; Rossi, M. J.; Troe, J.; Wallington, T. J. Evaluated kinetic and photochemical data for atmospheric chemistry: Volume VI - heterogeneous reactions with liquid substrates. *Atmos. Chem. Phys.* **2013**, *12*, 8045-8228.
(498) Sander, S. P.; Abbatt, J. P. D.; Barker, J. R.; Burkholder, J. B.; Friedl, R. R.; Golden, D. M.; Huie, R. E.; Kolb, C. E.; Kurylo, M. J.; Moortgat, G. K. *et al.* "Chemical Kinetics and Photochemical Data for Use in Atmospheric Studies, Evaluation No. 17, JPL Publication 10-6," Jet Propulsion Lab., 2011.
(499) Pöschl, U.; Shiraiwa, M. Multiphase Chemistry at the Atmosphere–Biosphere Interface Influencing Climate and Public Health in the Anthropocene. *Chem. Rev.* **2015**, *115*, 4440-4475.
(500) Pöschl, U.; Rudich, Y.; Ammann, M. Kinetic model framework for aerosol and cloud surface chemistry and gas-phase interaction-Part 1: General equation, parameters, and terminology. *Atmos. Chem. Phys.* **2007**, *7*, 5989-6023.
(501) Shiraiwa, M.; Pfrang, C.; Koop, T.; Poschl, U. Kinetic multi-layer model of gas-particle interactions in aerosols and clouds (KM-GAP): linking condensation, evaporation and chemical reactions of organics, oxidants and water. *Atmos. Chem. Phys.* **2012**, *12*, 2777-2794.
(502) Berkemeier, T.; Huisman, A. J.; Ammann, M.; Shiraiwa, M.; Koop, T.; Pöschl, U. Kinetic regimes and limiting cases of gas uptake and heterogeneous reactions in

atmospheric aerosols and clouds: a general classification scheme. *Atmos. Chem. Phys.* **2013**, *13*, 6663-6686.